Development of New Supported Bilayer Platforms for Membrane Protein Incorporation

By

Kirk M. Mulligan

Thesis submitted to the Faculty of Graduate & Postdoctoral Studies

University of Ottawa

In partial fulfillment of the requirements for the

Ph.D. degree from the

Ottawa-Carleton Chemistry Institute

University of Ottawa

Candidate	Supervisor
Kirk M. Mulligan	L. J. Johnston

Abstract

Membranes are essential components of all living organisms forming the borders of cells and their organelles. Planar lipid membranes deposited on solid substrates (solid supported membranes) provide models to study the functions of membrane proteins and are used as biosensing platforms. However, despite remarkable progress, solid supported membranes are not stable to harsh conditions such as dehydration, high temperature and pressure, and mechanical stress. In addition, the direct deposition of membranes onto a solid substrate often causes restricted mobility and denaturation of reconstituted membrane proteins.

Membrane stability can be addressed by altering the structure of the component lipids. Bolalipids are an interesting class of bipolar lipids that have been proposed for biosensing applications. Membranes formed from mixtures of a bolalipid, C_{20}BAS, and dioleoylphosphaphatidylcholine, POPC, were characterized by atomic force spectroscopy (AFM). The lipid mixtures produced a phase separated membrane consisting of thinner bolalipid-rich and thicker monopolar-rich POPC regions, with a height difference of approximately 1-2 nm. This confirmed an earlier prediction that some bolalipid/PC membranes would phase separate due to the hydrophobic mismatch between the two lipids. Interestingly, the surface coverage of the two phases was inconsistent with what one would expect from the initial starting lipid ratios. The complex membrane morphologies observed were accredited to the interplay of several factors, including a compositionally heterogeneous vesicle population, exchange of lipid between the vesicle solution

and solid substrate during formation of the supported membrane, and slow equilibration of domains due to pinning of the lipids to the solid support.

Decoupling the membrane from its underlying surface is one strategy to maintain the structure and mobility of membrane proteins. This decoupling can be achieved by depositing the membrane on a soft cushion composed of a water swelling hydrophilic polymer. A polyelectrolyte multilayer (PEM) and a tethered poly(ethylene) glycol (PEG) polymer are the two types of polymer cushions used in this study. The PEMs consist of the charged polysaccharides, chitosan (CHI) and hyaluronic acid (HA) which offer the advantage of biocompatibility over synthetic PEMs. DOPC lipid bilayers were formed at pH 4 and 6.5 on $(CHI/HA)_5$ films. At higher pH adsorbed lipids had low mobility and large immobile lipid fractions; fluorescence and AFM showed that this was accredited to the formation of poor quality membranes with defects and pinned lipids rather than to a layer of surface-adsorbed vesicles. However, more uniform bilayers with mobile lipids were produced at pH 4. Measured diffusion coefficients were similar to those for bilayers on PEG cushions and considerably higher than those measured on other polyelectrolyte films. The results suggest that the polymer surface charge is more important than the surface roughness in controlling formation of mobile supported bilayers.

The suitability of polymer supported membranes for the incorporation of integral membrane proteins was also assessed. The integral membrane protein Ste14p, a 26 kDa methyltransferase enzyme, was reconstituted into POPC membranes on PEM and PEG supports. A combination of fluorescence

microscopy, FRAP, AFM and an *in situ* methyltransferase activity assay were utilized to characterize the protein incorporated polymer supported membranes. Fluorescence measurements showed that more protein was incorporated in model membranes formed on the PEG support, compared to either glass or PEM cushions. However, the protein activity on a PEG support was comparable to that of the protein in a membrane on glass. FRAP measurements showed that the lipid mobilities of the POPC:Ste14p bilayers on the various supports were also comparable.

Lastly, as a new platform for manipulating and handling membrane proteins, nanodiscs containing reconstituted Ste14p were studied. Nanodiscs are small, soluble and stable bilayer discs that permit the study of membrane proteins in a uniform phospholipid bilayer environment. Empty and protein containing nanodiscs were deposited on a mica surface and imaged by AFM. AFM showed that protein containing samples possessed two subpopulations of nanodiscs with a height difference of ~1 nm. The taller discs, ~20% of the population, contained protein. Other experiments showed that the packing of the nanodisc samples was influenced by their initial stock concentration and that both imaging force and the addition of Mg^{2+} caused formation of larger bilayer patches.

Acknowledgements

At the completion of this project I feel it necessary to thank a few people that helped to make this project possible. I would like to thank my family members, Mother, Dad and Kyle. If it wasn't for their undying support over the last five years I would have probably not made it this far. I would also like to thank Dr. L. J. Johnston for her tremendous time, effort, advice, guidance, support and encouragement in the preparation of this thesis. Dr. Johnston provided a research environment that was stimulating and at the same time surprisingly relaxed. I would also like to thank the National Research Council, the Department of Chemistry and the University of Ottawa for their financial contributions. Many thanks are also extended to everyone else in the Dr. Johnston's lab that helped me with the finer points of this project. Lastly, my thanks must go to all of my friends who endured with me throughout this project.

To Mother and Dad…

Table of Contents

List of Abbreviations

ABC	ATP-binding cassette
AEBSF	4-(2-Aminoethyl) benzenesulfonyl fluoride hydrochloride
AFC	*N*-acetyl-*S*-farnesyl-L-cysteine
AFM	atomic force microscopy
AHAPS	aminopropyltrimethoxysilane
ATP	adenosine triphosphate
BACE	β-amyloid precursor protein cleaving enzyme
bR	bacteriorhodopsin
BSA	bovine serum albumin
bPC	brain phosphatidylcholine
bSM	brain sphingomyelin
C_{20}BAS	2,2'-di-*O*-decyl-3,3'-di-*O*-(1'',20''-eicosanyl)-bis-(*rac*-glycero)-1,1'-diphosphocholine
C_{34}phytBAS	2,2'-di-*O*-(3,7,11,15-tetramethylhexadecyl)-3,3'-di-*O*-(1'',32''-dotriacontanyl)-bis-(*rac*-glycero)-1,1'-diphosphocholine
CH	cholesterol
CHI	chitosan

CMC	critical micelle concentration
CPR	cytochrome P450 reductase
CV	cyclic voltammetry
Cy5	bisindeolenylpentamethine
CYP	cytochrome P450
C=C	carbon carbon double bond
D	diffusion coefficient
DDM	dodecyl β-D-maltoside
DHPE	1,2-dihexadecanoyl-*sn*-glycero-3-phosphoethanolamine
DiI	diindole
DLS	dynamic light scattering
DMPC	1,2-dimyristoylphosphatidylcholine
DMSO	dimethyl sulfoxide
DMPE	1,2-bis(dimethylphosphino)ethane
DODA	poly(2-ethyl-2-oxazoline)
DOPC	1,2-dioleoyl-*sn*-glycero-3-phosphocholine
DOPE	1,2-dioleoyl-*sn*-glycero-3-phosphoethanolamine

DPG	diphosphatidylglycerol
DPTL	glycol-D,L-R-lipoic acid ester lipid
DPhPC	1,2-diphytanoyl-*sn*-glycero-3-phosphocholine
DPPC	1,2-dipalmitoyl-*sn*-glycero-3-phosphocholine
DPPE	1,2-bis(diphenylphosphino)ethane
DSPE	1,2-distearoyl-*sn*-glycero-3-phosphoethanolamine
DTSP	3,3-dithio-bis(propionic acid *N*-hydroxysuc-cinimide ester)
EGFR	epidermal growth factor receptor
EIS	electrical impedance spectroscopy
EPR	electron paramagnetic resonance
F	mobile fraction
FCS	fluorescence correlation spectroscopy
FGFR3	fibroblast growth factor receptor 3
FLIM	fluorescence lifetime imaging
FRAP	fluorescence recovery after photobleaching
FTIR	fourier transform infrared
GDP	guanosine diphosphate

GFP	green fluorescent protein
GTP	guanosine triphosphate
GUV	giant unilamellar vesicles
HA	hyaluronic acid
hDOR	human delta-opioid receptor
His	histidine
ICMT	isoprenylcysteine carboxylmethyltransferase
k	spring constant
K	thousand
LB	Langmuir Blodgett
lbl	layer-by-layer
LH1-RC	light harvesting complex reaction center
LS	Langmuir Schaeffer
LUV	large unilamellar vesicles
MAC	magnetic AC
MOPS	3-(*N*-morpholino)propanesulfonic acid
MSP	membrane scaffolding protein

MUA	11-mercaptoundecanoic acid
NBD	nitro-2-1,3-benzoxadiazol-4-yl
NHS	sigma-*N*-hydroxysuccinimide
NMR	nuclear magnetic resonance
OG	Oregon Green
PAH	poly-(allylamine hydrochloride)
PC	phosphocholine
PDDA	polydiallyldimethylamonium
PDP	*N*-3-(2-pyridyldithio)propionate
PE	phosphatidylethanolamine
PEG	poly(ethylene) glycol
PEI	poly(ethyleneimine)
PEM	polyelectrolyte multilayer
PEMA	poly(ethane-alt-maleic anhydride)
PEOX	poly(ethyloxazoline)
PLL	Poly(L-Lysine)
POMA	Poly(octadecene-alt-maleic anhydride)

POPA	1-palmitoyl-2-oleoyl-*sn*-glycero-3-phosphate
POPC	1-palmitoyl-2-oleoylphosphatidylcholine
POPG	1-palmitoyl-2-oleoyl-*sn*-glycero-3-phosphoglycerol
POPS	1-palmitoyl-2-oleoyl-*sn*-glycero-3-phospho-L-serine
POX	poly(2-oxazoline)
PPMA	polymethylmethacrylate
PPy	polypyrrole
PS	phosphatidylserine
PSS	polystyrene sulfonate
QAC	quaternary ammonium compounds
QCM	quartz crystal microbalance
RCIM	raman chemical imaging microspectroscopy
SANS	small-angle neutron scattering
SAXS	small-angle x-ray scattering
SDS	sodium dodecyl sulfate
SIMS	secondary ion mass spectroscopy
SM	sphingomyelin

SMFM	single molecule fluorescence microscopy
SNARE	soluble NSF attachment protein receptor
SOPC	1-stearoyl-2-oleoyl-*sn*-glycero-3-phosphocholine
SPM	scanning probe microscopy
SPR	surface plasmon resonance
SPT	single particle tracking
Ste14p	enzyme from *Saccharomyces cerevisiae*
SUV	small unilamellar vesicles
TEM	transmission electron microscopy
TF	tissue factor
TIRF	total internal reflection fluorescence
TR	Texas Red
Tris	trisaminomethane
VF	vesicle fusion
x	times
X_b	fraction of C_{20}BAS
XPS	x-ray Photoelectron Spectroscopy

List of Figures

List of Tables

Chapter 1: Introduction

1.1 Biosensing Properties of Biomembranes

Biomembrane platforms that consist of membrane proteins and/or other components are novel materials for potential biosensor applications and for making artificial cells. The term biosensor is extremely broad and comprises any bio-related object that can be used for detection and measurement.[1] Organisms such as bacteria can even be considered as biosensors. Often times sensing or diagnostic systems that consist of large numbers of individual biosensors are referred to as biochips. Nano-fabrication and biomaterials allow the study of the interface between different materials and living organisms. Biomembranes that incorporate other biomolecules into or onto their surfaces, in order to study some specific properties, can be made by a controlled method. For example, one can study the function of membrane proteins via incorporation into a bilayer. In addition, one can also study the binding of ligands to membrane proteins in the bilayer. Many future potential biosensing applications are possible with the use of biomembranes and their modification.[1] As a result, it is of great interest to study biomembranes and exploit their potential in biosensing.

1.1.1 Models for Cellular Membranes

Biological membranes are important structures in all living organisms. In cells, membranes act as a barrier that separates the cell's interior organelles from its exterior environment. Membranes aid to control and maintain concentration gradients for various molecules passing into and out of the cell.[2] The membrane of a cell is also associated with growth, cellular differentiation and cell signaling. Many

of these functions are the result of dynamic processes within the cell membrane involving many of its cellular components. Some membrane functions require a balance between flexibility and stability of the lipid bilayer. For example, there are complex repair mechanisms that operate in the event of the creation of a defect in the membrane by an external mechanical or chemical stress.[3]

Membranes consist of three major components: lipids, proteins, and sugars. The main membrane matrix components are lipids. Lipids are amphiphilic molecules composed of a hydrophilic head group and a hydrophobic tail group. These molecules self assemble to form large two dimensional arrays or monolayers. Lipid membranes or bilayers are formed when two lipid monolayers are stabilized by hydrophobic interactions between their lipid tails. The packing together of the non polar hydrocarbon chains is energetically and entropically favoured. There are few possible arrangements of the hydrophobic tails since they can not form hydrogen bonds with the surrounding water molecules. This phenomenon is called the hydrophobic effect. The lipid component of the membrane matrix consists of several different lipid species such as, phospholipids and glycolipids. In addition, small molecules like cholesterol and the cytoskeleton also affect the structure and function of the membrane.[4] Finally, structural or functional proteins are embedded into lipid bilayers and in turn complete the composition of a typical membrane (Figure 1.1).

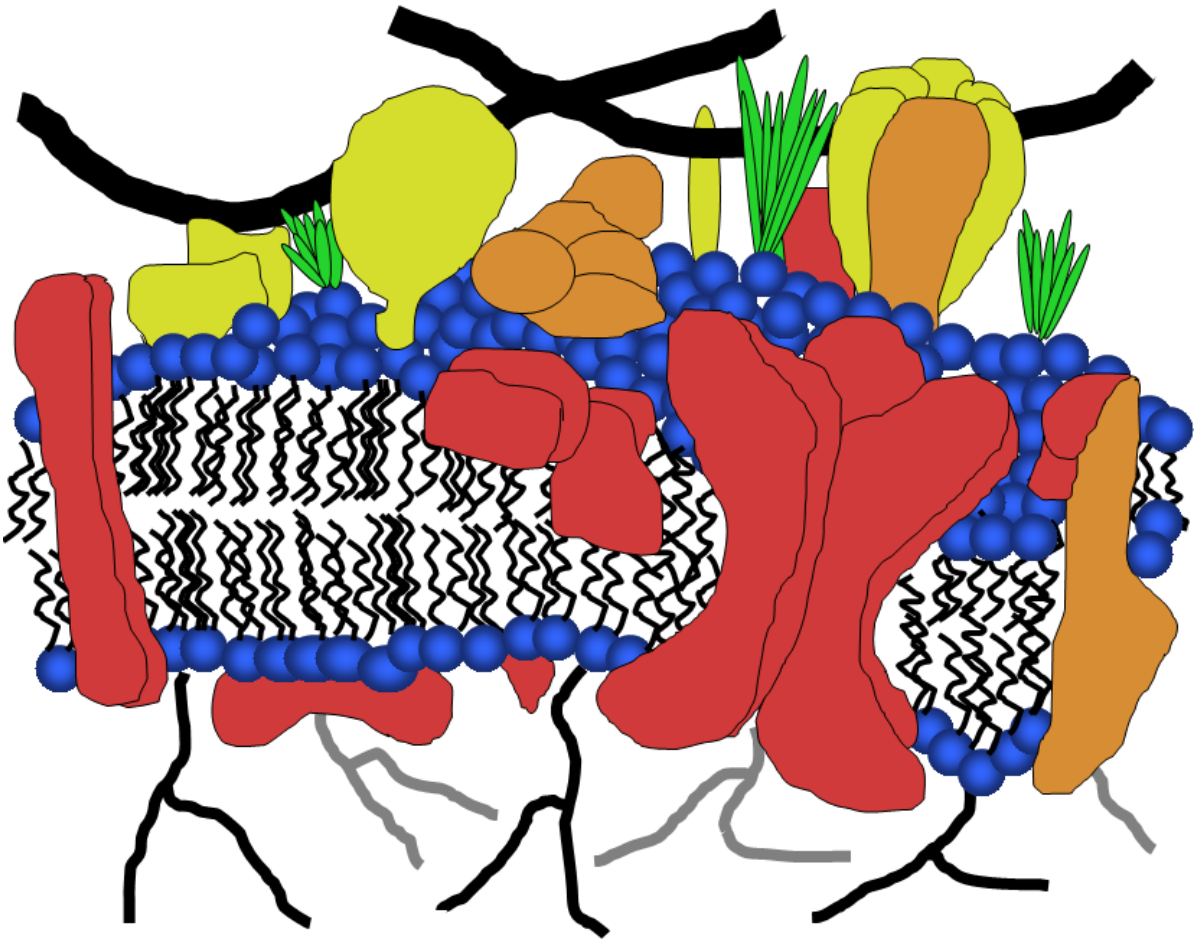

Figure 1.1 Model of a Biological Cell Membrane (Adapted from reference 5).[5]

In the early 1970's, membrane structure was explained by the fluid mosaic concept where proteins can diffuse freely in a two dimensional viscous liquid, the lipid bilayer.[6] More recently, research has shown that membranes are not as fluid as initially hypothesized. Small clusters in the membrane consisting of membrane proteins and different types of lipids were shown to affect membrane behavior at the molecular level.[7] For example important processes such as enzyme activation or ligand receptor recognition are facilitated by an enrichment of proteins in small lipid clusters. These small lipid clusters are also called lipid rafts.

The concept of lipid rafts was first hypothesized in 1988 to explain the production of a glycolipid-rich apical membrane in epithelial cells.[8] Later, the concept was generalized as the subcompartmentalization of membranes. Rafts were also shown to be involved in a broader range of cellular membrane functions, such as post-Golgi trafficking, endocytosis and signaling.[9] Lipid membrane rafts are presently defined as dynamic nanoscale regions of a membrane with higher sterol and glycosphingolipid content. Rafts can also contain ordered assemblies of specific proteins and their metastable resting state can be triggered to coalesce by specific lipid–lipid, protein–lipid, and protein–protein interactions.[10,11]

As membranes consist of many components and are very complex systems, several model membrane systems have been developed for studying membrane properties, structure and processes. Model membrane systems permit the study of membrane components and processes at the molecular level through quantitative methods such as scanning probe microscopy (SPM) techniques that are not generally applicable to natural cellular membranes. Applications of model membranes range from the study of structure and function of membrane proteins to drug discovery and delivery research. Many biochemical processes in cells occur inside or on the surface of the membrane; thus many drugs, ~60% of those in the marketplace, target membrane proteins.[12,13] Due to the difficulties of studying membrane proteins in the complex cellular environment, model membranes have been developed as drug screening tools for the study of specific integral membrane proteins. However, although model membranes can aid in developing therapeutics that target membrane proteins involved in various diseases, one must be careful not

to oversimplify the model system. A realistic model system must always be chosen in order to obtain conclusions that are relevant to the problem being studied. Over the last 50 years several lipid model membrane systems have been developed for the study of membrane related processes. These include black lipid membranes, vesicles and supported lipid membranes.

Black lipid membranes or free standing lipid membranes are lipid bilayers formed over a small 1 millimeter aperture (Figure 1.2). As a result, both leaflets of the black lipid membrane are easily available for investigation. After the creation of the lipid bilayer over the small aperture, the bilayer appears to be black in colour as a result of destructive interference from reflective light between the two hydrophilic and hydrophobic interfaces. Black lipid membranes were first reported by Mueller in the 1960's.[14] Mueller painted a black lipid membrane by brushing a solution of phospholipids across a 1 millimeter hole and then proceeded with electrochemical measurements across the membrane. The main drawback with Mueller's model membrane system was that often following the creation of the black lipid membrane small traces of solvent remained amongst the hydrophobic tails of the lipids. This small quantity of solvent was often shown to interfere with the function of sensitive membrane proteins. However, ten years later a solvent free[15] method was developed where two monolayer Langmuir films were used to form a bilayer over the aperture. Since the advent of black lipid membranes, they have been used to investigate various biophysical processes. Black lipid membranes have been used to study the formation and function of membrane pores[16], ion channels[17-20] and proton pumps.[21] However, the main drawback of this model system is the low

mechanical stability of these membranes which in turn lowers their ability for long term use in biosensing.[22]

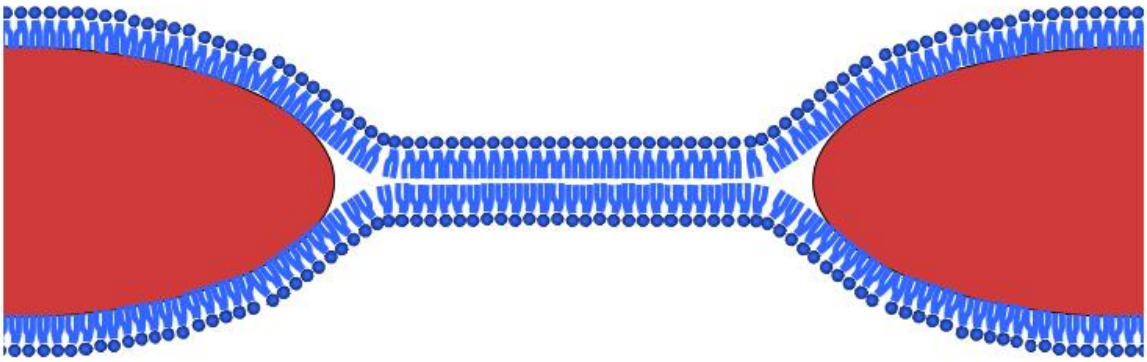

Figure 1.2 Black Lipid Membrane Model System

Lipid vesicles are an alternative model system. Lipid vesicles are bilayer structures where the bilayer terminals are joined together to form a spherical shape (Figure 1.3). Unlike black lipid membranes, vesicles can be tuned to a desired size, with diameters ranging from 20 nm to 100 μm. Due to this large range of sizes, typically vesicles are classified into 3 groups: small unilamellar vesicles (SUV), large unilamellar vesicles (LUV) and giant unilamellar vesicles (GUV). SUVs are vesicles < 100 nm and are used as precursors for supported lipid bilayers. The size of SUVs makes them difficult targets to be visualized for single object fluorescence measurements. LUVs are vesicles ranging from 100 nm – 1 μm and GUVs are vesicles with diameters > 1 μm. As a result, LUVs and GUVs can be viewed by a brightfield microscope. In addition, LUVs and GUVs can be dye labeled and viewed

by fluorescence microscopy. GUVs have been used to measure the lateral diffusion of components[23] or monitor the lipid phase behavior[24] within a membrane. Vesicles have also been used as a model system to study protein-lipid interactions[25] as well as the insertion of membrane proteins.[26] Vesicles can be more stable than black lipid membranes and are frequently stable with respect to aggregation for days to weeks. The major drawback with using vesicles as a model membrane system is that the interior leaflet of the membrane is not accessible. Therefore, although this model system is compatible with fluorescence methods it is not compatible with electrochemical methods.[1]

Figure 1.3 Lipid Vesicle Model System (Adapted from reference 1).[1]

Supported lipid bilayers are a second alternative to black lipid membranes. This model system offers robustness and can be analyzed by a variety of surface sensitive characterization techniques.[1] Supported lipid bilayers have been used to investigate cell adhesion[27] and the function of membrane proteins as well as lipid

phase behavior.[28] McConnell and Tamm first reported this new model system in the early 1980's where they deposited a single lipid bilayer directly onto a solid support (Figure 1.4).[29,30] There are several methods to prepare supported lipid bilayers that will be discussed in a later section. McConnell and Tamm made use of a technique called vesicle fusion[31] in which a quantity of a concentrated suspension of SUVs is deposited onto a surface. Supported lipid bilayers prepared by this technique have been heavily investigated by several characterization techniques such as quartz crystal microbalance (QCM),[32] surface plasmon resonance spectroscopy (SPR)[33] and atomic force microscopy (AFM).[34] The ability of a supported lipid bilayer to be studied by such a wide variety of surface analytical techniques is a major advantage that this model system offers over black lipid membranes and vesicles.

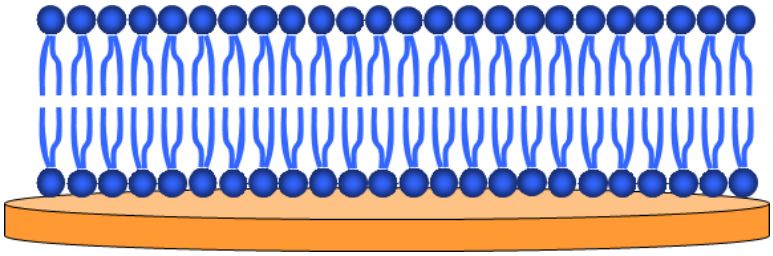

Figure 1.4 Supported Lipid Bilayer Model System

1.2 Solid Supported Bilayers as Models for Cell Membranes

Solid supported bilayers have generated much interest as models for cellular membranes and as platforms for membrane biosensing. They have been commonly

reported to form stable membranes on a small number of hydrophilic surfaces.[1,24,29,35] Solid supported bilayers can form homogenous membranes over large areas. The homogeneity of the membranes has been confirmed through a variety of techniques including fluorescence and AFM.[31,36] In addition, the homogeneity of the membrane is largely dependent on the surface roughness of the underlying support because defects in the support can disrupt the lipid bilayer.[1] Another important trait of supported lipid bilayers is the small water layer that separates the membrane and the solid support. This small lubricating water layer has a thickness of about 1 nm and preserves a lipid fluidity that is comparable to that of natural cell membranes and vesicles.[30,37,38] Peripheral membrane proteins attached to the outer leaflet of the membrane have also been shown to maintain a high degree of fluidity.[39] To summarize, the main advantages of the supported lipid bilayer model system are that it can be prepared over large areas, it possesses a thin lubricating water layer between the membrane and the support and it can be analyzed using a variety of surface-sensitive techniques.

1.2.1 Formation and Characterization of Supported Lipid Membranes

There are several methods to form solid supported lipid membranes. The three major methods described here are deposition by Langmuir Blodgett (LB) transfer, deposition by vesicle fusion (VF) and a hybrid method using a combination of LB and VF. The LB method consists of the formation of a lipid monolayer at the air-water interface in the LB trough, followed by the transfer of the monolayer to the solid support by dipping the support vertically into the LB trough. Transfer of the

initial monolayer forms the bottom leaflet of the membrane. Next, to form the outer leaflet the support coated with the first film is then dipped vertically (Langmuir-Blodgett), or horizontally (Langmuir-Schaeffer) a second time into the trough (Figure 1.5a). This method can be used to create symmetric and asymmetric bilayers by transferring monolayers of different lipid composition. In addition, the LB method allows one to control the pressure on the monolayer at the air-water interface and thus allows for the control of lipid packing. The second method, deposition by VF, is simpler. The process begins by hydrating a lipid film followed by extrusion or sonication to form SUVs. After the vesicles are prepared, they are added to a hydrophilic support such as a clean glass slide or a freshly cleaved mica sheet. The vesicles adsorb and subsequently rupture and spread to form planar membrane patches on the surface. Patches of lipid bilayer then fuse together due to the high lateral mobility of the lipids and form an extended lipid bilayer (Figure 1.5b).[40] The combination hybrid method makes use of both methods, LB and VF. Initially a LB film is transferred to the support to form the inner leaflet of the bilayer. Secondly, VF is used to form the outer leaflet of the bilayer (Figure 1.5c).[41,42] This method can also be used to create symmetric and asymmetric bilayers by using different lipid mixtures for the LB and VF steps.

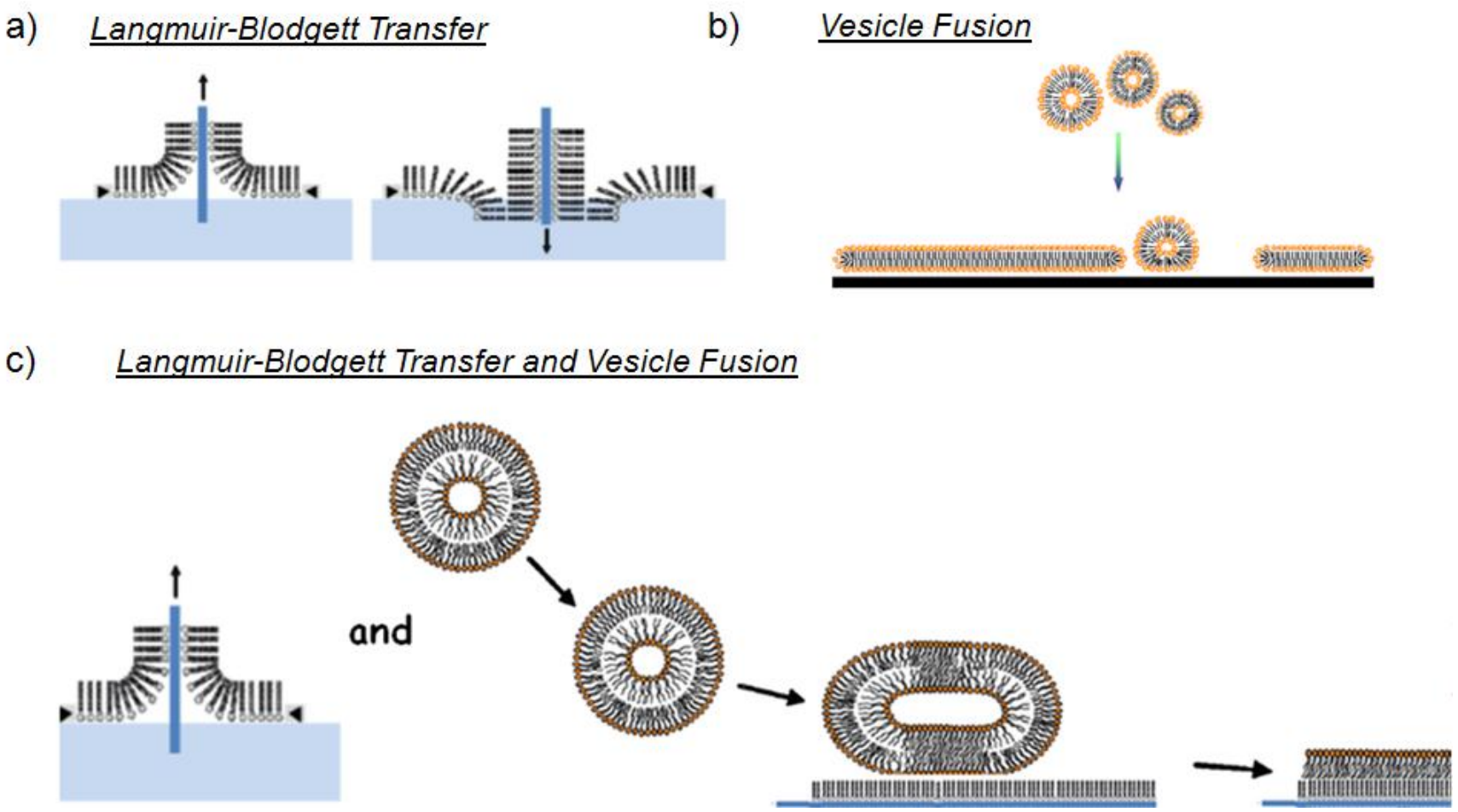

Figure 1.5 Methods to form a supported lipid bilayer model system. a) Langmuir Blodgett deposition (LB), b) Vesicle fusion deposition (VF), c) Combination of LB and VF

In this study two major characterization techniques were used to analyze supported lipid bilayers: i) fluorescence microscopy and ii) AFM. Fluorescence microscopy can be subdivided into a variety of methods such as: epi-fluorescence, confocal and total internal reflection fluorescence (TIRF) microscopy. Epi-fluorescence microscopy is the simplest variation of fluorescence microscopy. In this method, the entire sample is subjected to an intense illumination through an objective from an excitation source. The fluorescence emitted from the sample is then focused to the detector by the same objective that was used for excitation. Filters between the objective and the detector eliminate the excitation light from fluorescent light which results in a fluorescence image. The lateral resolution of the epi-fluorescence microscopy performed in this study was ~250 nm. Confocal microscopy, a more complex method, offers advantages over conventional epi-fluorescence microscopy such as a shallow depth of field, elimination of the out-of-focus glare and the ability to image optical cross-sections of thick samples. The fundamental principle of this method is the utilization of spatial filtering techniques to reduce out-of-focus light in samples whose thickness is larger than the immediate plane of focus. Illumination of the sample is performed by a laser beam through a pinhole aperture. The laser beam is situated in a conjugate plane with a scanning point on the sample. The resulting fluorescence emitted from the sample is then collected through a second pinhole aperture by a detector. The pinholes significantly reduce the amount of out-of-focus fluorescence emission.[43]

TIRF is a technique that applies an induced evanescent wave to selectively excite fluorophores in a thin sample region adjacent to the substrate-sample

interface (Figure 6a). The refractive index differences between the substrate and the water phase regulate the transmission/reflection of light at the interface as a function of incident angle. This refractive behavior is controlled by Snell's law:

$$(n_1)(\sin\theta_1) = (n_2)(\sin\theta_2) \qquad (1)$$

where n_1 is the higher and n_2 is the lower refractive index, respectively. The incident beam angle with respect to the normal to the interface is represented by θ_1. The refracted beam angle within the lower refractive index medium is represented by θ_2. The critical angle θ_c is where light hits the interface of two mediums at a high angle and the refraction direction becomes parallel to the interface. TIRF is achieved at the θ_c for light travelling from a medium with a higher refractive index to a medium with a lower refractive index.[43] The evanescent wave created at the interface of the two mediums can be regarded as an emerging oscillation from the solid medium and travelling some distance into the liquid medium before reentering the solid one (Figure 1.6b). As a result, TIRF is a method that offers a greater sensitivity measurement for fluorophores lying close to or on the surface.[44,45] The evanescent wave intensity decays exponentially according to the equation:

$$I_{(\perp Interface)} = I_{(Interface)}e^{(d(Interface)/d)} \qquad (2)$$

where $I_{(\perp Interface)}$ and $I_{(Interface)}$ represent the intensity at a perpendicular distance, $d_{(Interface)}$, from the interface and the intensity at the interface, respectively. The penetration depth is represented by d. The penetration depth at a specific wavelength λ is then given by:

$$d = \lambda/4\pi((n_1)^2\sin^2(-(n_2)^2))^{-1/2} \qquad (3)$$

The penetration depth usually ranges between 30 and 300 nm. The value is dependent upon the refractive indices of the different media and the reflection angle.[46] The number of biological investigations using TIRF is currently increasing. This technique can be implemented on standard epi-fluorescence microscopes and can be used simultaneously to compare images from different observation methods. For example, an area of a sample can be imaged by epi-fluorescence and then the same area can be immediately imaged again using TIRF. Finally, this method effectively enables investigators to localize fluorescence emission to specific regions within cells, membranes or complex biological structures that are close to the substrate-sample interface.[43,46]

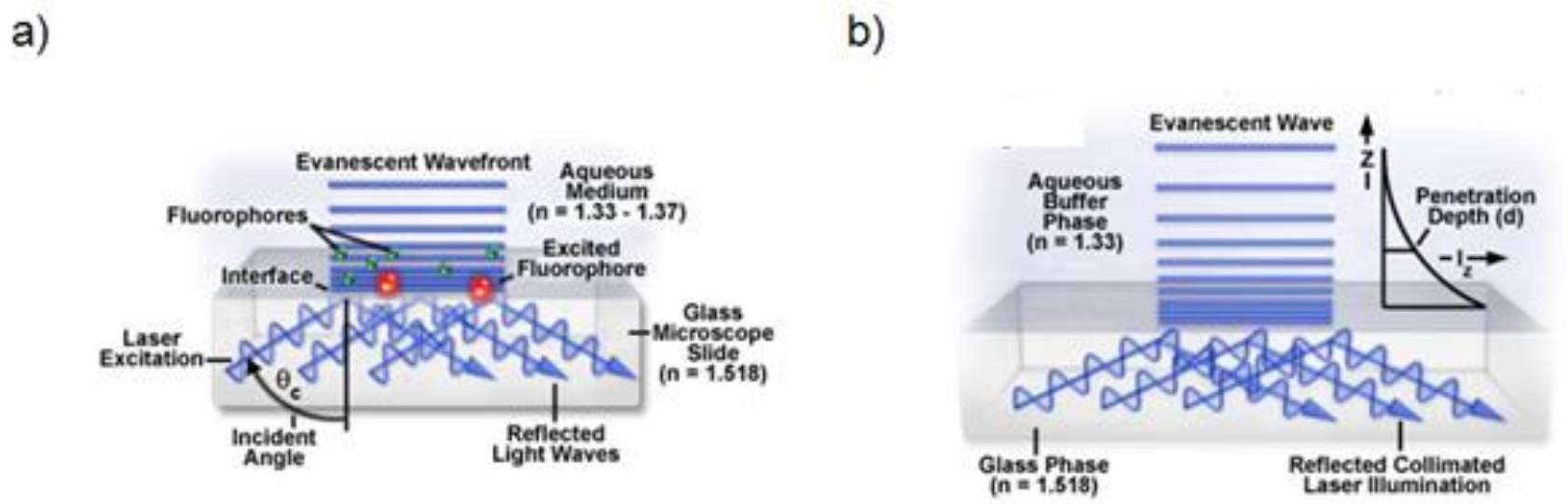

Figure 1.6 Total Internal Reflection Microscopy (TIRF) schematic showing an a) Evanescent wave that excites fluorophores at the interface and b) the penetration depth (Adapted from reference 46).[46]

Fluorescence recovery after photobleaching (FRAP) is a method based on the principle of photobleaching an area of a fluorescent sample and then monitoring the recovery of fluorescence due to the movement of fluorophores back into the bleached area.[47] As a result, FRAP can be used to measure the lateral diffusion of fluorescent dye linked to lipids in a bilayer. The lateral diffusion measurement can be used to confirm the fluidity and homogeneity of the lipid bilayer.[41] FRAP experiments involving lipid bilayers consist of collecting several fluorescence intensity measurements of a small area of bilayer before and after photobleaching (Figure 1.7). The recovery of fluorescence in the bleached area is plotted as a recovery curve and fit to determine a lipid diffusion coefficient and a mobile lipid fraction. A number of procedures have been developed to extract a two-dimensional diffusion coefficient from fluorescence recovery curves.[48] In this study, the two-dimensional diffusion equation described by Soumpasis[49] was used to fit the fluorescence recovery data since it had been previously used to fit recovery data for supported DOPC bilayers.[50] The equation is:

$$f(t) = e^{-2\tau_D t}[I_0(2_{\tau D}/t) + I_1(2_{\tau D}/t)] \qquad (4)$$

where I_0 and I_1 are modified Bessel functions, $\tau_D = r^2/4D$ is the characteristic diffusion time and r is the radius at half-height of the bleached area at t=0. As a result, a steep curve indicates a fast recovery revealing high molecular mobility. The mobile lipid fraction is determined by a percent recovery formula:

$$\% = (Y/X)(100) \qquad (5)$$

where Y is the increase in fluorescence intensity due to recovery and X is the decrease in fluorescence intensity due to photobleaching (Figure 1.7). Finally, FRAP is not limited to lipids it can also be utilized to determine a protein diffusion coefficient and mobile fraction.

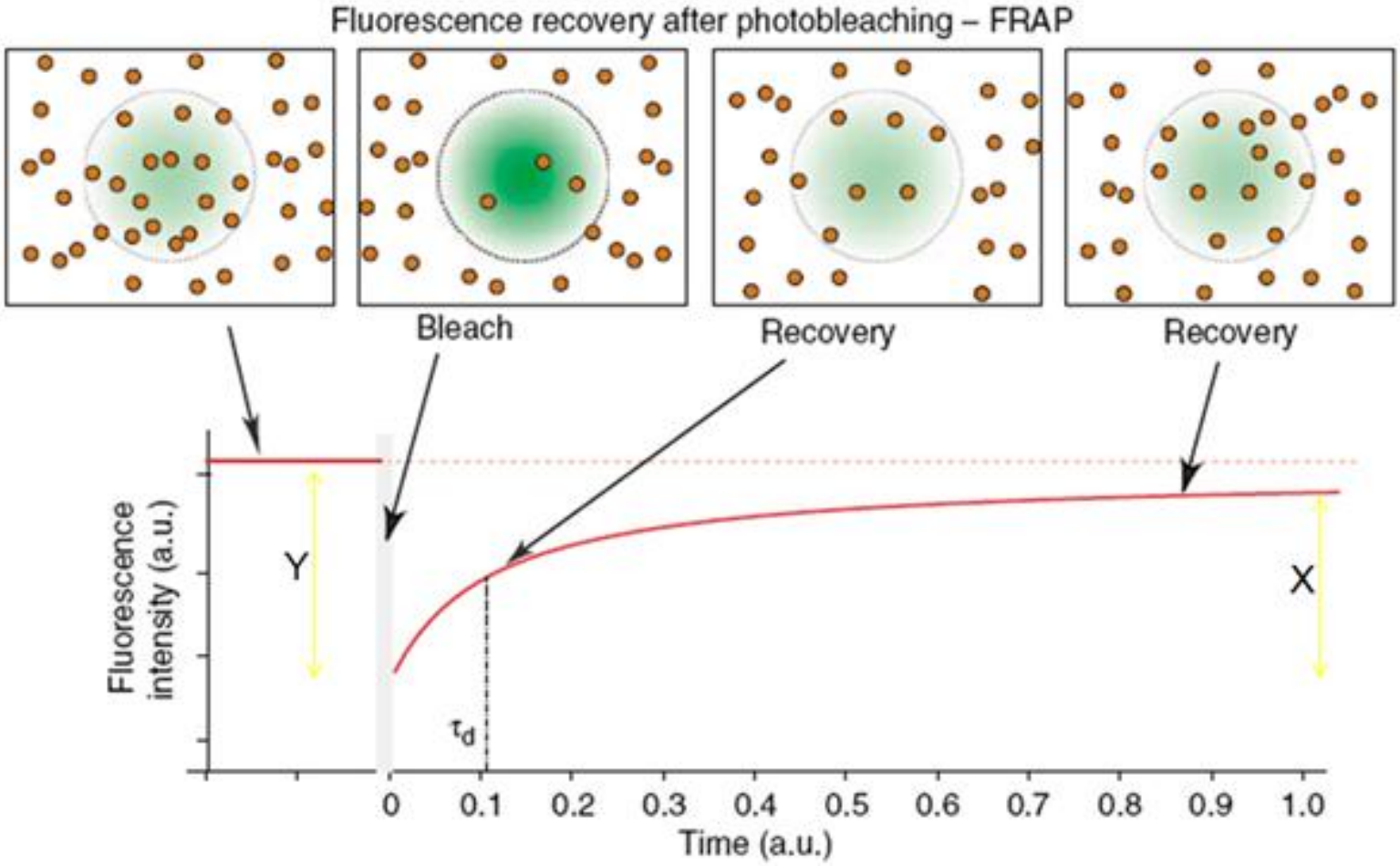

Figure 1.7 Schematic of the Fluorescence Recovery After Photobleaching (FRAP) technique (Adapted from reference 51).[51]

AFM is one of the most versatile methods of imaging nanoscale structures.[52] AFM characterization is used as a complementary method to fluorescence microscopy to observe supported lipid bilayers on the nanoscale. AFM is a high resolution measurement method that characterizes a sample by bringing a sharp probe attached to the end of a flexible cantilever in close proximity to the sample surface and raster scanning across it. The tip of the probe is affected by the forces from the surface of the sample. The forces from the surface of the sample cause a deflection of the cantilever on which the tip resides and the deflection is detected (Figure 1.8). The method of detection used to detect this deflection is called the optical lever, where a laser beam is bounced off the back of the cantilever and back onto a split photo detector.[53] Photo detectors possess four quadrants which permit the detection of both longitudinal bending modes and lateral torsional modes of the cantilever. The tip-sample interaction force can then be controlled by monitoring the deflection in the cantilever. This technique provides three dimensional molecular resolution without additional contrast agents such as fluorescent probes. AFM is commonly used to confirm the uniformity of a supported lipid bilayer through topography measurements of the membrane. Drawbacks of this technique include lack of chemical specificity and the requirement to immobilize the sample on a substrate with low surface roughness. Flat surfaces are required or small changes in sample height will be overshadowed by the roughness of the substrate.[34,54]

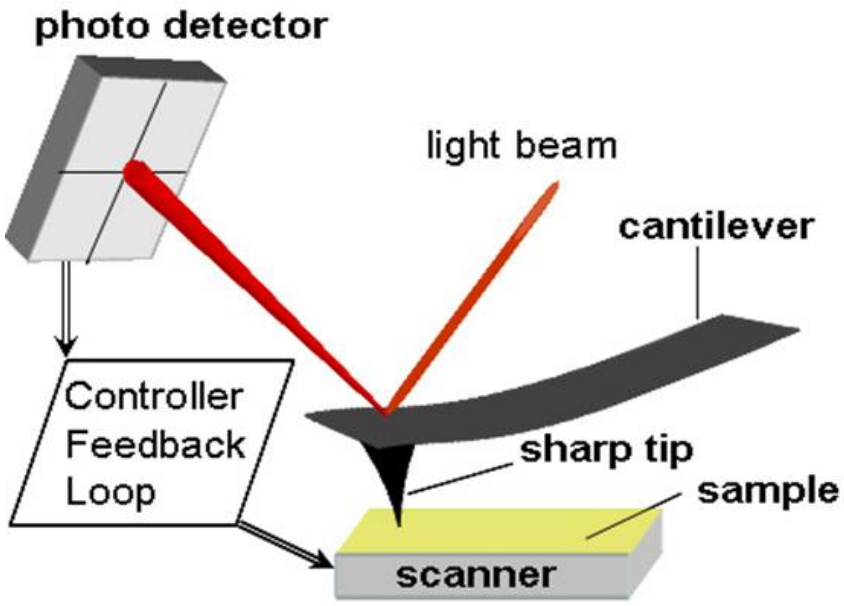

Figure 1.8 Schematic of the Atomic Force Microscopy (AFM) technique (Adapted from reference 55).[55]

AFM can be performed in two modes: contact mode and dynamic mode. Contact mode is the simplest mode where the tip is dragged over the surface of the sample and remains in contact with it over the course of the entire scan. The drawback with this method is that the lateral force exerted on the sample can be quite high. As a result, this force can damage or displace sections of soft samples. Dynamic mode AFM, sometimes called tapping mode AFM, solves this issue by oscillating the cantilever during imaging. High lateral forces are avoided by having the tip contact the surface for only a short time. There are many different methods of dynamic mode AFM. This study was used MAC Mode which uses a magnetically coated cantilever that is driven by an oscillating magnetic field. The magnetic field is applied to the cantilever from a magnetic plate that sits below the sample cell. MAC mode reduces false responses that can be generated by the cantilever holding

mechanism, the surrounding medium or from the sample. The cantilever can then be operated at much smaller amplitudes since there is less system noise. MAC mode AFM is a method that produces detailed images without damaging soft samples.[55]

Other commonly used techniques to analyze supported lipid bilayers that were not used in this study are: electrical impedance spectroscopy (EIS), secondary ion mass spectroscopy (SIMS), QCM-D, SPR and ellipsometry. EIS is a method that produces information about the permeability of the supported bilayer by measuring its resistance and capacitance. This technique is a non-invasive and label free technique that can be used to study ion transport through supported lipid bilayers. The impedance is measured by applying an alternating current potential to an electrochemical cell and monitoring the current through the bilayer. The data can then be plotted and analyzed to extract kinetic information. The only drawback is that this method is limited to the use of conductive surfaces such as gold.[56,57] SIMS is a method that can directly image the lateral distributions of specific membrane components.[58,59] SIMS makes use of a primary ion source focused on a supported lipid bilayer to produce secondary ion fragments. The collection time of the secondary ion fragments to the detector produces an image of the bilayer. SIMS has been used to characterize unlabeled lipid membranes composed of multiple lipid components such as, phosphatidylcholines, sphingomyelin and cholesterol.[60] Distributions of the characteristic secondary ions revealed that these membranes possessed domains enriched with sphingomyelin and cholesterol but deficient in monopolar lipid.[61] QCM-D is a method used to monitor the formation of

a supported lipid bilayer in real time by measuring changes in both resonance frequency and dissipation shift of the oscillator. The microbalance can quantify the amount of material bound to its surface and elucidate the acoustic mass and viscoelastic properties of the deposited bilayer.[54,62-64] SPR can also monitor the formation of bilayers with the use of an electromagnetic evanescent wave. Light is directed through a sample to a thin layer of gold that lies on the border of the support. Surface plasmons are generated at the surface of the gold when the incident light reaches a critical angle. The plasmons absorb the light causing a decrease in the intensity of the reflected light.[54,64-66] The critical angle is dependent upon the refractive index within a small distance or on the substrate's surface. The refractive index is changed when molecules bind to the surface, making it possible to monitor the formation of a lipid bilayer on a substrate. Lastly, ellipsometry can be used to characterize bilayer thickness and heterogeneity. Ellipsometry measures the reflectivity difference of a laser beam on a substrate surface. The changes in reflectivity allow this technique to measure the kinetics of bilayer formation, structure and swelling.[64,67]

1.2.2 Limitations of Supported Lipid Membranes

Solid supported lipid bilayers are widely used as model membranes due to their ease of formation and characterization. Although solid supported membranes are more stable than black lipid membranes, they are not stable to dehydration, to storage over extended periods of time, or to harsh conditions such as high temperature, high pressure, and mechanical stress.[68] This is a major drawback for

biosensing applications. Furthermore, supported lipid membranes have restricted compatibility with the incorporation of integral membrane proteins. The limited space between the lower membrane leaflet and the solid support can interfere with large external domains of integral membrane proteins causing denaturation (Figure 1.9).[30] The spacing could also cause the adsorption of the protein domains to the solid support resulting in the immobilization of the protein. Immobilization of a protein prevents its diffusion and makes the formation of multi-protein complexes difficult.[69] In addition, the limited spacing of supported lipid bilayers does not allow the bulk transport of water, ions and solutes across the membrane,[41,70] making this model system incompatible with separation applications.[70] Supported lipid membranes are also limited by the choice of substrate. In order to obtain a high quality membrane with few membrane defects and high lipid mobility the surface of the support should be hydrophilic, smooth, and clean.[38] There is only a small number of solid supports commonly used for biomimetic membranes including silica,[71-73] mica,[74,75] silicon nitride,[76] and gold.[77] In addition, supports that consist of transition metals have also been used such as titanium oxide,[78] indium-tin oxide,[79] silver[80] and platinum.[80] Lastly, solid-supported membranes are constrained by the fact that access to only one side of the membrane is possible.

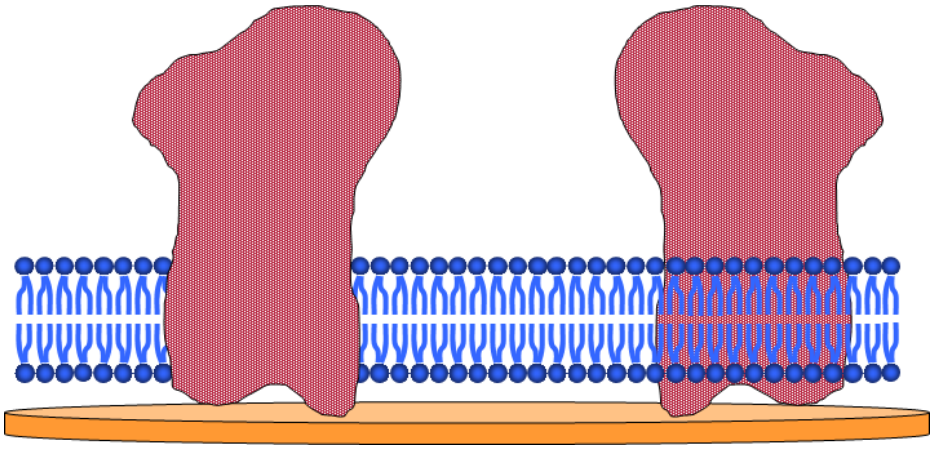

Figure 1.9 Supported Lipid Bilayer Model System with an Integral Membrane Protein

1.3 Bolaamphiphiles for Supported Lipid Bilayers

The problem of bilayer stability with respect to dehydration and harsh conditions can be addressed by modifying the lipid structure. One approach is to use bolaamphiphiles, also known as bolalipids. Bolalipids have two polar headgroups connected covalently by one or more transmembrane spanning alkyl chains[81] (Figure 1.10). The name "bola" was used due to the similarity of this lipid shape with an ancestral missile weapon named bola that is composed of two weights attached at both ends of a rope.[82] Bolalipids were originally extracted from Archaea. These unicellular organisms contain a large fraction of bolalipids, which enable them to survive in a severe environment. For example bolalipids permit these organisms to survive in high temperatures, high salt concentrations, acidic pH and anaerobic conditions. Bolalipids possess two key features that provide them enhanced chemical and physical stability. Firstly, bolalipids have one or more transmembrane spanning chains which counter delamination of the membrane

when under a physical stress. Secondly, most bolalipids consist of an ether-linkage between the head group and the alkyl chain as opposed to an ester-link. Unlike most bacteria and eukaryotes, this ether-link between the carbon chains and the glycerol backbone makes the bolalipid more hydrolysis-resistant.[81] These strengths of bolalipids have been exploited to develop planar supported membrane,[83-85] to reconstitute and study integral membrane proteins,[86-89] as gene and vaccine delivery vehicles,[90-92] and as molecular fossils.[93]

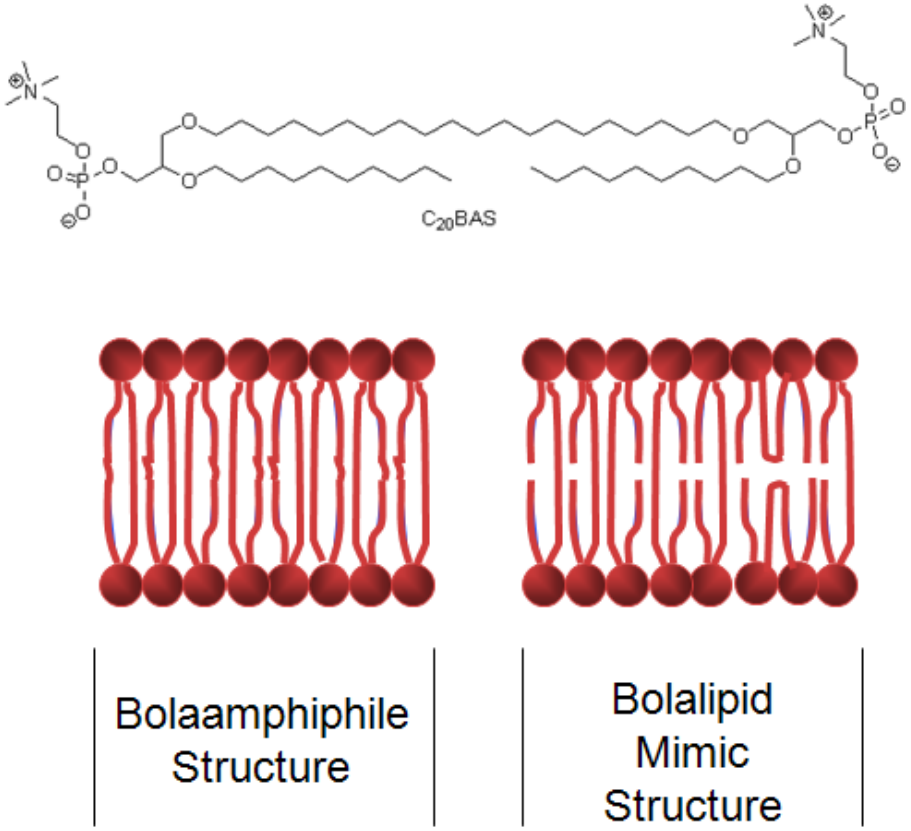

Figure 1.10 Structure of Bolaamphiphiles

Physical stresses to test the permeability and the resistance to increased temperatures have been performed on bolalipid membranes.[94-96] In fact bolalipid membranes are extremely impermeable to the addition of other molecules and ions. It was shown that dye labeled bolalipid vesicles heated to high temperatures released a significantly lower amount of dye in contrast to dye labeled vesicles made from monopolar lipids such as POPC and DPhPC. Bolalipid vesicles maintained their impermeability when heated to 100 °C however, monopolar lipid vesicles did not maintain their membrane impermeability above 50 °C.[94] Bolalipids were designed to survive during extreme conditions such as at very high temperatures. However, at lower temperatures bolalipids membranes have shown reduced lateral mobility, as much as an order of magnitude less than monopolar lipids.[87,97,98] The reduced lateral mobility was attributed to their unique structures.

Biomembrane studies require a large amount of lipid material. Purification of naturally occurring bolalipids from archaea is very costly. In addition, separation of an individual bolalipid from a bulk lipid extract matrix is very difficult. Synthetic routes to achieve these bolalipids have also been found to be very costly. As a result, a bolalipid mimic, C_{20}BAS, was designed and synthesized by the Thompson group (Figure 1.10).[69,70,90,99-104] C_{20}BAS consisted of two polar headgroups connected covalently by one transmembrane spanning alkyl chain. Factors such as conformational flexibility, lateral fluidity, membrane thickness and ease of use were considered in order to select the appropriate structure to synthesize C_{20}BAS.[87,102] The Thompson group has previously shown that C_{20}BAS has the ability to form stable membrane vesicles.[105] In addition, area-pressure isotherm experiments

confirmed that C_{20}BAS possessed all of the structural features necessary to provide the unique bolalipid properties. One other example of bisphosphocholine bolalipid mimics has been reported in the literature. The Vogel group developed bolalipid mimics consisting of phosphatidylcholine lipids cross-linked by thiol group. Supported lipid bilayers were formed by the LB technique where mixtures of DMPC/bolalipid were transferred to glass. The resulting bolalipid bilayers incorporating 25, 75 and 100 mol% bolalipid mimic were found to be stable and possess no measurable lateral diffusion.[100]

1.3.1 C_{20}BAS: Phosphocholine Lipid Mixed Membranes

C_{20}BAS lipids were found to form stable membranes existing in fluid liquid-crystalline phases at ambient temperatures. In addition, C_{20}BAS lipids displayed significant lateral mobility unlike typical bolalipids found in nature.[97] C_{20}BAS membranes have also been shown by a ^{2}H NMR study to be highly ordered.[106] However, this bolalipid mimic has the ability to exist in two conformers in the membrane. The major conformation is postulated to be a transmembrane conformer with the two polar headgroups on opposite leaflets of the membrane. The minor conformation is a U-shaped conformer with the headgroups in the same leaflet (Figure 1.11). Despite this flexibility in the C_{20}BAS structure, experimental and theoretical evidence has found that the bolalipid membranes are predominately composed of transmembrane conformers.[106-110]

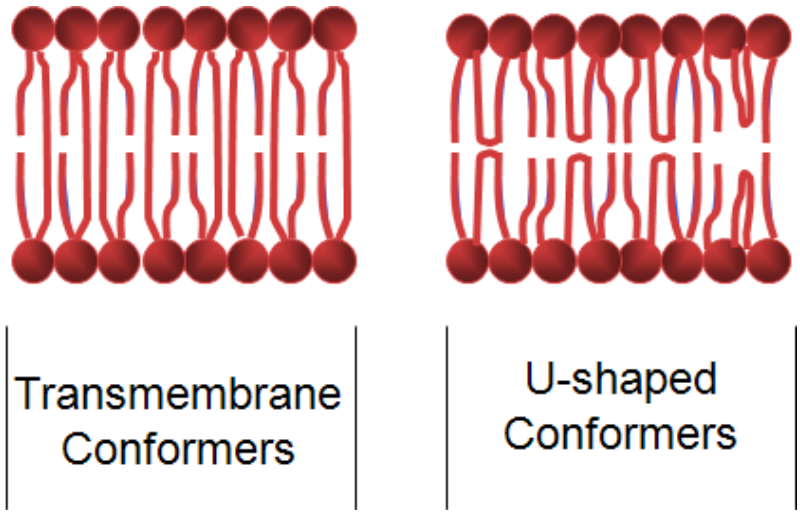

Figure 1.11 Bolalipid Mimic Structures: Transmembrane versus U-shaped Conformers

Membrane permeability is higher for mixtures of bolalipids and monopolar lipids than for pure bolalipid membranes.[111] The lateral mobility of a mixed monopolar lipid DMPC bilayer with small quantities of bolalipids (molar ratios $\leq$ 25%) was shown to be similar to that of a pure DMPC bilayer.[100] In another study, the Thompson group reconstituted the transmembrane protein, Ste14p, in membranes prepared from C_{20}BAS and monopolar lipid mixtures. Functional assay experiments for Ste14p in these mixed membranes demonstrated that bolalipid mimics may form heterogeneous membranes with monopolar lipids.[87] Molecular mean field theory was utilized by Longo to probe the possibility of phase separation of a lipid bilayer composed of a lipid mixture of C_{20}BAS and a monopolar lipid. This study suggested that phase separation between the two types of lipids would occur based on the hydrophobic mismatch induced by the significant differences in their membrane thicknesses (Figure 1.12).[109] For example, the theory predicted that the

bolalipid mimic C_{20}BAS when mixed with the monopolar lipid POPC would form two phases. One domain would consist of transmembrane C_{20}BAS with a small quantity of POPC, and the second domain would consist of POPC with a small amount of U-shaped C_{20}BAS. It is important to understand the behavior of mixed C_{20}BAS/monopolar lipid membranes for applications of these lipid mixtures for biosensing. In addition, C_{20}BAS mixtures offer a useful tool in terms of flexibility and stability for the design of new membrane-based biotechnologies.

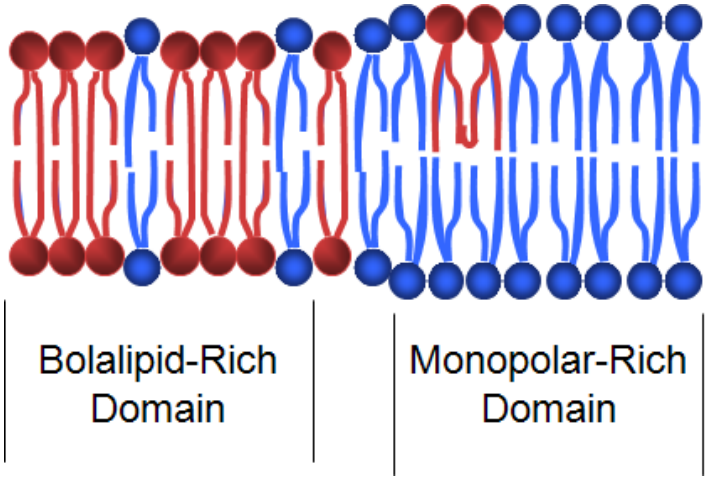

Figure 1.12 Phase Separated Bolalipid Mimic: Monopolar Lipid Mixture

1.4 Polymer Supported Bilayers as Models for Cell Membranes

A major drawback of supported lipid bilayers is the small thickness of the water layer between the membrane and the support. As a result, integral membrane proteins with large extracellular or intracellular domains come into contact with the hard solid substrate and this may lead to frictional coupling

between the protein and the support.[112] This may cause a decrease in lateral mobility or even prevent free diffusion of the protein in the supported lipid bilayer. In addition, the interaction of protein domains with the surface may lead to protein denaturation. One possible solution utilized to tackle the issue of protein domains contacting the solid support is to decouple the membrane from the support by a polymer cushion. The addition of a polymer cushion layer to a supported membrane system still offers a solid support for the membrane but reduces the risk of protein denaturation.[112,113] However, in order for the polymer cushion to mimic the extracellular matrix, an appropriate polymer that remains thermodynamically and mechanically stable must be selected. The polymer supported membrane will only be stable if there is complete wetting between the two interfaces (surface/polymer and polymer/membrane).[112] In addition, the polymer cushion must act as a water reservoir which should improve the self-healing properties of local defects in the membrane.[112]

Many polymer cushions have been studied and developed (Table 1.1). There are four methods to prepare a stable polymer cushioned supported bilayer: i) the deposition of a soft polymer layer, bound to the support by electrostatic forces, followed by the subsequent deposition of a bilayer, ii) the use of reconstituted lipopolymers, lipids with polymers coupled to their head group, to separate the bilayer from the support, iii) the chemical grafting of a polymer film to the solid support followed by subsequent deposition of a lipid bilayer and iv) a combination of ii and iii where the polymer is grafted to both the surface and the membrane. The polymer support should be hydrophilic, weakly charged, soft and not extensively

cross-linked in order to facilitate successful bilayer formation.[1] Most polymer supports have been constructed to thicknesses ranging from 1 to 10 nm. However, some studies have made use of much larger thicknesses ranging 30 to 80 nm. Renner[114] explains that a spacing of only 5 nm between the membrane and the support limits significantly the effect of a polymer cushion on sterically demanding transmembrane proteins. Other important factors that must be considered to evaluate the usefulness of a polymer cushion system are membrane homogeneity, lipid diffusion and mobile lipid fraction. The majority of lipid diffusion coefficient values of lipid bilayers on polymer supports have ranged from 0.5 to 3.5 $\mu m^2/s$. Diffusion coefficients in the literature for fluid-phase supported bilayers on glass without a polymer cushion range from 1-6 $\mu m^2/s$.[16] Therefore, most polymer supports have produced lipid bilayers with slower lipid diffusion. A couple of examples reported lipid diffusion coefficient values greater than 3.5 $\mu m^2/s$. In fact, Naumann[115] reported that a DMPC bilayer cross-linked to a DODA-E_{85} polymer cushion showed a lipid diffusion coefficient of 17.7 $\mu m^2/s$ which is similar to that of lipid vesicles. Some polymer cushioned systems have incorporated an integral membrane protein and this will be covered in a later section. Lastly, a wide variety of characterization methods have been used to analyze and evaluate these polymer cushioned systems.

Table 1.1 Polymer cushioned supported lipid bilayers

i) Polymer cushion without attachment to the substrate or the lipid bilayer.							
Support	Polymer	Thickness (nm)	Lipid Bilayer	Diffusion Coefficient ($\mu m^2/s$)	Characterization Method	Other Notes	Reference
Gold	PPy(DBS)		DPhPC		EIS, CV		116
Gold	MUA-PDDA	1-4	SOPS:POPC	1-2	Fluorescence, FRAP, SPR	SPR suggested that the membrane fusion protein formed a mixture with the bilayer.	117
Gold	MUA-PDDA-PSS	0.5-2.0	SOPS:POPC	1.2-2.1	Fluorescence, FRAP, SPR		118
Quartz	PEI	4-18	DMPC		Neutron Reflectometry	Thickness of the polymer was dependent on the addition method.	119-121
Glass	PLL-PEG-QAC		Egg-PC:DOPE (65:35), POPC:POPA (98:2)&(70:30), POPC:POPG (80:20), DOPC:DOPE: SM:CH (35:30:15:20)	10	Fluorescence, FRAP, QCM-D	Lipid diffusion was for DOPC: DOPE:SM:CH (35:30:15:20)	122
Glass	Cholesteryl-PEG		Egg-PC	1.3	Fluorescence, FRAP		123
Glass	Cellulose	4.9	SOPC	2	Neutron		124

					Reflectometry, DLS, Fluorescence, FRAP, Cryo TEM, AFM		
Glass	Cellulose		DMPC	3.3	Fluorescence, FRAP, RCIM		125
Silicon	Agarose, Chitosan		DMPC	0.6-1.6	Fluorescence, FRAP, RICM		126
Silicon	PEI-PSS/PAH	31.4	DMPC		Neutron Reflectometry		127
Silica Particle	PSS/PAH		POPC,POPS, POPS:POPC (1:1)(1:3)(3:1)	0.001-0.4	Fluorescence, FRAP, AFM, TEM, QCM-D, FTIR, Flow Cytometry		128
Silica Particle	PSS/PAH		POPC:POPS (1:1)		NMR, Fluorescence, FLIM		129
ii) Polymer cushion attached to the lipid bilayer.							
Support	Polymer	Thickness (nm)	Lipid Bilayer	Diffusion Coefficient ($\mu m^2/s$)	Characterization Method	Other Notes	Reference
Gold	DPTL	4.7	DPhPC		EIS, SPR, AFM, DSC		83,130
Gold	S-layer protein-DPPE, S-layer protein-PEG-DSPE	4-8	DPhPC, DOPC		QCM-D, EIS, Neutron Reflectometry		131

Mica	Acrylamide-DMPE-sulfide	1.5	DMPC		AFM		132,133
Glass	DSPE-PEG2K-CF	2.7-3.0	DOPC	2.6-6.6	PER, Fluorescence, FRAP	Diffusion increased as the concentration of lipopolymer decreased.	134
Glass	DSPE-PEG-PDP	3.1-6.5	Egg-PC	2	FRAP, Fluorescence, Ellipsometry, Contact angle, Fluorimetry, SPR	Thickness was dependent on the concentration of PEG.	135
Glass, Quartz	Et_3Osi-PEG-DMPE (DPS)	4.8	POPC:POPG (9:1), POPC:Chol (4:1), bPC:bSM/Chol (2:2:1)&(1:1:1)	0.9-1.4, 0.0-1.0 (Phase separated)	Fluorescence, FRAP, XPS, FLIC, SPT		136-139
Glass	PEG-DOPE		Egg-PC	3-4	Fluorescence, FRAP		140
Glass	Me_3Osi-polyoxazoline-lipid (POX)		SOPC	0.9-1.6	Fluorescence, FRAP		141,142
Glass	PEG-DOPE	7	DPhPC	1.5-2.5	EIS, Fluorescence, FRAP	Peptide diffusion varied from 0-0.02 $\mu m^2/s$ dependent on the bilayer preparation method.	143,144

Glass	BSA-PEG-PE		POPC	0.3-3.5	Fluorescence, FRAP		145
Silicon, glass	PEG-PE	3-5	POPC	1.1-2.6	Fluorescence, FRAP, QCM-D, AFM (Force)		146
Silicon	PEG-PE		DPhPC		EIS		147
iii) Polymer support attached to the substrate.							
Support	Polymer	Thickness (nm)	Lipid Bilayer	Diffusion Coefficient ($\mu m^2/s$)	Characterization Method	Other Notes	Reference
Glass	POMA, PPMA, PEMA	4-60	PC:PS:PE:Chol (5:2:1:2)	0.2-2.5	Fluorescence, FRAP, FCS, QCM-D	Diffusion was increased at lower pH.	114,148
Glass	NHS-PEG-biotin-avidin		DOPC	6.6-8.0	Fluorescence, SMFM		149
Glass	Polyacrylamide brushes	5-10	POPC	1.2-2.0	Fluoresecence, FRAP, SMFM, FTIR		150
Silicon, glass	Dextran	60-80	DMPC	2.8	RCIM, Ellipsometry, Fluorescence, FRAP, Contact angle		151,115
iv) Polymer support attached to both the substrate and the lipid bilayer.							
Support	Polymer	Thickness (nm)	Lipid Bilayer	Diffusion Coefficient ($\mu m^2/s$)	Characterization Method	Other Notes	Reference
Glass	DODA-E_{85}, DODA-E_{85}	5-10	DMPC, SOPC (Chol)	1.1-17.7	Fluorescence, FRAP, AFM, SMFM	D (at 40°C) corresponds to different tethering lipopolymer	115,152-154

						densities. In SOPC bilayers cholesterol was shown to relieve lipid pinning.	
Glass, Aluminum oxide	Streptavidin-biotinylated lipid		Egg-PC, Egg-PC+DOPE	1.9-2.5	Fluorescence, FRAP, AFM		155
Glass, Quartz	Et_3OSi-PEG-DMPE (DPS)	4.8	POPC:POPG (9:1)	0.5-0.9	Fluorescence, FRAP, XPS		136
Glass	AHAPS-PEG-DSPE	1-9	DOPC, DOPC:DOPS (9:1)&(4:1)	3.3	Fluorescence, FRAP, AFM, XPS	Lipid diffusion was for DOPC	156
Glass	Si-PEG-DSPE	5-7	SOPC	3.1	Fluorescence, FRAP, XPS		157
Glass	Biotin-PEG-DSPE	3-4	POPC:DOPS (85:15)	5.5	Fluorescence, SMFM, AFM		158
Glass	Si-PEOX-PEI		DMPC	0.1	SPR, Fluorescence, FRAP, AFM		159
Silicon	Si-PEG-DSPE	3.5	SOPC	2.2	XPS, Fluorescence, FRAP		160
Gold	DTSP-NTA	1	DPhPC		SPR, EIS, QCM		161
Gold	Phytanyl lipid polymer	1-3	DPG, DPEPC		EIS		162
Gold-Porous Alumina	ADMS-PEG-DSPE	5-15	DMPC:DMPE (80:20)	4	CV, SANS		163

1.4.1 Polyelectrolytes as Floating Polymer Supports

Polyelectrolytes are an interesting class of polymer cushions. Polyelectrolytes can be adsorbed from solution onto a number of different substrates such as mica,[120] quartz[119,121] or gold.[117,118] The absorption process occurs by layer-by-layer (lbl) deposition in which a polymer multilayer is constructed by alternating addition of oppositely charged polyelectrolytes (Figure 1.13).[164,165] This technique allows one to control the resulting film thickness by choosing the number of layers deposited. The deposition process is based on the electrostatic interactions of the polyelectrolytes with the support and can be tuned by changes in the ionic strength, molecular weight, concentration, temperature and pH of the polyelectrolyte solutions used. Careful attention must be given to the charge of the outer layer of the film since the surface can adversely affect the function and mobility of membrane constituents and incorporated proteins.[113]

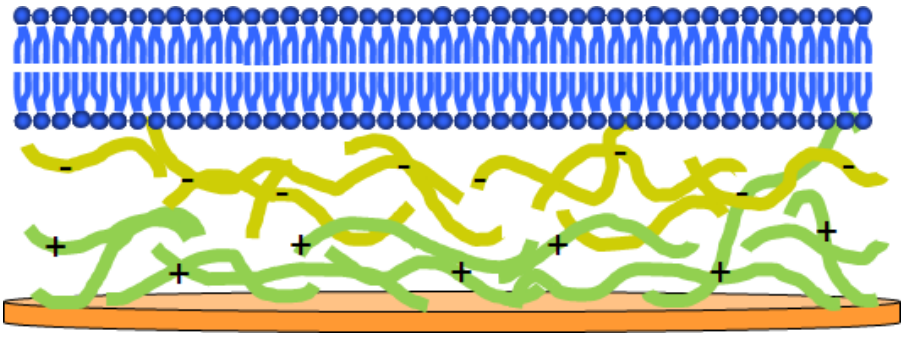

Figure 1.13 Floating Polyelectrolyte Supported Lipid Membrane

Initial investigations involving polyelectrolyte polymer cushions and supported lipid bilayers made use of alternating layers of polystyrenesulfonate (PSS) and poly(allylamine hydrochloride) (PAH).[127-129] Delajon[127] showed by neutron reflectivity measurements that a 5 nm DMPC lipid layer was formed on a 6 layer PSS/PAH polymer cushion. In addition, it was reported that when the outer layer of the multilayer was PAH the sample displayed a higher roughness of ~3 nm making it difficult to assess the thickness of the DMPC layer. Bunge[129] reported NMR and fluorescence data consistent with homogenous coverage of a POPS:POPC lipid bilayer on a 7 layer PSS/PAH polymer cushion. However, results of a Mn^{2+} quenching experiment gave contrasting findings, indicating that there were significant defects in the membrane.

Charged polysaccharides are also well known polyelectrolytes that have potential to be used as a polymer cushion.[164,165] Polysaccharides offer the advantages of biocompatibility, ready availability, and low cost over other synthetic polymers. In addition charged polysaccharides have been used in many biomimetic applications such as drug delivery vehicles based on lipid-polyelectrolyte particles, biocompatible surfaces for controlling cell growth, and tissue biomimetics, making them attractive targets as polymer cushions.[165-170] Polysaccharide-lipid interactions have been exploited for drug delivery applications, however, polysaccharide multilayers have yet to be used as supports for lipid bilayers. A biocompatible polysaccharide multilayer would extend the utility of polyelectrolyte polymer cushions as possible substrates for supported membranes for biosensing applications.

1.4.2 Tethered Polymer Supports

Another promising approach that effectively increases the distance between the support and membrane is the introduction of tethered polymer cushions.[138,144,171] The lipid bilayer can be tethered by attaching the polymer to the membrane, the substrate or both the membrane and the substrate (Figure 1.14). The structures of the polymer tethers are mainly determined by their length and chemistry and by their grafting density on the surface. The tethers are usually chemically bonded via thiol- or silane chemistry onto Au and SiO_2 surfaces, respectively.

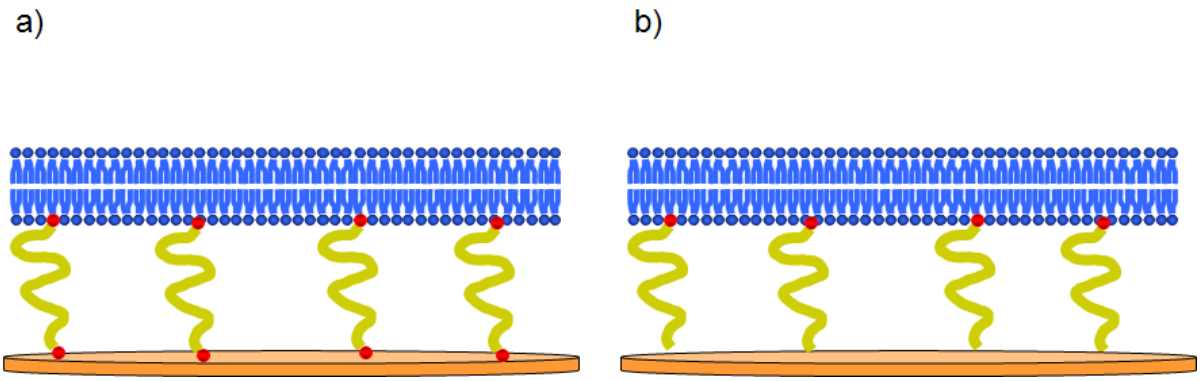

Figure 1.14 Tethered Supported Lipid Membrane. Tether attached to a) both solid support and the lipid membrane b) only the lipid membrane

Membrane stabilization through a photocross-linking reaction between a benzophenone silane-functionalized glass substrate and a dioctadecylamine anchored lipopolymer, DODA, was reported by Naumann.[115,152-154] In these examples, DMPC bilayers were formed on 5-10 nm thick DODA polymer cushions.

Lipid mobilities were dependent on the polymer concentration. The lowest polymer concentration of 5 mol% saw lipid mobilities similar to those of lipids in vesicles. The major advantage of this approach was the fact that the stability of the polymer cushion did not rely on electrostatic interactions. As a result, it was suggested that the system would be inert to changes in ionic strength or pH making it an excellent candidate for the incorporation of a broad variety of different integral membrane proteins.

Polyethylene glycol (PEG) is another excellent candidate for use as a tethered polymer support for supported membranes. PEG is commercially available and is the most widely used polymer support for lipid bilayers. It is a water soluble polymer that is biocompatible, used in many medical devices and drug delivery vehicles and has been shown to prevent nonspecific adsorption of biomolecules.[172-176] In turn, this aids in the prevention of membrane protein denaturation as well as any loss in protein lateral mobility. The Tamm group pioneered the use of supported lipid membranes on a PEG tether in 2000; in this study the PEG tether was tethered to both the quartz support and the membrane. The PEG tether consisted of a DMPE lipid component, a PEG moiety of 77 subunits and a triethoxysilane group for covalent linkage to silanols at the surface of quartz substrates. They demonstrated that uniform fluid bilayers of POPC could be formed on this type of cushion. In addition, reconstituted membrane proteins, cytochrome b_5, annexin V and SNARE, were shown to maintain mobility in the polymer supported membrane.[136,138,177,178] More complex lipid membranes such as phase separated systems were deposited with ease on this polymer cushion system.[137]

Later, to avoid the extra step of covalent attachment of polymer to the support, stable, fluid supported membranes were formed on PEG-lipid conjugates.[135,140,179] Similar values for lipid diffusion were obtained for bilayers on PEG cushions, independent of whether or not the PEG lipid conjugate was tethered to the surface.

Studies have been performed to determine the optimal chain length and coverage of PEG-lipid conjugate in the bilayer. The PEG polymer is available in many different molecular weights. However, Merzlyakov[180] showed that lipid diffusion in POPC bilayers on PEG cushions was unaffected by the molecular weight of the polymer. PEG is also known to exist in two conformers on a solid surface. At low concentrations PEG adopts a mushroom conformation whereas at high concentrations PEG adopts a brush conformation (Figure 1.15). The brush conformer is formed because of steric repulsions from neighboring polymers which forces the PEG structure to adopt a more linear conformer.[181,182] Attaching PEG at higher concentrations to ensure the prevention of nonspecific adsorption of proteins to the surface can be difficult due to steric repulsion between PEG molecules. Varying the molecular weight of PEG molecules can sometimes solve this issue. Smaller molecular weight PEG polymers link to the surface much easier then larger polymers because the steric repulsions are decreased. The concentration at which PEG changes from the mushroom conformer to the brush conformer is known as the crossover concentration. Higher lipid diffusion has been observed for concentrations above the crossover concentration.[180] Finally, the length and density of the PEG polymer control the size of the aqueous reservoir between the

support and the membrane which results in a significant variable for the reconstitution of membrane proteins.[183]

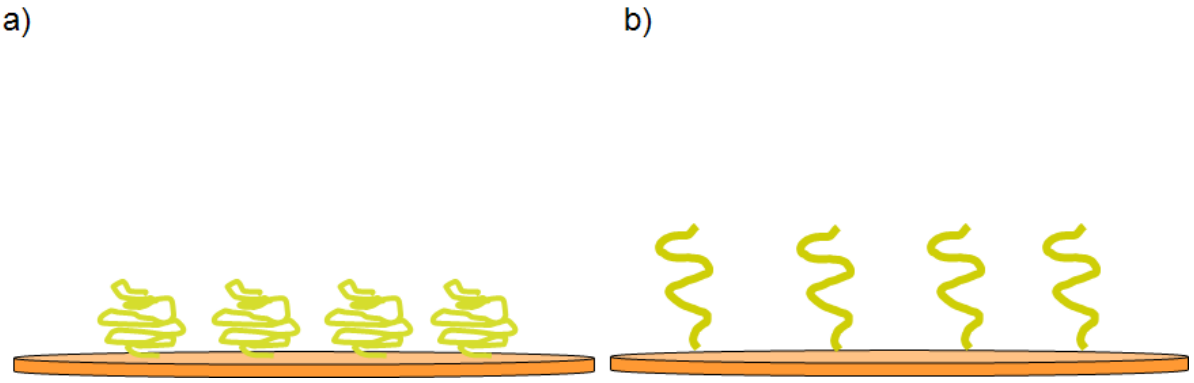

Figure 1.15 PEG Conformers. a) Mushroom conformation, b) Extended conformation

1.5 Membrane Proteins

Membrane proteins are a large group of proteins that can be divided into two major classes: i) peripheral membrane proteins and ii) integral/transmembrane proteins. The transmembrane protein class can then be subdivided into two subclasses based on their topology. The two subclasses consist of simple and complex transmembrane proteins. Simple transmembrane proteins possess only a single membrane spanning domain. Complex transmembrane proteins possess multiple transmembrane spanning α-helices or consist of a β-barrel type structure (Figure 1.16).[184] The hydrophobic domains of a transmembrane protein are usually embedded in the lipid bilayer membrane because of the restrictions of the hydrophobic/hydrophilic interface of the membrane. The lipid composition of a

membrane can significantly influence the mobility and function of transmembrane proteins.[185]

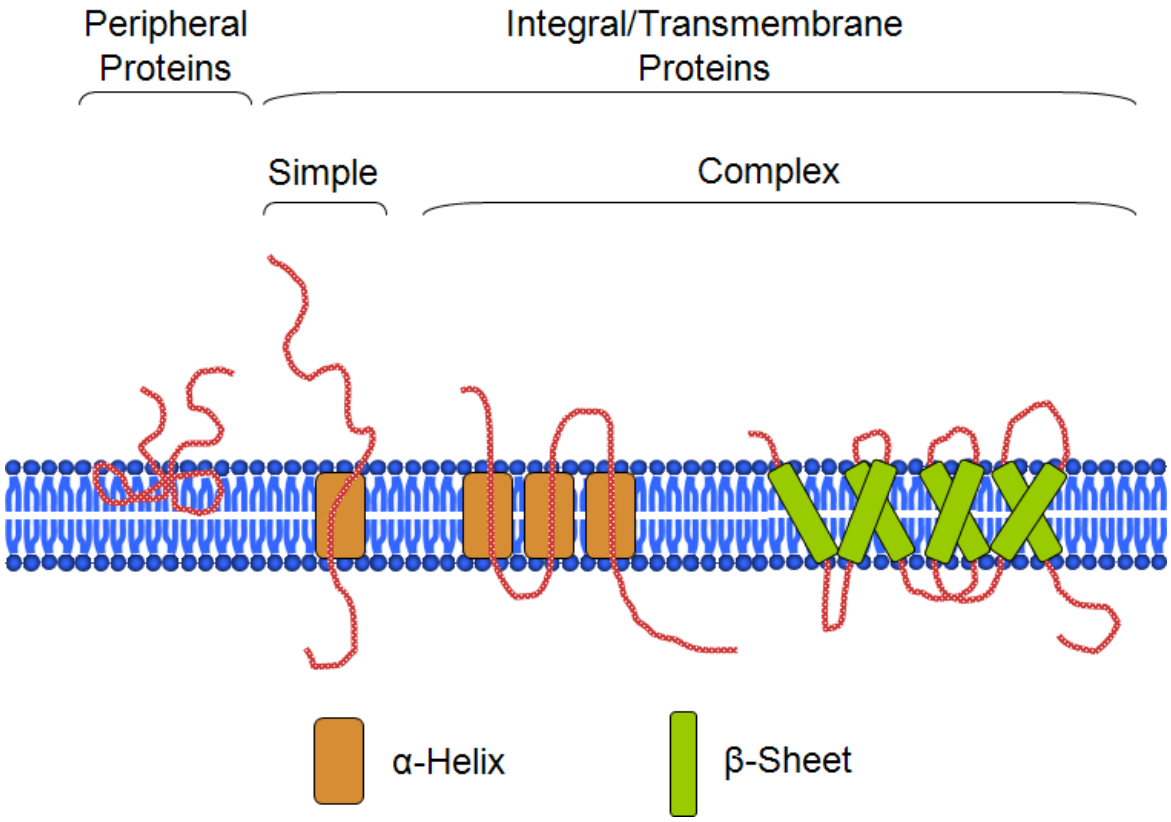

Figure 1.16 Membrane Protein Classes

Various strategies can be utilized to insert proteins into supported lipid membranes.[186] Small peptides such as gramicidin or alamethicin can be directly incorporated into supported membranes from solution.[187,188] Other proteins require solubilization by a detergent to be incorporated into a supported membrane. In this case, proteins are solubilized above the detergent's critical micelle concentration

(CMC). The solubilized protein is then diluted below the CMC when it is added to the cell containing a preformed supported membrane. In turn, the protein inserts itself into the supported membrane.[189] However, for larger transmembrane proteins the detergent dilution method is not as effective. Large transmembrane proteins can only be inserted into a supported membrane using proteoliposomes.[186] Proteins are solubilized in detergent and then rapidly diluted into liposomes forming proteoliposomes. The detergent is removed by dialysis or by passing the liposome solution through a column. These proteoliposomes are then deposited on a support to form a planar lipid membrane.[186] Rupture and fusion of the proteoliposomes to give a planar membrane can be confirmed via various assays or fluorescence techniques.[190] The incorporation of membrane proteins into supported membranes can be performed during membrane creation or after the membrane is formed. Factors such as protein size and experimental requirements often determine the optimal technique to use.

1.5.1 Membrane Proteins on Polymer Supported Membranes

Protein insertion into polymer supported membranes has recently started to emerge as an important direction for biomimetic membranes (Table 1.2).[186] Typically protein domains can extend up to several nm from the membrane. Thus, polymer cushioned supported membranes have become the method of choice when attempting to insert membrane proteins into biomimetic membranes.[5] The majority of examples of the incorporation of membrane proteins into supported membranes make use of a tethered polymer cushion (Figure 1.17a). The Tamm group has

incorporated a variety of transmembrane proteins into PEG cushioned supported membranes. Proteins such as cytochrome b_5, annexin V and a SNARE complex have been used with moderate success.[136,138,178] Cytochrome b_5 and annexin V were found to be largely immobile with mobile fractions of $\leq$25%. However, the protein portion that was mobile diffused with diffusion coefficients ranging from 0.02-1 $\mu m^2/s$. Tamm indicated that the protein diffusion was dependent on the polymer concentration suggesting that the protein weakly interacted with the underlying polymer network. However, the use of a SNARE complex protein on the same polymer cushion resulted in 70% lateral mobility. Diffusion coefficients for the SNARE proteins were determined to 1 $\mu m^2/s$.[178]

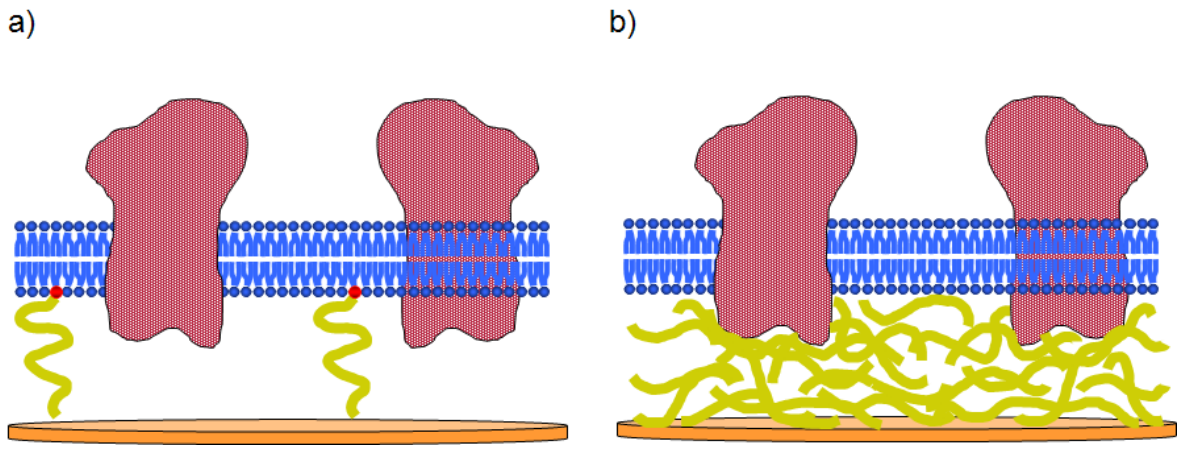

Figure 1.17 Polymer Supported Lipid Membrane Containing a Membrane Protein. a) Polyelectrolyte Polymer Cushion, b) PEG Polymer Cushion

A study by Purrucker investigated the incorporation of the transmembrane protein $\alpha_{IIb}\beta_3$ integrin on a lipopolymer tethered supported membrane.[142] Slow

diffusion of the protein was observed and suggested to be the result of frictional coupling due to the tethering of the polymer. By contrast, Gonnenwein reported a diffusion coefficient 6 times greater for the same $\alpha_{IIb}\beta_3$ integrin protein on a floating cellulose supported membrane.[125] Merzlyakov[180] studied lipid and peptide mobilities in bilayers on various PEG-cushioned supports. In particular the lateral mobility of the transmembrane domain of FGFR3 in a PEG supported membrane was compared to solid supported membranes without a PEG cushion. A reduction in lateral mobility was observed for the bilayer on a PEG cushion and they concluded that the decrease was not the result of the protein-cushion interactions. The authors believed that the method of bilayer deposition was the most important factor in determining the lateral mobility.

Another study made use of a maleic anhydride copolymer cushion for the integration of a transmembrane protein, the β-amyloid precursor protein cleaving enzyme (BACE), into a lipid bilayer. The copolymer system produced a supported bilayer with a homogeneous distribution, high lateral mobility and enhanced activity of the reconstituted BACE whereas in the absence of the copolymer low mobility, inhomogeneous clustering and reduced activity was observed.[148] Integration, mobility and activity of the protein seem to be dependent on factors such as the type of polymer used and the method of bilayer assembly.

Presently, there are a number of examples that incorporate membrane proteins into a polymer supported membrane; however, there are few comparisons of a single membrane protein on multiple polymer supports. As a result, there is no clear consensus as to which polymer cushion approach is optimal for multiple

membrane proteins. Finally, the use of biocompatible polymers, cellulose and PEG, have produced protein containing polymer supported bilayers with the highest protein diffusion coefficients although few studies have attempted to validate this method and show the function or activity of these membrane proteins in a polymer supported bilayer.

Table 1.2 Proteins reconstituted in supported lipid bilayers on polymer cushions

i) Polymer cushion without attachment to the substrate or the lipid bilayer.								
Support	Polymer	Thickness (nm)	Lipid Bilayer	Lipid Diffusion Coefficient ($\mu m^2/s$)	Characterization Method	Protein	Protein Diffusion Coefficient ($\mu m^2/s$)	Reference
Gold	PPy(DBS)		DPhPC		EIS, CV	Alamethicin		116
Gold	MUA-PDDA	1-4	SOPS: POPC	1-2	Fluorescence, FRAP, SPR	Wt-20		117
Gold	MUA-PDDA-PSS	0.5-2.0	SOPS: POPC	1.2-2.1	Fluorescence, FRAP, SPR	Protegrin-1		118
Glass	Cholesteryl-PEG		Egg-PC	1.3	Fluorescence, FRAP	Phospholamban		123
Glass	Cellulose	4.9	SOPC	2	Neutron Reflectometry, DLS, Fluorescence, FRAP, Cryo TEM, AFM	F_0F_1 ATP Synthase		124
Glass	Cellulose		DMPC	3.3	Fluorescence, FRAP, RCIM	$\alpha_{lib}\beta_3$	0.6	125
ii) Polymer cushion attached to the lipid bilayer.								
Support	Polymer	Thickness (nm)	Lipid Bilayer	Lipid Diffusion Coefficient ($\mu m^2/s$)	Characterization Method	Protein	Protein Diffusion Coefficient ($\mu m^2/s$)	Reference
Glass, Quartz	Et_3Osi-PEG-DMPE	4.8	POPC:POPG (9:1), POPC:Chol	0.9-1.4, 0.0-1.0 (Phase	Fluorescence, FRAP, XPS, FLIC, SPT	Cytochrome b_5, Annexin V, SNARE	0.02-1	136-139

	(DPS)		(4:1), bPC:bSM/ Chol (2:2:1) &(1:1:1)	separated)				
Glass	Me_3OSi-poly-oxazoline-lipid (POX)		SOPC	0.9-1.6	Fluorescence, FRAP	$\alpha_{IIb}\beta_3$	0.03-0.1	141,142
Glass	PEG-DOPE	7	DPhPC	1.5-2.5	EIS, Fluorescence, FRAP	FGFR3	0-0.02	143,144
Glass	BSA-PEG-PE		POPC	0.3-3.5	Fluorescence, FRAP	Annexin V	0.5-2.9	145
Silicon	PEG-PE		DPhPC		EIS	Gramicidin		147

iii) Polymer support attached to the substrate.

Support	Polymer	Thickness (nm)	Lipid Bilayer	Lipid Diffusion Coefficient ($\mu m^2/s$)	Characterization Method	Protein	Protein Diffusion Coefficient ($\mu m^2/s$)	Reference
Glass	POMA, PPMA, PEMA	4-60	PC:PS: PE:Chol (5:2:1:2)	0.2-2.5	Fluorescence, FRAP, FCS, QCM-D	BACE	0.04-0.1	114,148
Glass	NHS-PEG-biotin-avidin		DOPC	6.6-8.0	Fluorescence, SMFM	Gramicidin		149
Glass	Polyacrylamide brushes	5-10	POPC	1.2-2.0	Fluoresecence, FRAP, SMFM, FTIR	hDOR	0.3	150

iv) Polymer support attached to both the substrate and the lipid bilayer.

Support	Polymer	Thickness (nm)	Lipid Bilayer	Lipid Diffusion	Characterization Method	Protein	Protein Diffusion	Reference

				Coefficient ($\mu m^2/s$)			Coefficient ($\mu m^2/s$)	
Glass, Quartz	Et_3OSi-PEG-DMPE (DPS)	4.8	POPC:POPG (9:1)	0.5-0.9	Fluorescence, FRAP, XPS	Cytochrome b_5, Annexin V	0.02-1	136
Glass	AHAPS-PEG-DSPE	1-9	DOPC, DOPC:DOPS (9:1)&(4:1)	3.3	Fluorescence, FRAP, AFM, XPS	Annexin V		156
Glass	Biotin-PEG-DSPE	3-4	POPC:DOPS (85:15)	5.5	Fluorescence, SMFM, AFM	AF633-Syx	1	158
Gold	DTSP-NTA	1	DPhPC		SPR, EIS, QCM	Cytochrome *c*		161

1.5.2 Nanodiscs: An Alternate Support for Membrane Proteins

Nanodiscs are small assembled phospholipid membrane patches surrounded by two membrane scaffold proteins (MSP) which act as belts around the bilayer (Figure 1.18). The resulting bilayer patches are small discs of approximately 10 nm in diameter.[191] This alternative approach to supported membranes is a convenient method to encapsulate single membrane proteins. The incorporation of a protein in a nanodisc maintains membrane proteins in solution, provides a native-like phospholipid bilayer environment and permits control of the oligomeric state of the protein. The nanodisc support allows for the study of structure and function of individual proteins.[192] Relatively few proteins have so far been reconstituted into nanodiscs. One of the first examples was the incorporation of cytochrome P450 in nanodiscs. The function of cytochrome P450 is often affected by aggregation.[193] The use of nanodiscs prohibited any dynamic self-association of the protein and made it possible to cleanly monitor the function of cytochrome P450.[194,195] Nanodiscs have also been used in blood clotting studies.[196] The blood coagulation process is known to be initiated by the binding of an integral membrane protein tissue factor (TF) to a soluble factor, FVIIa. Nanodiscs were used to precisely couple TF to a gold surface so that the binding FVIIa could be measured by SPR.[196] Structure and function studies of individual bacteriorhodopsin[197] and G-protein coupled receptors[198] in nanodiscs have also been performed. Nanodiscs have an increasing potential as even more complex assemblies such as bacterial chemoreceptors[199] and peptide transcolon complexes[200] have been incorporated into them. The receptor for tyrosine kinase or the epidermal growth factor receptor

(EGFR) has also been reconstituted into nanodiscs.[201] The stability of an EGFR dimer was increased tremendously in nanodiscs. The activity monitored was 4 fold higher in nanodiscs as compared to the protein in the absence of the nanodiscs. Nanodiscs offer advantages such as their ability to stabilize proteins, size and a new means for surface attachment.[192] These qualities make nanodiscs an attractive platform that could be useful in the development of membrane-based biosensing.

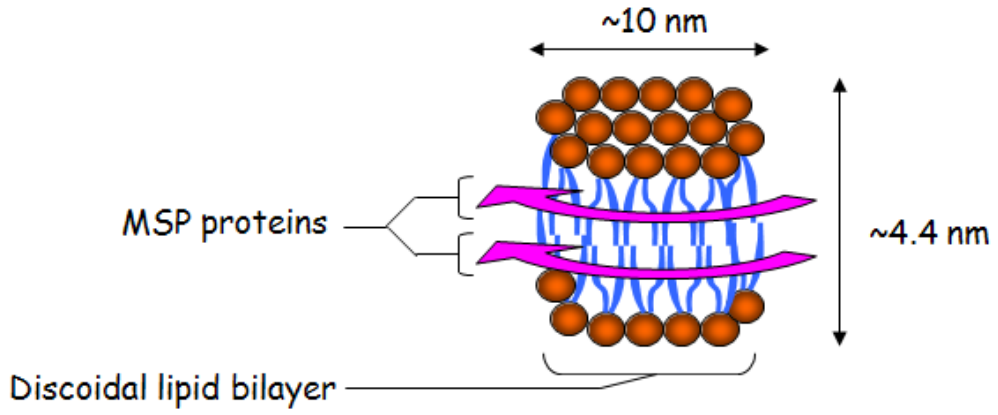

Figure 1.18 Structure of a Nanodisc[191]

1.5.3 Biosensing Using the Ste14p Membrane Protein

Ste14p is a 26 kDa protein that consists of six transmembrane helixes with a large active site localized on the cytosolic side of the membrane (Figure 1.19).[202] Ste14p is a more readily available yeast variant of the human isoprenylcysteine carboxylmethyltransferase (ICMT) from *S. cerevisiae*. ICMT is the methyltransferase enzyme responsible for the catalysis of α-carboxyl

methylesterification of the carboxylate on the terminal cysteine residue of *Ras* proteins (Figure 1.20). The *Ras* family of proteins is implicated in many metabolic processes such as cell growth, survival, differentiation, and angiogenesis.[203] *Ras* proteins are considered active when bound to guanosine triphosphate (GTP) and inactive when bound to guanosine diphosphate (GDP). Point mutations can occur in the sequence of a *Ras* gene, permanently locking the *Ras* protein in the active state. The *Ras* protein then becomes insensitive to induced hydrolysis of GTP to GDP. This insensitivity eventually leads to unregulated cell growth and proliferation that can possibly lead to cancer.[203-205] Mutated forms of the *Ras* protein have been found in high quantities in various types of cancers such as pancreatic, colorectal, lung, endometrium, gallbladder, multiple myeloma, and testicular.[206] Several attempts to target *Ras* proteins for cancer therapy have used methods such as the inhibition of *Ras* expression through antisense oligonucleotides or RNA interference, pursuing *Ras* effectors or employing mutant *Ras* proteins in combination with drugs. Initial research to develop inhibitors found that proteins should be inhibited later in the biochemical pathway.[207] This led to attempts to inhibit *Ras* post-translational processing[203] in which C-terminal–CaaX recognition sequences undergo a series of enzymatic reactions with ICMT. This methylesterification reaction is vital for proper localization of a *Ras* protein in a cellular membrane. The development of inhibitors for this reaction is a potential method to prevent or treat *Ras*-based cancers. The development of a biosensing platform for rapid detection of ICMT activity would greatly aid in the development of highly effective inhibitors of ICMT.

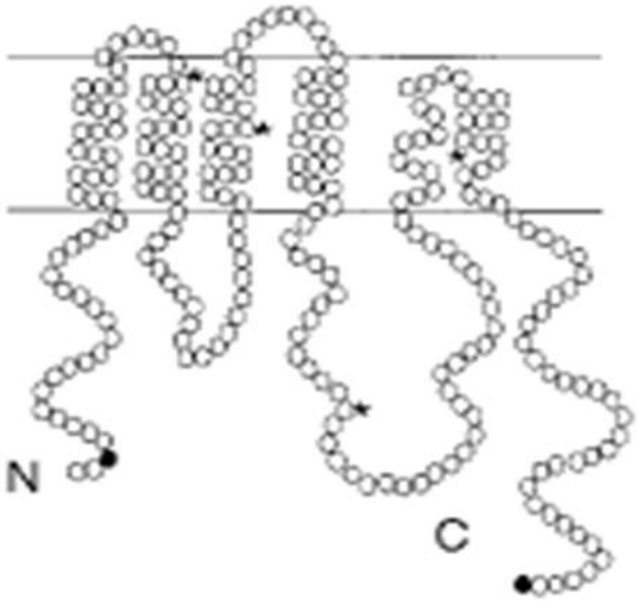

Figure 1.19 Six Transmembrane Domain Model of Ste14p (Adapted from reference 208).[208]

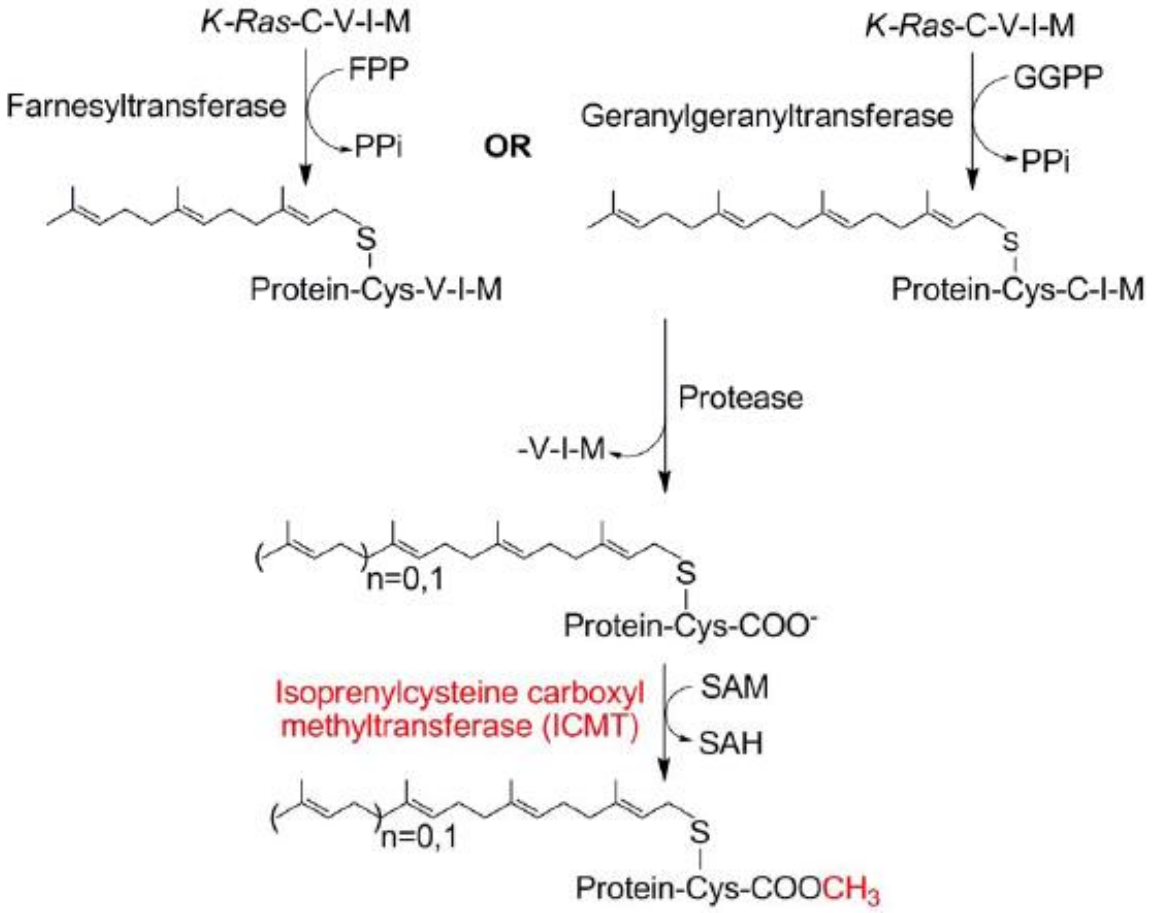

Figure 1.20 K-*ras* signaling pathway. The final step in the pathway is a α-carboxyl methylesterification catalyzed by ICMT.[208]

1.6 Objective of Thesis

An overview introducing many different methods to improve the supported lipid membrane system has been presented in this chapter. There is a necessity to establish new platforms for the supported membrane system to progress toward new methods of membrane-based biosensing. The supported membrane system possesses two major drawbacks of stability and spacing between the support and membrane. New membrane materials based on bolaamphiphiles combined with

monopolar lipids will be thoroughly investigated in an attempt to improve the stability of the supported membrane system. The spacing drawback will be addressed through the addition of a polymer cushion to the supported membrane system. Floating polymers such as cushions consisting of polyelectrolytes and tethered polymers such as cushions composed of PEG will be investigated. The incorporation of these polymers to the supported membrane system should increase the spacing in between the solid support and the membrane to allow a significant spacing for larger domains of integral membrane proteins. The effectiveness of these polymer supported membrane systems will be evaluated by the incorporation of the integral membrane protein Ste14p. Lastly, another new platform, the use of nanodiscs, to observe individual proteins will also be investigated.

Chapter 2: AFM Investigation of Phase Separation in Supported Membranes of Mixed POPC and Bola Lipids[209]

This chapter contains Material Adapted from the following manuscript

1. K. Mulligan, D. Brownholland, A. Carnini, D. H. Thompson, L. J. Johnston; AFM Investigations of Phase Separation in Supported Membranes of Binary Mixtures of POPC and an Eicosanyl-Based Bisphosphocholine Bolalipid; Langmuir, **2010**, *11*, 8525

2. CryO-TEM work was contributed by collaborators.

2.1 Bolalipid:POPC Membranes for Biosensing Applications

Membrane spanning alkyl chains of bolalipids[107,210] are one of the most important structural factors responsible for the enhanced stability of archaeal membranes relative to bilayer membranes. The robust character of bolalipids has led to their use in a number of potential applications, including gene and vaccine delivery and the development of planar supported membranes for biosensors incorporating integral membrane proteins.[83,85,87,88,130] The difficulty and costs associated with the isolation of pure bipolar archaeal lipids in practical quantities have motivated the development of efficient pathways for bolalipid synthesis.[110,211-215]

Thompson and coworkers have recently synthesized three symmetric, acyclic bolalipids with glycerophospholine headgroups and bearing either 20 or 32 carbon transmembrane chains;[87,211,216] they have also characterized the lamellar thickness[105,210] and fluidity[97] of these bolalipid membrane dispersions to evaluate their suitability for reconstitution of integral membrane proteins.[87,88] This work showed that the activity of Ste14p, a yeast membrane-associated enzyme in the family of isoprenylcysteine carboxyl methyltransferases, varied with the length of the bolalipid alkyl chain and the POPC molar ratio when reconstituted in mixed bolalipid:POPC membranes.[87] Significantly lower protein activity was observed in C_{20}BAS membranes with low POPC content (i.e., < 30 mol%) relative to the longer chain analogue, C_{32}phytBAS.[87] These findings were attributed to hydrophobic mismatch between the C_{20}BAS bolalipid and the hydrophobic, membrane-spanning sequences of Ste14p. Enzyme activity increased significantly when the bilayer-

forming lipid content exceeded ~30 mol% C_{20}BAS, however, fluorescence staining experiments provided no evidence of phase separation of either Ste14p from the vesicle membrane or the C_{20}BAS:POPC mixed membranes themselves on macroscopic length scales.

2.1.1 Bolalipid:POPC Membrane Phase Separation

A recent theoretical study has used mean field theory to examine the structure and phase behavior of mixed monopolar lipid:bolalipid membranes.[109] The results predict that phase separation is the thermodynamically stable state of mixed membranes containing approximately equimolar C_{20}BAS and double chain monopolar lipids with chain lengths exceeding fifteen carbons. The driving force for phase separation into two liquid phases was attributed to hydrophobic mismatch between the monopolar lipid hydrocarbon chains and the membrane spanning bolalipid chains. When the hydrophobic mismatch is sufficiently large, two liquid phases were predicted, one thinner membrane phase enriched in bolalipid and a second thicker bilayer phase enriched in monopolar lipid (Figure 2.1). Since bolalipids are capable of adopting two conformations, a transmembrane conformation with the headgroups on opposing sides of the membrane and a U-shaped conformer with both headgroups on the same side of the membrane, it was not clear how C_{20}BAS would be arranged in mixed membrane dispersions. Longo et. al. predicted that the thinner domain would be enriched in bolalipids that are predominately in their transmembrane conformations, while the thicker, monopolar lipid-rich domain would contain a small population of bolalipids in U-shaped

conformations (Figure 2.1). This prediction is consistent with experimental evidence reported for bolalipid systems. The ratio of looping to transmembrane conformers has been investigated by ^{2}H NMR for two phosphocholine-type bolalipids. A C_{28} bolalipid derivative was shown to exist with >90% transmembrane conformers;[107] similarly, C_{20}BAS showed no evidence for looping conformers at room temperature.[106] ^{2}H NMR spectra of POPC:C_{20}BAS mixtures with either perdeuterated POPC-d_{31} or bolalipid specifically labeled with deuterium in the middle of the transmembrane chain showed that two distinct liquid phases are detectable between POPC:C_{20}BAS ratios of 50:50 to 90:10.[210] It was further noted that (1) transmembrane conformers are the predominant species even at low fractions of bolalipid (e.g., 10 mol% C_{20}BAS) and (2) only a single lamellar thickness is detected by SAXS across the same range of compositions. Taken together, these findings provide strong evidence for the occurrence of microphase separated membranes in POPC:C_{20}BAS samples. This work, combined with the diffusion coefficient determined by pulsed field gradient NMR,[97] enabled an estimate of > 50 nm for the minimum domain radius in these dispersions.[210]

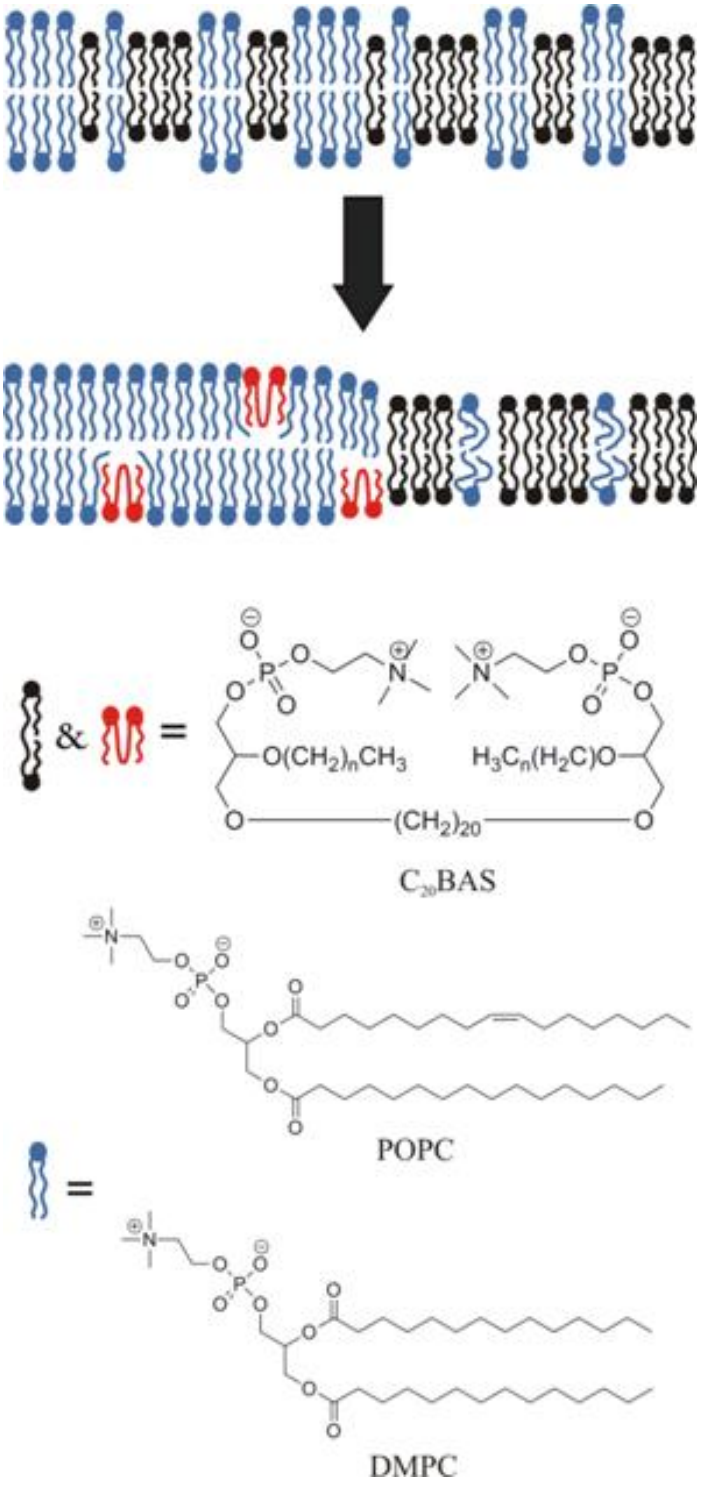

Figure 2.1 Structures of C_{20}BAS, POPC, and DMPC. The cartoon shows phase separation for a mixed C_{20}BAS/PC lipid membrane to give thinner domains that are predominantly transmembrane bolalipids and thicker domains that are enriched in monopolar lipid and have a small fraction of bolalipid U-conformers.

The theoretical prediction of phase separation for some C_{20}BAS:monopolar lipid membranes is consistent with experimental observations and computational studies of liquid-liquid phase separation for other fluid-phase phosphatidylcholine mixtures.[217,218] It also raises the interesting possibility that domain formation may play a role in determining the activity of membrane proteins that have been reconstituted in bolalipid:POPC membranes or other non-native membrane vesicle compositions. This is of practical importance for the development of bolalipid-stabilized supported membranes for biosensing applications. In this chapter we experimentally probe the role of hydrophobic mismatch between C_{20}BAS and POPC in pure C_{20}BAS bolalipid and mixed C_{20}BAS:POPC supported lipid membranes using atomic force microscopy (AFM). AFM has been widely used to probe domain formation in a variety of binary and ternary mixtures that exhibit mixtures of liquid-disordered and gel or liquid-ordered phases.[219,220] This method has a number of advantages, including the ability to detect small height differences between coexisting membrane phases and the capacity to examine domains across a range of length scales from tens of nm to tens of μm in aqueous solution under physiological conditions, without the requirement for labeling. Our studies confirm that C_{20}BAS:POPC lipid mixtures are microphase separated over a range of compositions. They also show that the morphology of the planar supported membranes varies significantly with the conditions used to prepare the vesicles and supported membrane samples. We conclude that three factors contribute to the complex membrane morphologies observed – (1) a compositionally heterogeneous vesicle population; (2) a non-uniform exchange of lipid between the bulk solution

and solid substrate during supported membrane formation; and (3) a slow equilibration between the surface-supported domain structures due to pinning of the lipids to the underlying solid support.

2.2 Characterization of Mixed Bolalipid:POPC Membranes

2.2.1 AFM Characterization of POPC and C_{20}BAS Membranes

AFM images of samples formed by incubating two different concentrations of sonicated POPC vesicles on mica for 1 hour, followed by washing to remove excess vesicles, produced bilayer patches and continuous bilayers as shown in Figure 2.2A & B. AFM imaging was performed in MilliQ at 23°C. At low lipid concentrations, there are many small bilayer patches with a height of 4.0 ± 0.2 nm, while at higher lipid concentrations, a uniform, featureless bilayer membrane is formed. Noticeably longer incubation times were required to produce supported membranes from C_{20}BAS vesicles at the same lipid concentration. Figure 2.2C shows large patches of C_{20}BAS bolalipid membrane, with a thickness of 2.7 ± 0.4 nm, formed with an incubation time of ~ 3 days. A smaller area with a continuous membrane in which a small area was scanned at high force to create a defect is shown in the insert of Figure 2.2C. AFM thickness measurements were determined by averaging the data obtained from three or more cross-sections of 3 or more areas of at least two independent samples. The measured thickness is consistent with the measured lamellar repeat distance of 32 Å by small angle x-ray scattering.[105,109] Shorter

incubation times gave either small membrane patches or adsorbed vesicles that were very difficult to image.

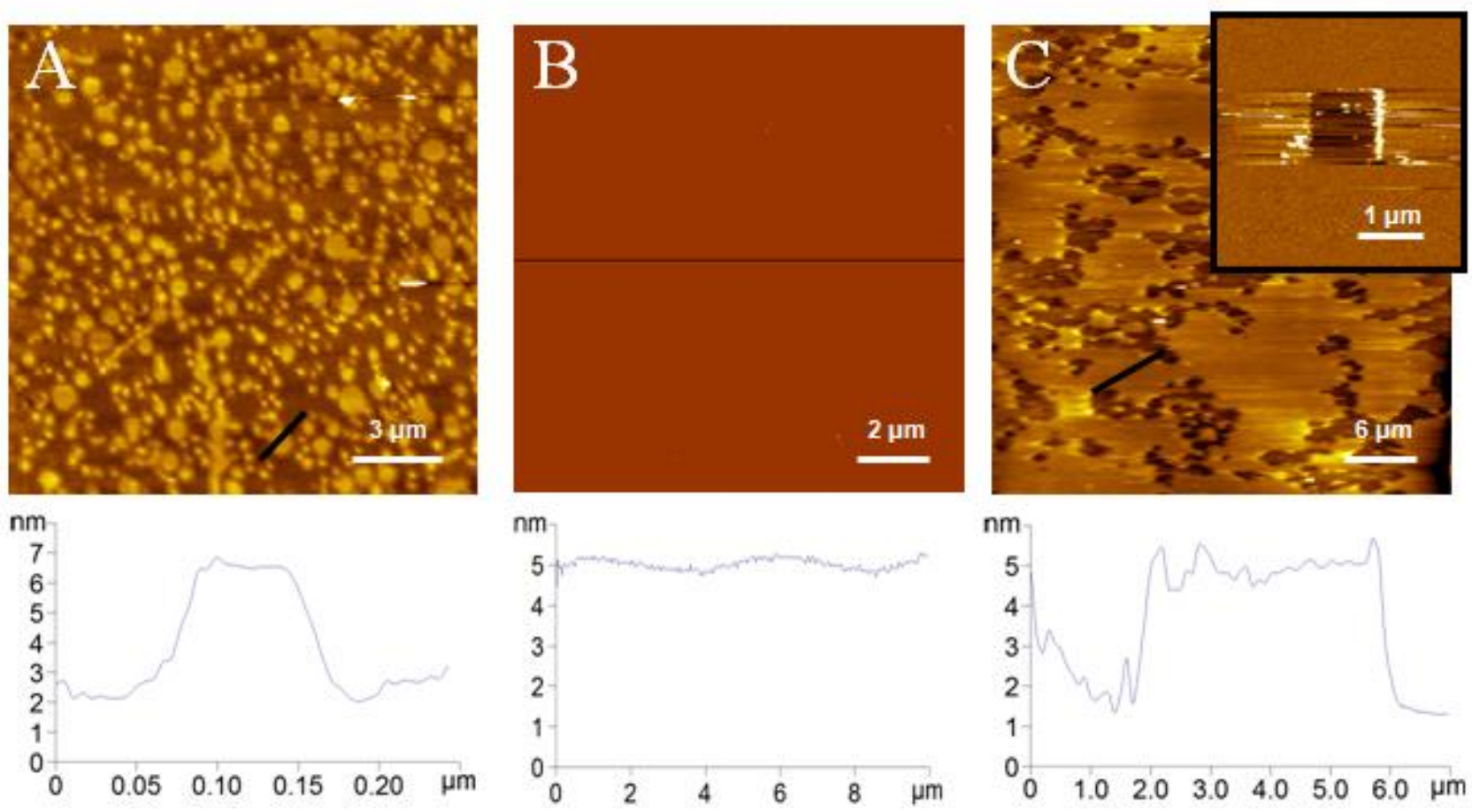

Figure 2.2 AFM images of POPC and C_{20}BAS supported membranes prepared from sonicated vesicles at room temperature on mica. (A) POPC patches and (B) a continuous bilayer formed by incubating 3 and 50 µg total lipid for 1h. (C) C_{20}BAS membrane patches produced by incubating 50 µg total lipid for 72 h; the inset shows an area of continuous membrane for a different sample for which a small region was scanned at high force to create a persistent defect. Cross sections for the lines marked on each image are shown below the images.

2.2.2 AFM Characterization of POPC:C_{20}BAS Membranes

Vesicles with mixtures of POPC and C_{20}BAS across a range of molar ratios were prepared by sonication and used to form supported membranes for AFM characterization. The results are shown in Figure 2.3. Uniform, featureless images were obtained for samples with 0.1 and 0.9 mol fractions of C_{20}BAS (X_B) after incubation for 3 hours. The X_B = 0.9 sample was scanned at high force to create a defect and verify that there was an intact membrane on the mica surface; however, it was not possible to maintain a defect in the X_B = 0.1 sample, presumably because the highly abundant monopolar POPC lipids are sufficiently mobile to rapidly refill defects created by the tip, as is commonly observed for fluid POPC bilayers. AFM images of samples prepared from sonicated vesicles with X_B = 0.6, 0.5 and 0.4 all showed evidence of microphase separation, with domains of thicker and thinner membrane regions apparent. For X_B = 0.6, there were a number of small raised islands that were 1.2 ± 0.2 nm higher than the surrounding lower phase (Figure 2.3B). The islands ranged in size from 10-15 nm in diameter and covered 6 ± 2 % of the surface area. Qualitatively similar results were obtained for X_B = 0.5, but both the number and size of the small raised islands increased; most of the islands ranged from 50 to 100 nm in diameter and there were a few larger features that appeared to be formed by coalescence of small adjacent islands. The islands were 1.9 ± 0.2 nm higher than the surrounding lower phase and covered 22 ± 2 % of the surface. The morphology was significantly different for X_B = 0.4, with a number of small lower areas (depth of 1.0 ± 0.1 nm) that were surrounded by a uniform membrane. Scanning at high force to create a defect indicated that there was an

intact membrane with small regions of lower phase, as opposed to an incomplete membrane with areas of bare mica. The higher phase covered 86 ± 2% of the surface. The overall membrane morphology, including the size and depth of the small regions of lower phase, did not change over a period of 24 hours. Similarly, no change in morphology was observed when a sample with X_B = 0.5 was imaged before and after heating at 40°C for 1 hour, followed by cooling (Figure 2.4).

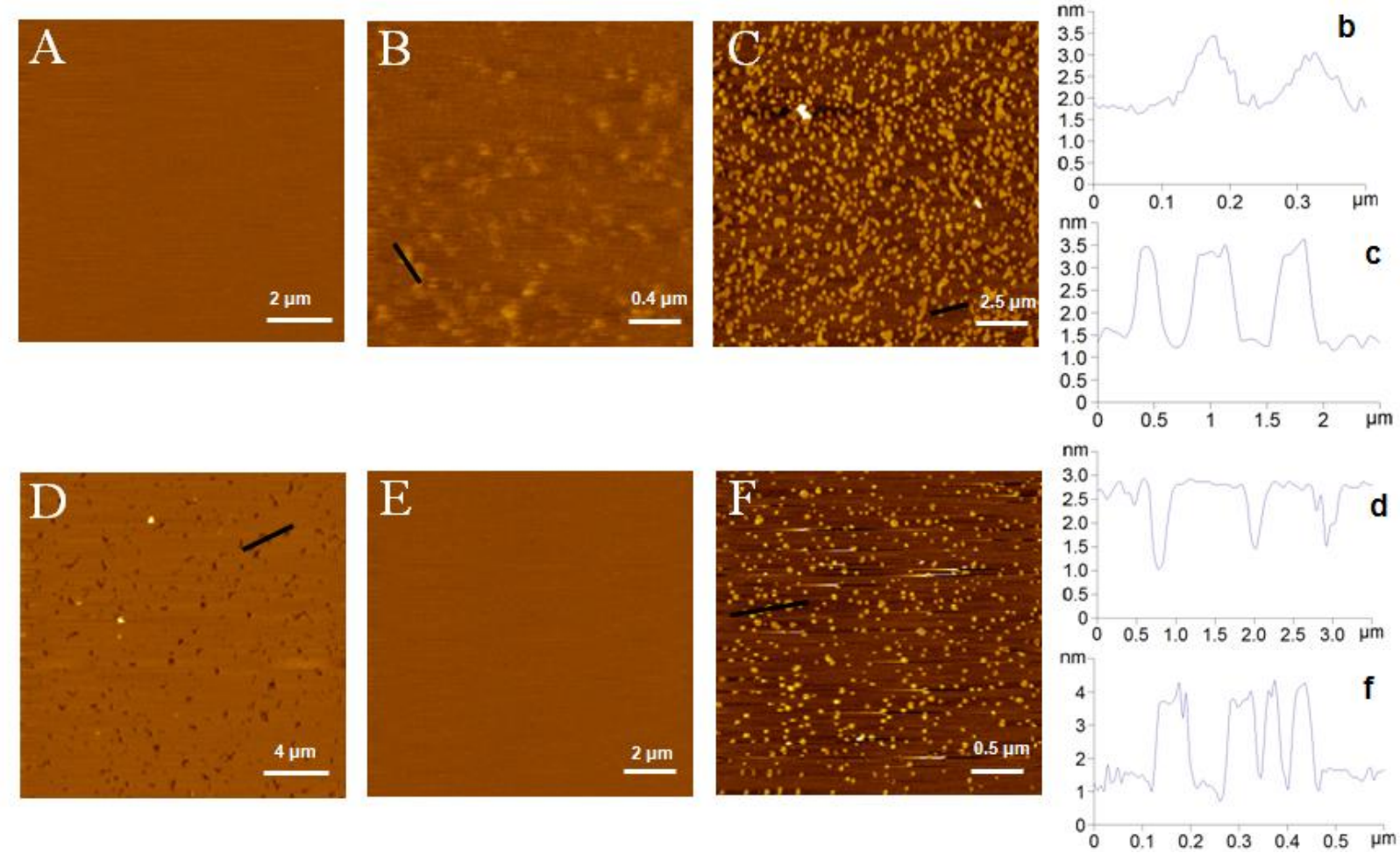

Figure 2.3 (A-E) AFM images of supported membranes prepared from sonicated vesicles with various POPC:C_{20}BAS ratios. Images A-E are for X_B = 0.9, 0.6, 0.5, 0.4 and 0.1, respectively. Image F shows a supported membrane prepared by mixing pure POPC and pure C_{20}BAS sonicated vesicles (1:1 ratio) immediately before incubation with the mica substrate. Cross sections for the lines marked on images, B, C, D and F are shown on the right.

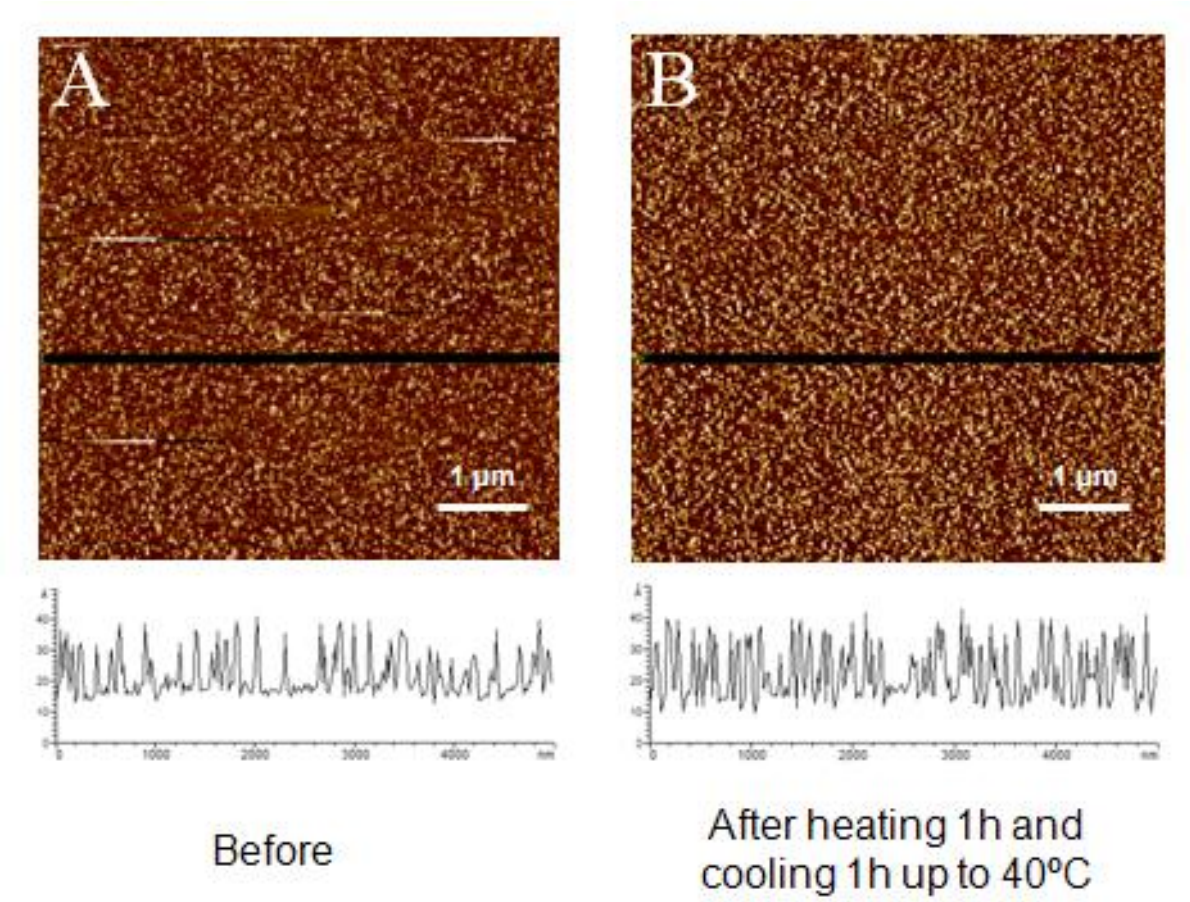

Figure 2.4 AFM images of a supported membrane prepared from sonicated vesicles (POPC:C_{20}BAS, X_B = 0.5). Image B shows the resulting supported membrane after reheating the membrane to 40°C for 1h and then cooling slowly for 1h to 23°C. Cross sections for the lines marked on each image are shown below the images.

Based on the measured thickness of pure POPC and C_{20}BAS membranes, it is reasonable to assign the higher phase observed for the lipid mixtures to a POPC-rich phase and the lower regions to a bolalipid-rich phase. This is also consistent with the observation that the amount of the higher phase decreases with increasing mole fraction of C_{20}BAS. However, the surface coverage data do not follow a

uniform trend with increasing POPC concentration. If one assumes that the area/molecule is similar for POPC and C_{20}BAS in the transmembrane configuration[211], then there is more C_{20}BAS phase than expected for X_B = 0.6 and 0.5 mixtures and less for the X_B = 0.4 mixture.

For comparison, membranes were prepared by physically mixing pure C_{20}BAS bolalipid and pure POPC vesicles before immediately incubating the vesicle mixture with mica, using the same conditions as for the samples in Figure 2.3. AFM images for both X_B = 0.5 and 0.4 showed small raised islands randomly distributed throughout the sample (see Figure 2.3F for X_B = 0.5). The surface coverage of the raised islands was 18 ± 2% and 26 ± 2% for X_B =0.5 and 0.4, respectively, and in both cases the islands were 2.3 ± 0.1 nm higher than the surrounding membrane. By analogy to the results above, we assign these islands to a POPC-rich phase. The relatively low fraction of the surface covered by the POPC-rich islands is surprising based on the very different incubation times required to form membranes from pure POPC and pure C_{20}BAS vesicles. Since POPC vesicles give a continuous bilayer with considerably lower lipid concentrations and shorter incubation times, one might have predicted the formation of a predominantly POPC bilayer from the physical mixture of vesicles. Interestingly, the morphologies for X_B = 0.5 are very similar when membranes are formed using either a physical mixture of pure lipid vesicles or vesicles with premixed lipids. By contrast, quite different results are obtained for the two methods for X_B = 0.4.

Diameters for sonicated vesicles were determined by dynamic light scattering and the results are summarized in Table 2.1. C_{20}BAS vesicles had a significantly

smaller mean diameter, 24 nm, than either POPC or POPC:C_{20}BAS vesicles, all of which had mean diameters between 40-45 nm.

Table 2.1 Mean diameters of sonicated vesicle dispersions determined by dynamic light scattering

Sample	Mean Diameter (nm)
C_{20}BAS	24
POPC	43
POPC:C_{20}BAS, X_B = 0.4	41
POPC:C_{20}BAS, X_B = 0.5	42
POPC:C_{20}BAS, X_B = 0.6	40
POPC:C_{20}BAS, X_B = 0.9	46
C_{20}BAS (after 3 days)	15

2.2.3 Effects of Vesicle Preparation and Incubation Conditions on Membrane Morphology

The size and shape of membrane domains and the kinetics for supported bilayer formation are affected by a variety of factors. These include (1) the size, net charge, lipid composition and concentration of the vesicles; (2) the aqueous environment present in the mica cell during vesicle adsorption and rupture; and (3) the characteristics of the solid support.[34,221] We hypothesized that the unusual trend in the ratios of higher and lower phases with changing lipid ratios could reflect a heterogeneous population of vesicles in the dispersed samples, with a significant fraction of the vesicles possessing lipid ratios that are different from the bulk

composition. If this were true, the process of vesicle adsorption and rupture on the surface could favor a specific vesicle population, thus leading to a membrane that does not reflect the nominal lipid ratios. An alternate possibility is that lipid exchange between the surface and vesicles occurs during supported membrane formation, thus leading to significant differences in composition between the final supported membrane and the initial vesicles. We carried out a number of experiments to further investigate these possibilities.

First, we examined the effects of vesicle sonication conditions on membrane morphology. We found no change in membrane morphology for samples prepared with X_B = 0.4 vesicles sonicated using several different protocols (e.g., variable times, bath vs. probe sonicator, or sonication temperatures between 20 and 60°C). It should be noted that the gel to liquid-crystalline phase transition temperatures of POPC and C_{20}BAS are -2°C and 17°C, respectively;[87] therefore, both lipids are in the fluid phase over the temperature range investigated. Vesicles sonicated at 56°C gave supported membranes with a different morphology featuring small raised areas that were 1.1 nm above the surrounding lower regions of the membrane. There were also occasional dark defects, indicating close to complete membrane coverage, although the defects were not large enough to obtain a reliable depth measurement. Increasing the incubation temperature from 20 to 60°C for vesicles sonicated at room temperature also produced a change in membrane morphology (Figure 2.5A,B). The higher resolution image (Figure 2.5B) shows that this sample has three distinct heights, with small and irregularly-shaped regions that are either

2.5 or 4 nm above the lowest (dark) regions that are assigned to exposed mica between membrane defects.

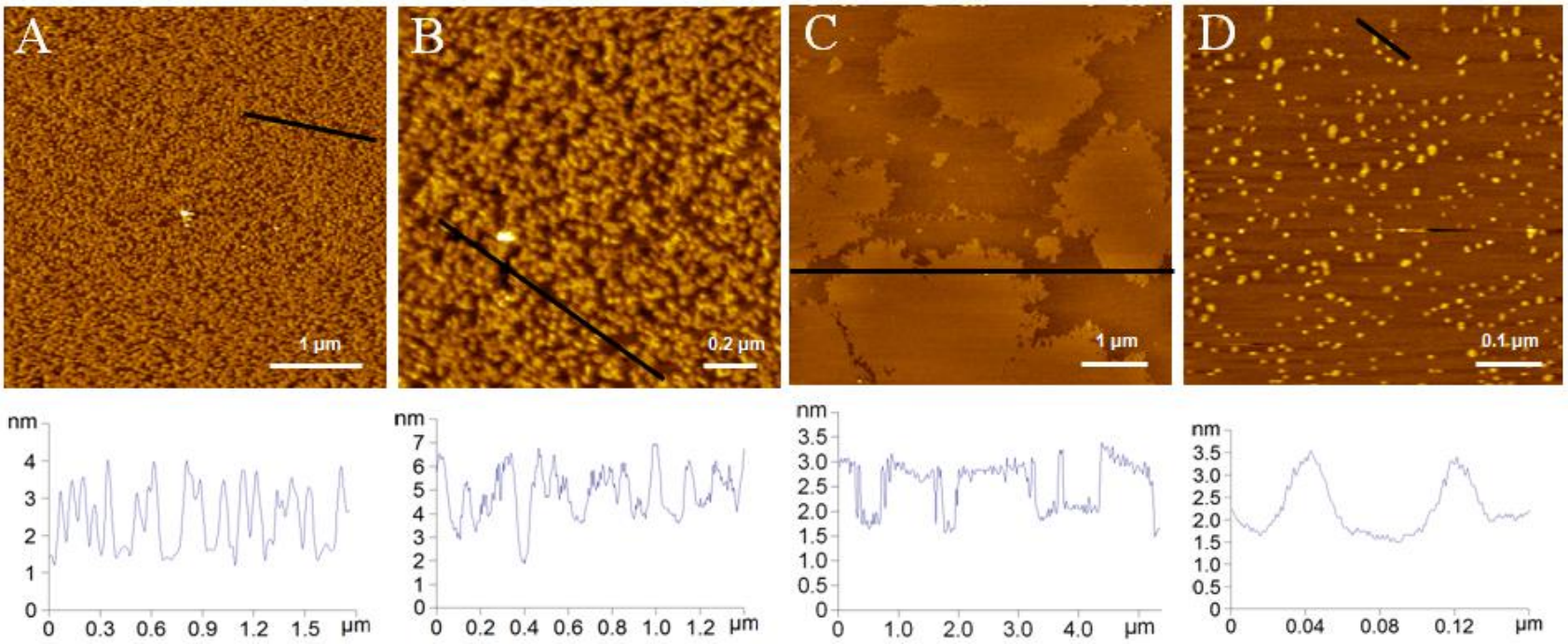

Figure 2.5 (A,B) AFM images of supported membranes prepared from sonicated vesicles (POPC:C_{20}BAS, X_B = 0.4) after incubation at 60°C on mica. (C) AFM images of supported membranes prepared from extruded vesicles (POPC:C_{20}BAS, X_B = 0.4, mean diameter = 71 nm) on mica at room temperature. (D) AFM images of supported membranes prepared from sonicated vesicles (POPC:C_{20}BAS, X_B = 0.5) on silicon (111) at room temperature. Cross sections for the lines marked on each image are shown below the images.

Second, we probed the effect of vesicle composition by using extrusion to make vesicles of similar sizes. Multilamellar vesicles prepared by hydrating lipid films with X_B = 0.4, 0.5 and 0.6 were extruded through a 100 nm filter, giving vesicles with mean diameters of 71, 127 and 104 nm, respectively. Vesicles with X_B = 0.4 produced microphase separated membranes with raised domains (1.6 ± 0.2 nm higher than the surrounding lower phase) with a wide distribution of sizes and shapes (Figure 2.5C). The surface coverage of the domains varied significantly from area to area of the same sample, with an average value of 30% for 4 large images (>10 x 10 μm^2) for the sample shown in Figure 2.5C. They also varied from sample to sample, displaying in some cases smaller domains that covered a significantly lower fraction of the surface (7%). Membranes prepared from X_B = 0.4 extruded vesicles using lower lipid concentrations (~10 times less) showed qualitatively similar microphase separation. By contrast, extruded vesicles with X_B = 0.5 and 0.6 formed featureless bilayers.

Vesicles with X_B = 0.4 were also extruded through filters with pores sizes of 200 nm and 400 nm to give vesicles with a mean diameter of 120 and 150 nm, respectively. Both samples gave microphase separated membranes that showed an increased number of small domains as compared to samples prepared from vesicles with a smaller mean diameter (71 nm) as shown in Figure 2.5C. Surface coverages of the raised domains are 35 ± 2 % and 35 ± 3 % for samples prepared by extrusion through 200 and 400 nm filters, respectively.

We also investigated the effect of substrate on the appearance of the supported membranes. Mica was replaced with silicon for sonicated vesicle

samples containing X_B = 0.5 and the resulting supported membranes imaged by AFM. Figure 2.5D shows a supported membrane image on silicon (111); there are many small islands (30-60 nm in diameter) that are 1.6 ± 0.2 nm above the lower phase and that cover 20 ± 1.6% of the surface, similar to the result on mica.

A final experiment probed the effects of the detergent, octyl glucoside, on a bilayer formed from sonicated vesicles with X_B = 0.5. A phase separated bilayer was formed and imaged by AFM before, after and 40 minutes following the addition of detergent. The detergent was added to a final concentration of 0.23 mM, half the critical micelle concentration. Figure 2.6 shows that the islands in the phase separated bilayer were 1.9 ± 0.3 nm higher than the surrounding lower phase and covered 20 ± 2 % of the surface which was consistent with other bilayers made from vesicles with X_B = 0.5. Figure 2.6 also shows no change in the surface coverage of the small islands after the addition of detergent.

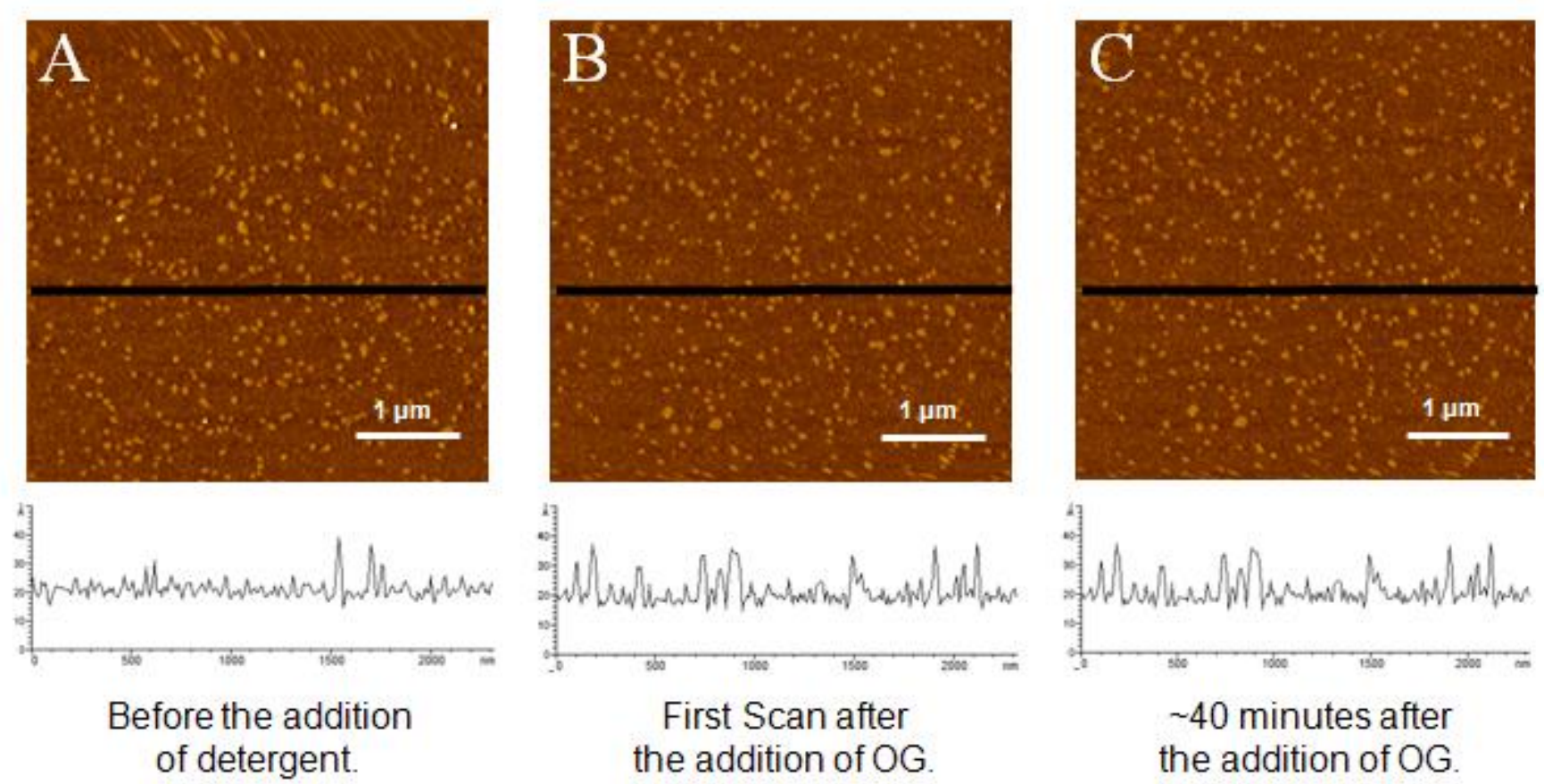

Figure 2.6 AFM images of a supported membranes prepared from sonicated vesicles (POPC:C_{20}BAS, X_B = 0.5). Images of the same supported membrane immediately (B) and 40 minutes (C) after the addition of 0.23 mM octyl glucoside.

2.2.4 Cryo-TEM of POPC:C_{20}BAS Vesicles

Cryo-TEM was utilized to examine the morphology of POPC:C_{20}BAS vesicles (X_B = 0.5) prepared by both sonication and extrusion with a 200 nm pore size filter. Representative cryo-TEM images of sonicated vesicles (measured 3 days after preparation) are shown in Figure 2.7A,B. This sample was heterogeneous with some areas having a distribution of vesicle sizes ranging from 10-70 nm in diameter (Figure 2.7A), consistent with the light scattering results, while other areas had much larger vesicles, some of which were elliptical in shape, as well as membrane fragments (Figure 2.7B). The larger structures presumably arise from fusion of smaller vesicles as has been previously reported for extruded bolalipid dispersions.[105] By contrast, cryo-TEM of extruded vesicles (X_B = 0.5) showed a range of vesicle sizes between 30-200 nm, but no evidence for the larger vesicles or membrane fragments observed for the sonicated vesicles (Figure 2.7C,D). Interestingly, thicker and thinner regions of the membrane could be clearly distinguished for some of the larger extruded vesicles (see arrows in Figures 2.7C,D). This is consistent with the presence of POPC-rich and C_{20}BAS bolalipid-rich regions within the same vesicle.

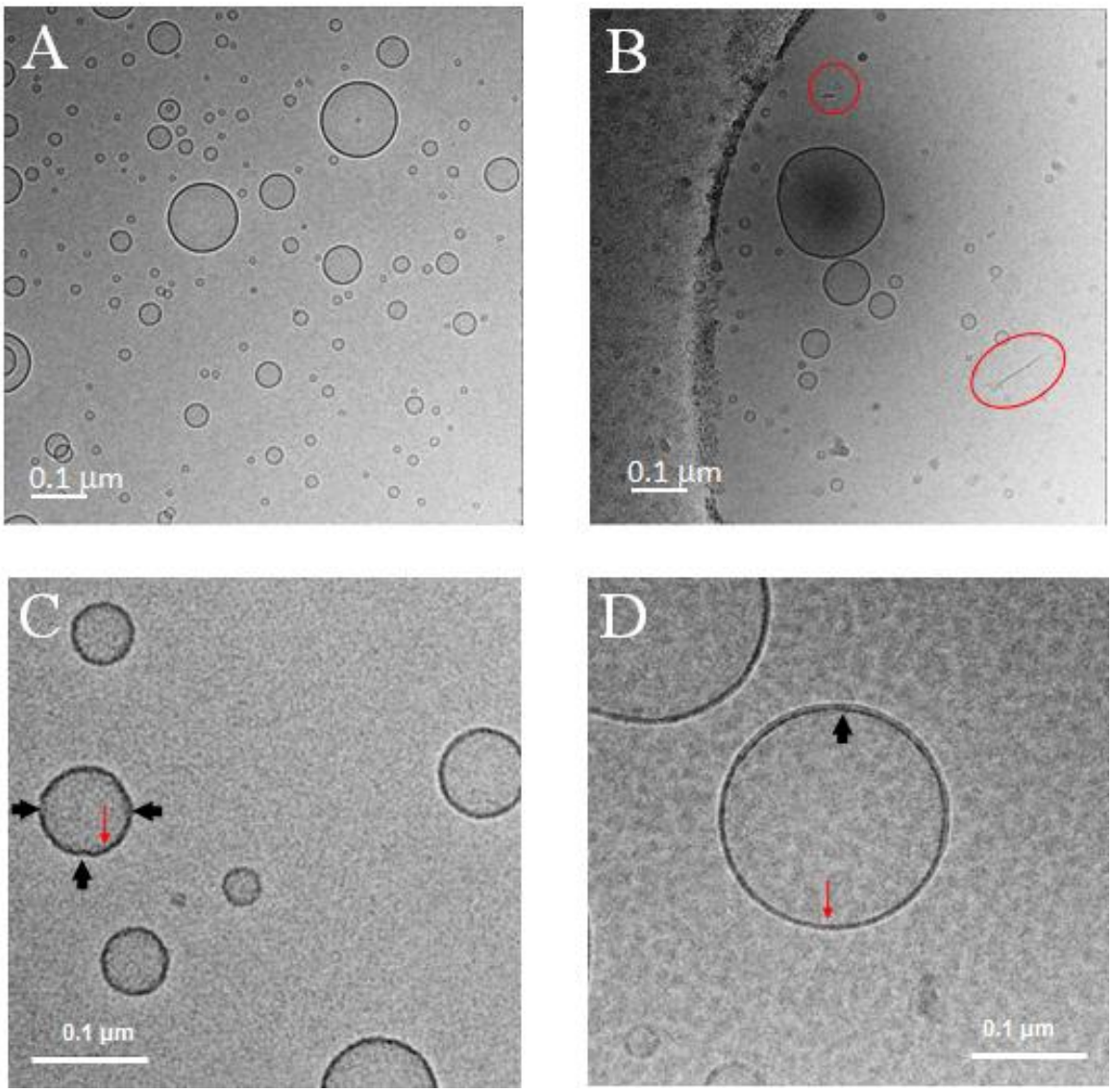

Figure 2.7 CryoTEM images at 50 000x magnification of POPC:C_{20}BAS vesicles (X_B = 0.5, 30 mM total lipid) prepared by sonication (A,B) and extrusion through 200 nm filters (C,D). Image B shows one large irregularly shaped vesicle as well as several membrane fragments (outlined in red). Images C and D show vesicles where there are noticeably thicker and thinner membrane regions, indicate with thick black arrows and thin red arrows, respectively.

2.2.5 AFM Characterization of DMPC:C_{20}BAS Membranes

Supported membranes on mica were also prepared for a DMPC:C_{20}BAS mixture (X_B = 0.4) using both sonicated and extruded (100 nm filter) vesicles. Sonicated vesicles gave a featureless lipid bilayer (Figure 2.8A). By contrast, the supported membrane produced from extruded vesicles had large raised domains (2.2 ± 0.2 nm) surrounded by a uniform lower phase (Figure 2.8B). The domains were interconnected, with irregular perimeters and covered 64 ± 4% of the sample.

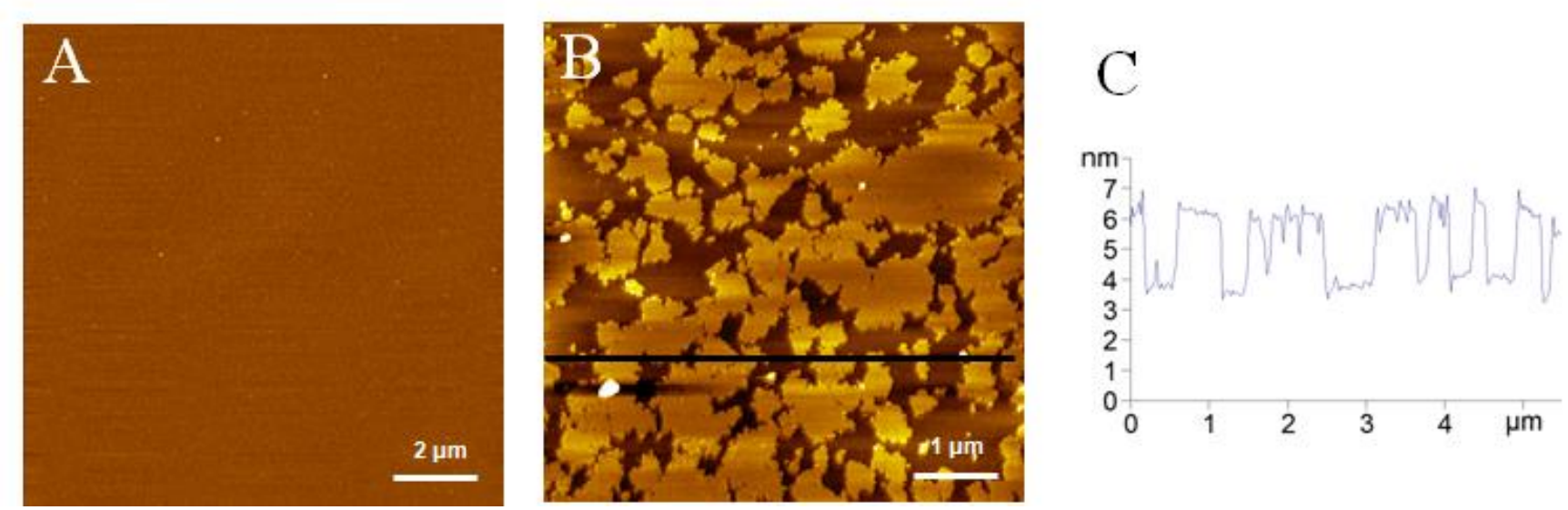

Figure 2.8 AFM images for membranes prepared from extruded (A, 100 nm filter) and sonicated (B) DMPC:C_{20}BAS (X_B = 0.4) vesicles on mica. (C) Cross section for the line marked on image B.

2.3 Discussion of Mixed Bolalipid:POPC Membranes

2.3.1 Mixed POPC:C_{20}BAS Phase Separated Membranes

The AFM results demonstrate that POPC:C_{20}BAS mixtures phase separate to give thicker POPC-rich and thinner C_{20}BAS-rich regions across a range of compositions in supported membranes on solid substrates, an observation that is qualitatively confirmed by cryo-TEM data for their binary lipid mixtures. This is consistent with previous computational and experimental findings that membranes comprised of C_{20}BAS and monopolar lipids with significantly different hydrocarbon chain lengths undergo phase separation due to hydrophobic mismatch.[109,210] The earlier computational study predicted that phase separated membranes would be obtained for approximately equimolar mixtures of bolalipid and monopolar lipids with chain lengths greater than 15 carbons. The calculated miscibility diagram further indicated that mixtures of C_{20}BAS with a C_{18} monopolar lipid would be phase-separated between 20 and 80 mol% bolalipid, in remarkably good agreement with the AFM results we obtained for POPC:C_{20}BAS membranes.[21]

Although POPC-bolalipid membranes exhibit clear phase separation, there are a number of puzzling aspects for the morphologies obtained using different sample preparation methods. First, although the C_{20}BAS bolalipid-rich phase area generally increases with increasing bolalipid content for bilayers prepared from sonicated vesicles, the surface coverage does not follow a uniform trend. Assuming that the area/molecule is similar for both lipids[211], there is more C_{20}BAS bolalipid-rich phase than expected for X_B = 0.6 and 0.5 mixtures and less for the X_B = 0.4 mixture. Second, the membrane morphology (i.e., the size and shape of the POPC-

rich domains and their fractional surface coverage) for some lipid mixtures varies significantly with temperature and with the method of preparation of the vesicles and the supported membranes. One possible explanation for these observations is that the composition of the supported membranes may be significantly different from that of the initial vesicles for some of the sample preparation methods. A change in lipid ratio between the bulk vesicle population and the substrate-supported membrane could occur during membrane formation, either by selective deposition of a compositionally-heterogeneous vesicle sub-population or by exchange between the developing surface-supported membrane and the bulk vesicle solution. Some of the variation in domain morphology may also reflect slow membrane equilibration. The role of these factors in determining the complex morphologies for POPC:C_{20}BAS supported membranes is discussed below.

Formation of supported bilayers from unilamellar vesicles on glass and mica has been studied in detail using AFM and quartz crystal microbalance techniques.[34,221] Following adsorption to the surface, vesicles can (1) remain intact on the surface, eventually giving a layer of adsorbed vesicles; (2) rupture rapidly giving small bilayer disks that then merge with other bilayer patches or promote rupture of adjacent vesicles, eventually forming a continuous membrane; or (3) fuse to give larger vesicles before rupturing to give bilayer patches. The stability of individual adsorbed vesicles depends on their size, lipid composition, solution composition (particularly the presence of divalent cations) and the properties of the surface.

A heterogeneous population of vesicles will lead to a bilayer that does not reflect the bulk lipid composition if one vesicle population adsorbs and ruptures to form membrane patches more rapidly than another. Small unilamellar vesicles prepared by either sonication or extrusion have been used extensively for the preparation of supported bilayers from multi-component lipid mixtures, in most cases with the implicit assumption that both individual vesicles and the supported bilayer have the same lipid ratio as the bulk vesicle solution. However, compositional heterogeneity of vesicles has been reported in some cases. For example, giant unilamellar vesicles prepared from ternary lipid mixtures with co-existing liquid phases occasionally show a mixture of vesicles with and without phase coexistence by fluorescence microscopy; these results have been attributed to differences in lipid composition between vesicles.[222] Similarly, a study of ternary lipid mixtures has concluded that lipid demixing leads to changes in phase diagrams when the vesicle samples are prepared by different methods.[223] It has been suggested that lipid demixing artifacts may be particularly problematic for cholesterol-rich mixtures. The presence of C_{20}BAS bolalipid, which can exist in both transmembrane and U-shaped conformers, may also promote lipid demixing when significant hydrophobic mismatch is present, resulting in a heterogeneous population of vesicles.

The unexpected trends in the percentages of C_{20}BAS-rich surface coverage with increasing bolalipid content for membranes prepared from sonicated vesicles could be partially due to a heterogeneous population of vesicles with different POPC:C_{20}BAS ratios that possess different intrinsic rates of supported membrane

formation. Consistent with this hypothesis, pure POPC vesicles form a continuous membrane much more rapidly than do pure C_{20}BAS vesicles. This can be attributed to the fact that the C_{20}BAS vesicles were smaller than the critical radius for vesicle adsorption and rupture reported for unilamellar vesicles of fluid phosphatidylcholines (PC).[224] This study showed that isolated vesicles with radii <25 nm remained intact on mica, whereas larger vesicles (>75 nm) rapidly ruptured to form bilayer disks. At high lipid concentrations, formation of a supported bilayer from small vesicles (<75 nm) was shown to proceed by fusion of vesicles to give larger vesicles that rupture on the surface. Although cryo-TEM images provide evidence for membranes with two different thicknesses for some larger vesicles, they do not allow us to address the questions of compositional variation in the smaller vesicle population or in the supported membrane itself.

Variations in preparation methods for sonicated vesicles gave consistent membrane morphologies in most cases. However, heating the samples above 50°C during either sonication or incubation did show some differences. Although membranes were still microphase separated, the surface coverage of POPC-rich and C_{20}BAS-rich domains was different and there were more membrane defects apparent. These changes may be due to a higher contribution of the bolalipid U-shaped conformer at higher temperature, consistent with the observations reported in ^{2}H NMR studies of POPC:C_{20}BAS mixtures.[210] In spite of the increased population of U-shaped conformers that occurs at elevated temperatures, ^{2}H NMR results showed that these conformers were capable of relaxing into the transmembrane conformation upon cooling the vesicle dispersion to room

temperature. This relaxation process may be more difficult, however, for supported membranes that may possess a significant fraction of pinned lipids.

The morphology of membranes prepared from extruded POPC:C_{20}BAS vesicles was significantly different from that obtained for sonicated vesicles with X_B = 0.4, with a much lower coverage of the POPC-rich phase and the formation of relatively large domains. POPC:C_{20}BAS membranes prepared from extruded vesicles with X_B = 0.5 and 0.6 were also significantly different than those for the corresponding sonicated samples, with small islands of POPC-rich phase present in the sonicated vesicle samples, but uniform featureless membranes arising from extruded vesicle samples. Heterogeneous sizes and compositions of vesicles prepared by sonication and extrusion may partially account for these results.

Several observations indicate, however, that vesicle heterogeneity is unlikely to be the only factor that contributes to the complex sample morphologies that were observed for POPC:C_{20}BAS supported membranes. For example, there is a larger fraction of the C_{20}BAS bolalipid-rich phase than expected for X_B = 0.6 and 0.5 mixtures and less for the X_B = 0.4 mixture. This cannot be explained simply by POPC-rich vesicles forming a membrane more rapidly than bolalipid-rich vesicles. Furthermore, the 1:1 physical mixture of pure POPC and pure C_{20}BAS vesicles would be expected to give a predominantly POPC membrane, based on the faster kinetics for membrane formation from POPC vesicles. The observation of a supported membrane with a relatively small fraction of POPC-rich phase requires a mechanism for lipid scrambling, either by rapid fusion of small adsorbed vesicles to produce larger vesicles that rupture to give membrane patches or by lipid exchange

between the surface and vesicles in solution during or after membrane formation. In this regard, neutron diffraction studies have shown that DOPC:DPPC bilayers on silica have a substantially different composition from the bulk vesicles, with an enrichment of DPPC in the lower leaflet.[225] These results were attributed to exchange of material between the surface bilayer and the bulk vesicle solution during bilayer formation. In agreement with this hypothesis, lipid exchange between small unilamellar vesicles containing charged lipids and supported bilayers has also been observed.[226,227] It is plausible that adsorbed C_{20}BAS vesicles undergo an accelerated fusion and planar surface deposition that is facilitated by the presence of the more dynamic POPC component.

In most cases, the domains for POPC:C_{20}BAS membranes are small (<100 nm) and do not coalesce to give larger domains when the membrane is stored at room temperature for 1 day or is heated to 50°C. The observed domain size is consistent with the estimates of >50 nm from NMR and SAXS data for POPC C_{20}BAS dispersions.[5] However, these results differ from data for a variety of phase separated bilayers composed of binary and ternary lipid mixtures, which typically have domain sizes ranging from several hundred nanometers up to tens of micrometers.[219,220] Domain sizes are determined by the balance between entropy, line tension at the domain perimeter and long-range dipole-dipole repulsion. Several recent studies have demonstrated that line tension increases with increasing hydrophobic mismatch between the domain and the surrounding membrane, and decreases in the presence of cholesterol.[228-230] A quantitative model for creation and evolution of domains in multicomponent bilayers predicts that for sufficiently

small line tensions (1) the decrease in the entropy term that results from domain merger is larger than the decrease in boundary energy; and (2) nanodomains are in quasi-equilibrium and do not increase in size. [231,232] At high line tension, however, nanodomains rapidly merge to give larger micron-sized domains because the decrease in boundary energy dominates the unfavorable entropy of merger. Based on the dependence of line tension on hydrophobic mismatch for binary and ternary lipid mixtures,[229,230,233] the >1 nm hydrophobic mismatch for C_{20}BAS/POPC mixtures would be predicted to give a relatively high line tension, thus favoring large domain size. This contrasts with our results for POPC:C_{20}BAS membranes prepared from sonicated vesicles, although it is not clear if one can extrapolate line tension behavior from bilayer membrane lipid mixtures to bolalipid membranes with predominantly transmembrane conformations.

An alternate possibility is that pinning of the bolalipid to the support prevents equilibration and limits the domain size. Coupling of domains to the surface is affected by the ionic strength of the aqueous medium, with the presence of salts helping to decouple the bilayer from the underlying support.[234,235] Bilayers are frequently prepared in the presence of Ca^{2+}, which promotes vesicle rupture and may reduce pinning of the lipids to the underlying support. We have avoided the use of Ca^{2+} in these experiments since it may affect the equilibrium between transmembrane and U-shaped bolalipid conformers in a manner that is not presently understood. This choice may have contributed to increased pinning of individual lipids onto the solid substrate, thereby resulting in small domains for sonicated vesicles and irregular domain boundaries for membranes prepared from

larger extruded vesicles. Experiments to relieve pinning with the addition of detergent were attempted, but, were unsuccessful. It is also possible that the formation of featureless membranes for some samples reflects very slow domain nucleation and growth from POPC:C_{20}BAS supported membranes, so that a membrane containing both lipids does not appear phase-separated, even at the spatial resolution of AFM. This is consistent with the expectation that domain growth may be slower for transmembrane bolalipids than for monopolar lipids.

Finally, we have shown that DMPC:C_{20}BAS membranes (X_B = 0.4) produce qualitatively similar results to those for POPC:C_{20}BAS, with phase-separated and apparently uniform membranes observed for extruded and sonicated vesicles, respectively. The similar behavior for phosphatidylcholine lipids with either saturated or unsaturated hydrocarbon chains could indicate that pinning of the lipid head groups is a dominant factor in controlling membrane morphology. Nevertheless, the large difference between sonicated and extruded vesicles argues for involvement of vesicle heterogeneity and/or lipid exchange, and we hypothesize that the same factors are responsible for variations in morphology of membranes prepared from mixtures of C_{20}BAS bolalipid with either POPC or DMPC.

2.3.2 Summary of Mixed Bolalipid:POPC Membranes

Microphase separated membranes prepared from mixtures of POPC and C_{20}BAS bolalipid have been examined in detail by AFM. The results indicate that the membrane morphology varies significantly for these samples as a function of

the methods used to prepare vesicles and supported membranes. We infer from our findings that the membrane lipid composition is different from that of the bulk vesicle solution for at least some of the sample preparation methods, leading to complex changes in membrane morphology. Further experiments are needed to discern whether the ratios of monopolar lipid and bolalipid are changing during the deposition process and whether appreciable partial mixing of the lipids in the microphase separated state is occurring. It is conceivable that processes involving selection of a subset of vesicles from an initial compositionally heterogeneous vesicle sample and exchange of lipid between the solid surface and the bulk solution may also be occurring during membrane formation to contribute to the observed effects. Finally, the small domain size obtained for some samples probably reflects pinning of lipids to the support, resulting in slow sample equilibration. This complex interplay of factors means that it is quite difficult to control the morphology of supported membranes prepared from POPC:C_{20}BAS mixtures, an important observation in the context of applications of bolalipid mixtures for membrane biosensing. Whether this is related to the large hydrophobic mismatch between POPC and C_{20}BAS or is an inherent property of transmembrane bolalipids remains to be determined.

2.4 Experimental

2.4.1 Materials

C_{20}BAS was synthesized as described previously.[211,216] 1-Palmitoyl-2-oleoylphosphatidylcholine (POPC) and 1,2-dimyristoylphosphatidylcholine (DMPC) were obtained from Avanti Polar Lipids and were used as received. All aqueous solutions were prepared with 18.3 MΩ·cm Milli-Q water. All other materials were obtained from Aldrich (≥98% pure) and used as received.

2.4.2 Preparation of Small Unilamellar Vesicles

Separate 5 mM chloroform stock solutions of POPC and C_{20}BAS were mixed in the appropriate ratios, the solvent was removed and the film was dried under vacuum overnight. The lipid films were then hydrated in water and vortexed to obtain multilamellar vesicles. Vesicles were formed either by sonication or extrusion. Sonicated samples were prepared from the multilamellar vesicles using a bath sonicator with an initial temperature of 20 ºC (or between 20-60 ºC, as noted in the text) to form clear dispersions of small unilamellar vesicles with a final lipid concentration of 1mg/mL. Extruded vesicles were formed by passing multilamellar vesicle suspensions (250 µL) 11 times through polycarbonate membranes with pore sizes of 100, 200 or 400 nm using a Liposofast extruder. Vesicles were used immediately after their formation for the preparation of supported membranes.

2.4.3 Preparation of Supported Membranes

Aliquots of vesicle solution (50 µL) and Milli-Q water (400 µL) were added to freshly cleaved mica clamped into a Molecular Imaging AFM liquid cell. After incubation at room temperature for 3 hours, the bilayers were rinsed extensively with Milli-Q water to remove unattached vesicles before imaging. Scanning at high force with the AFM tip over a small area in MAC-mode to create a bilayer defect allowed us to measure the bilayer thickness, confirming the presence of a single bilayer. For higher incubation temperatures, samples were incubated at the desired temperature for 2 hours and then cooled to room temperature at a rate of 20 ºC/h. For experiments involving detergent, bilayers were formed and 10 nM octyl glucoside (10 µL) was added to the AFM cell. In some experiments membranes were prepared on n-type silicon (111) wafers polished on one side with a thickness of 250 ± 25 µm and a resistance of 1.0-5.0 Ohm•cm. The silicon was cleaned using a standard piranha solution (3:1 sulfuric acid:hydrogen peroxide) for 20 minutes at 120 ºC. The wafers were then rinsed using copious amounts of Milli-Q water and stored in water until further use.

2.4.4 Atomic Force Microscopy

The AFM images were obtained at room temperature (23 ± 1 °C) using a PicoSPM atomic force microscope (Molecular Imaging) in MAC-mode. Magnetic coated silicon tips with spring constants of ~0.5 N/m and resonance frequencies between 5 and 40 kHz in aqueous solution were used. A 30 x 30 μm^2 scanner was operated at a scan rate between 0.7 and 1.3 Hz. The images shown are flattened

raw data. Two or more independently prepared samples were imaged for each bilayer composition, with several areas scanned for each sample. Reported heights are based on averaging data for at least two independent samples with a minimum of 9 areas imaged.

2.4.5 Dynamic Light Scattering

Vesicle samples were diluted, typically ~1:10, with Milli-Q water prior to DLS measurements. Vesicle size distributions were determined using a Nicomp Model 370 Laser Particle Sizer (Nicomp Instruments, Santa Barbara, CA) which utilized a measurement angle of 90º and a 5mW Ne laser operating at 632.8 nm.

2.4.6 Cryo-TEM

C_{20}BAS:POPC liposomes (1:1 mol:mol, 30 mM total lipid concentration) were extruded 11 times through 200 nm track-etch membranes. The liposome solution was then transferred by pipet to a bare Quantifoil grid, the excess blotted away using filter paper, and the sample vitrified in liquid ethane slush cooled by liquid nitrogen. The grid was then transferred to a Philips CM200 transmission electron microscope equipped with a liquid nitrogen-cooled stage and a field-emission gun operating at 200 kV accelerating voltage. The cryoTEM images were collected at 50,000x magnification under low dose conditions to minimize radiation damage to the samples.

Chapter 3: Supported Lipid Bilayers on Biocompatible PEMs[236]

This chapter contains Material Adapted from the following manuscript

1. K. Mulligan, Z. J. Jakubek, and L. J. Johnston; Supported Lipid Bilayers on Biocompatible Polysaccharide Multilayers; Langmuir, **2011**, *23*, 14352

3.1 Supported Lipid Bilayers on Polymer Cushions

Solid-supported phospholipid bilayers are widely used as models to understand the function of cellular membranes and as platforms for membrane protein biosensing applications based on electrical or optical detection.[1,58,113] Supported lipid bilayers have a number of advantages over other types of model membranes however, the proximity of the membrane to the solid support is a major limitation for applications that involve incorporation of integral membrane proteins. Interactions with the underlying solid surface interfere with both the lateral mobility and function of the protein. Several approaches have been employed to decouple the supported bilayer from the underlying support. One method utilizes modified lipids in which the head groups have long chain tethers that can be covalently attached to the underlying surface, thus providing space under the bilayer to accommodate bulky membrane domains.[37,237,238] Tethers are usually attached to the surface using either silane or gold-thiol chemistry. A second and more widely used approach is to construct lipid bilayers on soft polymer cushions.[112,113,239] In some cases bilayers are constructed directly on top of thin layers of surface adsorbed polymers, such as cellulose, or a surface grafted polymer.[114,124] Another method involves the use of polymer spacers which have one end attached to lipid head groups and the other end functionalized for surface attachment using either radical or silane chemistry.[136,137] This method provides flexibility to modify the thickness and viscosity of the polymer layer, but requires a multi-step fabrication process with the initial construction of the polymer layer and lower membrane leaflet by Langmuir-Blodgett transfer of a monolayer containing the polymer-modified lipid;

this is followed by addition of the upper bilayer leaflet by either vesicle fusion or Langmuir-Schaeffer transfer of a second lipid monolayer and finally treatment to covalently attach the polymer layer to the surface. Several recent studies have shown that covalent attachment of the polymer to the surface is not essential, somewhat simplifying the procedure.[143,153,180,240] Nevertheless, the requirement for lipid-polymer conjugates, and the complex assembly (relative to vesicle fusion methods) are limitations for eventual scale-up and/or multiplexing for biosensing applications.

3.1.1 Supported Lipid Bilayers on Polysaccharide PEMs

Polyelectrolyte multilayers (PEMs) provide an interesting alternative to other types of polymer cushions. Several studies have shown that stable supported lipid bilayers can be formed on PEMs composed of alternating layers of polystyrenesulfonate (PSS) and poly-(allylamine hydrochloride) (PAH).[127-129] Charged polysaccharides are also well-known to form PEMs by the layer-by-layer assembly method.[164,165] The biocompatibility, ready availability and low cost of charged polysaccharides have made them attractive choices for a range of applications, including drug delivery vehicles based on lipid-polyelectrolyte particles, biocompatible surfaces for controlling cell growth and tissue biomimetics.[165-170]

In this chapter, we have examined the suitability of PEM films constructed from alternating layers of chitosan (CHI) and hyaluronic acid (HA) as polymer cushions for supported lipid bilayers (Figure 3.1). Although polysaccharide-lipid

interactions have been exploited for drug delivery applications, to the best of our knowledge polysaccharide PEMs have not been used as supports for lipid bilayers. Hyaluronic acid is an anionic linear polysaccharide (pKa ~3.0) with a repeating disaccharide structure consisting of 2-acetamide-2-deoxy-β-D-glucose and β-D-glucuronic acid residues.[241] HA is found in the extracellular matrix of all higher animals and has been shown to affect cellular functions such as migration, adhesion, and proliferation. Chitosan is a random copolymer of *N*-acetyl-β-D-glycosamine and β-D-glycosamine that is obtained by deacetylation of chitin and has a pKa of ~6.5.[242] CHI/HA PEMs were prepared and characterized by atomic force microscopy (AFM) and ellipsometry and used as substrates for preparation of supported DOPC bilayers by vesicle fusion. Bilayers were characterized by a combination of AFM, fluorescence microscopy and fluorescence recovery after photobleaching (FRAP). The results show that the formation of bilayers with mobile lipids is dependent on the pH used for bilayer preparation. At pH 6.5 heterogeneous bilayers with slowly diffusing lipids and large immobile fractions are formed; we conclude that a combination of the surface roughness of the underlying polymer and pinning of individual lipids may contribute to the complex behavior. By contrast, uniform bilayers with diffusion coefficients that are similar to bilayers on glass and other polymer supports are obtained at pH 4, indicating the utility of polysaccharide PEMs for preparation of supported lipid bilayers.

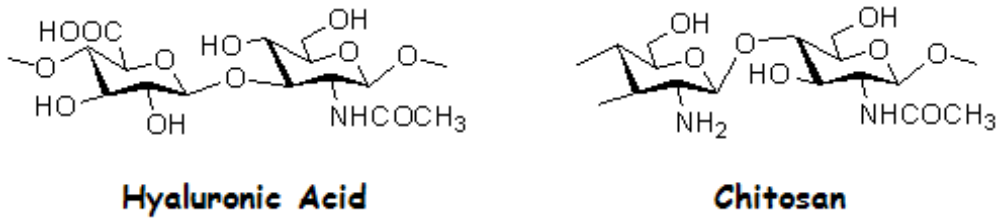

Figure 3.1 Structures of charged polysaccharides used to PEMs

3.2 Supported Lipid Bilayers Formed on CHI/HA PEMs

3.2.1 Preparation and Characterization of CHI/HA Films

The assembly of PEM films composed of alternating layers of HA and CHI has been examined in considerable detail by several groups.[164,165,167,243-245] Based on the literature data we selected films consisting of 5 bilayers, starting with adsorption of CHI to either glass or silicon surfaces; this selection provided a reasonable compromise between having a polymer film of sufficient thickness to provide good surface coverage while minimizing the surface roughness, which tends to increase with film thickness. We also reasoned that the use of a negatively charged top HA layer would be the most suitable for forming bilayers of zwitterionic lipids based on the rapid formation of bilayers by vesicle fusion on hydrophilic, negatively charged surfaces such as mica and glass.[34] AFM images of a $(CHI/HA)_5$ film on a glass substrate imaged in water (pH 6.5) are shown in Figure 3.2A,B. The film surface is covered with densely packed, round or slightly elliptical features that range in height from ~20 nm to ~150 nm, with typical widths of several hundred nanometers. The film thickness was assessed by scratching away part of the film to

expose the bare substrate and measuring the step height by AFM, as shown in a representative image in Figure 3.2C. The average thickness and rms roughness of the $(CHI/HA)_5$ polymer film were found to be 57±3 nm and 25±2 nm, respectively, Table 3.1. For comparison, films were also prepared by sequential addition of 5 CHI/HA bilayers to glass coated with a poly(ethyleneimine) (PEI)/HA bilayer; similar film morphology, thickness and surface roughness were measured, indicating that there was no particular advantage to the presence of the initial PEI surface layer. Since bilayer formation was attempted at several pHs, the $(CHI/HA)_5$ film thickness and roughness were also measured at pH 4; a reduced film thickness and roughness of 31±4 nm and 15±3 nm were obtained. Previous studies have shown that HA/CHI films are stable in contact with aqueous solutions with pH between 3.5 and 9, and show modest changes in thickness over this range.[243] The films are not stable in more basic or more acidic solutions, since neutralization of one of the polyelectrolytes leads to a charge imbalance that destroys the film.[243]

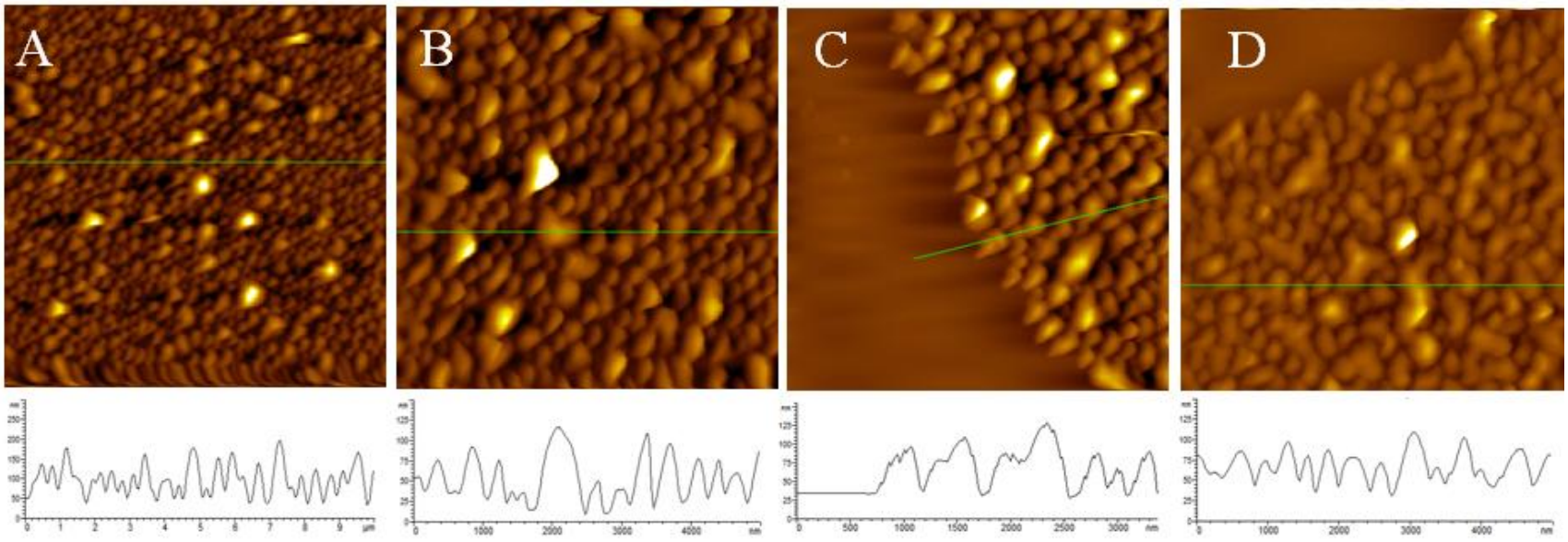

Figure 3.2 AFM images of $(CHI/HA)_5$ polymer films on a glass substrate imaged in water at pH 6.5. Images B and C show samples before and after scratching away part of the polymer film. Image D is for $(CHI/HA)_5$ on silicon.

Table 3.1 Surface thickness and RMS roughness measured by AFM for CHI/HA films on various supports.

PEM-Support	pH	Thickness (nm)	RMS (nm)
glass	4.0-6.5	--	1±0.2
$(CHI/HA)_5$ – glass	6.5	57±3	25±2
$(CHI/HA)_5$ – glass	4.0	31±4	15±3
PEI/HA/$(CHI/HA)_5$ – glass	6.5	54±4	25±3
$(CHI/HA)_5$ – silicon	6.5	52±5	23±2

For comparison, $(CHI/HA)_5$ polymer films were prepared on a silicon (111) substrate. The representative AFM image shown in Figure 3.2D indicates a similar film morphology to that obtained on glass, although the raised features were more elongated and interconnected. The thickness and rms roughness of the $(CHI/HA)_5$ polymer film were found to be 52±5 nm and 23±2 nm, respectively. Ellipsometry was used to measure an average thickness of 32±4 nm for a dry $(CHI/HA)_5$ film on silicon (111).

The film thickness and morphology are analogous to those reported in the literature for CHI/HA films prepared under similar conditions. For example, Picart and coworkers obtained films with comparable structures as assessed by AFM for $(CHI/HA)_n$ films, although neither film thickness nor roughness was reported for a sample with n = 5 bilayers.[165] Winnik and coworkers prepared films with similar morphologies on a PEI-coated thiol monolayer formed by self-assembly on a gold surface; for PEI-$(HA/CHI)_5$ films they report surface thickness and roughness of 70 nm and 20 nm, respectively.[244] These results are in good agreement with those obtained here considering the differences in the substrate and the molecular weight

of the polyelectrolytes and the opposite charge for the top polyelectrolyte layer in the two cases. Previous studies have shown that PEM film formation occurs by initial formation of small individual islands that grow in size and eventually coalesce as additional polyelectrolyte is adsorbed on or between them.[165] The slight change in film morphology observed for films on glass and silicon indicates that for our experimental conditions the adsorption of 5 bilayers is close to the transition between growing islands and interconnected structures.

3.2.2 Formation of DOPC Bilayers on $(CHI/HA)_5$ Films

In initial attempts to form supported bilayers on $(CHI/HA)_5$ films, DOPC vesicles containing 0.2 mol % TR-DHPE were incubated with polymer-coated glass in water in the presence of 10 mM $CaCl_2$ and 140 mM NaCl overnight at pH 6.5, followed by extensive washing to remove adsorbed vesicles. Fluorescence microscopy was used to assess the quality of the adsorbed lipid sample. As shown in Figure 3.3A, the samples showed patchy fluorescence with occasional small dark areas and bright features that are assigned to defects and adsorbed vesicles, respectively. For comparison a TR-DHPE-labeled DOPC bilayer on glass is shown in Figure 3.3B; the DOPC bilayer on glass is significantly more uniform than the membrane obtained on the PEM film. In order to test for lipid mobility a FRAP experiment was attempted for a bilayer labeled with 0.2 mol % OG-DHPE on a $(CHI/HA)_5$ film (Figure 3.3C). Images before and after photobleaching are shown in Figure 3.4, along with a plot demonstrating a large immobile lipid fraction. Replicate experiments on several samples indicated that the mobile lipid fraction was typically

between 10-30%, with diffusion coefficients, D, that varied between 0.1 and 0.5 $\mu m^2/s$. For comparison, FRAP experiments for OG-DHPE in DOPC bilayers prepared by vesicle fusion on glass gave a diffusion coefficient of 4.4 $\mu m^2/s$ (Table 3.2) with a mobile fraction of ~100%. Literature values for D for fluid-phase supported lipid bilayers on either glass or mica are in the range of 1-6 $\mu m^2/s$, depending on the lipid, substrate and presence of salt and buffer.[28,246]

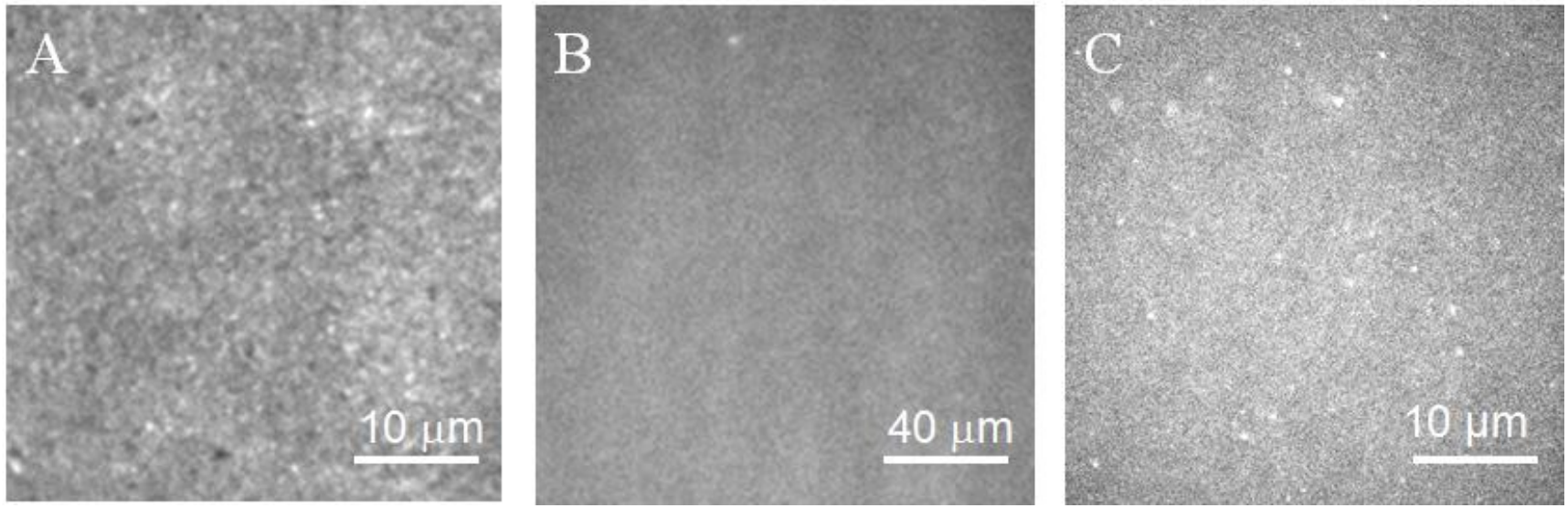

Figure 3.3 Fluorescence images of membranes obtained by incubating DOPC vesicles containing 0.2 mol% Texas Red-DHPE (A,B) or OG-DHPE (C) on a $(CHI/HA)_5$ polymer film (A, C) on a glass substrate and on glass (B). Samples were prepared by incubation at pH 6.5

Table 3.2 Diffusion coefficients, D, and mobile lipid fractions, F, obtained by FRAP measurements for OG-DHPE in DOPC bilayers on various supports.

Support	pH	D ($\mu m^2/s$)	F (%)
Glass	6.5	4.4±0.3	>99
$(CHI/HA)_5$	6.5	0.3±0.4	20±14
$(CHI/HA)_5$	6.5[#]	<0.05	>5
$(CHI/HA)_5$	7.0[##]	2.8±0.2	>99
$(CHI/HA)_5$	4.0	2.49±0.07	>99
PEG	4.5	2.16±0.07	>99

[#]Bilayer was formed and FRAP experiment was performed after the addition of Co^{2+}. [##]Bilayer prepared at pH 4 and then washed with pH 7 buffer prior to FRAP experiment.

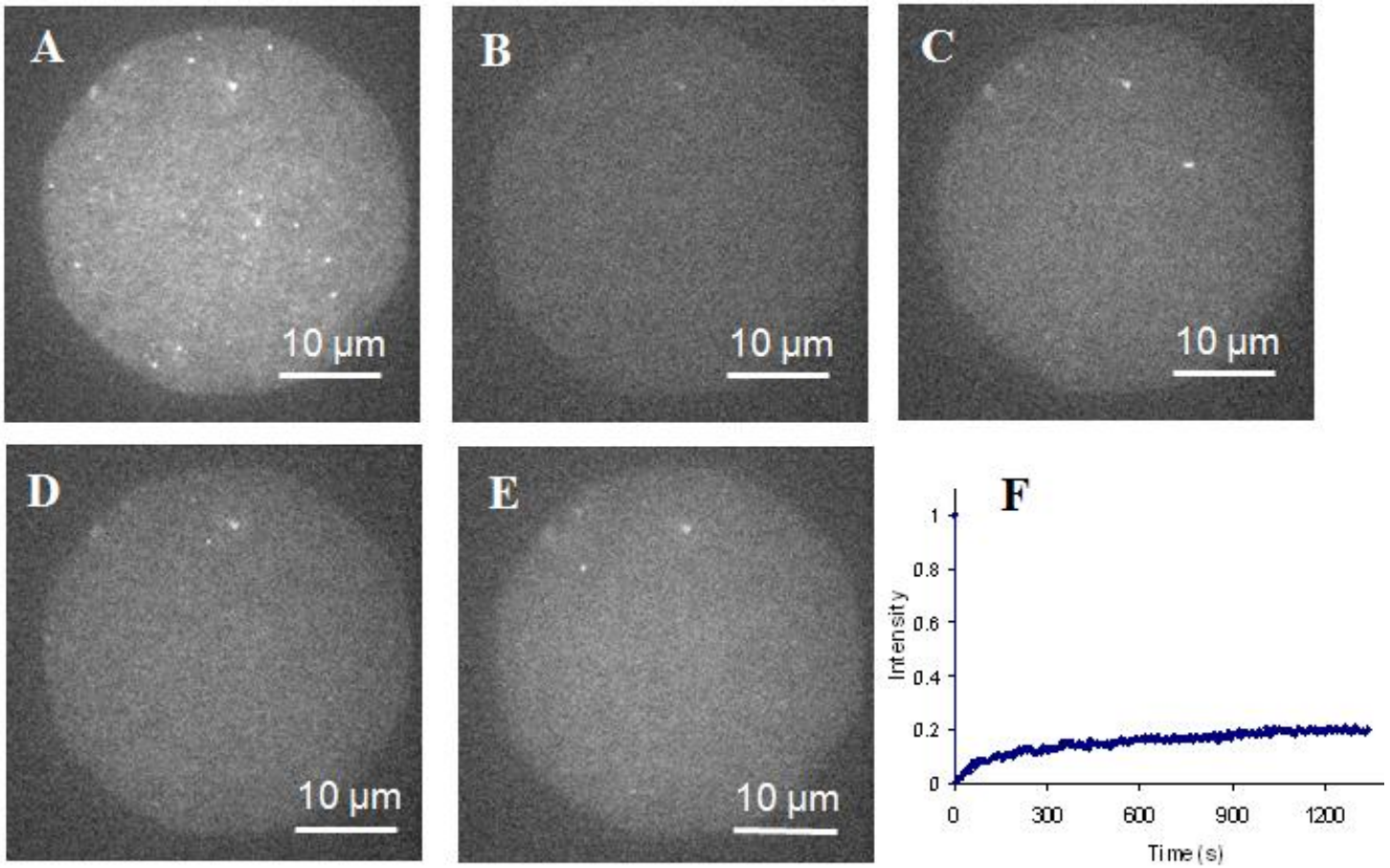

Figure 3.4 FRAP experiment for a membrane obtained by incubating DOPC vesicles containing 0.2 mol% Oregon Green-DHPE on a $(CHI/HA)_5$ polymer film on glass: A, before bleaching; B, immediately after bleaching; C, D, E at 118, 183 and 1330 s after bleaching. F shows a plot of fluorescence intensity as a function of time, demonstrating a large immobile lipid fraction.

The low diffusion coefficients, large fraction of immobile lipids and variable results for individual samples could indicate a significant fraction of surface adsorbed vesicles that have not ruptured and fused to give a supported membrane. Alternately, this observation may reflect the formation of a heterogeneous bilayer with many small defects and/or with lipids pinned to the underlying polymer. In order to distinguish between these possibilities, a similar sample was imaged by AFM, Figure 3.5. The images show an uneven surface that reflects the roughness of the initial polymer surface. However, the measured roughness of 17±3 nm is significantly smaller than that for the initial hydrated PEM film (>50 nm), and the surface morphology shows no evidence for the presence of a layer of surface-adsorbed vesicles. The combined results from the fluorescence imaging, FRAP and AFM analysis suggest that incubation of DOPC vesicles with $(CHI/HA)_5$ films at pH 6.5 gives a surface adsorbed bilayer with a large fraction of immobile lipids, either due to numerous defects, the presence of a rough polymer surface or lipid pinning to the PEM film. Note that the surface roughness makes it impossible to detect small membrane defects that would normally be observable by AFM for bilayers on glass or mica.

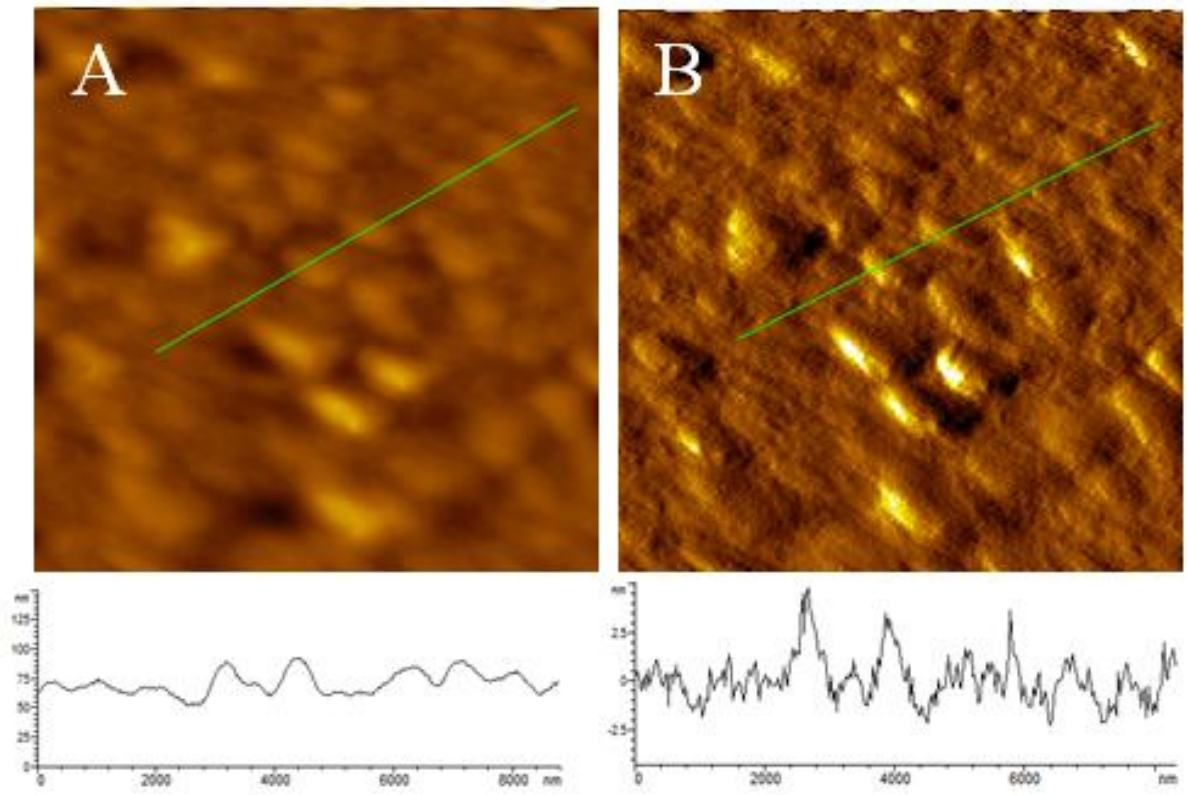

Figure 3.5 AFM images of a membrane prepared by incubating DOPC vesicles on a $(CHI/HA)_5$ polymer film on glass at pH 6.5: A, height; B, deflection.

An additional fluorescence quenching experiment was carried out to probe whether differences in the distribution of dye between the two bilayer leaflets contributed to the variable results for lipid mobility and mobile fraction. Cobalt ions have been shown not to penetrate lipid bilayers at concentrations below 100 mM[247] and are thus compatible with selectively quenching fluorophores in the top leaflet of a supported bilayer.[248] Fluorescence images were measured for a DOPC bilayer on a $(CHI/HA)_5$ film at pH 6.5 before and after addition of 50 mM $CoCl_2$ (Figure 3.6A,B). The total intensity decreased by 50 ± 5 % (average of two experiments) after adding Co^{2+}, indicating that approximately half of the dye was accessible to the

quencher, presumably due to its location in the top leaflet of the bilayer (Figure 3.6). A FRAP experiment for a bilayer at pH 6.5 before Co^{2+} addition gave D = 0.5 $\mu m^2/s$, with a mobile fraction of 44% (Figure 3.6C); a FRAP experiment for the same bilayer after the addition of Co^{2+} showed no recovery of photobleaching over the same time period, indicating D < 0.05 $\mu m^2/s$ (Figure 3.6D). These experiments indicate that lipid pinning of the lower bilayer leaflet is a major contributor to the slow lipid diffusion and variable mobile fractions for DOPC bilayers on PEM films.

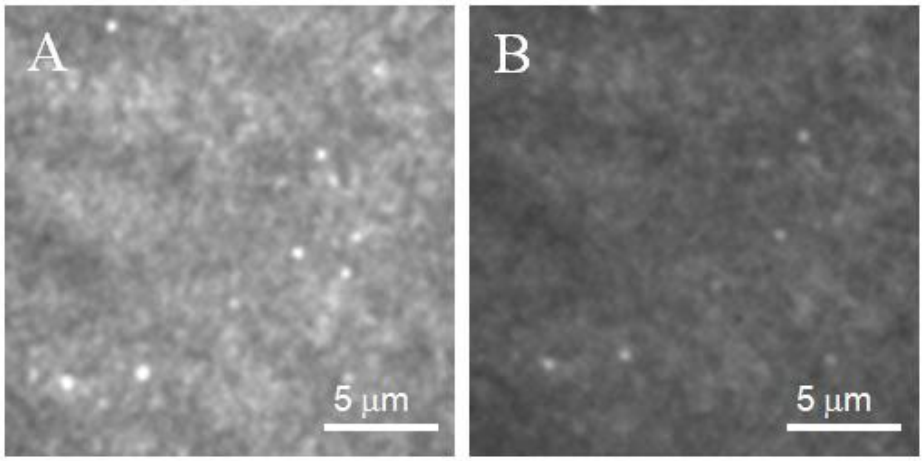

Sample	Mean Intensity	Corrected Intensity
Defect in Sample (background)	872	
DOPC/PEM pH 6.5 before Co^{2+}	2464	1592
DOPC/PEM pH 6.5 after Co^{2+}	1668	796

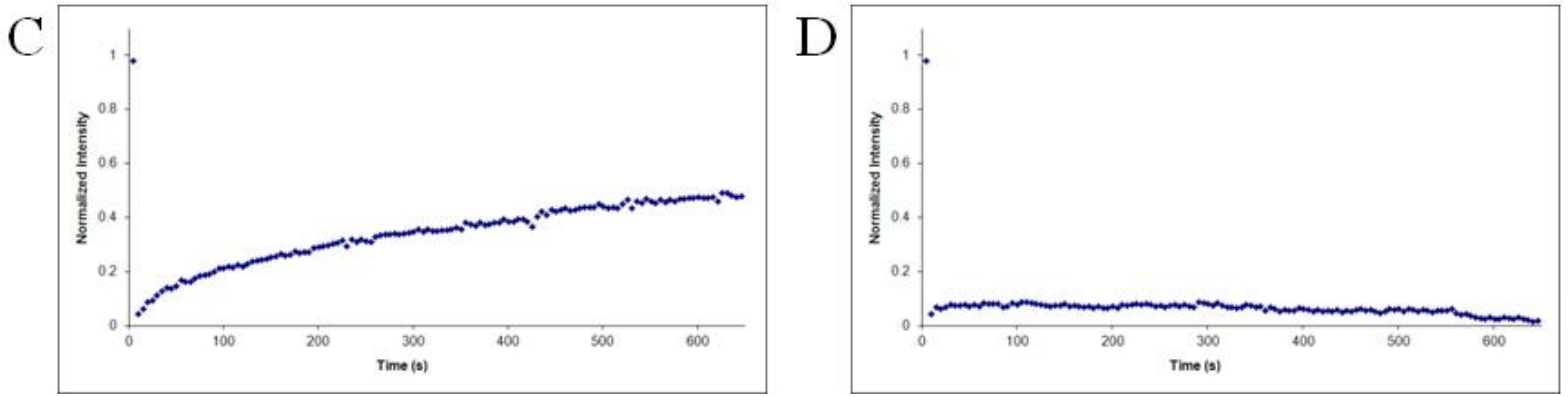

Figure 3.6 Fluorescence images of bilayers obtained by incubating DOPC vesicles on a $(CHI/HA)_5$ polymer film on glass (A, Oregon Green-DHPE) at pH 6.5 followed by the addition of 50 mM Co^{2+} (B). Fluorescence intensity measurements and FRAP recovery curves before (C) and after (D) the addition 50 mM Co^{2+}.

The formation of lipid bilayers by vesicle fusion is very sensitive to the surface properties, including charge, with surfaces such as glass, mica or silicon being the most widely used.[34] A recent study has shown that adjusting the surface charge by varying pH is a useful approach to promote formation of a homogeneous bilayer on a surface-grafted film of maleic acid copolymers; in this case variation of the pH was used to minimize electrostatic repulsion between vesicles with 20% negatively charged lipids and the negatively charged polymer layer.[114] Similarly, systematic variation of the surface charge density using functionalized alkanethiol self-assembled monolayers demonstrated that there is an optimal charge density for formation of supported bilayers from PC vesicles.[249] Although neither of these examples is identical to the current system of charged polyelectrolytes, we tested the impact of varying the pH within the range of stable CHI-HA films on the quality of the bilayers. TIRF images for a $(CHI/HA)_5$ film incubated with DOPC vesicles (labeled with either TR-DHPE, A or OG-DHPE, B) at pH 4 are shown in Figure 3.7. The bilayers are slightly more homogeneous than those formed at pH 6.5, although occasional defects and adsorbed vesicles are still visible. However, in this case the lipid mobility was considerably higher, as assessed by FRAP experiments. A representative experiment is shown in Figure 3.8, demonstrating complete recovery of the bleached area, with D = 2.49 $\mu m^2/s$, Table 3.2. The measured diffusion coefficient is approximately half that measured for DOPC on glass, indicating relatively minor effects of the PEM support on lipid diffusion. The surface roughness may partially account for the lower apparent diffusion coefficient since

the actual surface area covered by the bilayer is larger than the area of the bleached spot.

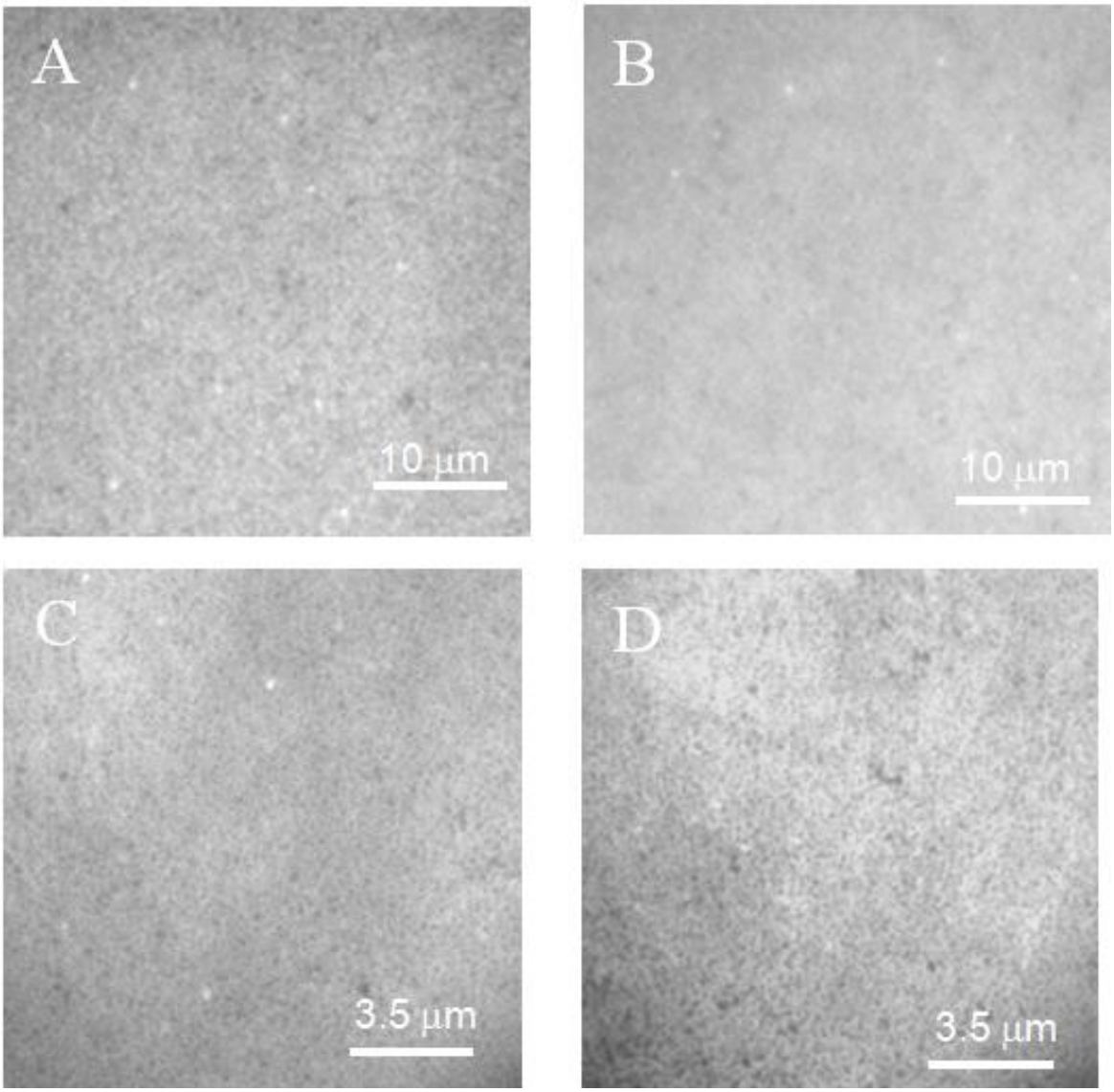

Figure 3.7 Fluorescence images of bilayers obtained by incubating DOPC vesicles on a $(CHI/HA)_5$ polymer film on glass (A, Texas Red-DHPE; B, Oregon Green-DHPE) at pH 4. (C,D) Fluorescence images obtained at higher magnification (150x) for DOPC (C) and DOPC/egg sphingomyelin/cholesterol (D) vesicles incubated on $(CHI/HA)_5$ polymer films.

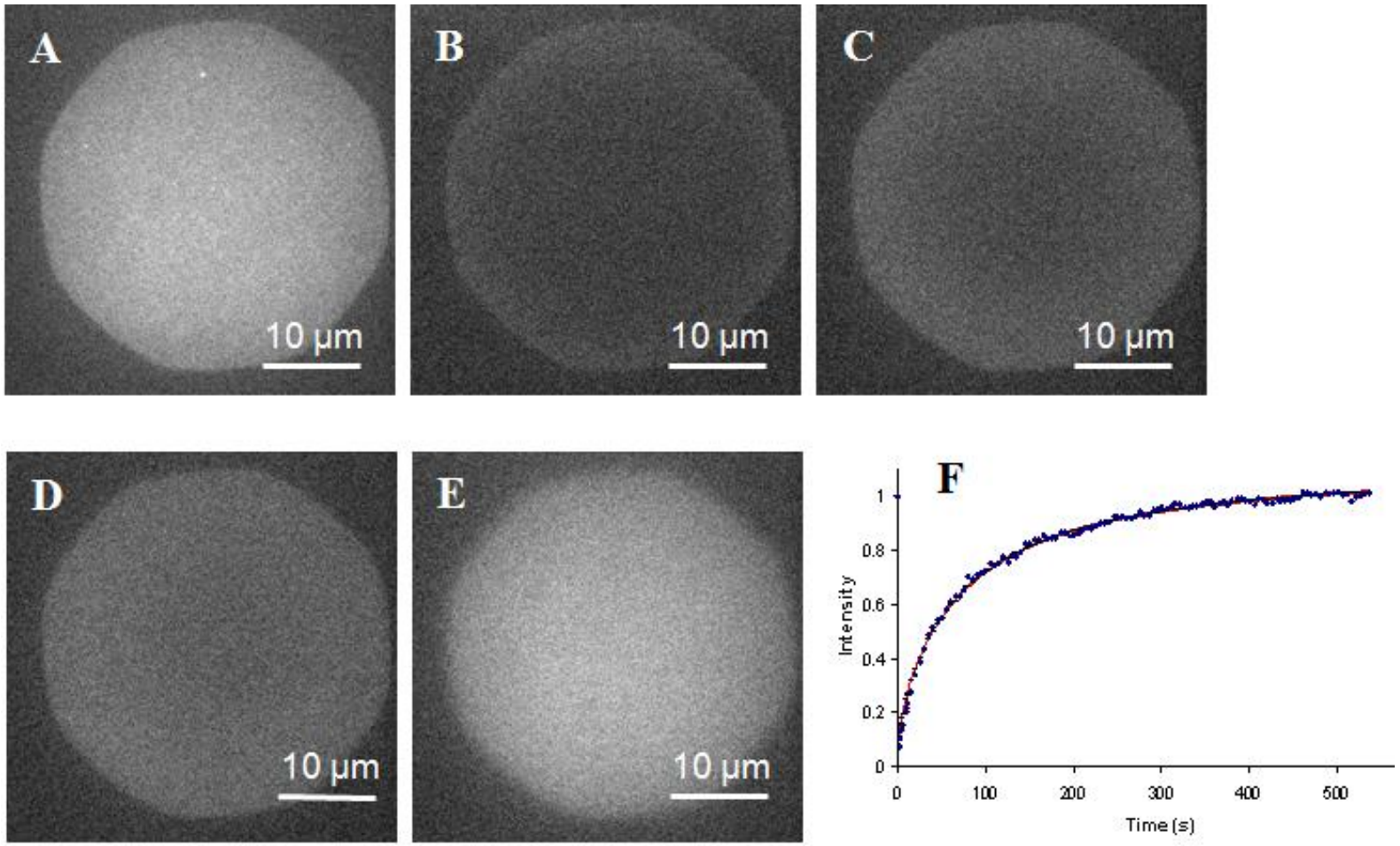

Figure 3.8 FRAP experiment for a DOPC bilayer on a $(CHI/HA)_5$ polymer film. Images were recorded before (A), immediately after (B) and 11, 45 and 750 (C, D, E) seconds after photobleaching, respectively. (F) The corresponding FRAP recovery curve, with D = 2.49 $\mu m^2/s$

DOPC bilayers at pH 4 showed similar quenching behavior to those at higher pH, with 46% quenching of the initial intensity after addition of 50 mM Co^{2+}. However, FRAP experiments before and after Co^{2+} addition did not show the large difference observed at pH 6.5. FRAP for a DOPC bilayer before Co^{2+} addition gave D= 2.8 $\mu m^2/s$ with 98% mobile fraction. After Co^{2+} addition FRAP measurements for the lower leaflet gave D = 1.9 $\mu m^2/s$ with 98% mobile fraction, indicating only a modest reduction in mobility for lipids in the lower leaflet (Figure 3.9).

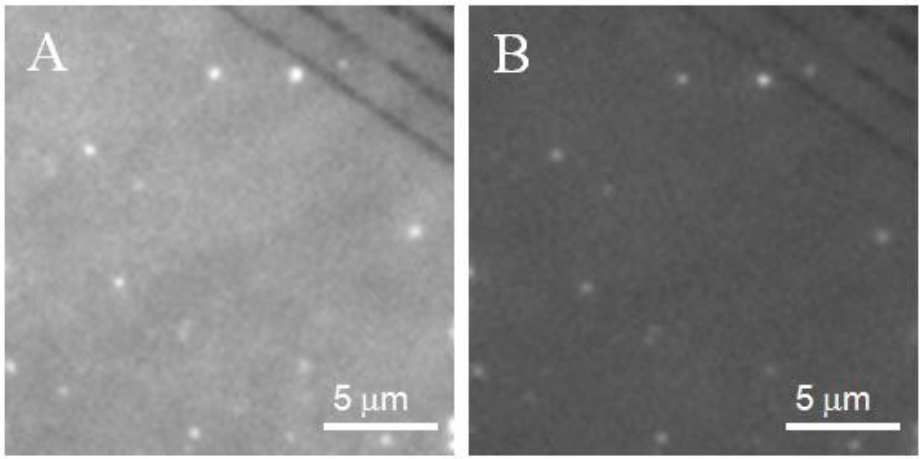

Sample	Mean Intensity	Corrected Intensity
Defect in Sample (background)	896	
DOPC/PEM pH 4 before Co^{2+}	2671	1775
DOPC/PEM pH 4 after Co^{2+}	1711	815

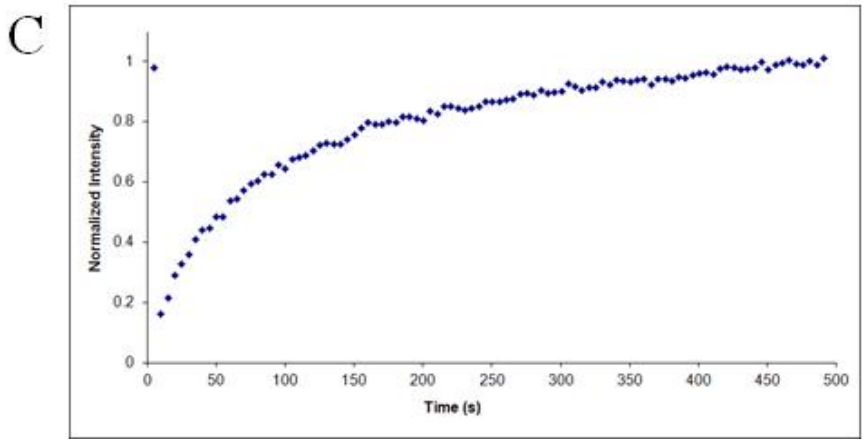

Figure 3.9 Fluorescence images of bilayers obtained by incubating DOPC vesicles on a $(CHI/HA)_5$ polymer film on glass (A, Oregon Green-DHPE) at pH 4.0 followed by the addition of 50 mM Co^{2+} (B). Fluorescence intensity measurements and a FRAP recovery curve after (C) the addition 50 mM Co^{2+}.

To confirm that bilayers containing lipids that are in the gel phase at room temperature could also be formed on PEM films, we prepared bilayers from a ternary lipid mixture that forms phase separated liquid-ordered domains surrounded by a fluid phase.[220,250] Fluorescence images of samples obtained after incubating DOPC/egg sphingomyelin/cholesterol (2:2:1 molar ratio, 0.2 % TR-DHPE) vesicles with PEM films were similar to those obtained for DOPC vesicles, with no evidence for formation of dark domains that exclude the dye (data not shown). Both samples were also imaged using a higher magnification objective (150x, Figure 3.7C,D). There are slight differences between the two suggesting that small domains may be present for the ternary lipid mixture, although they are considerably smaller than those typically observed for bilayers on mica substrates.[250]

In order for PEMs to be generally useful as biocompatible supports for protein-containing bilayers, it may be necessary to work at closer to neutral pH. Therefore we tested the lipid mobility for DOPC bilayers that were formed by incubation at pH 4, and then rinsed with aqueous NaCl solution at pH 7. FRAP data gave a similar diffusion coefficient, D = 2.8 $\mu m^2/s$ (Table 3.2), indicating that the pH can be re-adjusted after bilayer formation without reducing lipid mobility. The latter may be an important consideration for applications involving membrane proteins. The effect of pH on a membrane formed at pH 6.5 was also tested. A FRAP experiment for an initial bilayer at pH 6.5 gave D = 0.2 $\mu m^2/s$ with 16% mobile fraction. The bilayer was then washed with pH 4 solution and stored overnight at this pH prior to a second FRAP experiment which gave D= 0.5 $\mu m^2/s$ and a mobile fraction of 32%. This indicates that equilibration of the supported bilayer at low pH

leads to a somewhat higher mobile fraction and diffusion coefficient, presumably due to equilibration of the sample and repair of defects. However, the bilayer quality as assessed by lipid diffusion is still significantly better when the supported bilayer is formed at pH4. It should also be noted that the pH of the lower bilayer leaflet may not have equilibrated to the value of the bulk solution.

3.2.3 Comparison to Other Polymer Supported Bilayers

Several recent reports have characterized supported lipid bilayers on polyethylene glycol (PEG) cushions.[136,137,143,180] For comparison, a PEG-supported bilayer was prepared by the following procedure. First a DOPC monolayer with 7% PEG-DPPE was prepared at the air water interface and transferred to a glass slide; the polymer concentration is in the brush regime, slightly past the crossover point where the PEG chains are in contact with each other.[143] The second bilayer leaflet was then constructed by fusion of DOPC vesicles containing 0.2% OG-DHPE. FRAP gave a measured diffusion coefficient of 2.16 $\mu m^2/s$ (Table 3.2), slightly lower than D for DOPC bilayers on CHI/HA PEMs. This measurement is in good agreement with the D values of 1.5 $\mu m^2/s$ and 2.3-2.7 $\mu m^2/s$ for diffusion of NBD-PE in DPhPC and POPC bilayers prepared by vesicle fusion to a PEG-containing monolayer[143,251] and with D values of ~1.8 $\mu m^2/s$ for a SOPC bilayer supported on a physioabsorbed lipopolymer, dioctadecylamine [poly(ethyloxazoline)].[153] Similarly, D values of 1-2.5 $\mu m^2/s$ with mobile fractions >70% have been reported for fluid PC bilayers on PEG cushions grafted to a glass surface.[137] In addition to these results using LB-LS or LB-vesicle fusion methods, vesicle fusion of POPC vesicles doped

with low mol fractions of PEG-PE can also be used to produce PEG cushioned-bilayers. However, this method may not be of general utility due to the presence of polymer attached to the upper leaflet of the bilayers, thus reducing the accessibility for binding for biosensing applications.[146]

A recent detailed study by Fischlechner and coworkers employed a combination of fluorescence, lipid adsorption measurements using a quartz crystal microbalance and infrared spectroscopy to investigate the adsorption of POPC/POPS vesicles on PSS/PAH PEMs.[128] FRAP measurements indicated that the best quality bilayer (D = 0.38 $\mu m^2/s$) was formed from equimolar mixtures of POPC/POPS on PEMs with a positively charged PAH top layer.[128] POPC vesicles adsorbed strongly to PEM films with either PAH or PSS as the top layer but did not rupture and spread to give a continuous bilayer, resulting in negligible lipid diffusion (D ~ 0.001 $\mu m^2/s$ for PAH). Although POPS vesicles did rupture on the surface to give bilayer patches, the strong binding of lipid to PAH amino groups as assessed by IR studies resulted in patchy and immobile bilayers. These results led to the conclusion that the ability to form mobile bilayers on the PSS/PAH films involves a subtle balance between the long range electrostatic interactions that are necessary for vesicle adsorption, spreading and rupture and the lipid mobility required for formation of a continuous bilayer. A related NMR and fluorescence study concluded that a “somewhat” continuous POPC/POPS bilayer was formed on a $PAH(PSS/PAH)_3$ PEM, since there was evidence for small defects that allowed access of ions to both leaflets of the bilayer.[129]

Our results indicate that it is possible to form mobile zwitterionic bilayers on polysaccharide PEMs with negatively-charged HA in the top layer at pH 4, by contrast to the results for PSS/PAH films. The polysaccharide PEM cushions therefore provide a useful alternative to other polymer films for preparation of supported bilayers. The polysaccharides are biocompatible and the layer-by-layer assembly fabrication of PEM films is straightforward to use and does not require chemical modification of the surface. Bilayers on CHI/HA films have lipid mobilities that are comparable to those on various PEG polymer cushions and only slightly lower than those on glass. Our results show that the bilayer quality is poor when membrane formation is carried out at close to neutral pH. However, homogeneous bilayers formed at pH 4 retain their high lipid mobility in neutral solutions. These results are analogous to an earlier report showing that a low density of surface-adsorbed vesicles on anionic maleic acid copolymer films at pH 7 impedes bilayer formation for vesicles containing 20% negatively charged lipids; by contrast, lowering the pH reduces the electrostatic repulsion between the polymer film and vesicles, allowing the adsorption of a higher vesicle concentration and formation of a supported bilayer.[114] The same study found that a strong correlation between lipid mobility and surface hydrophilicity with a measured diffusion coefficient of 1.2 $\mu m^2/s$ for the most hydrophilic surface and a five-fold reduction for the most hydrophobic. In the present study we find that a less charged surface is also advantageous for preparation of more homogeneous, defect free bilayers. Since electrostatic interactions are less likely to interfere with initial vesicle absorption for

the zwitterionic lipids used in the present study, we hypothesize that the lower surface charge is more advantageous for vesicle spreading and rupture.

Bilayers on PEM films have already found a number of applications, for example in creating bilayers on PEM-filled nanopores for biochip development and for delivery of lipophilic cholesterol-based oligonucleotides.[252,253] The use of biocompatible polysaccharides may be advantageous for these applications. Furthermore, there is scope for modulating the behavior of polysaccharide PEMs by functionalization. For example, a recent study by Winnik has shown that phosphorylcholine-modified chitosan forms similar PEM films with HA; however, conversion of a fraction of the primary amino groups to secondary amines by covalent attachment of PC groups results in multilayers with higher water content that behave as soft, fluid gels as compared to the hard gels of HA/CHI films.[244]

Finally, it is worth considering the role of surface roughness in formation of supported lipid bilayers. Several studies have concluded that surface roughness is not a major factor in controlling the formation of supported bilayers.[34,114] For example, bilayers formed by vesicle fusion on silica xerogels follow the surface curvature and have diffusion coefficients that are only a factor of two lower than those on mica, consistent with continuous defect-free bilayers.[254] It has been argued that most of the decrease in D is due to the roughness of the surface, which cannot be easily corrected for when determining the diameter of the bleached spot. Similarly, a study of bilayer formation on nanoparticles adsorbed on a mica surface demonstrated that bilayers enveloped and closely followed the particle structure for particles larger than 22 nm in diameter.[255] However smaller particles (1.2 -22 nm)

were located in pores in the membrane. Other studies have shown that the rate and mechanism of bilayer formation via vesicle fusion can be modulated by the use of nanocorrugated versus nanosmooth topographies, with faster vesicle adsorption on the nanocorrugated regions[256] and that membranes can readily bend to accommodate complex topographies.[257] The results presented here indicate that surface properties (charge, hydrophilicity) are considerably more important in facilitating vesicle adsorption, spreading and rupture to form bilayers and also in allowing sufficient lipid mobility to form a continuous bilayer with few surface defects.

3.3 Summary of Supported Lipid Bilayers on Polysaccharide PEMs

Supported lipid bilayers were formed on polysaccharide multilayers produced by sequential adsorption of five CHI/HA bilayers with a top negatively-charged layer to mimic the behavior of glass and mica substrates. At approximately neutral pH, the adsorbed lipids were immobile but a combination of AFM and fluorescence microscopy indicated that this was attributable to formation of a lipid membrane with a combination of defects and pinned lipids, rather than to a layer of unruptured vesicles. At pH 4, supported lipid bilayers with mobile lipids were obtained, and diffusion coefficients measured by FRAP were very similar to those on PEG polymer cushions and approximately a factor of two slower than those on glass. The formation of mobile lipid bilayers for zwitterionic lipids is in contrast to earlier results indicating that a mixture of charged and zwitterionic lipids was necessary for formation of mobile bilayers on PSS/PAH PEMs with a positively charged top

layer.[128] The ability to generate zwitterionic bilayers on biocompatible polysaccharide films extends the range of utility of PEMs as possible substrates for supported membranes for biosensing applications. Furthermore, the results provide further insight on the relative importance of surface charge and roughness in modulating lipid bilayer formation. Although surface roughness is less important than electrostatic interactions between lipids and the polysaccharide in regulating bilayer formation, it may be responsible for the complex diffusion behavior observed for supported bilayers on PEMs.

3.4 Experimental

3.4.1 Materials

Lipids (1,2-dioleoyl-*sn*-glycero-3-phosphocholine (DOPC), egg sphingomyelin and cholesterol) and 1,2-dipalmitoyl-*sn*-glycero-3-phosphoethanolamine-*N*-[methoxy(polyethylene glycol)-2000] (PEG-DPPE) were obtained from Avanti Polar Lipids and were used as received. All aqueous solutions were prepared with 18.3 MΩ cm Milli-Q water. Texas Red 543 1,2-dihexadecanoyl-*sn*-glycero-3-phosphoethanolamine (TR-DHPE) and Oregon Green 488 1,2-dihexadecanoyl-*sn*-glycero-3-phosphoethanolamine (OG-DHPE) were obtained from Invitrogen. Low molecular weight chitosan (CHI, MW = 5 x 10^4 g/mol), hyaluronic acid sodium salt (HA, MW = 1.63 x 10^6 g/mol) from *Streptococcus equi* and all other materials were obtained from Aldrich ($\geq$98% pure) and used as received. Branched poly(ethyleneimine), MW 1800, 99% was obtained from

Polysciences, Inc. Cobalt (II) chloride hexahydrate was acquired from Riedel-deHaën. Glass coverslips (No. 1, 25 mm) from Fisher Scientific and n-type silicon (111) wafers polished on one side with a thickness of 250±25 μm and a resistance of 1.0-5.0 ohm·cm were used for preparation of PEMs.

3.4.2 Assembly of PEM

The polyelectrolyte multilayers were constructed following the previously described layer-by-layer assembly method on either glass or silicon substrates.[164,244] Substrates were cleaned prior to use by dipping in a piranha solution consisting of 70% concentrated sulfuric acid and 30% hydrogen peroxide, followed by rinsing with Milli-Q water, and nitrogen drying. Polyelectrolyte solutions (1.0 g L^{-1}) were prepared in 0.15 M NaCl and the pH was adjusted to 4.5 using aqueous concentrated acetic acid solution. Polymer solutions were filtered through a 0.45 μm Millipore PVDF filter prior to use. The cleaned substrate was placed in a homemade glass fluid cell holder. The cell was immersed in aqueous CHI solution for 15 min and then removed and placed in a beaker containing 350 mL of NaCl solution (0.15 M, pH 4.5) for 1 min. The cell was then removed and placed in a second beaker containing 150 mL of NaCl solution (0.15 M, pH 4.5) for another 5 min to ensure the removal of excess CHI. HA was then deposited on the substrate surface following the dipping/rinsing procedure described above for CHI. The assembly of the PEM was continued up to 5 bilayers. Rinsing beakers containing aqueous NaCl solution were changed after 3 uses. The PEM coated substrates were dried by a stream of N_2 and stored in a nitrogen box until used for bilayer preparation, typically within 1-2 days and never more than 1 week.

3.4.3 Preparation of Small Unilamellar Vesicles

Chloroform solutions of lipids were mixed in the appropriate ratios, the solvent was removed, and the film was dried under vacuum overnight. The lipid films were then hydrated in Milli-Q water containing (a) 10 mM $CaCl_2$ and 140 mM NaCl at the desired pH, 4 or 7 (for preparation of PEM-supported bilayers) or (b) 10 mM NaH_2PO_4 and 100 mM KCl (for preparation of PEG-supported bilayers) and vortexed to obtain multilamellar vesicles. Small unilamellar vesicles were prepared by bath sonication with an initial temperature of 20ºC to form clear dispersions with a final lipid concentration of 1 mg/mL. Vesicles prepared by bath sonication were 38±12 nm in diameter, as assessed by dynamic light scattering. Vesicles were stored at 4ºC and used within 1 week.

3.4.4 Preparation of Supported Bilayers

(a) PEMs: An aliquot of vesicle solution (100 µL) and Milli-Q water (400 µL) containing 10 mM $CaCl_2$ and 140 mM NaCl at the desired pH, 4 or 7, were added to a $(CHI/HA)_5$ PEM substrate and clamped into a TIRF or AFM liquid cell. After incubation at room temperature overnight, the bilayers were rinsed extensively with Milli-Q water containing 140 mM NaCl at the corresponding pH to remove unattached vesicles before imaging. (b) PEG polymers: A polymer-doped monolayer was prepared by Langmuir-Blodgett deposition on a Nima 611 trough. A 1 mg/mL solution of DOPC with 7 mol% PEG-DPPE was prepared in chloroform

and 20 µL of the lipid solution was deposited at the air-water interface. After waiting 15 minutes to allow for chloroform evaporation, the lipids were compressed to a surface pressure of 32 mN/m. Two glass coverslips placed back to back were then raised vertically out of the trough at a rate of 15 mm/min, allowing the deposition of a PEG-supported lipid monolayer on only the exposed side of each coverslip. An aliquot of vesicle solution (100 µL) and Milli-Q water (300 µL) containing 10 mM NaH_2PO_4 and 100 mM KCl, were added to the monolayer-coated substrate and clamped into a TIRF or AFM liquid cell. After incubation at room temperature for 1h, the bilayers were rinsed extensively with Milli-Q water containing 10 mM NaH_2PO_4 and 100 mM KCl to remove unattached vesicles before imaging.

3.4.5 Atomic Force Microscopy

The AFM images were obtained at room temperature (23±1ºC) using a PicoSPM atomic force microscope (Molecular Imaging) in MAC-mode. Magnetic coated silicon tips with spring constants of ~0.5 N/m and resonance frequencies between 5 and 40 kHz in aqueous solution were used. A 30 x 30 μm^2 scanner was operated at a scan rate between 0.7 and 1.3 Hz. The images shown are flattened raw data and imaged at minimal force (15-170 pN). Two or more independently prepared samples were imaged for each set of conditions with several areas scanned for each sample. Reported PEM thicknesses are based on the removal of polymer with a razor blade and measuring the AFM step height for at least two independent samples with a minimum of nine areas imaged. In addition, after

image flattening, RMS roughness measurements were measured using PicoSPM software. The software calculates the RMS roughness from (6)

$$RMS = (\Sigma((Z_n - Z_{Av})^2)/N)^{1/2} \quad (6)$$

where Z_{Av} is the mean value of the surface height relative to the center plane and N is the number of points in the sample area. The RMS values reported were averaged values of three same sized areas of two or more independently prepared samples.

3.4.6 Fluorescence Microscopy

Fluorescence images of bilayers were taken on an Olympus IX81 total internal reflection fluorescence (TIRF) microscope equipped with a back-illuminated electron multiplying CCD camera (Cascade 512B, Photometrics) and a 60×/1.45 NA Plan Apochromat TIRF objective (Olympus). Supported bilayers containing either Texas Red DHPE or Oregon Green DHPE (0.2 mol%) were excited at 543 or 488 nm, respectively. A 150x objective was used for several experiments (pixel size – 107 x 107 nm, compared to 267 x 267 nm for the 60x objective). Images shown are all measured in TIRF mode, although comparison of TIRF and epi-fluorescence images gave very similar results except for reduced interference from adsorbed vesicles in the TIRF images.

3.4.7 Fluorescence Recovery After Photobleaching (FRAP)

FRAP experiments for bilayers labeled with 0.2 % Oregon Green DHPE were conducted on an Olympus IX81 microscope (epifluorescence mode) by bleaching a ~45 μm diameter spot with full laser power (~11 mW) at 488 nm for 1-3 s. The fluorescence recovery was recorded with a 150x objective with a 1-5 second interval (depending on the recovery kinetics) between images at a reduced laser power (<2.3 mW). Image analysis was performed using National Institutes of Health Image J software (http://rsb.info.nih.gov/ij/). Diffusion coefficients were estimated following the approach of Soumpasis with normalized intensities fit to a two-dimensional diffusion equation.[49] Reported diffusion coefficients and mobile fractions are the average of bleaching experiments on multiple areas for at least 2 independently prepared bilayers.

3.4.8 Ellipsometry

Thickness measurements of dry PEM coated silicon substrates were estimated using a Gaertner model L116S single wavelength (633 nm) ellipsometer at an angle of incidence of 70º. A two-layer model with n=1.46 as the refractive index of the PEM layer and the silicon substrate described by n=3.85 and k=0.02 was used to estimate the PEM dry thickness.

Chapter 4: The Incorporation of a Membrane Protein into Polymer Supported Lipid Bilayers

This chapter contains Material Adapted from the following manuscript

1. K. Mulligan, B. Schilling, D. H. Thompson, C. A. Hrycyna, L. J. Johnston; Functional Reconstitution, and characterization of the *Saccharomyces cerevisiae* Isoprenylcysteine Carboxylmethyltransferase Ste14p in Polymer Supported Lipid Membranes. *In preparation*.

2. Ste14p protein and activity measurements were contributed by collaborators.

4.1 Platforms for Incorporating Membrane Proteins

4.1.1 Polymer Supported Lipid Bilayers

A major limitation of the supported lipid bilayer model system is the spacing between the membrane and the solid support. This small spacing can interfere with the integration and activity of an integral membrane protein within a lipid bilayer. Few platforms that incorporate polymer tethers or cushions to decouple supported lipid bilayers from their underlying supports have been shown to successfully integrate large transmembrane proteins.[64,112] SNARE and cytochrome *b* membrane proteins have been incorporated into bilayers on a PEG tethered polymer system.[136] The PEG cushion measured from 2 to 4 nm in thickness.[138] The conclusion that different proteins behave differently on the same polymer cushion was based on the observation that SNARE proteins diffused in the bilayer three times faster than cytochrome *b* proteins.[178] Another study made use of lipopolymers tethers consisting of polymerized 2-methyl-2-oxazoline. In this case, the polymer cushion measured a thickness of less than 5 nm. The large transmembrane cell receptor integrin $\alpha_{IIb}\beta_3$ was incorporated into the polymer supported bilayer system and low protein diffusion coefficients and mobile protein fractions were reported.[141] However, the use of the same cell receptor integrin $\alpha_{IIb}\beta_3$ on a different polymer cushion, trimethylsilyl cellulose, and preparation method gave higher protein diffusion coefficients and mobile fractions.[125] As a result, the same membrane protein has behaved differently in different polymer cushion systems. Protein diffusion coefficients and mobile fractions are the most common characterization method and very few studies have attempted to show the function or activity of

membrane proteins incorporated into different polymer supports. Renner measured the activity of the transmembrane protein β-amyloid precursor protein cleaving enzyme (BACE) in a lipid bilayer supported by maleic anhydride copolymers. In this example, the copolymer system produced a supported lipid bilayer with enhanced activity of the reconstituted BACE compared to a supported lipid bilayer without underlying copolymer.[148]

In the previous chapter, we have shown the usefulness of polyelectrolyte multilayer (PEM) films constructed from alternating layers of chitosan (CHI) and hyaluronic acid (HA) as polymer cushions for supported lipid bilayers.[236] Uniform bilayers with diffusion coefficients similar to bilayers on glass and other polymer supports such as a PEG tethered system were obtained at pH 4. In this chapter, we examined the suitability of the same PEM system and of a PEG tethered system for reconstitution of an integral membrane protein, Ste14p, into a polymer supported lipid bilayer. Ste14p is a 26 kDa integral membrane protein with six transmembrane domains responsible for the carboxyl methylation of C-terminal CaaX sequences.[87] Reconstitution of functional Ste14p into a polymer supported lipid bilayer is an essential first step toward the development of a sensor based on this enzyme. In this chapter, GFP-Ste14p will be incorporated into POPC lipid bilayers supported by a PEM or a PEG polymer cushion. The systems will be characterized using AFM, fluorescence microscopy, FRAP and by an *in situ* methyltransferase activity assay. Finally, the GFP-Ste14p in supported lipid bilayers on polymer supports will be compared to the GFP-Ste14p in supported lipid bilayers prepared on glass.

4.2 Results and Discussion

4.2.1 Preparation and Characterization of the Polymer Supports

In the previous chapter, we examined polymer supports of a PEM film composed of alternating layers of HA and CHI as well as a 7% PEG-DPPE supported system.[236] We showed that PEM films consisting of 5 bilayers, starting with adsorption of CHI to a glass surface, produced a polymer film with sufficient thickness and provided good surface coverage while minimizing the surface roughness. AFM images of the $(CHI/HA)_5$ films on a glass substrate imaged in water (pH 6.5) are shown in Figure 4.1A,B. The average thickness and rms roughness of the $(CHI/HA)_5$ polymer films used in this study were consistent with our previous study's result of 57±3 and 25±2 nm.[236] The PEG-supported monolayer was also characterized by AFM under dry conditions as shown in Figure 4.1C. The rms roughness of the PEG monolayers used in this study was found to be 0.5±0.2 nm. This measurement is similar to the rms roughness of glass, ~0.6 nm.[258] Lower molecular weight PEG monolayers prepared in the brush regime have been shown to retain the native surface roughness of the underlying surface.[259]

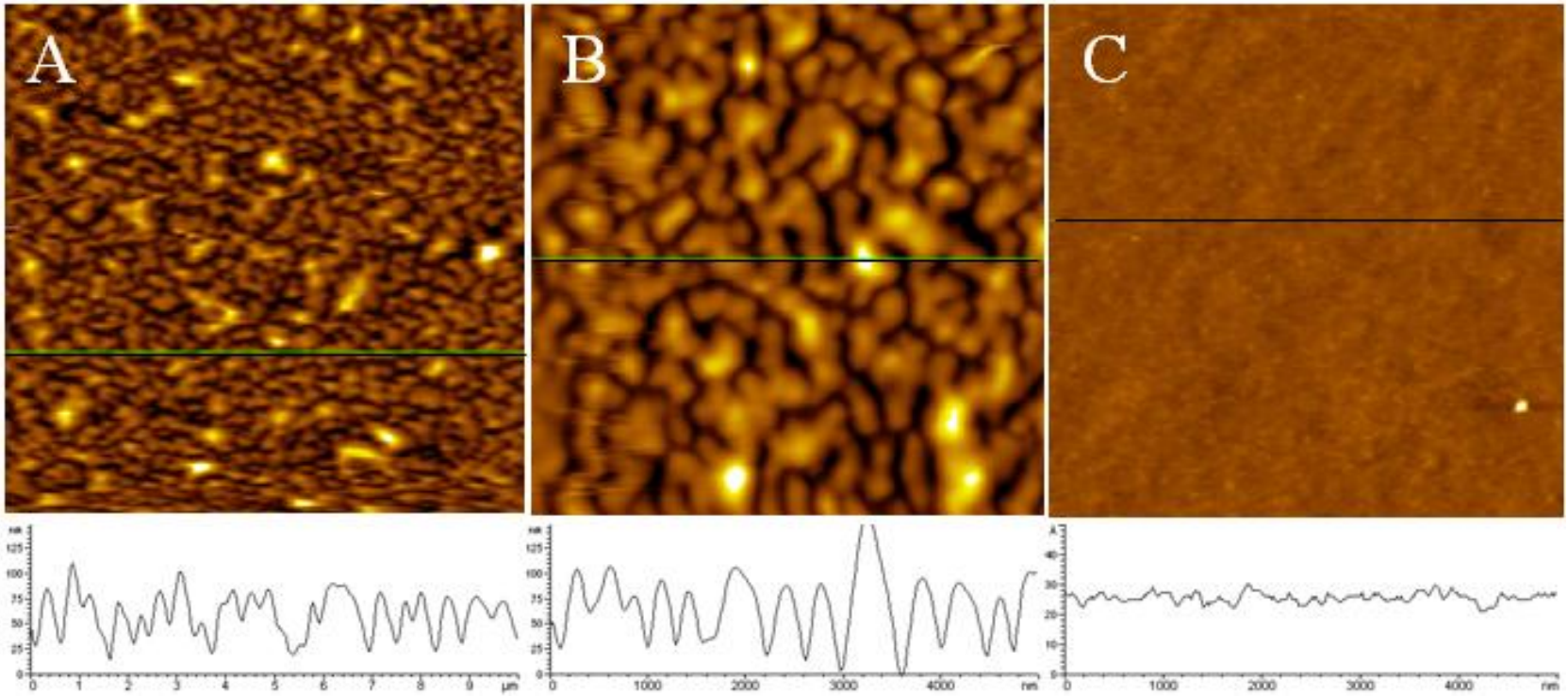

Figure 4.1 AFM images of a $(CHI/HA)_5$ polymer film (A,B) and of a PEG-DPPE-POPC monolayer (C) on glass.

4.2.2 Formation of POPC Bilayers on Polymer Supports

Ste14p protein activity has been previously measured in POPC lipid membranes.[87] POPC and DOPC, as used in chapter 3, are similar phosphocholine lipids that differ solely by an additional unsaturation in the hydrocarbon chain of DOPC (Figure 4.2). POPC bilayers on polymer supports were characterized before the incorporation of a membrane protein. In the previous chapter, DOPC lipids were labeled using Oregon Green-DHPE. Oregon Green is excited using 488 nm light. In this chapter, we intended to study the incorporation of GFP-Ste14p in a supported lipid bilayer, which also requires 488 nm excitation. Diindole dye, DiI C_{22} (5), is another commonly used lipid dye that is excited using 633 nm light. DiI C_{22} (5) was selected to label the lipid component of this system instead of Oregon Green-DHPE in order to avoid exciting both the lipid and protein components at the same time. Therefore, POPC vesicles containing 0.2 mol% DiI C_{22} (5) were incubated with bare and polymer-coated glass in 138 mM MOPS overnight at the desired pH, followed by extensive rinsing to remove adsorbed vesicles. In addition, 10 mM $CaCl_2$ was used when depositing vesicles on $(CHI/HA)_5$ polymer films. The quality of the lipid bilayers on the different substrates was evaluated by fluorescence microscopy. The POPC bilayer on glass, as shown in Figure 4.3A, showed uniform membrane fluorescence with occasional small bright features that were assigned to adsorbed vesicles. Conversely, as shown in Figure 4.3B, the POPC bilayer formed at pH 4 on a $(CHI/HA)_5$ film showed a more patchy fluorescence with small dark areas that were assigned to defects. A POPC bilayer

formed on the PEG polymer support, as shown in Figure 4.3C, showed membrane fluorescence similar to that of a POPC bilayer prepared on bare glass.

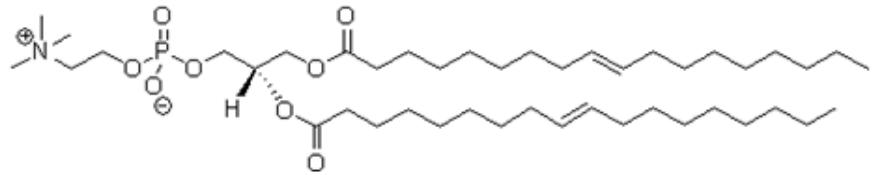

DOPC

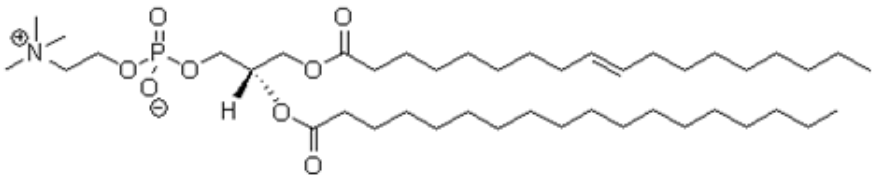

POPC

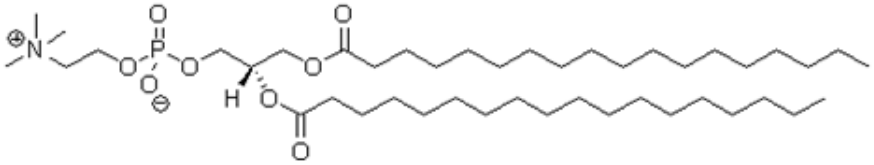

DPhPC

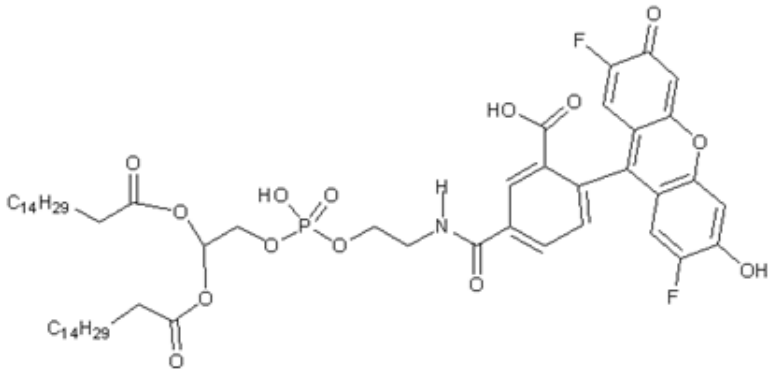

Oregon Green-DHPE

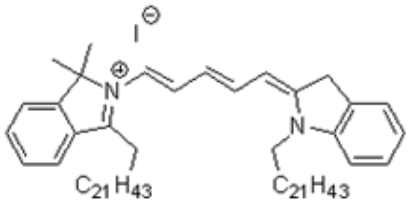

DiI C_{22} (5)

Figure 4.2 Structures of lipids and dyes used to make supported lipid bilayers.

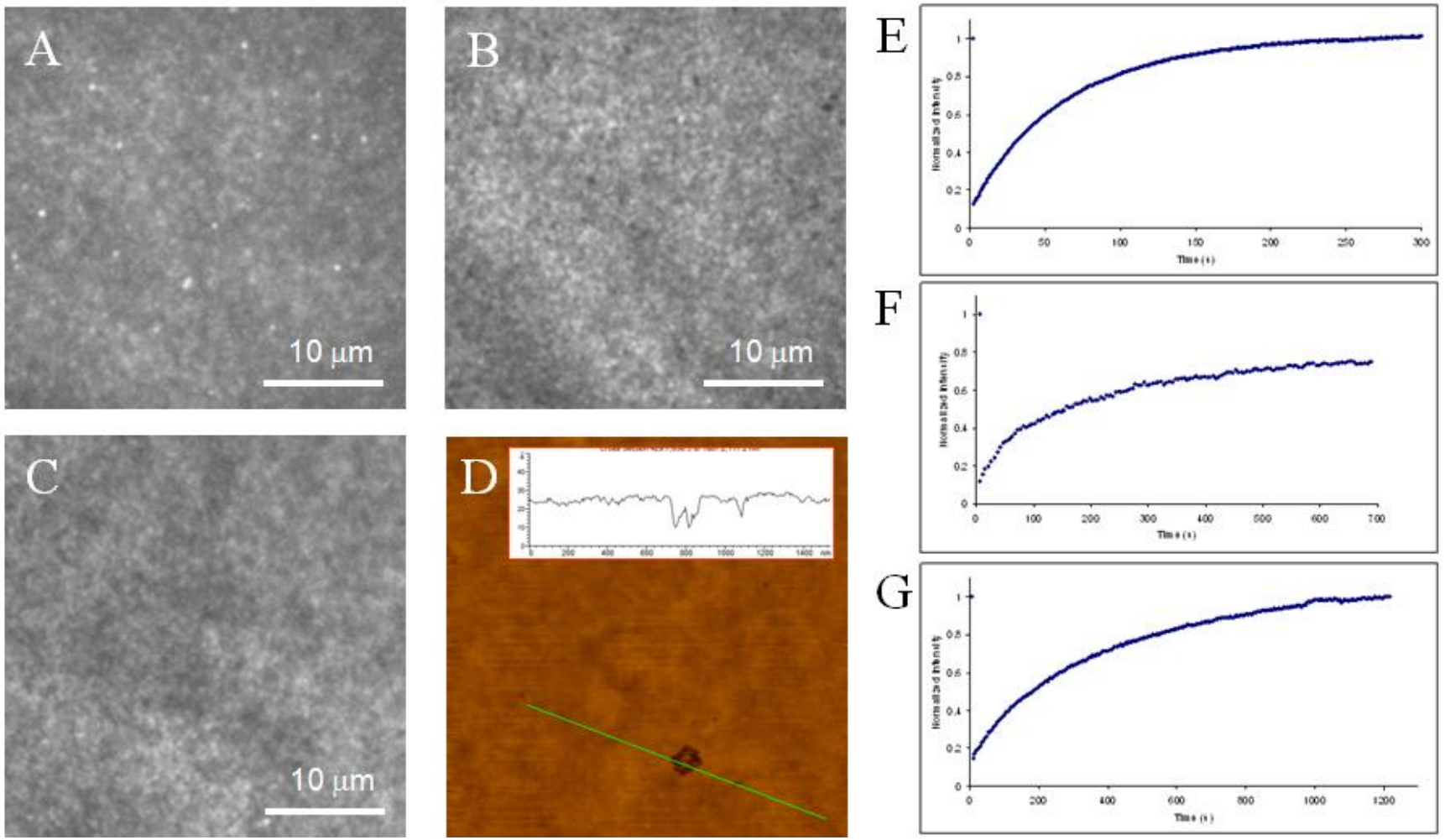

Figure 4.3 Fluorescence images, an AFM image and FRAP recovery curves of bilayers obtained by incubating POPC vesicles on a glass substrate (A, DiI $C_{22}(5)$; E, FRAP), on a $(CHI/HA)_5$ polymer film on glass (B, DiI $C_{22}(5)$; F, FRAP) at pH 4 and on a DPPE-PEG-POPC monolayer on glass (C, DiI $C_{22}(5)$; D, AFM; G, FRAP).

Lipid mobility was investigated using FRAP experiments. The diffusion coefficients, D, and mobile lipid fractions for the three types of supports using different dyes are reported in Table 1. FRAP experiments for DiI C_{22} (5) in POPC bilayers prepared by vesicle fusion on glass gave a diffusion coefficient of 2.4 $\mu m^2/s$ with a mobile fraction of >99%, Figure 4.3E. This value is significantly lower than the diffusion coefficient of 6.2 $\mu m^2/s$ obtained for a POPC bilayer on glass labeled with Oregon Green-DHPE. The difference in diffusion coefficients could be attributed to the difference in chemical structures of the two dyes. The longer hydrocarbon chains found in the structure of DiI C_{22} (5), Figure 4.2, could lead to a hydrophobic mismatch with the POPC lipid tails in the bilayer, which could reduce its diffusion. However, the difference in size of the headgroup to which the alkyl chains are attached may partially offset this effect. In addition, unlike POPC where the alkyl chains are close together, the structure of DiI C_{22} (5) possesses two alkyl tails separated by a 5 carbon linker. The spacing between the alkyl chains of the DiI C_{22} (5) structure may also reduce its diffusion coefficient. Overall, although DiI C_{22} (5) has a lower diffusion coefficient than Oregon Green-DHPE in POPC bilayers the values are within the range of diffusion measurements for dye-labeled lipids in fluid-phase supported bilayers on glass. Typical measurements range, in the literature, from 1-6 $\mu m^2/s$, depending on the presence of salt and buffer.[28,246]

Diffusion coefficients measured on the PEM polymer support were found to be slightly lower than those for glass. However, measurements on the PEG polymer support were found to be lower by as much as a factor of two. The lower diffusion values may indicate the formation of heterogeneous bilayers with small

defects and/or lipids pinned to the underlying polymer. However, the uniformity of the membrane fluorescence of the POPC bilayer on the PEG polymer and the absence of small dark areas suggests that the lower diffusion measurements on the PEG polymer are the result of some lipid pinning or the presence of small nanoscale defects that are not observed by fluorescence methods. High mobile lipid fraction measurements of a POPC bilayer on a PEG cushion supports the absence of lipid pinning as it was consistent with that of a glass substrate.

AFM imaging of a POPC bilayer sample on a PEG cushion was used to determine whether there were nanoscale defects in the bilayer. The majority of AFM images acquired showed a smooth surface. This result indicated the formation of a uniform POPC bilayer. The AFM image of a POPC bilayer on a PEG cushion in Figure 4.3D shows a small defect which demonstrated that the smooth surface was in fact a bilayer and not the surface of the substrate.

Table 4.1 Diffusion coefficients, D, and mobile lipid fractions, F, obtained by FRAP measurements in POPC bilayers on various supports

Support	Dye	D ($\mu m^2/s$)	F (%)
Glass	DiI C_{22} (5)	2.4±0.1	>99
$(CHI/HA)_5$[#]	DiI C_{22} (5)	2.0±0.2	60-75
PEG	DiI C_{22} (5)	1.3±0.2	>99
Glass	Oregon Green-DHPE	6.2±0.4	>99
PEG	Oregon Green-DHPE	3.3±0.2	>99

[#]Bilayer was prepared at pH 4.
*All other bilayers were prepared at pH 6.5. Reported D and F are the average of FRAP experiments on two or more areas..

Bilayers formed on PEG polymer cushion supports were prepared using the combination hybrid method where first LB was used to deposit a monolayer of PEG-lipid and then VF was used to deposit the top leaflet of the bilayer. However, only vesicles contained the dye. As a result, a dye location study, using DPhPC lipids and Oregon Green-DHPE, was performed in order to determine whether the location of the dye had an effect on the lipid diffusion coefficient. DPhPC, as in Figure 4.2, is a fluid phosphocholine lipid at room temperature and has the advantage of being composed of hydrocarbon chains with saturated bonds which results in lipids with increased stability.[260] The absence of C=C unsaturations in the structure of DPhPC eliminates any issues of lipid oxidation. FRAP measurements were carried out on DPhPC samples prepared by incorporating dye in both leaflets of the bilayer as well as samples prepared by incorporating dye in only the top or bottom leaflet of the bilayer. The first sample using VF gave a DPhPC bilayer with dye in both the top and bottom leaflets of the bilayer on glass. The diffusion coefficient was measured to be 2.4±0.1 $\mu m^2/s$. Next, using the combination hybrid method, we prepared a DPhPC bilayer containing dye solely in the bottom leaflet. In this case the lipids solutions used to make the LB lipid monolayer contained dye and the vesicles used to make the top leaflet of the bilayer did not. The diffusion coefficient that was measured, 2.3±0.2 $\mu m^2/s$, was very similar to that of a bilayer containing dye in both leaflets. The same type of experiment was attempted using a PEG polymer support where dye was incorporated in either the top or bottom leaflets of the bilayer. Again the lipid diffusion coefficients of the bilayer were similar independent of the location of the dye (Table 4.2).

Table 4.2 Diffusion coefficients, D, obtained by FRAP measurements for Oregon Green-DHPE in DPhPC bilayers prepared by incorporation of dye in different locations

Supported Lipid Bilayer	Preparation Method	Dye Location	D ($\mu m^2/s$)
DPhPC/DPhPC	VF	Both Leaflets	2.4±0.1
DPhPC/DPhPC	LB and VF	Bottom Leaflet	2.3±0.2
PEG-DPhPC/DPhPC	LB and VF	Top Leaflet	1.5±0.1
PEG-DPhPC/DPhPC	LB and VF	Bottom Leaflet	1.4±0.2

*Reported D are the average of FRAP experiments on two or more areas for at least 2 independently prepared bilayers.

Lin and co-workers performed a similar study where the effects of a PEG cushion on the electrical properties of a supported DPhPC bilayer were investigated.[143] FRAP was used to further characterize their electrically optimal DPhPC bilayer platform. A lipid diffusion coefficient of 1.5 $\mu m^2/s$ was measured. Lin explained that this value was a factor of 2 lower than the values reported for POPC bilayers without a PEG cushion (2.3-2.7 $\mu m^2/s$). Lipid mobile fractions for the PEG supported DPhPC bilayers were observed to be >99%. The lower diffusion coefficient was explained by the interpenetration of the methyl groups of the DPhPC hydrocarbon chains. Our study, which used POPC instead of DPhPC, gave a diffusion coefficient of 1.3 $\mu m^2/s$. This result suggests that the methyl groups of the DPhPC have little effect on the lipid diffusion and that the slower diffusion is more likely due to the polymer cushion.

The mobile lipid fraction for a POPC bilayer on a $(CHI/HA)_5$ polymer film was found to be much lower, between 60 and 75% (Figure 4.3F), than that of the POPC bilayer on a PEG support. The decreased mobile lipid fraction and the appearance of small dark patches in the fluorescence images suggests that the POPC bilayer

on a $(CHI/HA)_5$ polymer film possessed many small defects and/or some lipid pinning effects. Unfortunately, due to the surface roughness of PEM supported bilayers, AFM is not a useful technique to confirm the uniformity of a bilayer on the nanoscale. In our previous study using the same conditions to make a DOPC bilayer on a $(CHI/HA)_5$ polymer film using 0.2 mol% Oregon Green-DHPE, mobile lipid fractions of >99% were achieved.[236] The decrease in mobile lipid fraction could be attributed to the structure of the dye used, as in Figure 4.2. At pH 4, Oregon Green-DHPE and DiI C_{22} (5) possess a negative and a positive charge, respectively. As a result, in this study the DiI C_{22} (5) dye may be electrostatically interacting with the negatively charged top HA layer of the $(CHI/HA)_5$ polymer film. The interaction of different cationic dyes with a polyanion, polystyrene sulfonate (PSS), has been previously investigated. The goal of the investigation was to synthesize capsules composed of polyelectrolyte complexes. Bisindeolenylpentamethine (Cy5), which has a similar structure to DiI C_{22} (5), was shown to absorb to PSS by absorption spectroscopy. However, it was also found that this monovalent dye can be replaced easily by other polyelectrolytes or "washed out" due to its weak binding with PSS.[261] Therefore, the DiI C_{22} (5) dye used in this study may be weakly interacting with the top HA layer of the $(CHI/HA)_5$ polymer film resulting in lower mobile lipid fractions.

4.2.3 Optimization of the Formation of POPC:Ste14p Bilayers on Mica

AFM was used to optimize conditions such as amount of lipid and incubation time for the formation of POPC:Ste14p bilayers on mica. POPC vesicles were

reconstituted with Ste14p using the rapid dilution method.[87,202] Briefly, purified protein dissolved in protein elution buffer was thawed, dissolved in buffer and combined with lipid vesicles. The protein elution buffer consisted of 35 mM Na_2PO_4, 210 mM NaCl, 8% glycerol, 1.6 mM AEBSF, 1.2 mg/mL Aprotinin, 0.1% DDM and 1 M Imidazole at pH 7.2. Next, a rapid dilution was performed to reconstitute the protein into the vesicles. A lipid to protein molar ratio of 7500:1 was selected as a starting point. Mica was chosen as the substrate for this optimization study because it is both atomically flat and inert. An atomically flat surface is advantageous when attempting to measure small height differences such as nanometer protrusions of small proteins from a bilayer. The first set of experiments investigated the effect of different amounts of lipid to make a POPC:Ste14p bilayer. Different amounts (30 µL, 120 µL and 240 µL of 0.4 mg/mL) of POPC:Ste14p vesicles were deposited on mica in 10 mM $CaCl_2$, 138 mM MOPS buffer at pH 7.2 to form a total volume of 500 µL and incubated for one hour at room temperature. The samples were washed with buffer to remove excess vesicles and then imaged by AFM (Figure 4.4).

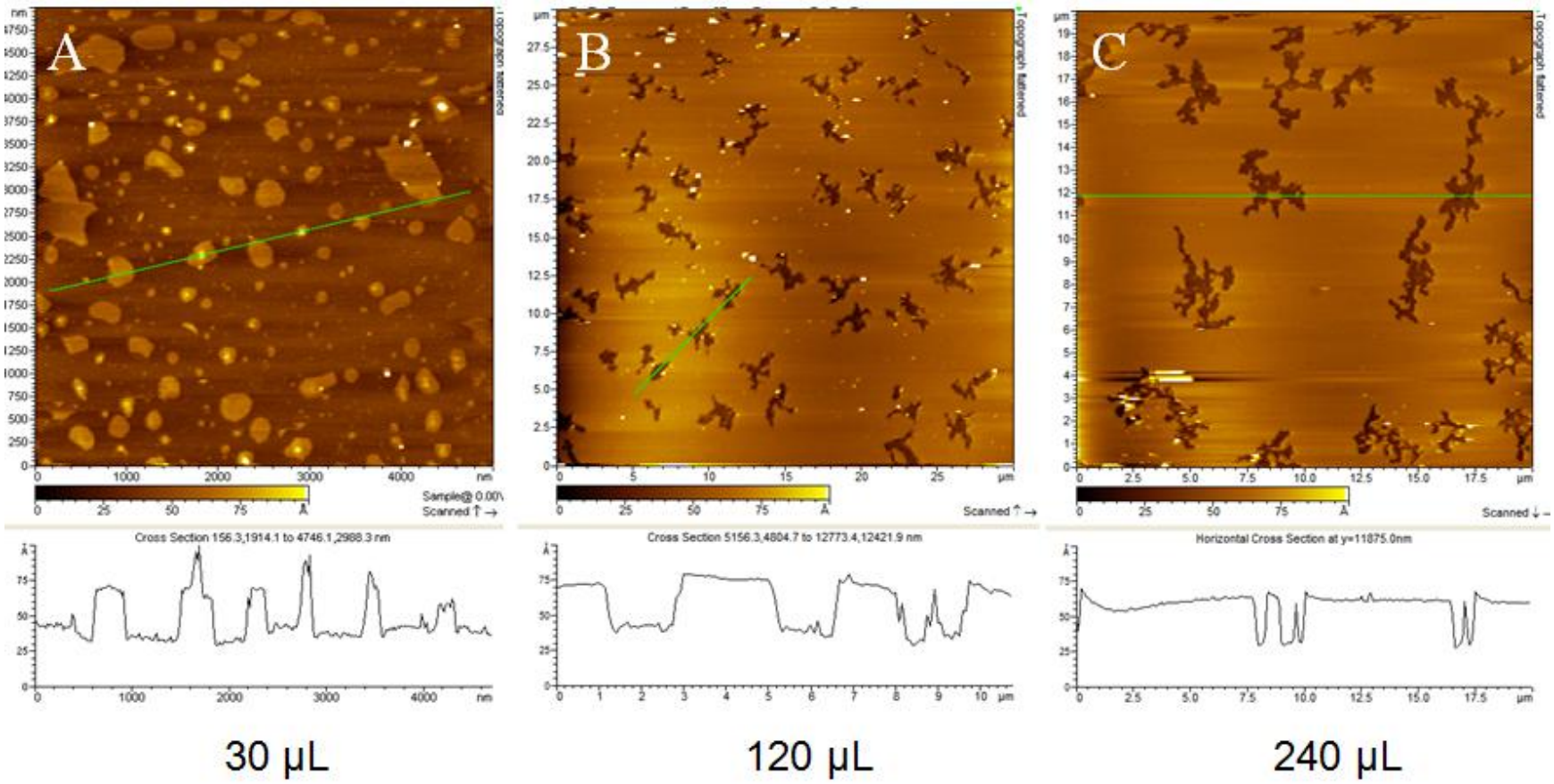

Figure 4.4 AFM image of bilayers obtained by incubating POPC:Ste14p (7500:1) vesicles on a mica substrate using different lipid amounts in a final volume of 500 µL, 138 mM MOPS at pH 7.2, 10 mM $CaCl_2$, room temperature and 1 hour incubation.

At low amounts of lipid (30 µL, Figure 4.4A), small bilayer patches were formed with a height of ~4 nm. Small features were observed to protrude from the patches of bilayer. The features measured heights of ~1-3.5 nm above the patches of bilayer. These features were smaller than unruptured vesicles (< 8 nm) and were assigned as protein. Based on the range of heights measured, the protein in the sample was thought to be either reconstituted in the bilayer or physioabsorbed on the top of the bilayer. The following samples containing higher amounts of lipid (120 µL and 240 µL, Figure 4.4B,C) produced large areas of bilayer. However, the bilayers possessed large defects. Cross sections measured over the defect areas gave a depth of ~4 nm. Distances of 4 nm are consistent with the thickness of a POPC bilayer.[209] Increasing the incubation time to 18 hours in an effort to reduce the number of defects produced a large change in the amount of lipid required to make a POPC:Ste14p bilayer. Intact bilayers could then be formed at low amounts of lipid (35 µL of 0.4 mg/mL) as in Figure 4.5A. Even at longer incubation periods, there were consistently ~4 nm defects in the bilayer although the number was fewer. The samples in figure 5 also showed the presence of small features measuring heights of ~1-4 nm above the bilayer. Although some features that appeared to be protein were present in the sample, it was believed that much more protein should be present. AFM may not be the most effective method to detect protein as protein can only be detected in scans of small areas. In addition, without optimal scanning conditions protein can be moved by the motion of the probe. The orientation of the protein in the bilayer can also be an issue. The protein can be reconstituted into the bilayer in two orientations. The two orientations can have the

larger C and N termini protruding from either the top or the bottom leaflet. In the event that the termini are pointed towards the support the small protruding areas could be difficult to image by AFM without optimal scanning conditions. However, if the termini are pointed outward from the support the larger area may be possible to detect by AFM.

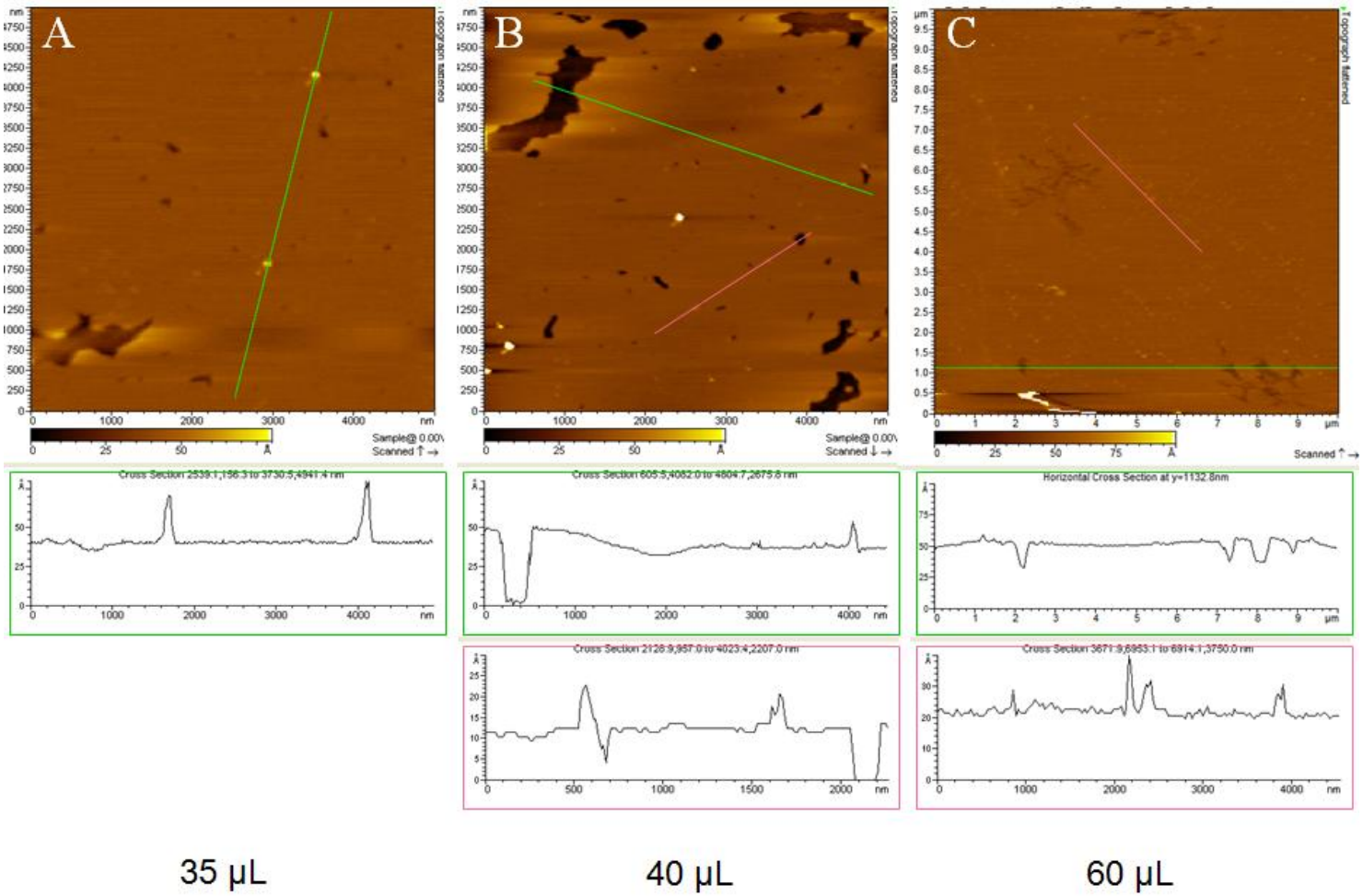

Figure 4.5 AFM images of bilayers obtained by incubating POPC:Ste14p (7500:1) vesicles on a mica substrate using different lipid amounts in a final volume of 500 µL, 138 mM MOPS at pH 7.2, 10 mM $CaCl_2$, room temperature and 18 hour incubation.

4.2.4 Formation of POPC:GFP-Ste14p Bilayers on Glass

The detection of individual proteins using AFM was difficult and required imaging very small areas. In addition, AFM imaging of several very small areas was time-consuming and only sampled small fractions of the bilayers. As a result, GFP-Ste14p was substituted for Ste14p so that the amount of protein incorporated in the bilayer could be monitored by fluorescence. DiI C_{22} (5) was incorporated into the POPC bilayer to confirm the integrity of the bilayer. Glass was also used as a substrate for the bilayer since it has better optical properties than mica. Thus, GFP-Ste14p was reconstituted in POPC vesicles containing 0.2 mol% DiI C_{22} (5) and incubated on glass in 138 mM MOPS overnight at pH 7.2. Although it was found that the use of AFM to detect protein was difficult, AFM was first used to confirm the successful formation of a bilayer after altering the initial conditions used on mica. Therefore, after extensive rinsing to remove any adsorbed vesicles the bilayer was imaged by AFM. As shown in Figure 4.6A,B, a continuous bilayer was formed possessing some small defects penetrating the bilayer to depths of ~ <3 nm. Figure 4.6A also showed a small amount of raised features. The islands were ~1-5 nm higher then the surrounding lower membrane. The islands possessed widths of ~20-200 nm. Using standard deconvolution techniques and assuming a spherical tip with a radius of <10 nm imaging a spherical feature, the smaller islands true widths can be estimated to ~5 nm.[262] These features were assigned to GFP-Ste14p protein or clusters in the POPC lipid bilayer. AFM diameter measurements of integral membrane proteins are typically <10 nm and vary depending on the molecular weight of the protein.[263] Milhiet measured the diameter of the membrane

protein LH1-RC (MW ~300 kDa), a light harvesting complex reaction center, in a DOPC/DPPC (1:1 mol/mol) supported lipid bilayer. High magnification topographs showed LH1-RC with a diameter of ~10 nm.[263] Another example was that of Slade where a 480 kDa heterodimer, the insulin receptor, was measured by AFM.[264] AFM topographs in combination with mathematical models showed the receptor to have a diameter in the range of 31-56 nm. The membrane protein used in this study possessed a molecular weight of 26 kDa. As a result, the features observed by AFM in the POPC:GFP-Ste14p bilayers are likely to correspond to small clusters of proteins.

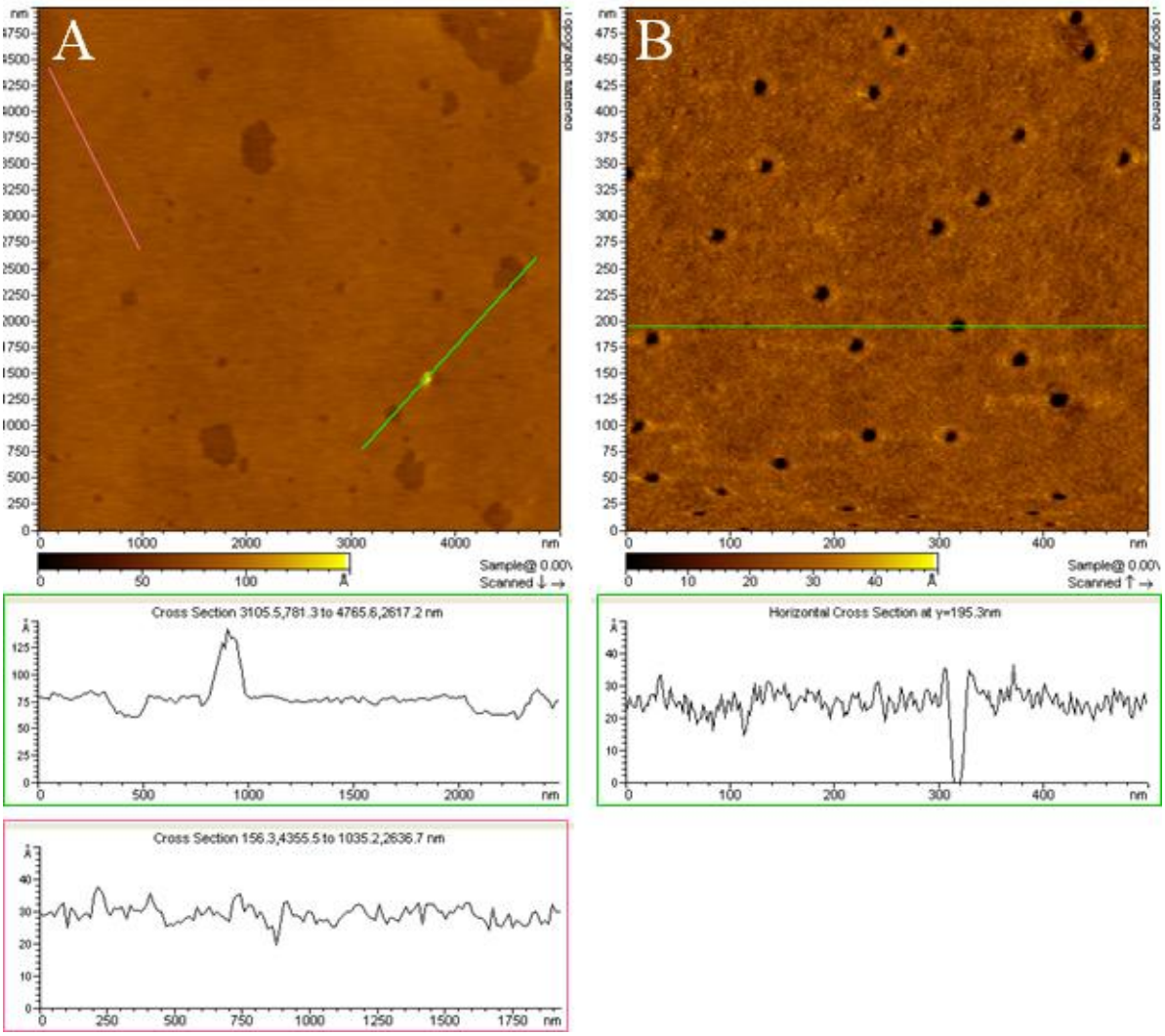

Figure 4.6 AFM images of a membrane prepared by incubating POPC:GFP-Ste14p (7500:1) vesicles on glass (A, B).

4.2.5 Formation of POPC:GFP-Ste14p Bilayers on a PEG Polymer Support

A POPC bilayer was prepared by incubating POPC/GFP-Ste14p proteoliposomes (lipid/protein ratio 7500:1 + 0.2 mol% DiI C_{22} (5)) on a PEG-POPC monolayer in 138 mM MOPS at pH 7.2. The formation of the lipid bilayer with reconstituted GFP-Ste14p was monitored using the DiI C_{22} (5) and the GFP

channels by excitation at 633 and 488 nm, respectively. Examples of 3 bilayers prepared from independently prepared proteoliposomes are shown in Figure 4.7. The DiI channel was used to confirm the successful formation of an intact POPC:GFP-Ste14p bilayer and the GFP channel was used to monitor the presence of protein. The DiI channel shows the formation of a reasonably uniform bilayer with occasional defects (Figure 4.7A-C) and/or occasional bright features that we assign to adsorbed vesicles (Figure 4.7C). In contrast, the GFP channel, Figure 4.7D-F, showed a heterogeneous distribution of intensities with some large bright features and many areas with much weaker signals. Comparison of DiI and GFP images (Figure 4.7C,F) indicated that some of the brighter GFP features overlapped with the bright features assigned to adsorbed vesicles in the DiI channel. The brighter features in the GFP channel that do not overlap with the adsorbed vesicles are presumably due to protein aggregates or clusters. Examination of multiple images for the same bilayer and images for independently prepared bilayers demonstrated that the amount of protein varied significantly for different bilayer regions and from one bilayer to another (Figure 4.7D-F).

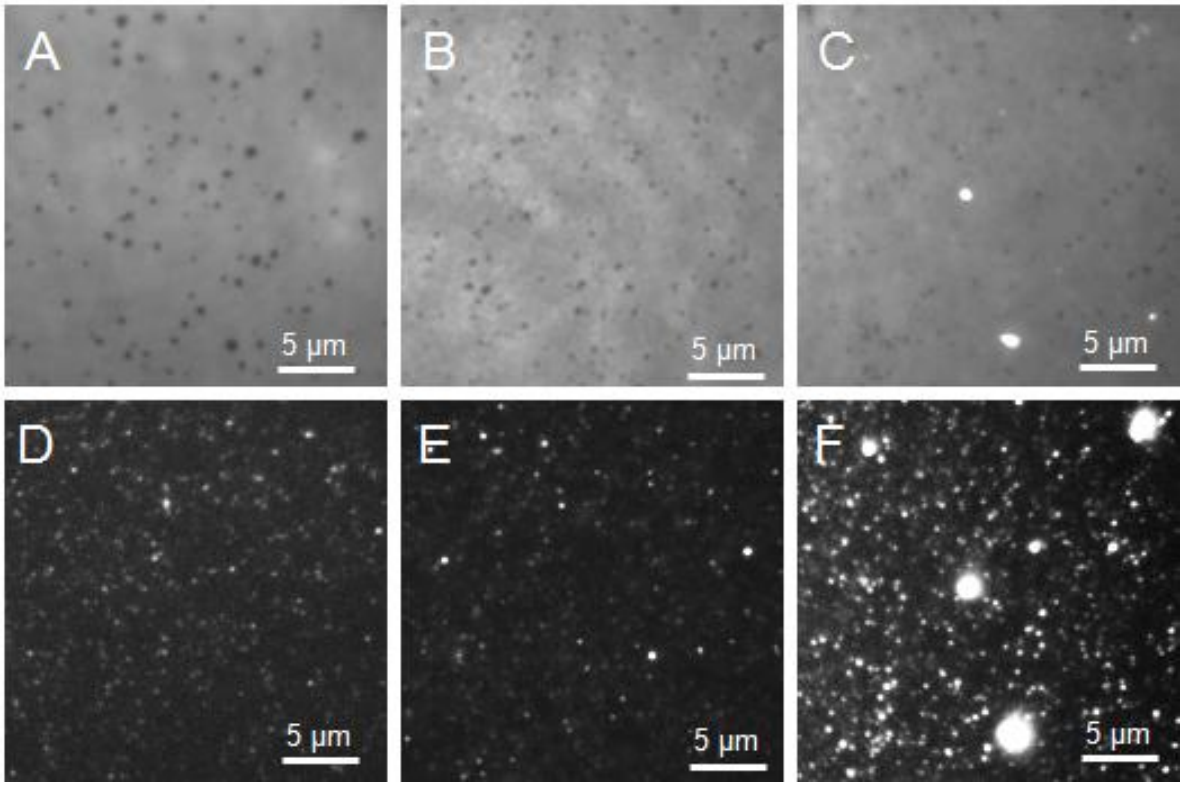

Figure 4.7 Fluorescence images of 3 independently prepared POPC:GFP-Ste14p bilayers on PEG polymer supports using 633 nm excitation (A-C, DiI $C_{22}(5)$) and 488 nm excitation (D-F, GFP). The fluorescence intensity scales are the same for images A-C and D-F.

Figure 4.8 shows a comparison of POPC:GFP-Ste14p bilayers prepared on a PEG support and on glass. The DiI channels show similar quality bilayers for both samples, but the GFP images provide a qualitative indication that there is more protein in the PEG (Figure 4.8E,F). Note that the two samples were prepared from the same proteoliposomes and measured on the same day. Although it is clear that there are a number of bright protein clusters in bilayers on both glass and the PEG support, it is difficult to tell from an initial inspection of the images how much protein is in less bright regions of the bilayer. This was addressed qualitatively by assessing the background signal for the 488 nm channel by imaging a POPC

bilayer on glass (ie, no protein or polymer) labeled with DiI C_{22} (5), Figure 4.8D. This reference background measurement corrects for dark counts as well as any fluorescence or scatter from 488 nm excitation in the absence of GFP. Images for the background reference and the two protein containing bilayers were displayed on the same intensity scale for smaller regions of the bilayer that were chosen to minimize the number of larger protein clusters (Figure 4.8G-I). It is clear from a comparison of these images that a considerable fraction of the bilayer has higher intensity than the background for the POPC:GFP-Ste14p bilayer on PEG. However, for the bilayer on glass, most of the protein fluorescence is localized in the bright features with much lower levels in the surrounding regions. This is illustrated in cross sections for the 3 images shown in Figure 4.8J. The bilayer on PEG shows few or no regions where the signal intensity returns to the background level, by contrast to the bilayer on glass which shows many regions of background only intensity.

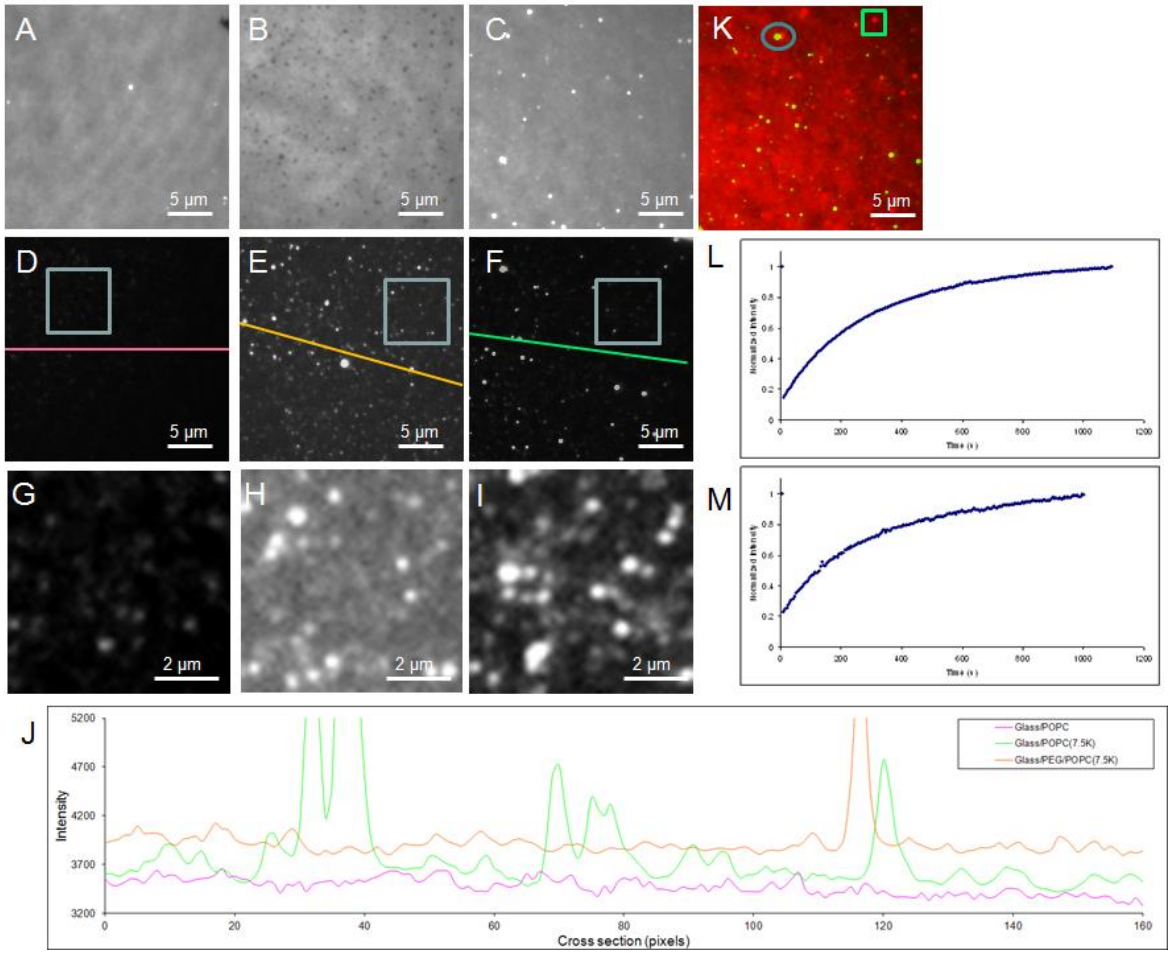

Figure 4.8 Fluorescence images and FRAP recovery curves for a POPC bilayer on a glass substrate (A, DiI $C_{22}(5)$; D,G GFP), a POPC:GFP-Ste14p (1:7500) bilayer on a PEG support (B, DiI $C_{22}(5)$; E,H GFP; L, FRAP) and a POPC:GFP-Ste14p (1:7500) bilayer on a glass support (C, DiI $C_{22}(5)$; F,I GFP; M, FRAP). Fluorescence images C and F have been overlaid to form the composite image K. Cross sections from the GFP fluorescence images are shown in J.

Figure 4.8K shows an overlay image of the DiI and GFP images of a POPC:GFP-Ste14p bilayer on glass. Similarly to Figure 4.7 of a POPC:GFP-Ste14p bilayer on PEG, some of the brighter GFP features overlapped with the bright features assigned to adsorbed vesicles in the DiI channel (blue circle). However, in this case some of the brighter features in the DiI channel did not overlap with bright features in the GFP channel (green square). This result further indicated that the distribution of protein in the ruptured vesicles is heterogeneous.

For comparison of multiple samples it is useful to calculate an average intensity integrated over a large part of the image, rather than to compare individual images. Since the protein distribution was heterogeneous, this was done by imaging multiple regions of the same bilayer and calculating an average intensity for 200 x 200 pixel regions in approximately the center of each image where the excitation beam profile is the most uniform. The same was done for the reference sample to provide an average background to subtract from the GFP signal intensity. We also tested whether similar values for the background were obtained by using an area outside the iris on the excitation beam or by creating a large defect in the sample to provide a bilayer-free region in which to measure the background. Although the 3 methods gave reasonably similar results for stronger signals, the approach of using a protein-free bilayer avoided the need to create defects in the sample, which is sometimes problematic for fluid bilayers in which defects recover by lipid diffusion. The average protein channel intensities for the two bilayers shown in Figure 4.8 are listed in Table 4.3, Entries 4,5 and confirm the qualitative conclusion based on inspection of individual images. Thus, the signal intensity for

the bilayer on PEG is ~ two times the value of that for the bilayer on glass. Note that the average intensities were measured under as closely matched conditions as possible (same exposure, laser intensity, integration of similar regions to avoid variations due to inhomogeneity in the excitation beam profile). Average intensities are based on at least 2 images and typically 4 images. Note that as much as possible, areas that were reasonably free of adsorbed vesicles in the DiI channel were chosen for measuring the average GFP intensities in order to avoid including signals from protein in adsorbed vesicles. However, the presence of a small number of adsorbed vesicles does not contribute significantly to the average (< 3%).

Table 4.3 Average Corrected Protein Fluorescent Intensity, Lipid diffusion coefficients, D, and Mobile Lipid Fractions, F, obtained for POPC:Ste14p bilayers on various supports

Entry	Protein Sample	Sample	Lipid: Protein Ratio	Average Corrected Fluorescence Intensity	D ($\mu m^2/s$)	F (%)
1	1-A	Glass/ POPC(DiI)	7500:1	66	0.94±0.01	96
2	1-A	Glass/PEG/ POPC(DiI)	7500:1	152	0.72±0.01	97
3	1-B	Glass/ POPC(DiI)	No protein	--	2.38±0.01	98
4	1-B	Glass/ POPC(DiI)	7500:1	221	1.08±0.09	97
5	1-B	Glass/PEG/ POPC(DiI)	7500:1	340	0.79±0.02	95
6	1-B	Glass/PEG/ POPC(DiI)	3800:1	688	0.67±0.05	96
7	1-C	Glass/PEG/ POPC(DiI)	7500:1	564	0.75±0.01	96
8	1-C	Glass/PEG/ POPC(DiI)	15000:1	192	1.12±0.16	98
9	2-A	Glass/ POPC(DiI)	No protein	--	--	--
10	2-A	Glass/ POPC(DiI)	7500:1	415	1.19±0.17	98
11	2-A	Glass/PEG/ POPC(DiI)	7500:1	1183	0.67±0.09	98
12	2-B	Glass/PEG/ POPC(DiI)	7500:1	960	0.69±0.01	98
13	2-B	Glass/PEG/ POPC(DiI)	3800:1	1042	0.57±0.03	96
14	2-C	Glass/ POPC(DiI)	No protein	--	--	--
15	2-C	Glass/PEM/ POPC(DiI)	7500:1	213	1.03±0.08	68
16	2-C	Glass/PEG/ POPC(DiI)	7500:1	491	0.98±0.12	98

*Reported D and F are the average of FRAP experiments on two or more areas.

FRAP experiments for the same POPC:GFP-Ste14p bilayers showed that the lipid mobilities were slightly larger on glass, D = 1.08 μm/s^2 (Figure 4.8L, Table 3, Entry 4), than on a PEG support, D = 0.79 μm/s^2 (Figure 4.8M, Table 3, Entry 5) which might be attributed to the lower amount of protein and protein clusters. In both cases the lipid mobility was significantly lower than that for a POPC bilayer on glass, D = 2.38 μm/s^2 (Table 4.3, Entry 3). Mobile lipid fractions for the POPC:GFP-Ste14p bilayers (F $\geq$ 97%) were comparable to those obtained in the absence of protein. Average diffusion coefficients and mobile lipid fractions are based on at least 2 FRAP experiments. These results are consistent with the incorporation of membrane proteins into lipid bilayers as membrane proteins are known to obstruct lateral lipid diffusion.[153]

Several applications such as drug screening devices require high protein concentrations.[265] Figures 4.9 and 4.10 demonstrates a comparison of POPC:GFP-Ste14p bilayers prepared on a PEG support using different protein concentrations. Figure 4.9 shows a comparison between bilayers formed with 7500:1 and 3800:1 lipid to protein ratios. Figure 4.10 shows a comparison between bilayers formed with 7500:1 and 15000:1 lipid to protein ratios. The DiI channels show similar quality bilayers for samples prepared using ratios of 7500:1 and 3800:1 (Figure 4.9A-D, 4.10A,B). However, bilayers prepared using a ratio of 15000:1 showed better quality bilayers in the DiI channel with the absence of small defects. This suggests that lower concentrations of protein form better quality lipid bilayers. The GFP images indicated that there was slightly more protein in the 3800:1 sample than in the 7500:1 sample, Figure 4.9E-H. In addition, the GFP images in Figure

4.10E-H showed that there is less protein in the 15000:1 sample than in the 7500:1 sample. As in the previous experiment the background signal for the 488 nm channel was addressed by imaging a POPC bilayer labeled with DiI C_{22} (5) on glass, in the absence of protein and polymer. Cross sections from the 7500:1 and 3800:1 images and a background sample are shown in Figure 4.9I. The figure shows the 3800:1 sample is similar to the 7500:1 sample where a significant fraction of the bilayer has higher intensity than the background. In contrast, a cross section from the 15000:1 image, shown in Figure 4.10I shows that the 15000:1 sample has most of its protein fluorescence in the bright features with little protein in the surrounding areas. The average protein channel intensities for the 3800:1 and 15000:1 bilayers are listed in Table 4.3, Entries 6 and 8. The intensities confirm the qualitative conclusions that the more concentrated sample has a higher fluorescence signal than the 7500:1 sample and that the less concentrated sample has lower fluorescence than the 7500:1 sample. However, it was also observed that the intensities of the two 7500:1 samples from Figure 4.9 and 4.10 listed in Table 4.3, Entries 5 and 7 were different by a factor of ~2. In this case the samples were measured on different days and the differences may be the result of inhomogeneity in the excitation beam intensity.

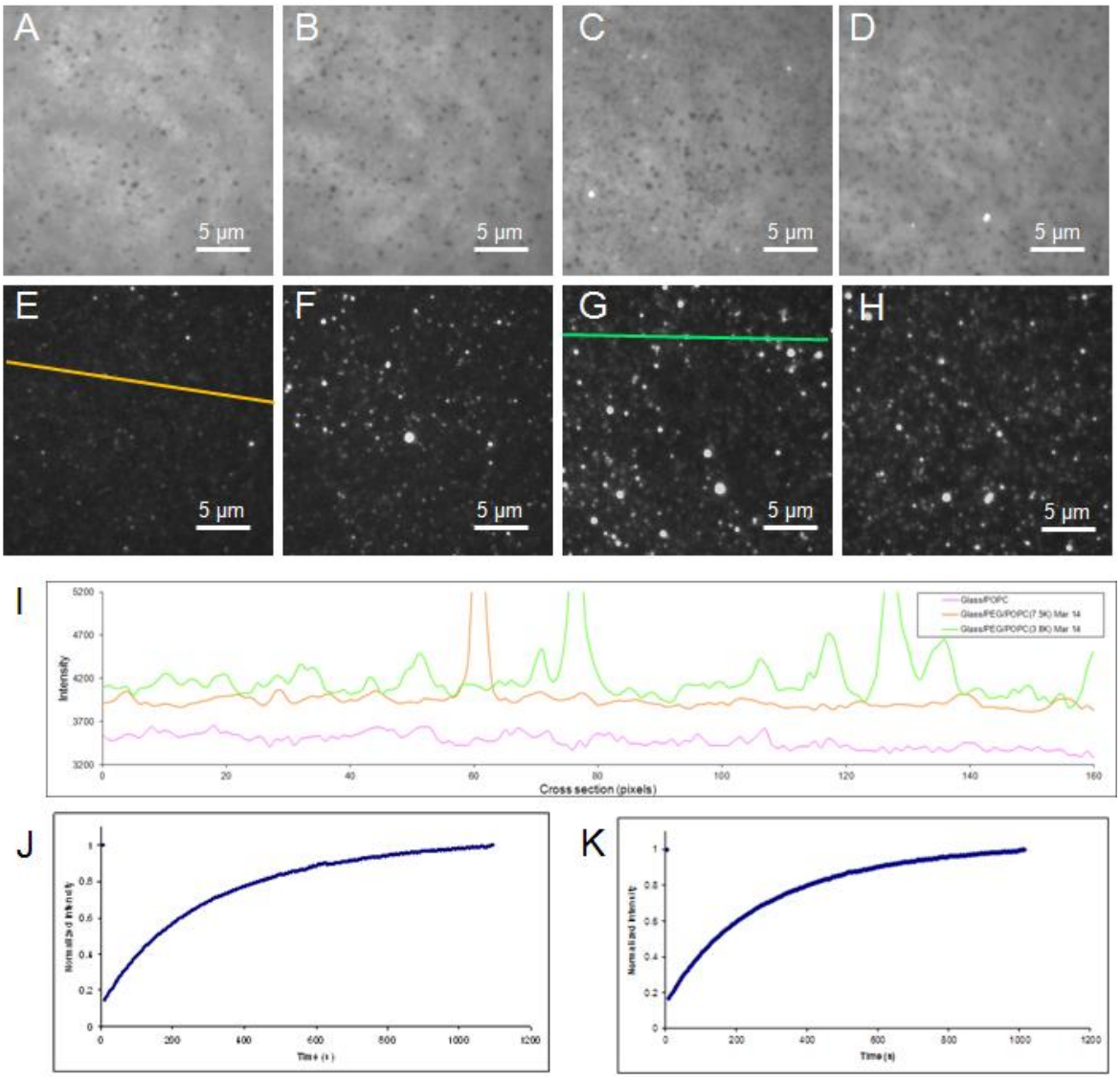

Figure 4.9 Fluorescence images and FRAP recovery curves for POPC:GFP-Ste14p bilayers on a PEG support with lipid to protein molar ratios of 7500:1 (A,B, DiI $C_{22}(5)$; E,F GFP; J, FRAP) and 3800:1 (C,D DiI $C_{22}(5)$; G,H GFP; K, FRAP). Cross sections from the GFP fluorescence images E and G are shown in I.

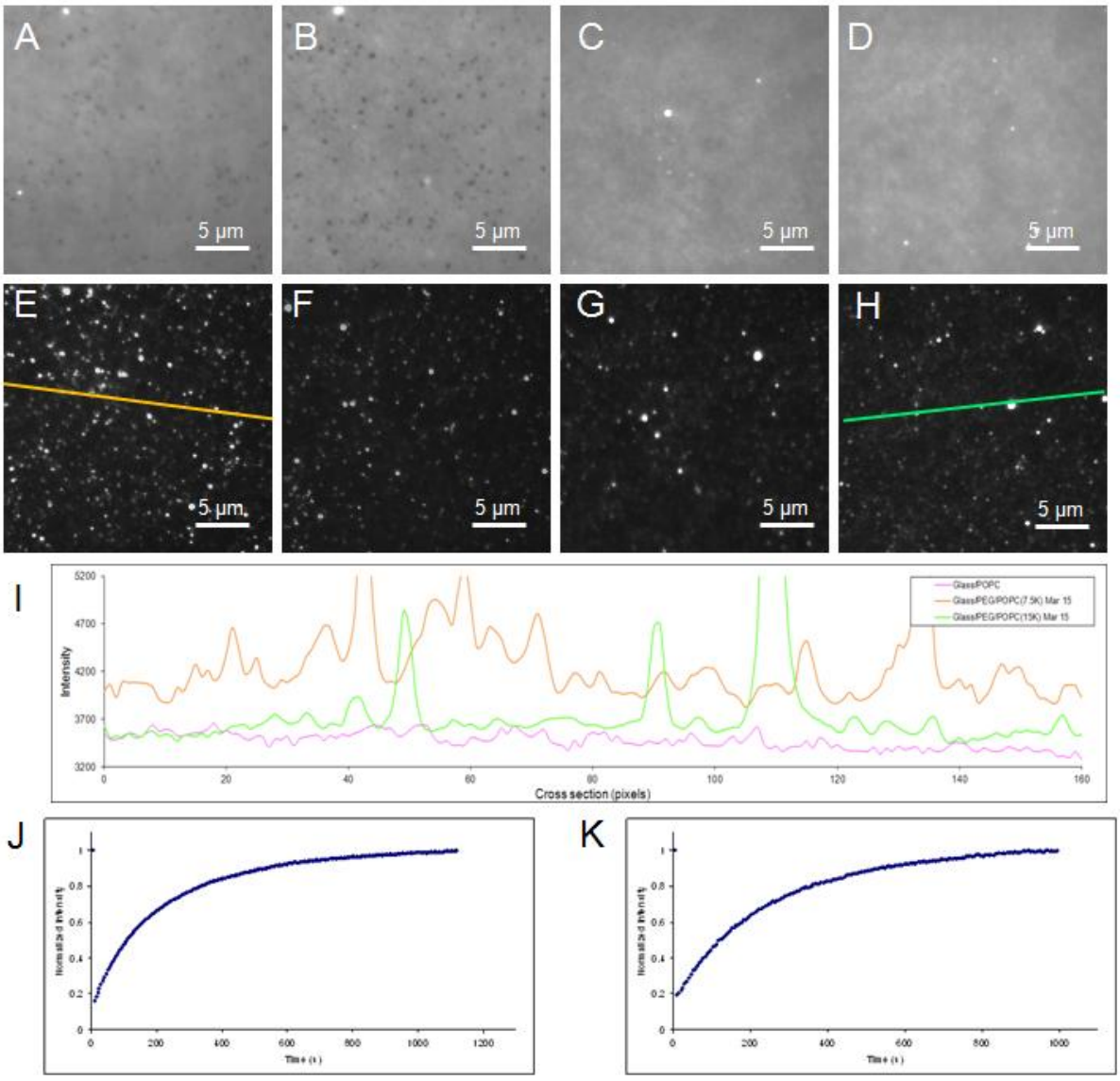

Figure 4.10 Fluorescence images and FRAP recovery curves of POPC:GFP-Ste14p bilayers on a PEG support with lipid to protein molar ratios of 7500:1 (A,B, DiI $C_{22}(5)$; E,F GFP; J, FRAP) and 15000:1 (C,D DiI $C_{22}(5)$; G,H GFP; K, FRAP). Cross sections from the GFP fluorescence images E and H are shown in I.

FRAP experiments for the POPC:GFP-Ste14p bilayers from Figures 4.9 and 4.10 showed that the lipid mobilities were slightly lower using a lipid to protein ratio of 3800:1, D = 0.67 μm/s^2 (Figure 4.9C,D, Table 4.3, Entry 6) and higher using a lipid to protein ratio of 15000:1, D = 1.12 μm/s^2 (Figure 4.10C,D, Table 4.3, Entry 8). The slower and faster diffusion coefficients are likely accredited to the higher and lower amounts of protein in the bilayers. A lipid to protein ratio of 7500:1 produced bilayers with lipid mobility consistent with previous experiments, D = 0.77 μm/s^2 (Figure 4.9A,B and 4.10A,B, Table 4.3, Entries 5,7). Mobile lipid fractions for the POPC:GFP-Ste14p bilayers at different protein concentrations (F $\geq$ 96%) were comparable to those obtained without protein. These results further support that membrane proteins obstruct lateral lipid diffusion.[153]

Lower diffusion coefficients might indicate that a significant fraction of the POPC:GFP-Ste14p bilayers on PEG may possess a large number of nanoscale defects. Nanoscale defects are not visible by fluorescence; thus a set of similar samples were imaged by AFM, as shown in Figures 4.11 and 4.12. Figures 11A,B show AFM images of a POPC:GFP-Ste14p bilayer with a lipid to protein ratio of 7500:1. The images show large areas of uniform bilayer with small defects measuring depths of ~1 nm. A small amount of raised features measuring ~1-3.5 nm higher than the bilayer were also observed in Figures 4.11A,B. The features were likely GFP-Ste14p protein clusters as they were too large to be individual proteins. Figure 4.11C is a fluorescence image of a POPC:GFP-Ste14p bilayer on PEG with a lipid to protein ratio of 7500:1. The fluorescence image suggests that the area scanned by AFM should contain much more reconstituted protein than the

amount that is detected. Therefore, either a large amount of protein is being removed by the scanning of the AFM tip or the protein is orientated into the bilayer such that it can not be detected by AFM.

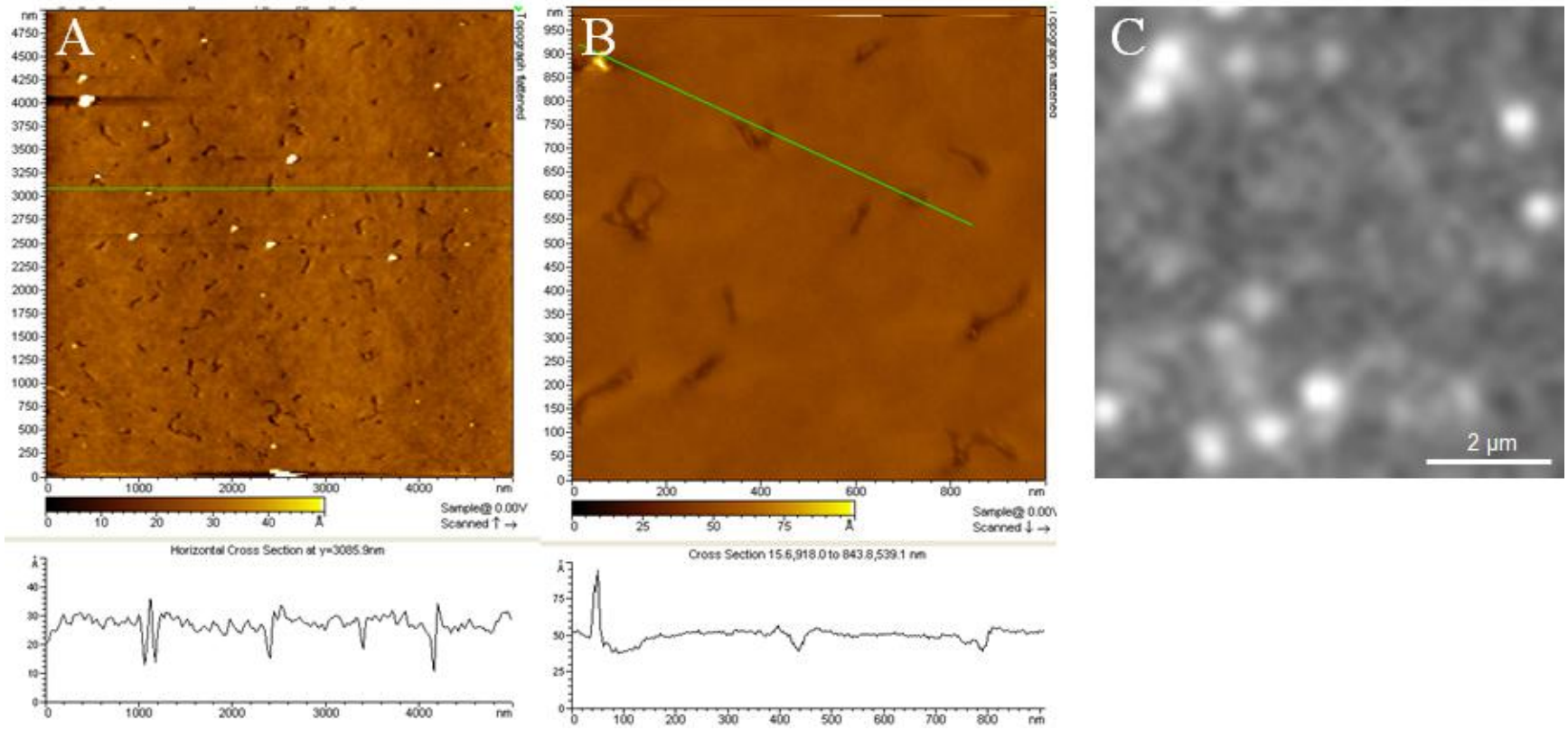

Figure 4.11 AFM images of POPC:GFP-Ste14p bilayers prepared on a PEG support (A,B) at a lipid to protein ratio of 7500:1. A fluorescence image of a POPC:GFP-Ste14p bilayer prepared on a PEG support (C) on a similar x-y scale.

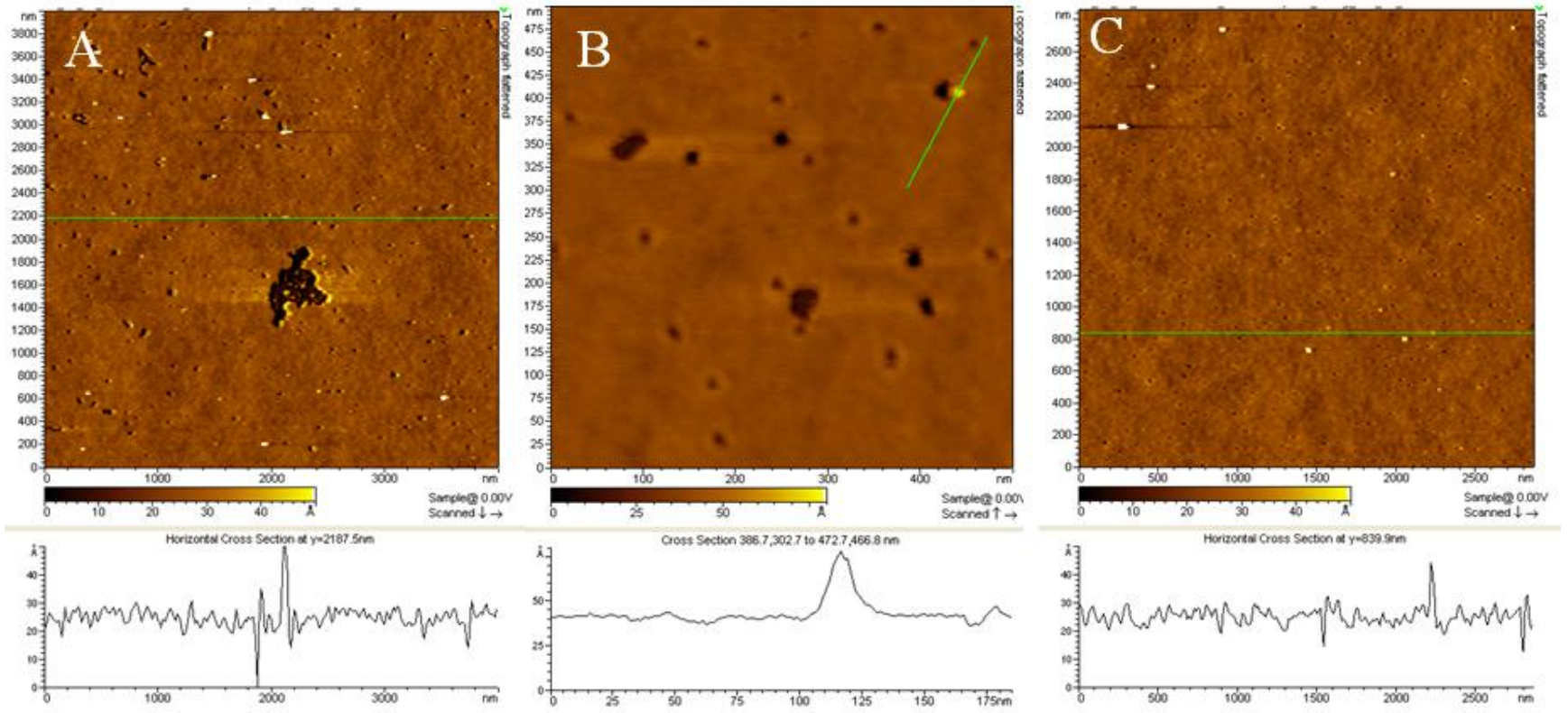

Figure 4.12 AFM images of POPC:GFP-Ste14p bilayers prepared on a PEG support at a lipid to protein ratio of 3800:1 (A,B) and 15000:1 (C).

Figure 4.12 shows AFM images of POPC:GFP-Ste14p bilayers prepared with a lipid to protein ratios of 3800:1 (Figures 4.12A,B) and 15000:1 (Figure 4.12C), respectively. The samples both possessed small defects similar to those in the 7500:1 sample. The samples both showed a small number of raised features measuring ~1-3.5 nm higher than the bilayer. Again the features found in these AFM images were likely protein clusters as they were too large to be individual proteins. The large number of defects found in these samples is likely to have some effect on the lipid diffusion. However, due to the small size of the defects it's likely that the incorporation of protein into these bilayers that has a greater effect on lipid diffusion.

Purified proteins are often stored for an extended period of time while maintaining their original activity. The length of time that they can be stored can vary from a few days to months and is dependent on the nature of the protein and the storage conditions used.[266] Although the protein sample in this study was kept in the appropriate buffer and at -80°C, a fresh sample of protein was obtained from collaborators at Purdue University to test whether the bilayer quality was affected by the age of the protein sample. POPC/GFP-Ste14p proteoliposomes (lipid/protein ratio 7500:1) were formed and deposited on PEG polymer supports using freshly purified protein. POPC:GFP-Ste14p bilayers that were formed at different times are shown in Figure 4.13 and listed in Table 4.3, Entries 11, 12 and 16. The DiI channel shows the formation of three uniform bilayers (Figure 4.13A-C). The GFP channel, Figure 4.13D-F, showed that the samples possessed heterogeneous distributions of intensities similar to the bilayers in Figure 4.7. However, assuming

that the laser intensity was the same in both experiments, the fluorescence intensities of bilayers in Figure 4.13A,B, were ~2 times larger than the intensities of the bilayers formed in Figure 4.7. Inspection of various images for independently prepared bilayers demonstrated that the amount of protein again varied significantly for different bilayer regions and from one bilayer to another. The results suggested that the age of the protein has a slight effect on the amount of protein deposited into a supported lipid bilayer.

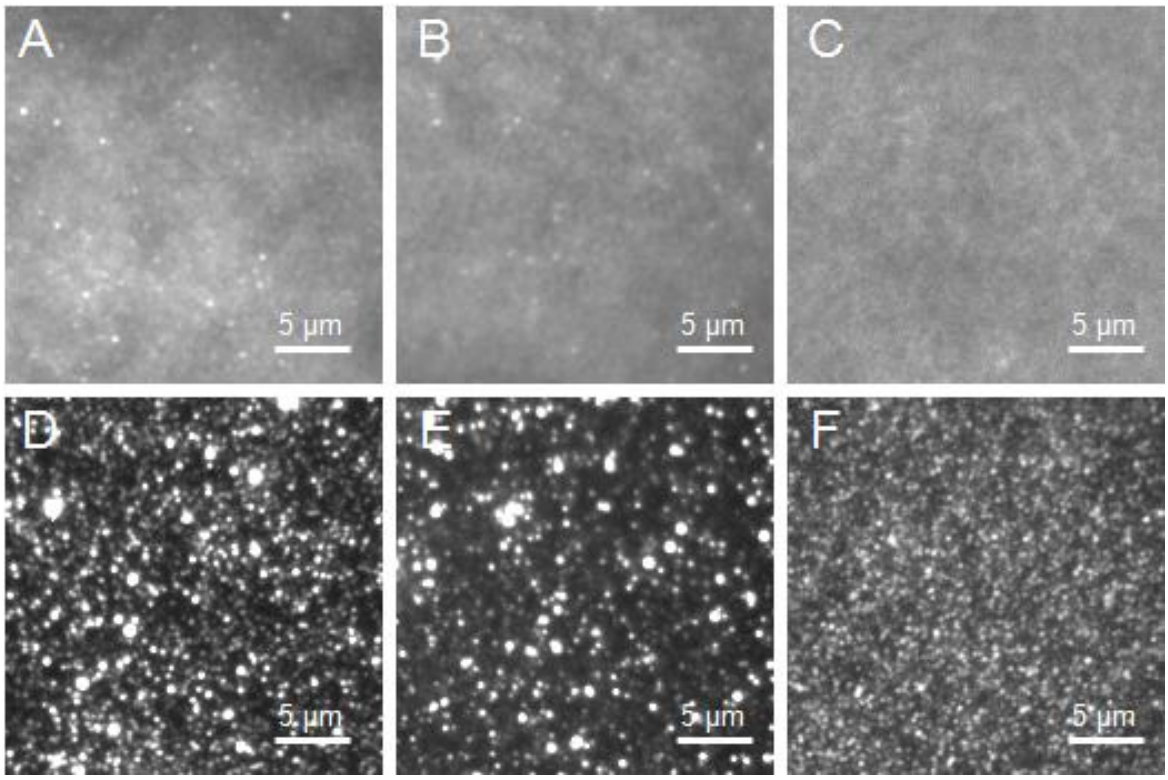

Figure 4.13 Fluorescence images of 3 independently prepared POPC:GFP-Ste14p bilayers using a fresh protein sample on PEG polymer supports using 633 nm excitation (A-C, DiI $C_{22}(5)$) and 488 nm excitation (D-F, GFP).

Figure 4.14 shows a comparison of POPC:GFP-Ste14p bilayers prepared using the new protein sample on a PEG support and on glass. The trend is consistent with the results from Figure 4.8 where the DiI channels show similar quality bilayers for both samples and the GFP images suggest that there is more protein on the PEG support (Figure 4.14E,F). However, similarly to Figure 4.13, the GFP intensities of the samples on both PEG and glass are larger by a factor of ~2 (Table 4.3, Entries 10,11). Smaller regions displayed on different intensity scales for the background reference and the two protein containing bilayers (Figure 4.14G-I) again showed that the majority of the protein signal on PEG was above the background. In addition, the bilayer on glass showed more protein fluorescence but again it was mainly found the bright features. Cross sections from the 3 bilayer images shown in Figure 4.14J, further support the presence of different levels of protein seen in the two protein containing bilayers.

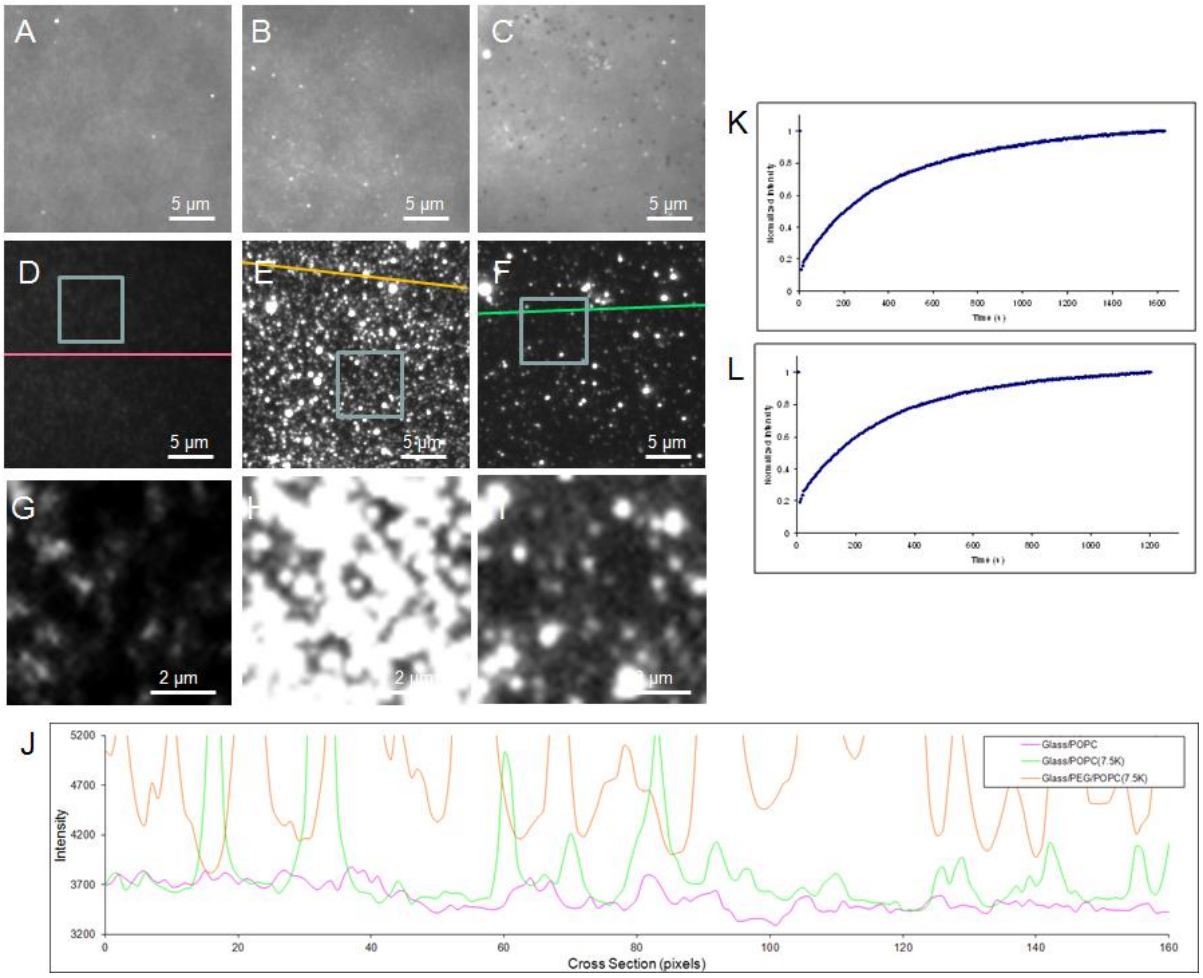

Figure 4.14 Fluorescence images and FRAP recovery curves for a POPC bilayer on a glass substrate (A, DiI $C_{22}(5)$; D,G GFP), a POPC:GFP-Ste14p (1:7500) bilayer on a PEG support (B, DiI $C_{22}(5)$; E,H GFP; K, FRAP) and a POPC:GFP-Ste14p (1:7500) bilayer on a glass support (C, DiI $C_{22}(5)$; F,I GFP; L, FRAP). Cross sections from the GFP fluorescence images D-F are shown in J.

The greater GFP fluorescence intensities shown in Figures 4.13 and 4.14 suggested the age of the protein could have a significant effect on the amount of protein deposited in the supported lipid bilayer. Thus, the comparison of POPC:GFP-Ste14p bilayers prepared on a PEG support using different protein concentrations was repeated with the new protein sample. Figure 4.15 shows a comparison between bilayers formed with 7500:1 and 3800:1 lipid to protein ratios. Similarly to other bilayers prepared with the fresh protein sample, the DiI channel showed the formation of good quality bilayers for both samples (Figures 4.15A-D). Conversely, unlike the previous experiments using different concentrations of protein the DiI channel showed the absence of small defects. The GFP images qualitatively indicated that there was a similar amount of protein in the 3800:1 sample than in the 7500:1 sample in most cases, Figure 4.15E-H. However, in some instances the 7500:1 sample showed different amounts of protein in different areas within a given sample (Figure 4.15E,F). The average intensities of the samples are listed in Table 4.3, Entries 12,13. The 3800:1 sample produced a GFP fluorescent intensity only slightly higher than the 7500:1 sample. Cross sections from the 7500:1 and 3800:1 images and a background sample are shown in Figure 4.15I. The figure shows the 3800:1 sample is very similar to the 7500:1 sample where most of the bilayer has higher intensity than the background and only a few sections have higher intensity than the 7500:1 sample.

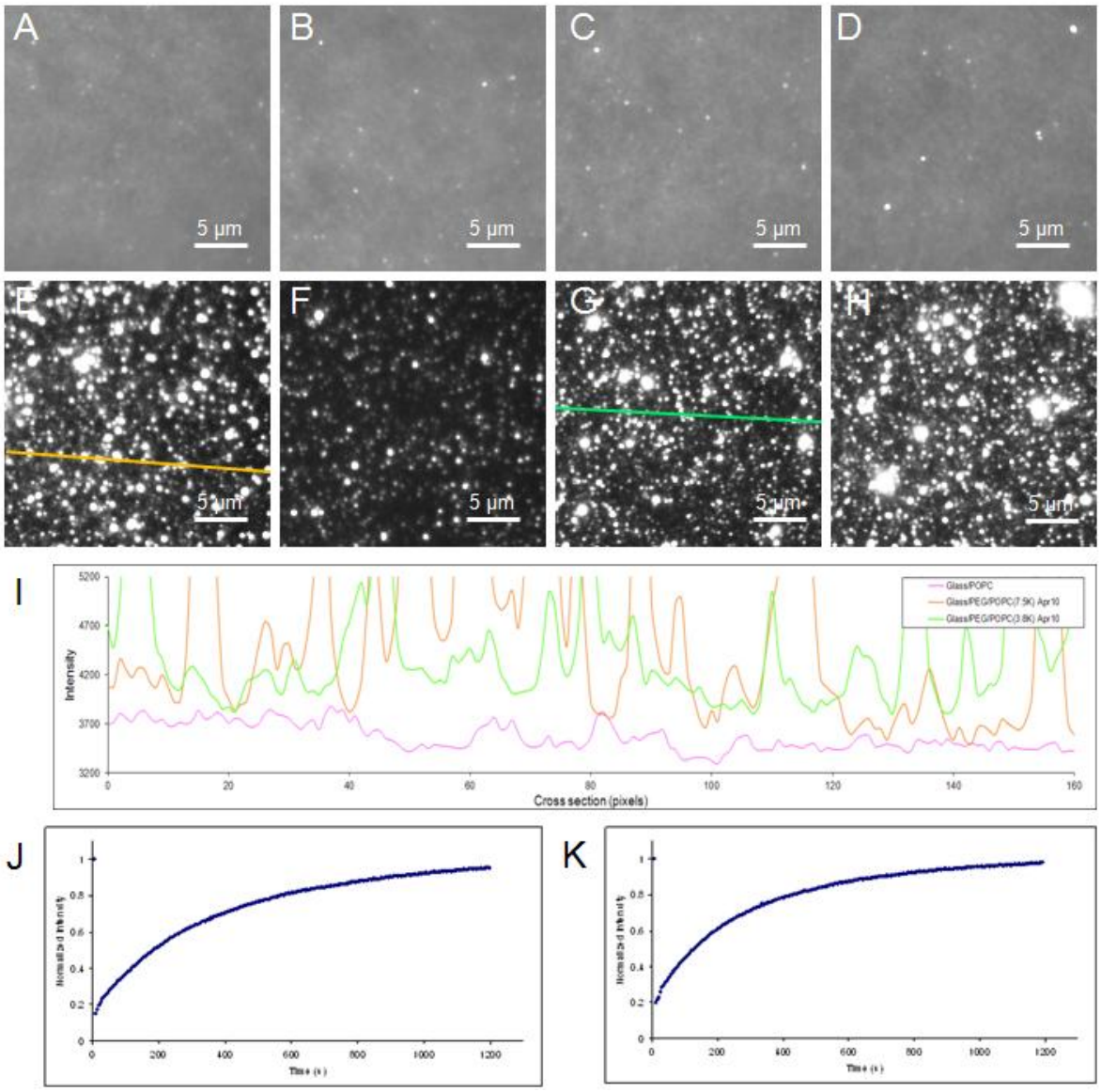

Figure 4.15 Fluorescence images and FRAP recovery curves for POPC:GFP-Ste14p bilayers formed with fresh protein on a PEG support with lipid to protein molar ratios of 7500:1 (A,B, DiI $C_{22}(5)$; E,F GFP; J, FRAP) and 3800:1 (C,D DiI $C_{22}(5)$; G,H GFP; K, FRAP). Cross sections from the GFP fluorescence images E and G are shown in I.

FRAP experiments for the same POPC:GFP-Ste14p bilayers using the new protein sample showed that the lipid mobilities were consistent with bilayers formed using the old protein sample. POPC:GFP-Ste14p bilayers formed on glass, D = 1.19 μm/s^2 (Figure 4.14L, Table 4.3, Entry 10) were slightly larger than those on a PEG support at both protein concentrations, D = 0.67 μm/s^2 (7500:1)(Figure 14M, Table 4.3, Entry 11,12) and D = 0.57 μm/s^2 (3800:1)(Figure 15K, Table 4.3, Entry 13). Mobile lipid fractions for the POPC:GFP-Ste14p bilayers (F $\geq$ 96%) were comparable to the previous experiments in Figures 8-9. These results further demonstrate that the incorporation of membrane proteins into lipid bilayers reduces lateral lipid diffusion.

These results are in good agreement with a study by Graneli *et al.*[71] Graneli showed using the quartz crystal microbalance and surface plasmon resonance techniques that proteoliposomes with lower concentrations of protein, less than 1:1000 protein:lipid molar ratio, produced supported lipid bilayers. Higher concentrations of protein were believed to have reduced proteoliposome-surface interaction and the steric hinderance of liposome-liposome interactions prevented the formation of a supported lipid bilayer. The DiI channel fluorescence images in Figures 4.10-4.12 of the POPC:GFP-Ste14p bilayers at different protein concentrations showed the successful formation of uniform bilayers. Graneli also showed that the more concentrated protein samples possessed a higher quantity of protein in the resulting supported lipid bilayer. In this study there was a slight difference in protein fluorescence intensity for the older protein sample however, the same result was not observed using the newest protein sample. Protein

fluorescence intensities of the least concentrated sample of 15000:1 were much lower than the 7500:1 sample which is consistent with the study performed by Graneli.

A study by Merzlyakov and co-workers made use of FRAP measurements to study the effects of various PEG cushions on the lipid and protein mobilities.[180] The transmembrane peptide FGFR3 was incorporated in POPC PEG supported bilayers. The study aimed to test whether protein mobility in surface supported bilayers was influenced by the method of supported bilayer assembly. Merzlyakov's study examined 160 bilayers using PEG1K to PEG5K variants. Lipid diffusion coefficients for bilayers on these PEG variants ranged between 0.6-3.0 $\mu m^2/s$. PEG2K had the highest peptide diffusion coefficient and the same PEG polymer was used in this study. One of the best bilayer preparation methods was found to be the LB followed by VF method. This was also the technique used to make a PEG supported bilayer in this study. The combination of PEG2K with the LB/VF bilayer preparation method produced lipid and peptide diffusion values of 2.5 $\mu m^2/s$ and 0.0065 $\mu m^2/s$, respectively. Contrary to expectation, the PEG cushion at several molecular weights did not increase the peptide mobility in surface supported bilayers. It was also found that the low protein diffusion was not due to the formation of aggregates within the supported bilayer. In fact, it was shown that the majority of the protein had formed dimers due to sequence-specific protein interactions.[267] Thus, Merzylyakov proposed that the mobility for this peptide is intrinsically low and that further study was required to uncover the general and sequence specific factors that govern protein mobility for this peptide.

Merzylyakov used the FRAP technique to measure diffusion coefficients for the transmembrane peptide FGFR3 in POPC PEG supported bilayers. In this study, we initially planned to use the GFP tag to measure the diffusion coefficients of GFP-Ste14p by FRAP. Initial attempts were unsuccessful as GFP undergoes photobleaching when illuminated with 488 nm light but interestingly, the fluorescence of the GFP completely recovers equally over the photobleached area. This suggests that the fluorescence signal recovers due to reversible photobleaching,[268] not due to diffusion. In fact, illumination of the bleached state of GFP using light between 360-500 nm accelerates the recovery of the fluorescent state. In addition, reversible photobleaching is more pronounced in acidic pH. As a result, the GFP tag on GFP-Ste14p could not be used to measure diffusion coefficients for the protein.

As a comparative method to the use of POPC:GFP-Ste14p proteoliposomes, preliminary experiments using the detergent method to incorporate GFP-Ste14p protein into a POPC bilayer were performed. POPC vesicles were deposited on glass to form a uniform bilayer, Figure 4.16A. Next, the bilayer was incubated for 20 minutes with *N*-dodecyl β-D-maltoside (DDM) at a concentration of 0.085 mM. The sample was then washed and imaged by AFM, Figure 4.16B,C. The AFM images of the sample showed large defects in the bilayer ~4.0 nm. Samples had been previously incubated with DDM for longer time periods; however, unless the sample was washed the sample remained an intact bilayer. Following the formation of a bilayer with large defects, solubilized protein in DDM was added to the sample. Preliminary experiments with the addition of protein revealed that the method

required much more optimization to produce bilayers containing Ste14p. Thus the detergent method was abandoned.

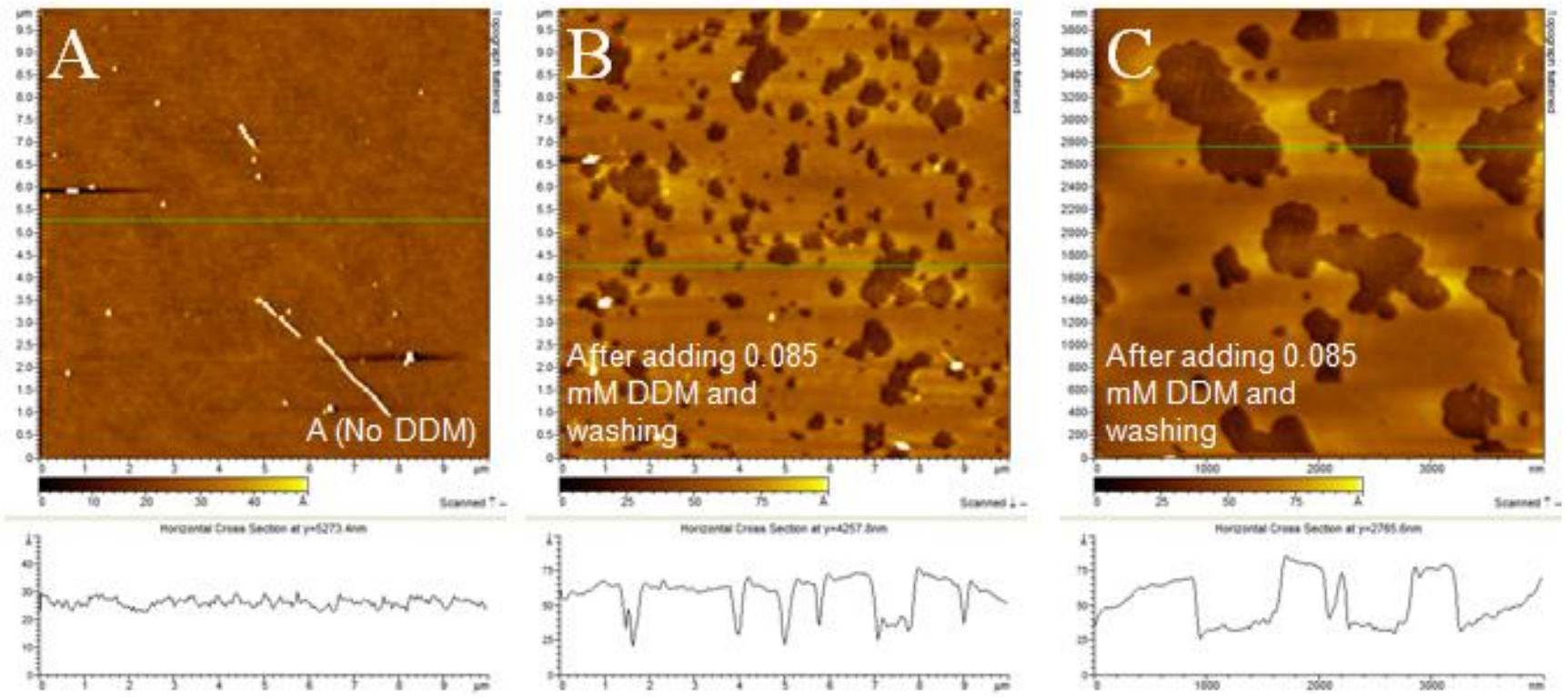

Figure 4.16 AFM images of a POPC bilayer prepared on glass before (A) and after the addition of 0.085 mM DDM (B,C).

4.2.6 Comparison of POPC:GFP-Ste14p Bilayers on Polymer Supports

In the last chapter, we showed the successful formation of a POPC bilayer on a PEM $(CHI/HA)_5$ polymer support at pH 4. Thus, the optimized conditions used to make a POPC:GFP-Ste14p bilayer on mica were altered to pH 4 in order to successfully make a POPC:GFP-Ste14p bilayer on a $(CHI/HA)_5$ substrate. POPC/GFP-Ste14p proteoliposomes (lipid/protein ratio 7500:1 + 0.2 mol% DiI C_{22} (5)) were incubated on a $(CHI/HA)_5$ film on glass in 10 mM $CaCl_2$ and 138 mM MOPS at pH 7.2. Figure 4.17 shows a comparison of POPC:GFP-Ste14p bilayers prepared on a $(CHI/HA)_5$ film and on a PEG support. The DiI channels show similar quality bilayers for both samples (Figures 4.17B-E), although in some areas the bilayers prepared on $(CHI/HA)_5$ films possess some small defects (Figure 4.17B). The GFP images suggest that there is more protein on the PEG support than on the $(CHI/HA)_5$ film (Figure 4.17G-J). The two samples were prepared from different proteoliposomes since different pH conditions were required but, the samples were prepared and measured on the same day. Initial inspection indicates that a heterogeneous layer of protein is present on the PEG support. However, it was unclear whether the a more homogeneous layer of protein existed on the $(CHI/HA)_5$ film or whether the protein signal existed only in the very bright features. Cross sections from the three images show that the majority of the protein fluorescent signal on the $(CHI/HA)_5$ film originates from the brighter features and that the surrounding areas contain very little protein or are in fact background signal. The average GFP fluorescence intensities of the samples are listed in Table 4.3, Entries 15,16. The POPC:GFP-Ste14p bilayer on PEG produced a GFP fluorescence

intensity a factor of ~2 higher than the bilayer prepared on a $(CHI/HA)_5$ film. The intensities confirm the qualitative conclusions that the PEG sample has more GFP fluorescence signal than the $(CHI/HA)_5$ film sample.

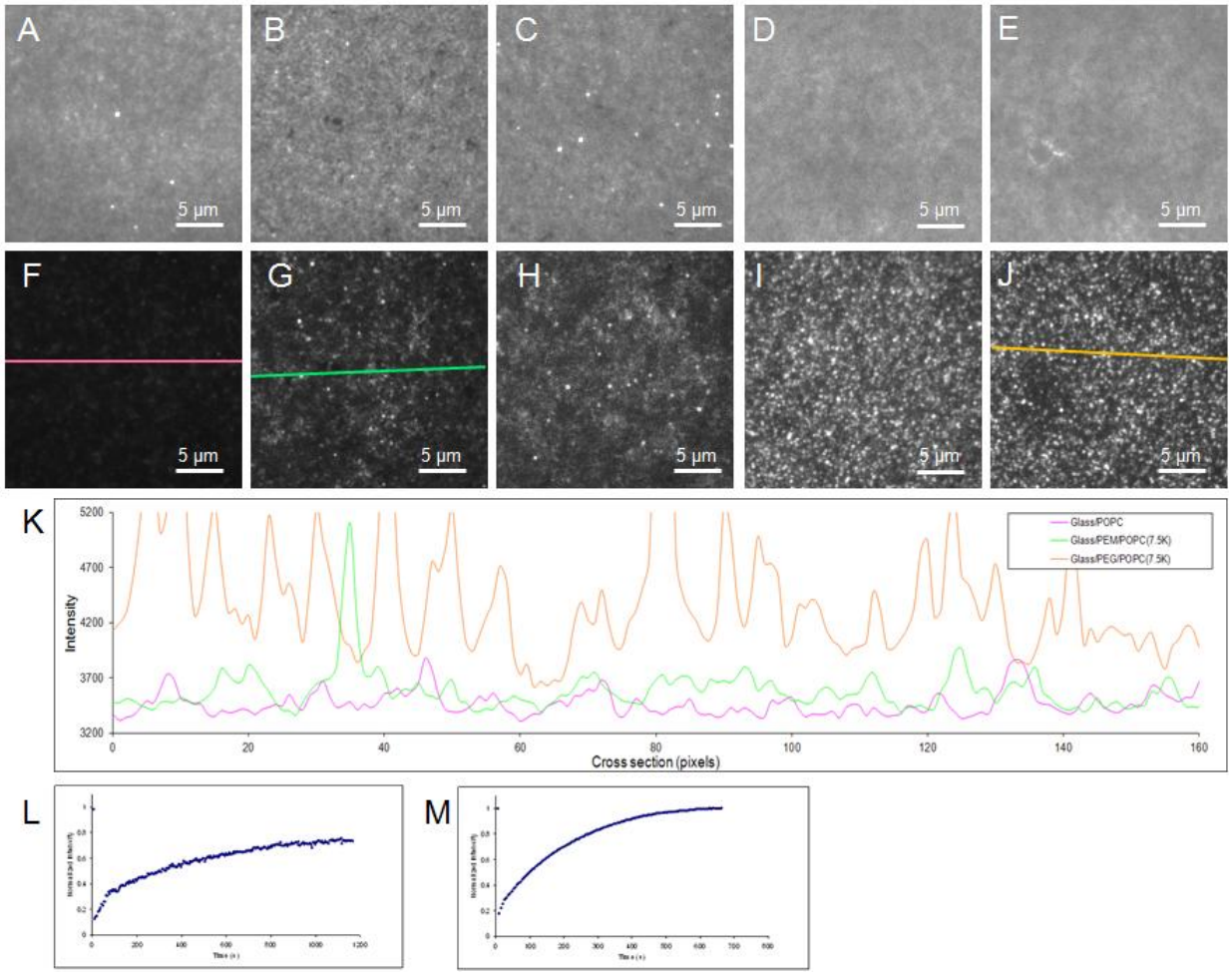

Figure 4.17 Fluorescence images and FRAP recovery curves of a POPC bilayer on a glass substrate (A, DiI $C_{22}(5)$; F GFP), a POPC:GFP-Ste14p (1:7500) bilayer on a PEM support (B,C DiI $C_{22}(5)$; G,H GFP; L, FRAP) and a POPC:GFP-Ste14p (1:7500) bilayer on a PEG support (D,E DiI $C_{22}(5)$; I,J GFP; M, FRAP). Cross sections from the GFP fluorescence images F,G and J are shown in K.

FRAP experiments for POPC:GFP-Ste14p bilayers on a $(CHI/HA)_5$ film produced lipid diffusion coefficients, D = 1.03 $\mu m^2/s$, (Figure 4.17L, Table 4.3, Entry 15) that were lower than in the absence of protein, D = 2.0 $\mu m^2/s$. However, lipid mobilities for POPC:GFP-Ste14p bilayers on $(CHI/HA)_5$ were slightly higher than those on a PEG support, D = 0.98 $\mu m^2/s$ (Figure 4.17M, Table 4.3, Entry 16). Mobile lipid fractions of the POPC:GFP-Ste14p bilayers formed on a $(CHI/HA)_5$ film were similar to that of POPC bilayers formed on a $(CHI/HA)_5$ film, but were significantly lower than for bilayers formed on the other supports. Finally, as in the previous section, the large fraction of immobile lipids is possibly due to electrostatic interaction of the DiI C_{22} (5) dye with the $(CHI/HA)_5$ film.

An investigation by Ma and co-workers used a combination of SPR and FRAP measurements to study the integration of protegrin-1 peptide into SOPS/POPC lipid bilayers on a PEM.[118] The PEM consisted of a PDDA/PSS/PDDA polyion layer, ~2 nm thick, on a mercaptoundecanoic acid (MUA)/gold surface. FRAP measurements indicated that the bilayer with the highest lateral diffusion (D = 2.1 $\mu m^2/s$) consisted of 75% SOPS and 25% POPC. SPR was used to measure the kinetics of the addition of the ion-channel-forming peptide protegrin-1 to the bilayer. The reflectivity of the sample increased instantaneously after addition of the peptide to the bilayer and showed a two-step interaction. The bilayer thickness was found to increase by 1.2 nm which was stated to be in agreement with the successful insertion of the peptide into the polyion supported bilayer. However, the use of SPR alone does not allow for the discrepancy between the insertion of protein into the lipid bilayer and the absorption

of protein on the bilayer surface. As a result, related orientation studies of protegrin-1[269] and other helical antimicrobial peptides[270] were used to support the hypothesis of the successful integration of protegrin-1 in the SOPS/POPC bilayer. The authors suggested that the two-step interaction observed in the SPR measurements corresponded to a surface state, where the peptide is adsorbed to the head group region of the lipid bilayer, and an insertion state, where the peptide is inserted perpendicular to the bilayer plane. The authors make no comparison of this system to other PEM systems or to a system in the absence of a PEM. However, they do state that the supported lipid membrane system is lifted by the PEM cushion and that this system has potential for the study of membrane proteins. Our results are in agreement that a PEM does separate the bilayer from the support and that a small amount of protein is incorporated into the bilayer. However, the amount of protein incorporated into the bilayer is comparable to the amount in the absence of a PEM.

The results presented in this study show that it is possible to incorporate the integral membrane protein into PEM and PEG supported POPC bilayers. The amount of protein incorporated into the samples varies from sample to sample and within a sample. The age of the protein also has an effect on the amount of protein deposited onto the support. The PEM and PEG cushions provide a useful alternative to other solid supports for the preparation of supported bilayers. The PEM and PEG systems make use of biocompatible polymers that act as a soft cushion to increase the spacing between the membrane and the support. The increase in spacing reduces any interactions between the protein and the support

that could affect protein activity. POPC:Ste14p bilayers on PEM and PEG polymer films have lipid mobilities that are comparable to those on a glass support. However, our results demonstrate that the incorporation of protein into the POPC bilayer is greater when membrane formation is performed on a PEG polymer cushioned support than on a glass or PEM support.

4.2.7 Activity of GFP-Ste14p in POPC Bilayers on Polymer Supports

Activity measurements were performed on POPC:GFP-Ste14p bilayers on glass, PEG and PEM supports using an *in vitro* methyltransferase vapor diffusion assay. Protein activity measurements were performed at our collaborators laboratory (Hrycyna Laboratory) at Purdue University. The vapor diffusion assay makes use of scintillation counting to measure the amount of ^{14}C labeled methanol released from the base catalyzed cleavage of methyl esters formed by the reaction between ^{14}C *N*-acetyl-*S*-farnesyl-L-cysteine (AFC) substrate and Ste14p. The results are summarized in Figure 4.18. The PEG supported bilayers showed a small increase in activity over bilayers formed on glass. Bilayers formed at higher protein concentrations showed the expected result of higher activity. As a comparative measurement, unlabeled Ste14p was used to make POPC:Ste14p bilayers on the various supports. Unlabeled Ste14p bilayers at the lower protein concentration (7500:1) produced higher activities than for GFP-Ste14p bilayer but the two proteins had similar activity at a higher concentration (3800:1). POPC:Ste14p bilayers formed on the PEM support showed minimal activity.

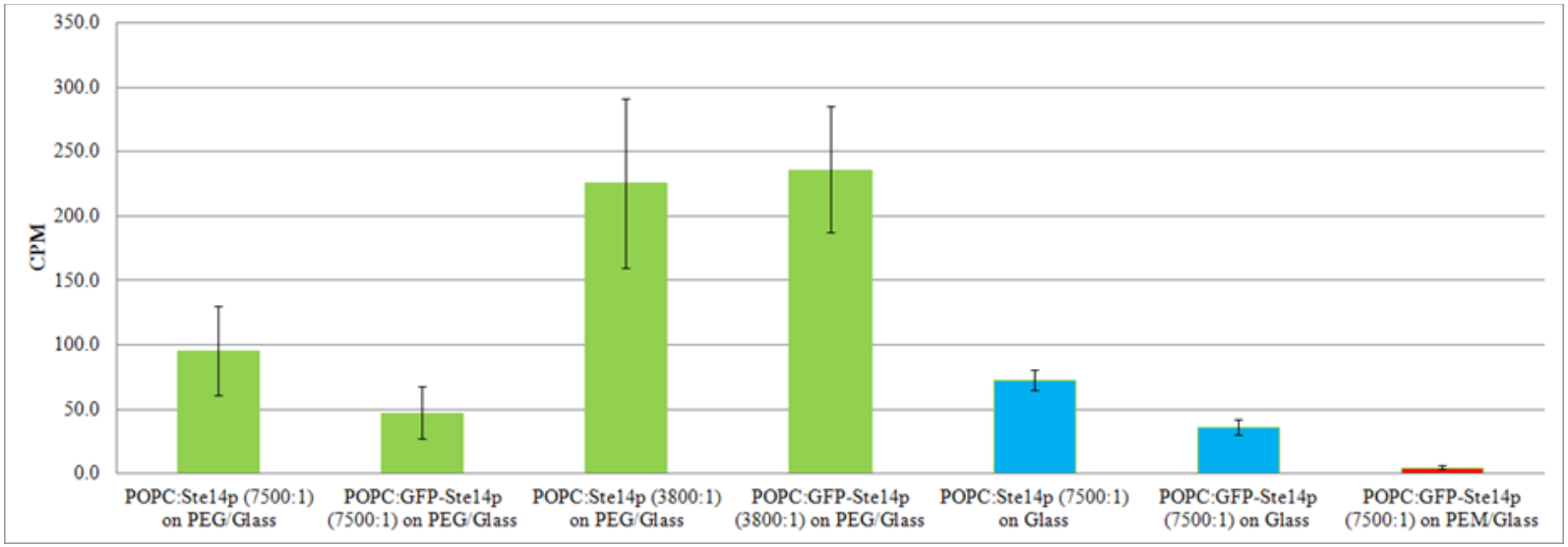

Figure 4.18 Activity measurements of POPC:GFP-Ste14p and POPC:Ste14p bilayers on different supports.

A recent study by Renner *et al.* made use of fluorescence and an activity assay to examine the reconstitution of a transmembrane protein, BACE, into a PC:PS:PE (6:2:2 molar ratio) supported lipid bilayer on maleic anhydride copolymer films.[148] It was shown that the best integration of BACE was on a poly(ethane-*alt*-maleic anhydride) (PEMA) support. The lipid and protein mobilities were found to be 1.24±0.14 $\mu m^2/s$ and 0.11±0.024 $\mu m^2/s$, respectively. In addition, the successful integration of BACE was also correlated to the thickness of the polymer (PEMA thickness = 60 nm) which was believed to have decreased the protein-support interactions. The activity of BACE at various concentrations integrated into a supported lipid bilayer was also investigated. The results showed an enhanced BACE activity on the polymer cushions. The BACE protein integrated into supported lipid bilayers on a polymer support converted 1.5-2.5 times more amyloid precursor substrate analogue, FS-1, per minute than on a silica support. These results led to the conclusion that the polymer cushion decoupled the transmembrane protein from the solid support resulting in an increase in protein mobility and activity.

In order for a model membrane system on a polymer support to be deemed useful, integrated membrane proteins must retain their integrity and activity. The activity assay results in this study suggest that the activity of Ste14p in POPC supported lipid bilayers is slightly increased with the use of a PEG polymer cushion. However, the GFP fluorescence data suggests that much more protein is present on the PEG support than on the glass support. The activity measurements support the fluorescence data showing that there is active protein in the lipid bilayers on

PEG and glass. However, to make a quantitative comparison between samples one needs to determine the protein concentration in the bilayer. Due to the small amounts of protein incorporated into the bilayer, <10 µg, a direct calibration on the amount of protein in the bilayers was not obtained. Thus, the activity results can only be reported as apparent values as the concentration of protein in the supported bilayer can not be determined. The activity results suggested that the use of a biocompatible PEM as a polymer cushion to make supported POPC:Ste14p bilayers was detrimental to the activity of the membrane protein. It was hypothesized that maintaining a protein at pH 4 for a long period of time could reduce the activity of the protein. As a control measurement, the activity of a sample of Ste14p placed in buffer at pH 4 for 18 hours was measured. The protein showed that 90% of the activity remained after incubation. The PEM and PEG cushions provide membrane spacing of ~60 nm and ~6 nm, respectively. If the successful integration of Ste14p was correlated to the thickness of the polymer we would expect to have observed a greater protein activity on the PEM support than on the PEG support. The pH of our system was different and the results obtained were in fact the opposite of this hypothesis. As a result, other factors must be taken into account when trying to develop an ideal polymer support for the incorporation of a membrane protein into a supported bilayer.

4.2.8 Conclusions

Supported lipid bilayers incorporating an integral membrane protein, GFP-Ste14p, were formed on glass, PEM and PEG polymer supports. PEG supported

POPC:Ste14p bilayers incorporated the greatest amount of protein by fluorescence measurements and showed slightly better protein activity than other supports. Glass supported POPC:Ste14p bilayers incorporated a lower amount of protein by fluorescence measurements and showed moderate protein activity indicating that it possessed a higher fraction of active protein. Detection of protein by AFM was difficult however, the presence of some protein clusters in the supported POPC:Ste14p bilayers on PEG and on glass was observed. Lipid diffusion measurements for the POPC:Ste14p bilayers on the various types of supports were comparable. These results of incorporating an integral membrane protein into a polymer supported bilayer can be extended to apply these systems as possible substrates for supported membranes for biosensing applications. Furthermore, the results demonstrate that a variety of factors must be considered when attempting to choose a polymer support to successfully incorporate an active membrane protein.

4.3 Experimental

4.3.1 Materials

Lipids 1-palmitoyl-2-oleoylphosphatidylcholine (POPC), 1,2-diphytanoyl-*sn*-glycero-3-phosphocholine (DPhPC) and 1,2-dipalmitoyl-*sn*-glycero-3-phosphoethanolamine-*N*-[methoxy(polyethylene glycol)-2000] (PEG-DPPE) were obtained from Avanti Polar Lipids and used as received. All aqueous solutions were prepared with 18.3 MΩ cm Milli-Q water. DiI C_{22} (5) was obtained from Molecular Targeting Technologies, Inc. Low molecular weight chitosan (CHI, MW = 5 x 10^4 g/mol),

hyaluronic acid sodium salt (HA, MW = 1.63 x 10^6 g/mol) from *Streptococcus equi*, MOPS and all other materials were obtained from Aldrich (>98% pure) and used as received. Glass coverslips (No. 1, 25 mm) were obtained from Fisher Scientific.

4.3.2 Assembly of PEM

Using the previously described layer-by-layer (lbl) assembly method the polyelectrolyte multilayers were constructed a glass substrates [164,244]. Briefly, substrates were firstly cleaned in a piranha solution consisting of 70% concentrated sulfuric acid and 30% hydrogen peroxide, followed by rinsing with copious amounts of Milli-Q water and then nitrogen drying. The polyelectrolyte solutions (1.0 g/L) were prepared in 0.15 M NaCl, and the pH of the solutions was adjusted to 4.5 using aqueous concentrated acetic acid solution. Prior to use the polymer solutions were filtered through a 0.45 µm Millipore PVDF filter. Using a homemade glass fluid cell holder the glass substrates were immersed in aqueous CHI solution for 15 min and then removed and placed in a beaker containing 350 mL of NaCl solution (0.15 M, pH 4.5) for 1 min. The glass substrates were then removed and placed in a second beaker containing 150 mL of NaCl solution (0.15 M, pH 4.5) for another 5 min to ensure the removal of excess CHI. HA was then deposited on the substrate surface following the same dipping/rinsing procedure described above for CHI. After 5 bilayers of the CHI/HA polymers, the PEM assembly was completed and the PEM-coated substrates were dried using a stream of N_2. Rinsing beakers containing aqueous NaCl solution were changed after 3 uses. The PEM-coated

substrates were stored in a nitrogen box until used for bilayer preparation, typically within 1-2 days and never more than 1 week.

4.3.3 Preparation of Small Unilamellar Vesicles

Chloroform solutions of lipids and dyes were mixed, the solvent was removed, and the film was dried under vacuum overnight. The lipid films were then hydrated in Milli-Q water containing (a) 138 mM MOPS and 140 mM NaCl at the desired pH, 4 or 7.2 (for preparation of PEM supported bilayers) or (b) 138 mM MOPS at pH 7.2 (for preparation of PEG-supported bilayers) and vortexed to obtain multilamellar vesicles. Small unilamellar vesicles were prepared by bath sonication with an initial temperature of 20°C to form clear dispersions with a final lipid concentration of 0.75 mg/mL. Vesicles were stored at 4°C and used within 1 week.

4.3.4 Reconstitution of Ste14p into POPC Vesicles (Lipid:Protein Molar Ratio = 7500:1)

Purified Ste14p was reconstituted by rapid dilution in the presence of POPC lipid vesicles as previously described [202]. A sample of 5 µL of protein (3.2 mg/mL) in elution buffer consisting of 35 mM Na_2PO_4, 210 mM NaCl, 8% glycerol, 1.6 mM AEBSF, 1.2 mg/mL Aprotinin, 0.1% DDM and 1 M Imidazole at pH 7.2 was set on ice and left to thaw. In a separate vial 231 µL of POPC lipid vesicles (0.75 mg/mL) in 138 mM MOPS at pH 7.2 was measured out. The thawed protein sample was diluted in 25 µL of 10 mM MOPS. From the newly formed diluted protein sample, 3 µL was added to the vial containing the lipid vesicle suspension. The protein vesicle

containing solution was then reconstituted by rapidly adding 460 µL of 138 mM MOPS buffer at pH 7.2. The reconstituted sample was then incubated on ice for 10 minutes. Following the incubation time the sample was stored at 4°C and used within 1 week.

4.3.5 Preparation of Supported Bilayers

a. PEMs. An aliquot of vesicle solution (100 µL) and Milli-Q water (400 µL) containing 10mM CaCl2, 140 mM NaCl and 138 mM MOPS at the desired pH, 4 or 7.2, were added to a $(CHI/HA)_5$ PEM substrate and clamped into a TIRF or AFM liquid cell. After incubation at room temperature overnight, the bilayers were rinsed extensively with Milli-Q water containing 140 mM NaCl and 138 mM MOPS at the corresponding pH to remove unattached vesicles before imaging.

b. PEG Tether. A polymer-doped monolayer was prepared by Langmuir-Blodgett deposition on a Nima 611 trough. A POPC solution (1 mg/mL) with 7 mol % PEG-DPPE was prepared in chloroform, and 20 µL of the lipid solution was deposited at the air-water interface. After waiting 15 min to allow for chloroform evaporation, the lipids were compressed to a surface pressure of 32 mN/m. Two glass coverslips placed back to back were then raised vertically out of the trough at a rate of 15 mm/min, allowing deposition of a PEG-supported lipid monolayer on only the exposed side of each coverslip. An aliquot of vesicle solution (100 µL) and Milli-Q water (400 µL) containing 138mM MOPS at pH 7.2 were added to the monolayer-coated substrate and clamped into a TIRF or AFM liquid cell. After incubation at room temperature for 1 h, the bilayers were rinsed extensively with

Milli-Q water containing 138 MOPS buffer at pH 7.2 to remove unattached vesicles before imaging.

4.3.6 Atomic Force Microscopy

The AFM images were obtained at room temperature (23 ± 1°C) using a PicoSPM atomic force microscope (Molecular Imaging) in MAC mode. Magnetic coated silicon tips with spring constants of ~0.5 N/m and resonance frequencies between 5 and 40 kHz in aqueous solution were used. A 6 x 6 μm^2 scanner was operated at a scan rate between 0.7 and 1.3 Hz. The images shown are flattened raw data and imaged at minimal force. Two or more independently prepared samples were imaged for each set of conditions with several areas scanned for each sample.

4.3.7 Fluorescence Microscopy

Fluorescence images of bilayers were taken on an Olympus IX81 total internal reflection fluorescence (TIRF) microscope equipped with a back-illuminated electron multiplying CCD camera (Cascade 512B, Photometrics) and a 100x/1.30 NA Plan Fluar oil UV objective (Zeiss). Supported bilayers containing either DiI C_{22} (5) (0.2 mol%) or Ste14p-GFP were excited at 633 or 488 nm, respectively. Filter sets used were Cy5 and FITC for the images obtained using 633 and 488 nm, respectively. Images shown are all measured as epi-fluorescence images.

4.3.8 Fluorescence Recovery after Photobleaching (FRAP)

FRAP experiments for bilayers labeled with 0.2% DiI C_{22} (5) were conducted on an Olympus IX81 microscope (epi-fluorescence mode) by bleaching a >55 µm diameter spot with full laser power (1.69 mW) at 633 nm for 1-3 s. The fluorescence recovery was recorded with a 100x objective with a 5 s interval between images at a reduced laser power (<1.69 mW). Image analysis was performed using National Institutes of Health Image J software (http://rsb.info.nih.gov/ij/). Diffusion coefficients were estimated following the approach of Soumpasis with normalized intensities fit to a two-dimensional diffusion equation.[49] Reported diffusion coefficients and mobile fractions are the average of bleaching experiments on multiple areas for at least 2 independently prepared bilayers.

4.3.9 *In vitro* Methyltransferase Vapor Diffusion Assay of POPC:GFP-Ste14p Bilayers

The assay was developed and performed as previously described with some modifications.[271] The optimal concentration of AFC was determined to be 10 µM. The bilayer reaction mixtures contained 20 µM of AFC and 40 µM *S*-adenosyl-L-[^{14}C-methyl] methionine in a total volume of 60 µL. The bilayer reaction mixtures were prepared by the addition of 20 µL of a 120 µM *S*-adenosyl-L-[^{14}C-methyl] methionine solution, 1 µL of a 1.2 mM AFC solution, and 39 µL of 138 mM MOPS buffer at pH 7.2. The previously prepared 120 µM *S*-adenosyl-L-[^{14}C-methyl] methionine solution was diluted to 120 µM in 138 mM MOPS buffer at pH 7.2. The

AFC solution was prepared at 1.2 mM in DMSO to minimize the percentage of DMSO incubated with the lipid bilayers.

The 9 mm diameter wells containing lipid bilayers were submerged in approximately 60-70 µL of 138 mM MOPS buffer at pH 7.2 and 60 µL of the reaction mixture. This yielded a final concentration of 20 µM S-adenosyl-L-[14C-methyl] methionine and 10 µM AFC. The reactions were then incubated in a 30 °C water bath for 2 h. From each bilayer well, 80 µL was removed and placed into a 1.7 mL microcentrifuge tube. Next, 60 µL of 1% SDS was then added to each well and pipette mixed in order to solubilize each bilayer and remove the 14C-methylated AFC. After 45 seconds, the entire volume was removed from well and placed in the microcentrifuge tubes containing 80 µL of previously removed sample. Each centrifuge tube was charged with 60 µL of 1 M NaOH in 1% SDS, vortexed, and the mixtures were spotted onto filter paper. The filter papers were then wedged into the neck of 20 mL scintillation vials followed by incubation at room temperature for 2.5 hr. The filter papers were then pulled from the scintillation vials and 14C methyl groups transferred to the paper were counted by a Packard Tri-carb 1600CA liquid scintillation counter

Chapter 5: AFM Investigation of Ste14p in Nanodiscs

This chapter contains Material Adapted from the following manuscript

1. B. Schilling, K. Mulligan, D. H. Thompson, L. J. Johnston, C. A. Hrycyna; Functional Reconstitution and AFM Characterization of the *Saccharomyces cerevisiae* Isoprenylcysteine Carboxylmethyltransferase Ste14p in Nanodiscs. *In preparation*.

2. Nanodiscs samples were contributed by collaborators.

5.1 An Alternate Technique to Study Membrane Proteins: Nanodiscs

Recently, a technique to study membrane proteins has been invented that makes use of phospholipid nanodiscs.[191] The incorporation of membrane proteins into phospholipid nanodiscs has several advantages over other model membrane systems. Nanodiscs have the advantage of self assembly and the ability to encapsulate individual proteins. Nanodiscs provide a small native phospholipid environment for individual membrane proteins. The have also been shown to be reliably and reproducibly prepared.[192] The literature precedents demonstrate that a number of membrane proteins have been reconstituted into phospholipid nanodiscs. For example, lipid nanodiscs have been used to isolate monomeric and oligomeric forms of CYP34A, a cytochrome P450.[193,272] Kinetic binding differences were observed when comparing CYP34A in lipid nanodiscs and detergent solubilized CYP34A.[193] Differences were also discovered when comparing monomeric and aggregates of CYP34A.[193,273] Nanodiscs have been used to investigate the relationship between function and oligomerization states. G-protein coupled receptors, rhodopsin and the β-2 adrenergic receptor, as well as some bacterial chemoreceptors have all been studied using a nanodisc support.[198,274,275] Lipid nanodiscs have also been used to alleviate sample heterogeneity in the EPR analysis of MalFGK2, an ABC transporter.[276] The development of nanodiscs has aided researchers to address some of the challenges associated with the functional and biophysical studies of membrane proteins.[277,278]

5.1.1 Motivation for Incorporating Ste14p in Nanodiscs

The integral membrane protein, Ste14p, has been shown to exist as a homodimer or higher order oligomer through chemical crosslinking, co-immuno precipitation, and co-purification studies.[279] Immunoblot analysis of Ste14p in crude membranes as well as purified Ste14p revealed a homodimer as the predominant species with smaller amounts of higher order oligomers present, including trimers and tetramers. Untagged Ste14p was found to co-immunoprecipitate with His-Ste14p indicating that Ste14p exists as a homodimer in cells. Untagged Ste14p was also found to be co-expressed and co-purified with His-Ste14p and inactive variants of His-Ste14p. These results indicated indirectly that the interaction of Ste14p monomers is essential to enzymatic function and that Ste14p forms a homodimer or higher order oligomer.[279] Further experiments are required to conclusively demonstrate the oligomerization state of Ste14p, specifically if it is a homodimer. Our collaborators at Purdue University examined the oligomerization state of detergent solubilized His-Ste14p in nanodiscs utilizing analytical ultracentrifugation and size exclusion chromatography coupled with multi-angle light scattering. AFM is a complimentary technique that has previously been used to accurately discriminate different types of nanodiscs based on heights.[191-193,195,197,280] As a result, our part of the project that is described in this chapter was an AFM investigation of Ste14p reconstituted into lipid nanodiscs. AFM analysis of the incorporation of Ste14p into nanodiscs showed that two types of discs were present with a height difference of ~1 nm. The taller nanodiscs were believed to contain Ste14p.

5.2 Characterization of Nanodiscs

5.2.1 AFM Characterization of Empty Nanodiscs

Lipid nanodiscs were created by the solubilization of Ste14p in the presence of buffer (MOPS), detergent (DDM), phospholipids (*E coli.* lipid extract mixture) and a helical protein belt (MSP1D1E3).[191] Ste14p spontaneously assembles with the phospholipids to form a nanodisc once detergent is removed from the system by dialysis or adsorption to hydrophobic beads. The MSP MSP1D1E3 variant forms nanodiscs with diameters in the range of ~12.5-13 nm.[277] The nanodisc samples provided by our collaborators were obtained in several concentrations dissolved in 25 mM MOPS buffer with 150 mM NaCl at pH 7.2. The different concentrations arise from the purification step in the nanodisc synthesis. Different fractions collected during the removal of the detergent with hydrophobic beads possess different amounts of discs and thus different concentrations. Once received an aliquot of the nanodisc sample was diluted to a concentration of 0.1 mg/mL. The samples were further diluted to a concentration of 2.0×10^{-3} mg/mL in an AFM cell mounted on a sheet of freshly cleaved mica. The nanodisc samples were then incubated at room temperature for 15 minutes. The incubation time was sufficient for the discs to absorb to the mica surface. The sample was then washed to remove any unabsorbed nanodiscs and imaged by AFM.

AFM imaging of empty and GFP-Ste14p nanodiscs on mica was first performed in contact mode. Contact mode AFM has been shown to successfully image similar nanodiscs in previous studies.[191] Thus, it was hypothesized that a close packed layer of empty nanodiscs could be imaged using contact mode AFM

with good resolution. In addition, it was thought that a close packed layer of nanodiscs would prevent any slight movement of the discs during imaging. The contact mode AFM images, Figure 5.1, show a layer of nanodiscs with small spacings between discs. Although individual discs could be observed, their size and shape were not well-defined. Several attempts were performed to visualize nanodiscs by contact mode AFM at many different force setpoints with several types of AFM tips possessing low spring constants, $k < 0.05$ N/m. However, either the compression or the slight movement of the nanodiscs caused by the applied or lateral force produced images of the discs that were not well resolved.

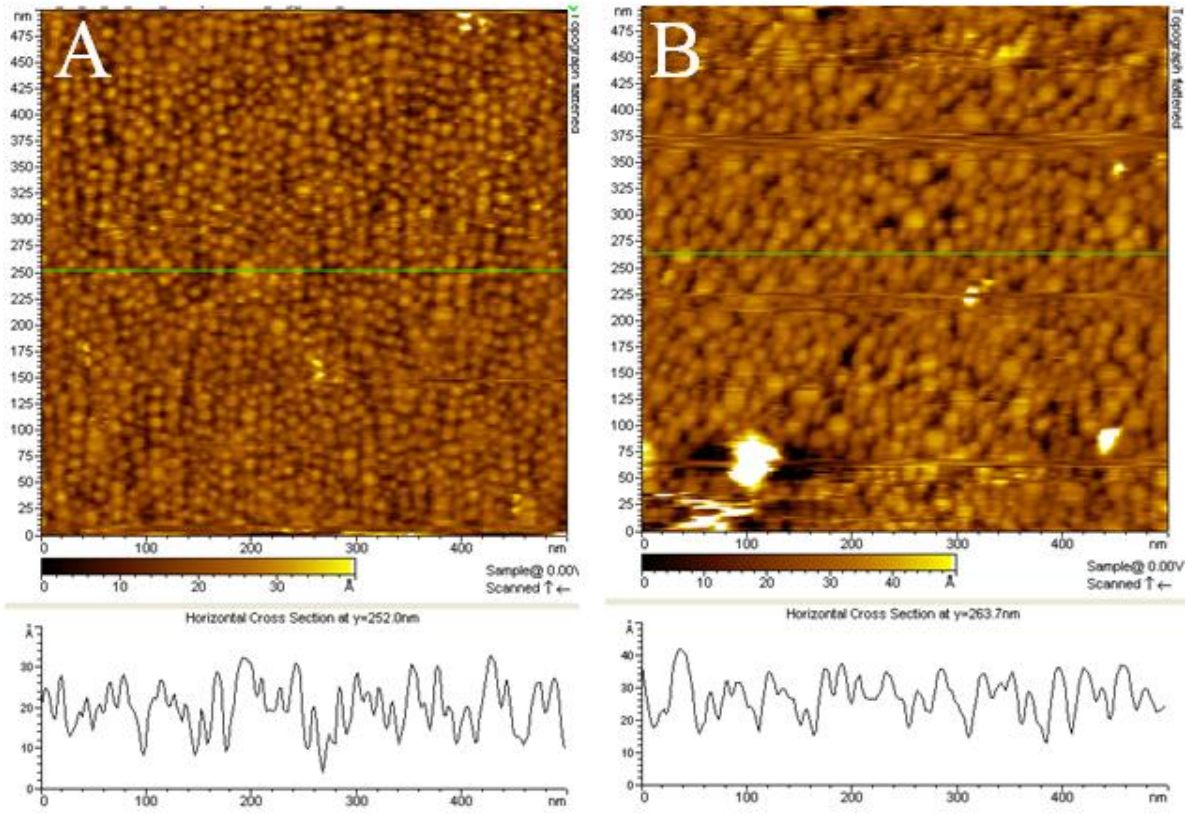

Figure 5.1 Contact mode AFM images of empty nanodiscs with an initial concentration of 1.4 mg/mL (A) and GFP-Ste14p nanodiscs with an initial concentration of 1.5 mg/mL (B) obtained by incubating nanodiscs on a mica substrate in 25 mM MOPS, 150 mM NaCl at pH 7.2, room temperature and 15 minute incubation.

The results achieved with contact mode indicated that the soft nature of the nanodiscs required a gentler scanning approach. To minimize the compression and movement of the discs, MAC mode AFM, with the use of a soft cantilever ($k < 0.14$ N/m), was applied to characterize the nanodiscs. The experiment using empty nanodiscs was repeated using MAC mode where the AFM tip was intermittently in contact with the surface of the nanodiscs. Imaging the nanodiscs again proved to be difficult and involved the use of several AFM scans to optimize the force applied

by the cantilever. Figure 5.2 shows the MAC mode AFM image of the nanodiscs. The majority of the images show small well-defined round nanodiscs. However, there were other features with irregular shapes and much larger sizes than the expected size of a nanodisc using the MSP1D1E1 scaffolding protein. The larger irregular shaped features (indicated by blue arrows) were assigned as patches of lipid bilayer. The nanodiscs in this sample again formed a layer of discs with a small spacing between them. The heights and widths of the empty nanodiscs (Figure 5.2) were found to be 4.0±0.1 nm and 30±5 nm, respectively. Widths were determined using the diameter of a disc at half maximum. After correcting for tip-feature convolution effects, the size of the nanodiscs was estimated to be ~8-15 nm.[262] Heights and widths were determined by averaging the values from two or more independent samples. Values were obtained by measuring 3 or more cross-sections of two or more different areas per sample. The heights of the nanodiscs were consistent with the thickness of an *E. coli* extracts lipid bilayer, ~4 nm.[281] Figure 5.2B is a 3 dimensional image of Figure 5.2A that clearly shows, with the exception of two small areas, that only one height of discs is observed. The two small brighter areas are in fact significantly higher, 7.8±0.5 nm, than the other discs. This may be due to the deposition of a disc on top of another or perhaps a number of discs that have formed an aggregate.

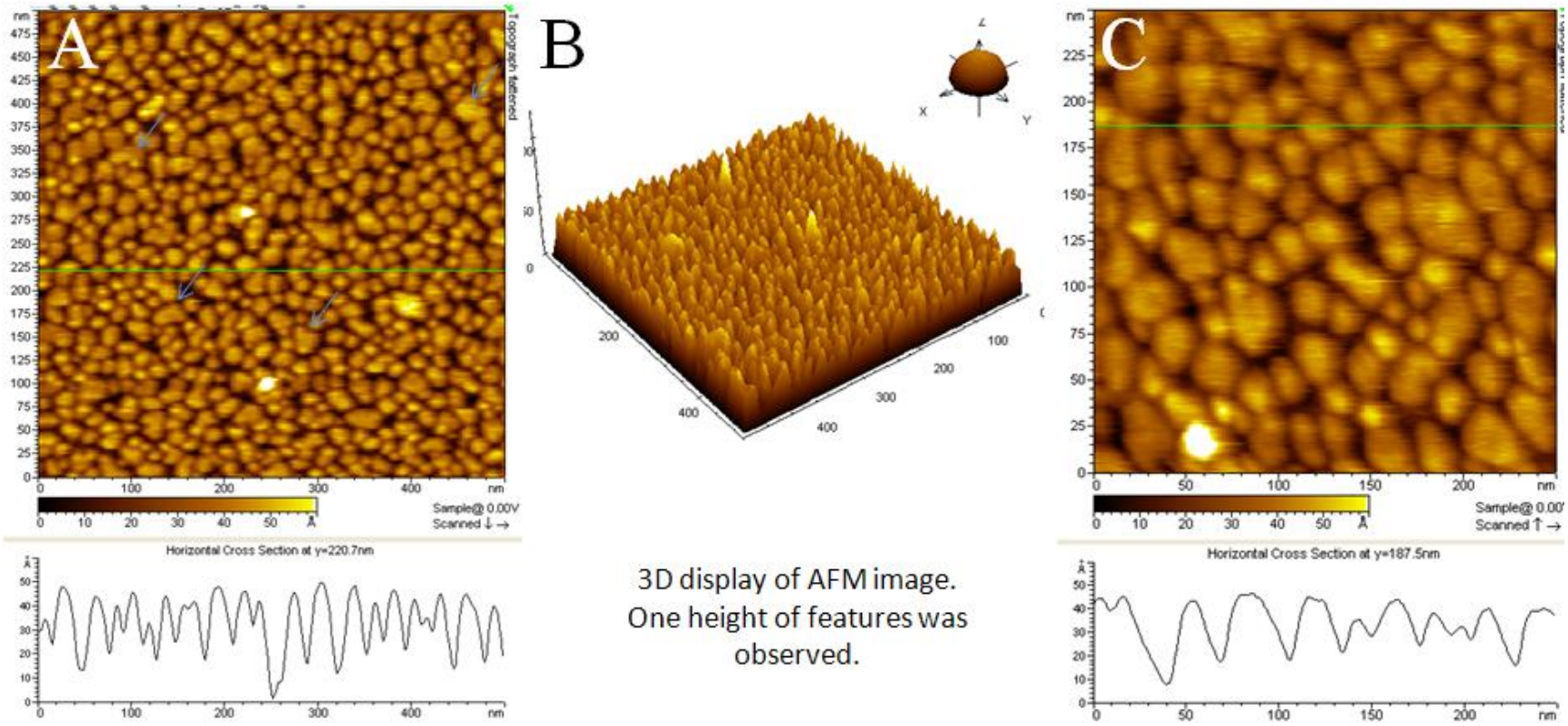

Figure 5.2 MAC mode AFM images of empty nanodiscs obtained by incubating discs with an initial concentration of 1.0 mg/mL in 25 mM MOPS, 150 mM NaCl at pH 7.2, room temperature and 15 minute incubation on a mica substrate.

The nanodisc samples were obtained with different initial concentrations. Although the discs were diluted to the same concentrations before deposition, a concentration effect was observed after AFM imaging. The concentration affected the packing density of the discs. The samples were imaged using MAC mode AFM. The sample with the lowest initial concentration of 0.64 mg/mL as in Figure 5.3A produced an AFM image that showed a larger spacing between discs than for the sample with an initial concentration of 1.0 mg/mL. The distance from the center of a nanodisc to the center of a neighboring nanodisc (center to center) was used as a measure of the spacing between the discs. Center to center distances were only obtained using discs of expected size and shape. The distances were measured using 3 cross sections for 3 separate images of a sample. The sample with an initial concentration of 0.64 mg/mL gave center to center distances between 33 and 40 nm. However, the sample with the highest initial concentration of 1.0 mg/mL as in Figure 5.2,5.3B showed smaller spacing between discs. In this instance, center to center distances between discs were between 25 and 35 nm. Although the discs showed different packing density the heights and widths of the discs remained similar from sample to sample.

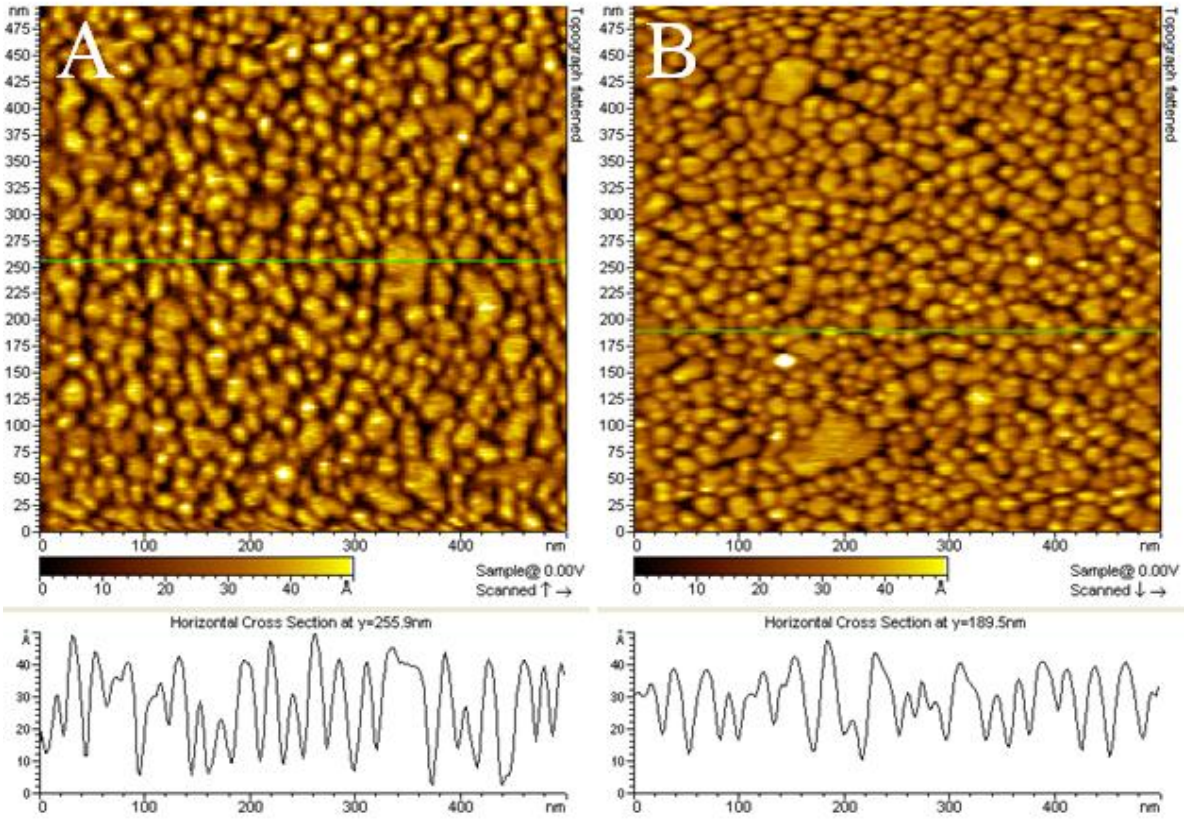

Figure 5.3 MAC mode AFM images of empty nanodiscs obtained by incubating nanodiscs on a mica substrate with the initial concentrations 0.64 mg/mL (A) and 1.0 mg/mL (B) in 25 mM MOPS, 150 mM NaCl at pH 7.2, room temperature and 15 minute incubation.

5.2.2 AFM Characterization of Ste14p Nanodiscs

Initial attempts to image GFP-Ste14p nanodiscs using contact mode AFM were unsuccessful. Unlabeled Ste14p is known to produce less protein aggregates than labeled Ste14p. Due to the behaviour and an increasing interest by our collaborators in the unlabeled Ste14p nanodiscs, the study was continued with unlabeled Ste14p. Sample of Ste14p:nanodiscs were obtained and imaged by MAC mode AFM. Based on analytical ultracentrifugation data approximately 20%

of the nanodiscs in the Ste14p:nanodisc sample contain protein. Based on previous studies[282] with nanodiscs containing protein, it was also hypothesized that nanodiscs containing Ste14p would possess higher heights, ~1 nm. The higher height would result from the protrusion of an individual protein or a small cluster from the nanodisc surface. The samples were prepared by the same method as the empty nanodiscs.

The Ste14p:nanodisc sample formed a layer of small, round, well resolved and separated nanodiscs as shown in Figure 5.4A. The AFM image also showed the presence of large irregularly shaped particles that were much wider than the expected width of a nanodisc. This result suggested that some discs were coalescing into larger patches of lipid bilayer. The majority of the AFM image, ~95%, was small individual nanodiscs. This value was calculated by visually counting the number of irregularly shaped discs and the total number of features. Both nanodiscs and patches of bilayer, as shown by the cross section in Figure 5.4A, appeared to have a smaller feature protruding from the bilayer surface by ~1 nm. The discs possessing this protruding feature and those with a higher height were assigned as protein containing discs. The heights of the two types of discs were measured to be 3.8±0.3 nm and 4.8±0.2 nm, respectively. The width of the discs was variable ranging from ~25-35 nm which gives an estimated width of ~8-15 nm after accounting for tip convolution. Figure 5.4B is a 3 dimensional image of Figure 5.4A which attempts to better depict a layer of discs at one height and occasional discs possessing a higher height. Finally, Figure 5.4C is the AFM image from Figure 5.4B where features that surpass the height of an empty nanodisc plus

three standard deviations have been marked in red. This was performed using Gwyddion SPM data analysis software. After the features were marked the number of discs was counted to determine the percentage of discs that likely contained protein. Irregularly shaped particles were excluded from the analysis and the analysis was performed on a minimum of three areas per sample. The analysis indicated that 23±6% of the discs contained protein which was consistent with the value of 20% observed in analytical ultracentrifugation data.

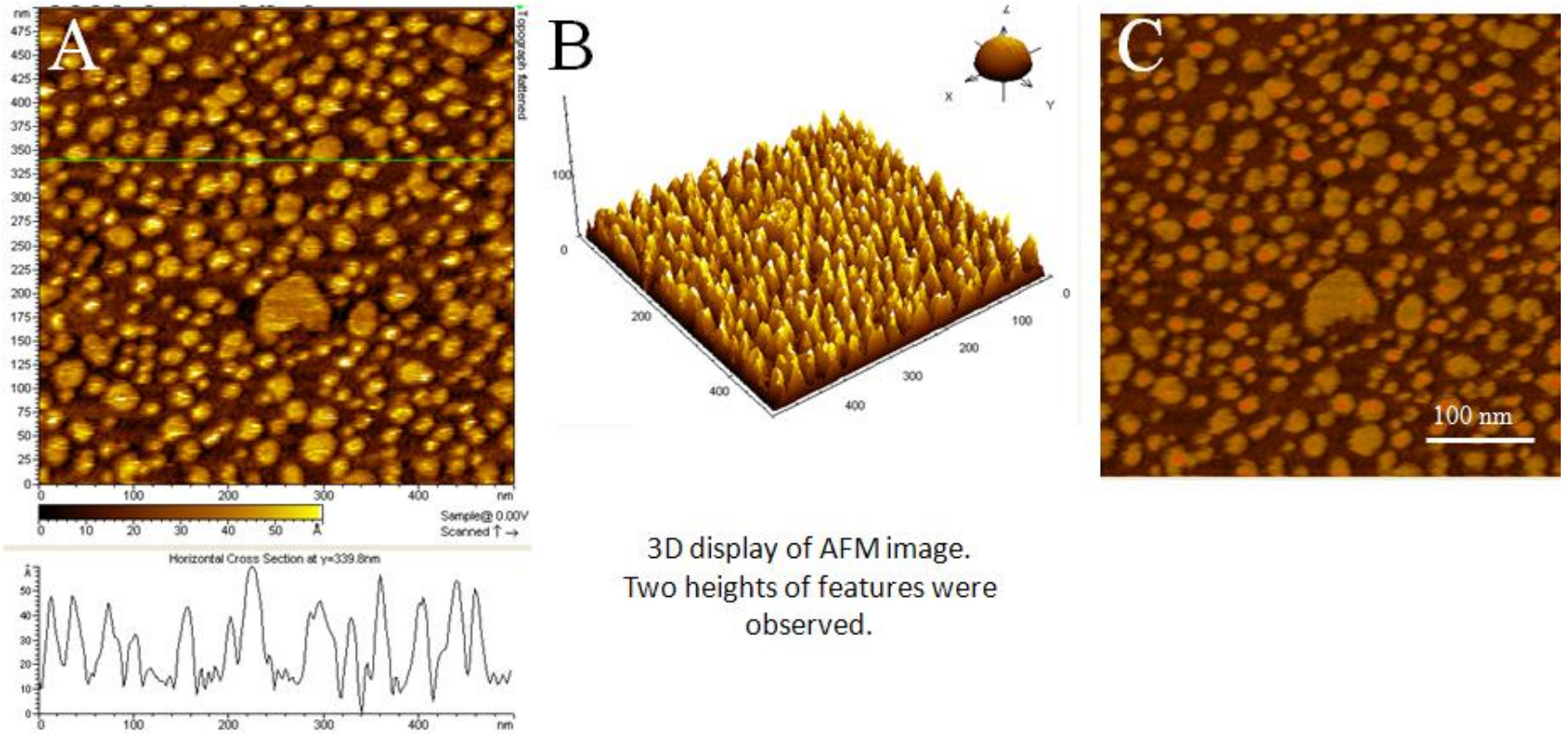

Figure 5.4 MAC mode AFM images of Ste14p:nanodiscs obtained by incubating nanodiscs on a mica substrate with the initial concentrations 0.65 mg/mL (A,B) in 25 mM MOPS, 150 mM NaCl at pH 7.2, room temperature and 15 minute incubation. Image C is the AFM image (A) where the higher feature heights have been marked in red.

A concentration effect on the disc packing densities was again observed even though the discs were diluted to the same concentrations before deposition. The sample with the lowest initial concentration of 0.65 mg/mL as in Figure 5.4,5.5A had an AFM image with a larger spacing between discs. The center to center distances of the sample were measured to be between 45 and 65 nm. The sample with the highest initial concentration of 0.92 mg/mL (Figure 5.5B) gave an AFM image that showed a smaller spacing between discs but many more of the discs had irregular shapes. The center to center distances of the rounder nanodiscs were between 30 and 40 nm. However, we observed the spacing between the discs to be similar for empty and Ste14p:nanodiscs with similar concentrations.

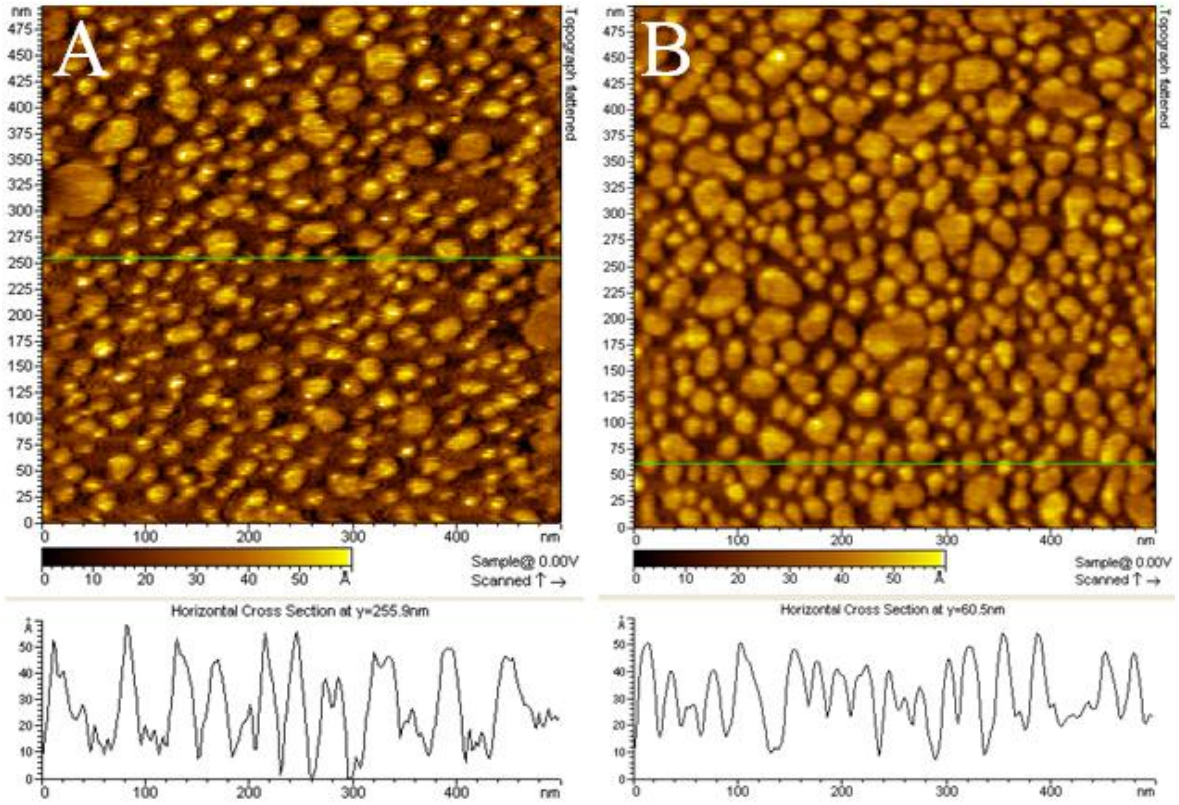

Figure 5.5 MAC mode AFM images of Ste14p:nanodiscs obtained by incubating nanodiscs on a mica substrate with the initial concentrations 0.65 mg/mL (A) and 0.92 mg/mL (B) in 25 mM MOPS, 150 mM NaCl at pH 7.2, room temperature and 15 minute incubation.

The Ste14p incorporated in nanodiscs has a positively charged His tag on it's C-terminus. It was hypothesized that the negative charge on the mica surface was perhaps affecting the orientation of the Ste14p within a nanodisc. If an electrostatic interaction between the His tag on the C-terminus and the mica surface was present, the Ste14p would be oriented with its large termini pointing towards the surface. Thus, AFM detection of the protein would be difficult since only smaller areas of the transmembrane domains would protrude from the membrane. It was thought that if the surface charge was neutralized, a smaller fraction of the Ste14p

would be oriented with the His tag on the substrate surface. Nanodiscs containing Ste14p where both termini were extended outward from the surface would possibly make the heights of protein containing discs more pronounced. In addition, this conformation would position the Ste14p active site above the nanodisc which is necessary for biosensing applications. The addition of the magnesium divalent cation Mg^{2+} was used in an effort to neutralize the mica surface. Thus, we deposited Ste14p:nanodiscs in the presence of 10 mM $MgCl_2$ in an attempt to obtain a layer of nanodiscs with a clearer height difference between empty nanodiscs and those that contain protein. The AFM image in Figure 5.6A shows that samples deposited in the presence of Mg^{2+} formed more irregular shaped discs than the previous samples that excluded Mg^{2+}. Discs appear to be coalescing into larger discs or patches of bilayer. Lipid bilayers are frequently prepared in the presence of divalent cations such as Mg^{2+}, which promote vesicle rupture and reduce pinning of the lipids to the underlying support.[234,235] The Ste14p:nanodiscs in the presence of Mg^{2+} formed a separated layer of discs with two heights of features measuring 3.6±0.3 nm and 4.8±0.3 nm. Finally, analysis of the AFM images of the Ste14p:nanodiscs in the presence of Mg^{2+} showed the expected result that 20±5% of the discs contained protein.

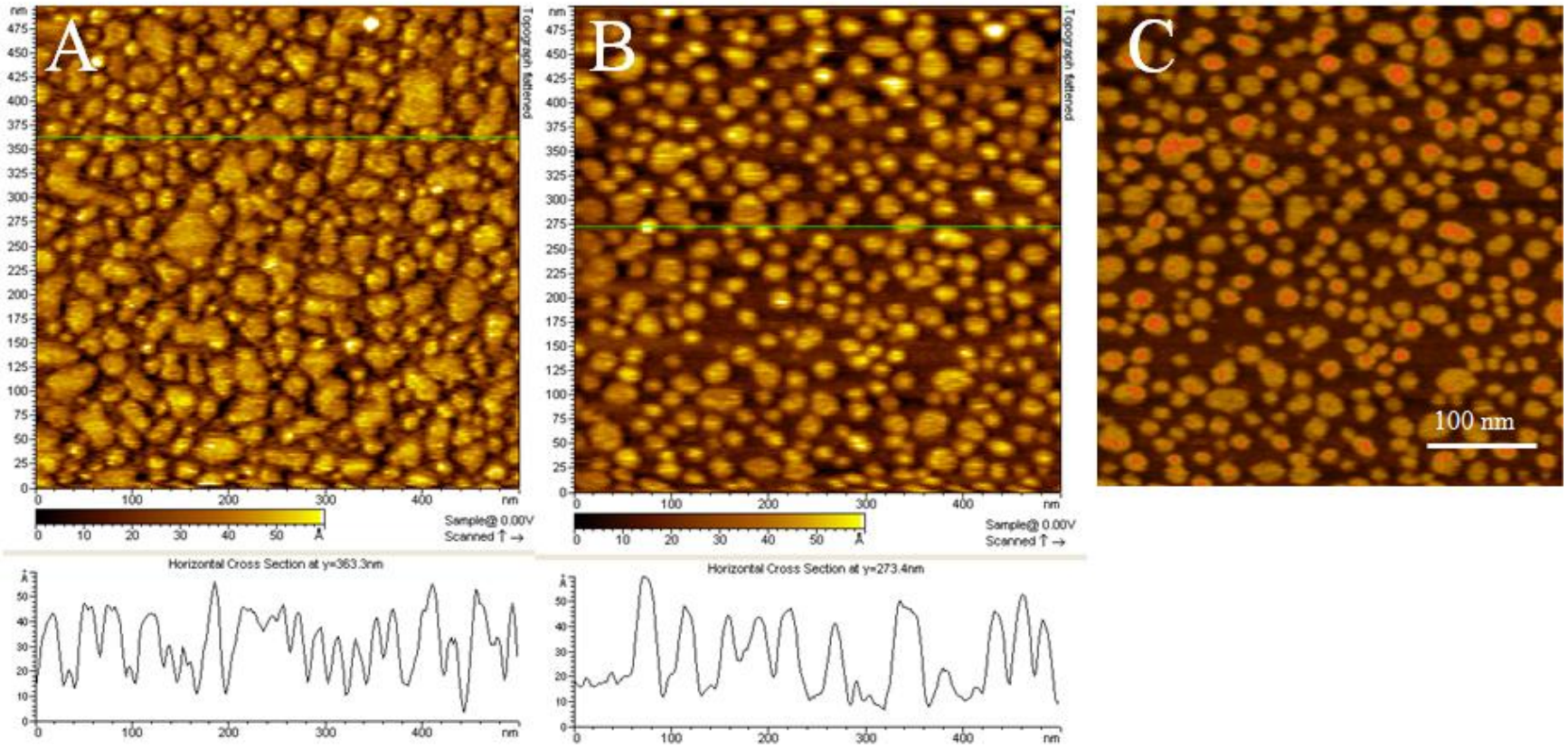

Figure 5.6 MAC mode AFM images of Ste14p:nanodiscs obtained by incubating nanodiscs on a mica substrate in the presence of 10 mM $MgCl_2$ (A) and of a mixed empty nanodisc/Ste14p:nanodiscs sample obtained by incubating a mixture (1:1) of empty nanodiscs (1.0 mg/mL) and Ste14p: nanodiscs (0.92 mg/mL) (B). Image C is the AFM image (A) where the higher feature heights have been marked in red.

Analysis of the AFM images of the Ste14p:nanodiscs showed that ~20% of the discs contained protein. Thus, it was hypothesized that if a sample of Ste14p:nanodiscs was manually mixed with a sample of empty nanodiscs in a 1:1 ratio, one would expect that only ~10% of the nanodiscs in the mixed sample would contain protein. Therefore, to test the hypothesis a sample of Ste14p: nanodiscs of initial concentration 0.92 mg/mL and a sample of nanodiscs of initial concentration 1.0 mg/mL were physically mixed in the AFM cell, incubated and imaged. The AFM image of the sample, as in Figure 5.6B, formed a layer of discs where the spacing between discs was greater than that of previous individual Ste14p:nanodiscs or empty nanodisc samples. Center to center distances of the nanodiscs were in the range of 52-78 nm. Fewer irregular shaped discs were observed. Similarly to the previous experiments with Ste14p:nanodiscs two heights of nanodiscs were observed that measured 3.6±0.2 nm and 4.6±0.2 nm. Interestingly, analysis of the AFM images of the mixed nanodisc and Ste14p:nanodiscs did not show the expected trend of ~10% of the discs containing protein. The analysis revealed that a lower number, 18±3%, of the discs contained protein but still this was much greater than expected.

As a reference sample, our collaborators prepared an affinity purified sample. The affinity purified sample was obtained by separating empty nanodiscs and Ste14p:nanodiscs on an affinity column. As a result, a sample where every nanodisc contained protein was created. AFM imaging of a sample consisting of only nanodiscs containing protein would provide a good reference height for comparison to samples consisting of a mixture of empty and Ste14p:nanodiscs.

The affinity purified sample was diluted, deposited and imaged by MAC mode AFM. The AFM image in Figure 5.7A,B showed the affinity purified discs formed a separated layer of Ste14p:nanodiscs where the heights of nanodiscs were observed to be 4.8±0.2 nm. The heights of some irregularly shaped discs were very large suggesting that discs were stacking on top of one another or that protein aggregates were forming. The width of the discs was also variable ranging from ~20-50 nm which produced an estimated width of ~5-30nm after accounting for tip convolution. Some discs appeared to be much wider which suggested that perhaps some discs are coalescing into larger patches of lipid bilayer. Figure 5.7C is an example of the AFM analysis used to confirm that the majority of affinity purified discs contained protein. It was observed that 92±1% of the discs contained protein.

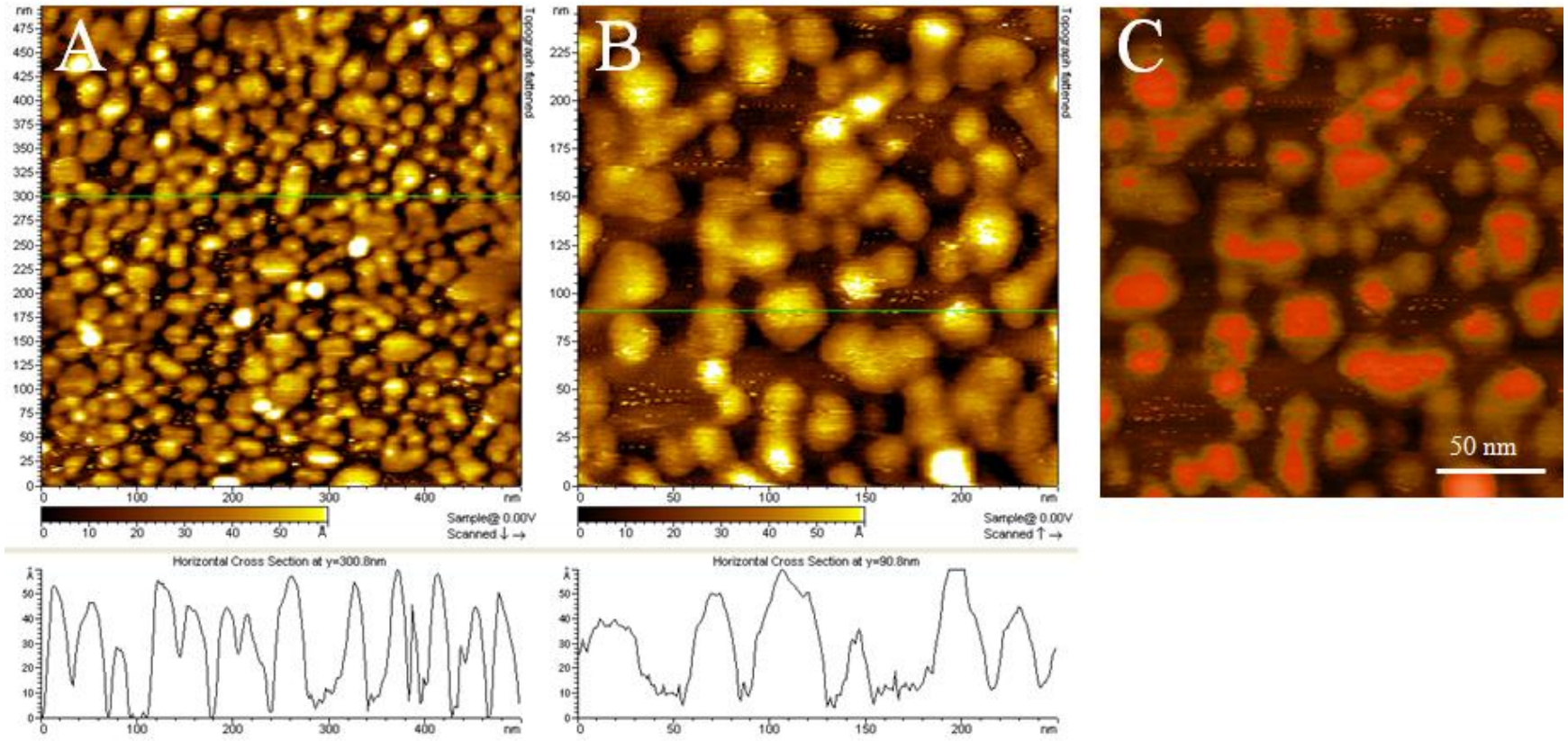

Figure 5.7 MAC mode AFM images of an affinity purified Ste14p:nanodiscs obtained by incubating nanodiscs on a mica substrate with the initial concentrations 0.65 mg/mL (A,B) in 25 mM MOPS, 150 mM NaCl at pH 7.2, room temperature and 15 minute incubation. Image C is the AFM image (A) where the higher feature heights have been marked in red.

5.3 Discussion and Conclusions

5.3.1 Imaging Empty Nanodiscs

Empty nanodiscs imaged by AFM in this study produced a layer of absorbed nanodiscs on mica with a single uniform height. Initially the discs were imaged using contact mode AFM. However, the imaging method was changed to MAC mode AFM after it was observed that contact mode did not give well-resolved images of the discs. MAC mode AFM images of the empty nanodiscs produced the expected result of a relative height of ~4 nm. Although previous studies by Bayburt *et al.*,[191,197] have used contact mode AFM, the light tapping of MAC mode AFM seemed to be less destructive and the method of choice for successful imaging of these soft samples.

Our study of nanodiscs composed of *E. coli* lipid extracts was consistent with the initial study of nanodiscs reported by Bayburt.[191] The initial study characterized DPPC nanodiscs using scanning probe microscopy. The discs were imaged in contact mode using a cantilever having a nominal spring constant of 0.03 N/m on a mica surface. The discs were adsorbed to the surface using and incubation time of 15 minutes and a buffer consisting of 10 mM Tris pH 8.0, 0.15 M NaCl and 10 mM $MgCl_2$. The height and diameter of the discs were found to be 5.6-5.9 nm and 9.7-9.9 nm, respectively. The height measurements were consistent with the thickness of a DPPC bilayer. Similarly, in our system the height of the nanodisc was consistent with the bilayer thickness of the *E. coli* extract lipid used to prepare the discs. Interestingly, in Bayburt's study the His tags on the MSP proteins used to surround the discs were found to form aggregates on the mica surface in the

presence of a divalent cation. Although the MSP protein used in this study contained a His tag, the presence of a divalent cation in our samples only seemed to make discs coalesce into small patches of bilayer. Discs were only found to coalesce in Bayburt's study when high force loads were used during imaging.

Previous AFM studies have also shown nanodiscs adsorb on mica substrates.[280] This fact was consistent with our study. Other studies by Carlson *et al.*,[283] have shown that the manipulation of nanodiscs can be performed mechanically with an AFM tip. Nanodiscs have been shown to form patterns on surfaces when directed by an AFM tip and a high force is applied. However, defects in the nanodiscs have been shown to occur when the tip scrapes the discs when scanning at high force.[283] Lipids from other discs fill in the defects on the scraped nanodiscs resulting in the coalescence of discs. Perhaps the coalescence of nanodiscs observed in this study in the absence of Mg^{2+} was the result of AFM scanning. The large difference in the range of heights of the empty nanodiscs ~3.4 to 4.2 nm, further suggests that too high a force was used in some cases during AFM imaging. As a result, careful attention must be given to the applied force when imaging these types of samples.

5.3.2 Imaging Nanodiscs Containing Membrane Proteins

Ste14p:nanodiscs imaged by AFM in this study produced a layer of absorbed nanodiscs on mica with two heights. The difference in heights was ~1 nm. The widths of the discs were estimated to be ~8-15 nm, which were slightly larger than

the widths of nanodiscs using the same MSP scaffolding protein (12 nm).[284] Cross sections of the Ste14p:nanodisc samples revealed that the taller discs actually contained features that protruded from the disc by ~1 nm. AFM imaging of affinity purified nanodiscs confirmed that the taller nanodiscs likely contained Ste14p. Few AFM studies of integral membrane proteins in nanodiscs have been performed. One of the first examples of an integral membrane protein incorporated into nanodiscs was that of self-assembling bacteriorhodopsin (bR).[197] Bacteriorhodopsin is a 26 kDa model protein containing 7 transmembrane helices. AFM imaging of nanodiscs consisting of bR, *E. coli lipid* extracts and MSP1 were found to be 10 nm in diameter which was consistent with previous calibrated size-exclusion chromatography data. AFM images used to characterize the bR nanodiscs showed nanodiscs that were not well defined. Nonetheless, in this study electron microscopy, AFM, size-exclusion chromatography, and bilayer probe orientation measurements showed that nanodiscs containing bR possess structures with ~10 nm in overall diameter. This is very similar in size to the previous AFM study of empty nanodiscs which had diameters of 9.7 nm.[191] However, the diameters measured by AFM of the nanodiscs observed in our study, containing a similar size protein, Ste14p, were found to be in a slightly higher range.

Recently, another study by Blanchette[282] contradicted the previous observation that only one average diameter is representative of the entire nanodisc sample. Nanodiscs were formed using DMPC lipids and an alolipoprotein E4. Empty nanodiscs and nanodisc containing bR were imaged by AFM. Protein containing discs were found to be an average of 1.0 nm higher than empty

nanodiscs. In addition, it was suggested that the diameters of the nanodiscs varied significantly. The nanodiscs were grouped into subpopulations that were classified by specific diameters ranging from 15-35 nm. Larger discs in diameter were shown to more likely to contain bR than smaller discs. The authors suggested that the membrane proteins must alter the mechanism of nanodisc assembly. This report, although it used a different scaffolding protein, is consistent with our study where a range of nanodisc diameters ~8-15 nm, was observed when incorporating the 26 kDa Ste14p protein.

Another AFM study examined cytochrome P450 (CYP) and NADPH-cytochrome P450 reductase (CPR) incorporated in nanodiscs.[285] Cytochrome P450 enzymes range in molecular weight from 45 to 60 kDa, which is a factor of 2 larger than the protein used in this study. AFM was used to determine the orientation and depth of the membrane proteins in nanodiscs. The average heights of the single proteins of CYP and CPR above the lipid bilayer of the nanodiscs were found to be 3.5 and 5.5 nm, respectively. These values were consistent with the crystal structures of CYP and CPR. The heights of the nanodiscs containing CYP are approximately a factor of two higher than the heights of the protein containing discs in this study. This is consistent with the fact that CYP is a factor of 2 larger in size than Ste14p.

Different concentrations of nanodiscs deposited onto mica have been shown to affect the packing density of the discs.[191,197,198] However, in this study the discs were all diluted to the same concentrations before the addition of the discs to the AFM cell. The addition of Mg^{2+} ions as well as the physical mixing of

Ste14:nanodiscs and empty nanodisc did not seem to increase closeness of the packing of the discs. The packing of the nanodiscs was similar both with and without protein present. Thus, although it was suggested that protein can affect the size of the nanodiscs, it likely does not play a role in the packing of the nanodiscs. Nanodiscs at low concentrations are known to be very stable.[282] Therefore, the poor packing must be purely a surface effect and perhaps a change in the substrate or incubation conditions such as, buffer, salts or pH would increase the packing of the nanodiscs.

5.3.3 Conclusions

The heights of empty nanodiscs and Ste14p:nanodiscs in this study were probed by AFM showing values that corresponded to that of an *E. coli* lipid extract bilayer and nanodiscs containing Ste14p, respectively. The height difference between the two types of discs was found to be ~1 nm. The nanodiscs were observed to naturally absorb to a mica substrate. Interestingly, some nanodisc samples showed the formation of lipid bilayer patches amongst the absorbed nanodiscs. This effect was increasingly observed with the addition of Mg^{2+} salt, which most likely increases the probability of fusion. Nanodiscs have many potential applications from the study of isolated individual proteins to their use as a carrier of membrane proteins into supported bilayers.

5.4 Experimental

5.4.1 Materials

Ste14p was reconstituted into nanodisc by collaborators using a method as described previously.[191,192,197] All aqueous solutions were prepared with 18.3 MΩ·cm Milli-Q water. All other materials were obtained from Aldrich (≥98% pure) and used as received.

5.4.2 Atomic Force Microscopy

The AFM images for all samples were obtained at room temperature (23 ± 1 °C) using a PicoSPM atomic force microscope (Molecular Imaging) in MAC-mode. Magnetic coated silicon tips with spring constants of ~0.14 N/m (Type VII) and resonance frequencies between 5 and 12 kHz in aqueous solution were used. Earlier experiments using contact-mode AFM made use of MSNL silicon tips with spring constants of ~<0.05 N/m. A 6 x 6 μm^2 scanner was operated at a scan rate between 0.4 and 1.0 Hz. The images shown are flattened raw data and imaged at minimal force. Two or more independently prepared samples were imaged for each nanodisc sample, with several areas scanned for each sample. Reported heights are based on averaging data from cross sections of at least 3 independent areas of a minimum of 2 samples imaged.

5.4.3 Preparation of Supported Nanodiscs

The nanodisc samples were received at various concentrations in 25 mM MOPS buffer with 150 mM NaCl at pH 7.2. Once received a fraction of the nanodisc sample was diluted to a concentration of 0.1 mg/mL. Aliquots of the nanodisc solution (10 µL) and 25 mM MOPS buffer with 150 mM NaCl at pH 7.2 (490 µL) were added to freshly cleaved mica clamped into a Molecular Imaging AFM liquid cell. After incubation at room temperature for 15 minutes, the discs were rinsed extensively with buffer to remove unabsorbed discs before imaging. For samples using $MgCl_2$, 50 µL of buffer was substituted with 50 µL of 100 mM $MgCl_2$ solution.

Chapter 6: Final Comments and Future Work

6.1 Conclusions and Suggested Future Work

The work described in this thesis represents the development of new platforms for membrane based biosensing applications, from an investigation of supported membranes formed from bolalipid and phosphocholine lipid mixtures to a comparison of supported lipid membranes formed on different types of polymer cushions. In addition, an integral membrane protein, Ste14p, was reconstituted into two types of polymer supported bilayers as well as lipid nanodiscs. We have demonstrated that a complex interplay of factors controls the morphology of supported membranes and that a variety of factors must be considered when selecting a polymer support for a model membrane containing active proteins.

Our results from the phase-separated phosphocholine and bolalipid membranes conclusively indicate that the morphology varies significantly as a function of the vesicle and bilayer preparation methods. The bulk lipid vesicle composition was significantly different from the deposited lipid membrane composition. It was believed that difference resulted from an exchange of lipid between the surface and the bulk solution during membrane formation. Future experiments are required to determine whether the changes in composition of the lipid membrane are occurring during the deposition process and whether significant mixing of the lipids in the phase separated state is occurring. Experiments using minimal amounts of lipid to give small patches of bilayer could provide some insight about preliminary stages of the deposition process. The small domain size obtained for some samples indicated that lipids may be pinned to the support resulting in slow sample equilibration. The observation of phase separated bolalipid/POPC

membranes confirms earlier predictions that C20BAS/phosphocholine lipid mixtures would phase separate based on the hydrophobic mismatch. Other future experiments to further probe this effect would be to vary the chain length of either the phosphocholine lipids or bolalipids and test for phase separation of the resulting supported membranes. In addition, other bolalipid/phosphocholine mixtures may give results that are easier to interpret which might indicate that the large hydrophobic mismatch may cause some of the complex effects.

Supported lipid bilayers on the novel polysaccharide PEM polymer support developed in this study extended the range of use of PEMs. The study also indicated the importance of factors such as surface charge and roughness in supported lipid bilayer formation. At low pH, the supported lipid bilayers on PEMs possessed lipid diffusion coefficients that were comparable if not better than those on other PEM polymer cushions as well as on PEG polymer cushions. However, lipid mobile fractions were found to be lower than other polymer systems. It is also worth noting that this PEM system is based on charged polysaccharides which are more biocompatible than other PEM systems. Future experiments such as the use of a thicker multilayer or of different lipids are required to further understand the complex diffusion behaviour observed in this study. Variations or substitution of the polysaccharides in the PEM could also be performed to improve properties such as biocompatibility and surface charge. A polysaccharide PEM that would allow for the deposition of a lipid bilayer at neutral pH could have promising applications.

The utility of PEM-supported bilayers for the incorporation of membrane proteins was assessed. Bilayers containing GFP-Ste14p, were prepared on a PEM

and a previously reported PEG polymer support. Protein fluorescence intensity and activity was found to be minimal in PEM supported lipid bilayers. However, the PEG system showed the greatest protein fluorescence intensity and a comparable if not higher amount of protein activity to that of lipid bilayers formed on a glass support. Further experiments to optimize the activity of Ste14p on the PEG system could provide a promising alternate model membrane system for this protein. An alternate method of labeling Ste14p would also be beneficial as GFP could be promoting aggregation in this system. The alternate label may also allow for the determination of the protein concentration in the supported bilayer, so that a direct comparison between activities for the three systems could be performed. In addition, further experiments using other membrane proteins could show the usefulness and range of this system. These results could also be extended to other sections of this thesis such as reconstituting Ste14p in bolalipid/phosphocholine bilayers. Finally, this system could be used as a possible substrate for membrane based biosensing.

For comparison, Ste14p reconstituted into nanodiscs was studied by AFM. Samples containing empty nanodiscs and protein containing discs were characterized and found to have a difference in height of ~1 nm. After analysis of the discs, it was found that the taller discs contained protein. The taller discs accounted for ~20% of the nanodisc sample, consistent with other data provided by collaborators. Concentration of the nanodisc sample was also found to influence the packing of the discs. Future experiments could include characterizing

nanodiscs with GFP-Ste14p, looking at the effects of a polymer supported nanodisc and observing the AFM of isolated nanodiscs, rather than a densely packed array.

6.2 Claims to Original Research

1. Mixtures of bolalipid and phosphocholine lipids were used to prepare supported lipid bilayers, confirming an earlier prediction that phase separation would occur for some bolalipid/phosphocoline mixtures due to hydrophobic mismatch. The morphology of the mixed supported membranes varied significantly with the preparation conditions. This revealed a complex trend between lipid membrane composition and the bulk vesicle solution for these mixtures. The trend was believed to be a combination effect of a heterogeneous vesicle population, the exchange of lipid between the vesicle solution and the support during deposition of the membrane and the slow equilibration of domains due to pinning of the lipids to the support.

2. The development of a novel biocompatible PEM system as a substrate for supported lipid bilayers. Lipid mobilities of bilayers prepared on the PEMs were shown to be greater than other PEMs and comparable to a previously reported PEG polymer cushion.

3. The reconstitution of the membrane protein Ste14p into polymer supported lipid bilayers. PEG supported bilayers were shown to possess the greatest amount of protein fluorescence and to have comparable protein activity to that of lipid bilayers formed on a glass support. PEM supported bilayers showed the lowest protein activity.

4. The elucidation of a ~1 nm height difference between empty and Ste14p reconstituted nanodiscs. A significant concentration effect was shown for both empty and protein containing discs as increasing the initial concentration increases the packing of the discs. The addition of divalent cations during the deposition process increases the fusion of nanodiscs to form lipid bilayer patches.

6.3 Publications

6.3.1 Published

K. Mulligan, D. Brownholland, A. Carnini, D. H. Thompson, L. J. Johnston; AFM Investigations of Phase Separation in Supported Membranes of Binary Mixtures of POPC and an Eicosanyl-Based Bisphosphocholine Bolalipid; Langmuir, **2010**, *11*, 8525

K. Mulligan, Z. J. Jakubek, and L. J. Johnston; Supported Lipid Bilayers on Biocompatible Polysaccharide Multilayers; Langmuir, **2011**, *23*, 14352

6.3.2 In Preparation

K. Mulligan, B. Schilling, D. H. Thompson, C. A. Hrycyna, L. J. Johnston; Functional Reconstitution, and characterization of the *Saccharomyces cerevisiae* Isoprenylcysteine Carboxylmethyltransferase Ste14p in Polymer Supported Lipid Membranes. *In preparation*.

B. Schilling, **K. Mulligan**, D. H. Thompson, L. J. Johnston, C. A. Hrycyna; Functional Reconstitution and AFM Characterization of the *Saccharomyces cerevisiae* Isoprenylcysteine Carboxylmethyltransferase Ste14p in Nanodiscs. *In preparation*.

6.3.3 Oral Presentations

K. Mulligan, Z. J. Jakubek, and L. J. Johnston. "Biosensing Platforms: Supported Lipid Bilayers on Polymer Cushions." **94th Canadian Chemistry Conference and Exhibition,** Montreal, Quebec, Canada (June 2011)

6.3.4 Poster Presentations

K. Mulligan, Z. J. Jakubek, and L. J. Johnston. "Polymer Supported Lipid Bilayers Using a Chitosan/Hyaluronic Acid Polyelectrolyte Multilayer." **93rd Canadian Chemistry Conference and Exhibition,** Toronto, Ontario, Canada (May 2010)

K. Mulligan, D. Brownholland, A. Carnini, D. H. Thompson, L. J. Johnston. "Supported Lipid Membranes for Biosensor Development: The Bolalipid-POPC System." **92nd Canadian Chemistry Conference and Exhibition,** Hamilton, Ontario, Canada (May 2009)

K. Mulligan, D. Brownholland, A. Carnini, D. H. Thompson, L. J. Johnston. "Supported Lipid Membranes for Biosensor Development: The Bolalipid-POPC System." **36th Ontario-Quebec Physical Organic Mini-Symposium,** Ottawa, Ontario, Canada (October 2008)

References

(1) Sackmann, E. *Science* **1996**, *271*, 43.

(2) Heijine, G. V.; Rees, D. *Curr. Opin. Struc. Biol.* **2008**, *18*, 403.

(3) McNeil, P. L.; Steinhardt, R. A. *Annu. Rev. Cell. Dev. Bi.* **2003**, *19*, 697.

(4) Cooper, G. M. In *A Molecular Approach*; 2nd ed.; Sinauer Associates: Sunderland, MA, 2000.

(5) Kiessling, V.; Domanska, M. K.; Murray, D.; Wan, C.; Tamm, L. K. *Supported Lipid Bilayers: Development and Applications in Chemical Biology*; John Wiley & Sons, Inc., 2008.

(6) Singer, S. J.; L.Nicolson, G. *Science* **1972**, *175*, 720.

(7) Vereb, G.; Szollosi, J.; Matko, J.; Nagy, P.; Farkas, T.; Vigh, L.; Matyus, L.; Waldmann, T. A.; Damjanovich, S. *Proc. Natl. Acad. Sci.* **2003**, *100*, 8053.

(8) Simons, K.; Meer, G. V. *Biochemistry* **1988**, *27*, 6197.

(9) Simons, K.; Ikonen, E. *Nature* **1997**, *387*, 569.

(10) Lingwood, D.; Simons, K. *Science* **2010**, *327*, 46.

(11) Simons, K.; Gerl, M. J. *Nat. Rev. Mol. Cell Biol.* **2010**, *11*, 688.

(12) Yildrim, M. A.; Goh, K. I.; Cusick, M. E.; Barabasi, A. L.; Vidal, M. *Nat. Biotechnol.* **2007**, *25*, 1119.

(13) Zheng, C. J.; Han, L.; Yap, C. W.; Xie, B.; Chen, Y. Z. *Drug Discov. Today* **2006**, 412.

(14) Mueller, P.; Rudin, D. O.; Tien, H. T.; Wescott, W. C. *Nature* **1962**, *194*, 979.

(15) Montal, M.; Mueller, P. *Proc. Natl. Acad. Sci.* **1972**, *69*, 3561.

(16) Schulte, A.; Ruamchan, S.; Khunkaewla, P.; Suginta, W. *J. Membrane Biol.* **2009**, *230*, 101.

(17) Bamberg, E.; Alpes, H.; Apell, H. J.; Bradley, R.; Harter, B.; M.J. Quelle; Urry, D. W. *J. Membrane Biol.* **1979**, *50*, 257.

(18) Gomezlagunas, F.; Pena, A.; Lievano, A.; Darszon, A. *Biophys. J.* **1989**, *56*, 115.

(19) Gelder, P. V.; Dumas, F.; Winterhalter, M. *Biophys. Chem.* **2000**, *85*, 153.

(20) Bezrukov, S. M.; Vodyanoy, I. *Biophys. J.* **1993**, *64*, 16.

(21) Schmies, G.; Luttenberg, B.; Chizhov, I.; Engelhard, M.; Becker, A.; Bamberg, E. *Biophys. J.* **2000**, *78*, 967.

(22) Schmitt, E. K.; Vrouenraets, M.; Steinem, C. *Biophys. J.* **2006**, *91*, 2163.

(23) Kahya, N.; Scherfeld, D.; Bacia, K.; Poolman, B.; Schwille, P. *J. Biol. Chem.* **2003**, *278*, 28109.

(24) Korlach, J.; Schwille, P.; Webb, W. W.; Feigenson, G. W. *Proc. Natl. Acad. Sci.* **1999**, *96*, 8461.

(25) Sanchez, S. A.; Gratton, E. *Acc. Chem. Res.* **2005**, *38*, 469.

(26) Nomura, S. M.; Kondoh, S.; Asayama, W.; Nishikawa, S.; Akiyoshi, K. *J. Biotechnol.* **2008**, *133*, 190.
(27) Groves, J. T.; Dustin, M. L. *J. Immunol. Methods* **2003**, *278*, 19.
(28) Seu, K. J.; Pandey, A. P.; Haque, F.; Proctor, E. A.; Ribbe, A. E.; Hovis, J. S. *Biophys. J.* **2007**, *92*, 2445.
(29) Brian, A. A.; McConnell, H. M. *Proc. Natl. Acad. Sci.* **1984**, *81*, 6159.
(30) Tamm, L. K.; McConnell, H. M. *Biophys. J.* **1985**, *47*, 105.
(31) McConnell, H. M.; Watts, T. H.; Weis, R. M.; Brian, A. A. *Biochim. Biophys. Acta* **1986**, *864*, 95.
(32) Keller, C. A.; Glasmastar, K.; Zhdanov, V. P.; Kasemo, B. *Phys. Rev. Lett.* **2000**, *84*, 5443.
(33) Morigaki, K.; Tawa, K. *Biophys. J.* **2006**, *91*, 1380.
(34) Richter, R. P.; Berat, R.; Brisson, A. R. *Langmuir* **2006**, *22*, 3497.
(35) Korlach, J.; Schwille, P.; Webb, W. W.; Feigenson, G. W. *PNAS* **1999**, *96*, 8461.
(36) Tamm, L. K.; Bohm, C.; Yang, J.; Shao, Z.; Hwang, J.; Edidin, M.; Betzig, E. *Thin Solid Films* **1996**, *284-285*, 813.
(37) Hughes, A. V.; Howse, J. R.; Dabkowska, A.; Jones, R. A. L.; Lawrence, M. J.; Roser, S. J. *Langmuir* **2008**, *24*, 1989.
(38) Johnson, S. J.; Bayerl, T. M.; McDermott, D. C.; Adam, G. W.; Rennie, A. R.; Thomas, R. K.; Sackmann, E. *Biophys. J.* **1991**, *59*, 289.
(39) Tamm, L. K. *Biochemistry* **1988**, *27*, 1450.
(40) Parikh, A. N.; Groves, J. T. *M.R.S. Bull.* **2006**, *31*, 507.
(41) Kalb, E.; Frey, S.; Tamm, L. K. *Biochim. Biophys. Acta* **1992**, *1103*, 307.
(42) Wenzl, P.; Fringeli, M.; Goette, J.; Fringeli, U. P. *Langmuir* **1994**, *10*, 4253.
(43) Ross, S. T.; Schwartz, S.; Fellers, T. J.; Davidson, M. W. **2012**.
(44) Heyse, S.; Stora, T.; Schmid, E.; Lakey, J. H.; Vogel, H. *Biochim. Biophys. Acta* **1998**, *1376*, 319.
(45) Thompson, N. L.; Drake, A. W.; Chen, L. X.; Broek, W. V. *Photochem. Photobiol.* **1997**, *65*, 39.
(46) Axelrod, D.; Davidson, M. W. **2012**.
(47) Gordon, G. W.; Chazotte, B.; Wang, X. F.; Herman, B. *Biophys. J.* **1995**, *68*, 766.
(48) Axelrod, D.; Koppel, D. E.; Schlessinger, J.; Elson, E.; Webb, W. W. *Biophys. J.* **1976**, *16*, 1055.
(49) Soumpasis, D. M. *Biophys. J.* **1983**, *41*, 95.
(50) Smith, K. A.; Gale, B. K.; Conboy, J. C. *Anal. Che.* **2008**, *80*, 7980.
(51) Marguet, D.; Lenne, P. F.; Rigneault, H.; He, H. T. *EMBO J.* **2006**, *25*, 3446.
(52) Abramovitch, D. Y.; Andersson, S. B.; Pao, L. Y.; Schitter, G. *P. Amer. Contr. Conf.* **2007**, 3488.
(53) Alexander, S.; Hellemans, I.; Marti, O.; Schneir, J.; Ellings, V.; Hansma, P. K.; Longmire, M.; Gurley, J. *J. Appl. Phys.* **1989**, *65*, 164.
(54) Rossi, C.; Chopineau, J. *Eur. Biophys. J.* **2007**, *36*, 955.

(55) In *Agilent MAC Mode Magnetic AC Mode-The Gentle Touch for AFM* 2006, p 1.
(56) Terrettaz, S.; Vogel, H. *M.R.S. Bull.* **2005**, *30*, 207.
(57) Terrettaz, S.; Vogel, H. *Surf. Sci. Nanotechnol.* **2005**, *3*, 203.
(58) Chan, Y.-H. M.; Boxer, S. G. *Curr. Opin. Chem. Biol.* **2007**, *11*, 581.
(59) Kraft, M. L.; Weber, P. K.; Longo, M. L.; Hutcheon, I. D.; Boxer, S. G. *Science* **2006**, *313*, 1948.
(60) McQuaw, C. M.; Sostarecz, A. G.; Zheng, L.; Ewing, A. G.; Winograd, N. *Langmuir* **2005**, *21*, 807.
(61) McQuaw, C. M.; Zheng, L.; Ewing, A. G.; Winograd, N. *Langmuir* **2007**, *23*, 5645.
(62) Cho, N. J.; Kanazawa, K. K.; Glenn, J. S.; Frank, C. W. *Anal. Chem.* **2007**, *79*, 7027.
(63) Dorvel, B. R.; Keizer, H. M.; Fine, D.; Vuorinen, J.; Dodabalapur, A.; Duran, R. S. *Langmuir* **2007**, *23*, 7344.
(64) Sackmann, E.; Tanaka, M. *Trends Biotechnol.* **2000**, *18*, 58.
(65) Stelzle, M.; Weissmuller, G.; Sackmann, E. *J. Phys. Chem.* **1993**, *97*, 2974.
(66) Stora, T.; Dienes, Z.; Vogel, H.; Duschl, C. *Langmuir* **2000**, *16*, 5471.
(67) Howland, M. C.; Szmodis, A. W.; Sanii, B.; Parikh, A. N. *Biophys. J.* **2007**, *92*, 1306.
(68) Daniel, S.; Albertorio, F.; Cremer, P. S. *M.R.S. Bull.* **2006**, *31*, 536.
(69) Tanaka, M. *M.R.S. Bull.* **2006**, *31*, 513.
(70) Hubbard, J. B.; Silin, V.; Plant, A. L. *Biophys. Chem.* **1998**, *75*, 163.
(71) Graneli, A.; Rydstrom, J.; Kasemo, B.; Hook, F. *Langmuir* **2003**, *19*, 842.
(72) Reimhult, E.; Hook, F.; Kasemo, B. *Phys. Rev.* **2002**, *66*.
(73) Reimhult, E.; Hook, F.; Kasemo, B. *J. Chem. Phys.* **2002**, *117*, 7401.
(74) Richter, R. P.; Brisson, A. *Langmuir* **2004**, *20*, 4609.
(75) Richter, R. P.; Brisson, A. R. *Biophys. J.* **2005**, *88*, 3422.
(76) Han, X. J.; Studer, A.; Sehr, H.; Geissbuhler, I.; Berardino, M. D.; Winkler, F. K.; Tiefenauer, L. X. *Adv. Mat.* **2007**, *19*, 4466.
(77) Terrettaz, S.; Ulrich, W. P.; Guerrini, R.; Verdini, A.; Vogel, H. *Angew. Chem. Int. Edit.* **2001**, *40*, 1740.
(78) Reimhult, E.; Hook, F.; Kasemo, B. *Langmuir* **2003**, *19*, 1681.
(79) Yang, J. L.; Kleijn, J. M. *Biophys. J.* **1999**, *76*.
(80) Salamon, Z.; Wang, Y.; Tollin, G.; Macleod, H. A. *Biochim. Biophys. Acta* **1994**, *1195*.
(81) Rosa, M. D.; Gambacorta, A. *Prog. Lipid Res.* **1988**, *27*, 153.
(82) Fuoss, R. M.; Edelson, D. J. *J. Am. Chem. Soc.* **1951**, *73*, 269.
(83) Cornell, B. A.; Braach-Maksvytis, V. L. B.; King, L. G.; Osman, P. D. J.; Raguse, B.; Wieczorek, L.; Pace, R. J. *Nature* **1997**, *387*, 580.
(84) Fuhrhop, A. H.; Wang, T. Y. *Chem. Rev.* **2004**, *104*, 2901.
(85) Sun, X.-L.; Biswas, N.; Kai, T.; Dai, Z.; Dluhy, R. A.; Chaikof, E. L. *Langmuir* **2006**, *22*, 1201.

(86) Elferink, M. G.; Dewit, J. G.; Demel, R.; Driessen, A. J.; Konings, W. N. *J. Biol. Chem.* **1992**, *267*, 1375.
(87) Febo-Ayala, W.; Moreira-Felix, S. L.; Hrycyna, C. A.; Thompson, D. H. *Biochemistry* **2006**, *45*, 14683.
(88) Kim, J.-M.; Patwardhan, A.; Bott, A.; Thompson, D. H. *Biochim. Biophys. Acta* **2003**, *1617*, 10.
(89) Veld, G. I.; Elferink, M. G.; Drienssen, A. J.; Konings, W. N. *Biochemistry* **1992**, *31*, 12493.
(90) Denoyelle, S.; Polidori, A.; Brunelle, M.; Vuillaume, P. Y.; Laurent, S.; ElAzhary, Y.; Pucci, B. *New J. Chem.* **2006**, *30*, 629.
(91) Patel, G. B.; Sprott, G. D. *CRC Cr. Rev. Biotechn.* **1999**, *19*, 317.
(92) Rethore, G.; Montier, T.; Gall, T. L.; Delepine, P.; Cammas-Marion, S.; Lemiegre, L.; Lehn, P.; Benvegnu, T. *Chem. Commun.* **2007**, 2054.
(93) Huguet, C.; Hopmans, E. C.; Febo-Ayala, W.; Thompson, D. H.; Damste, J. S.; Schouten, S. *Org. Geochem.* **2006**, *37*, 1036.
(94) Chang, E. L. *Biochem. Bioph. Res. Co.* **1994**, *202*, 673.
(95) Elferink, M. G.; Dewit, J. G.; Driessen, A. J.; Konings, W. N. *Biochim. Biophys. Acta* **1994**, *1193*, 247.
(96) Gliozzi, A.; Relini, A.; Chong, P. L. *J. Membrane Sci.* **2002**, *206*, 131.
(97) Febo-Ayala, W.; Holland, D. P.; Bradley, S. A.; Thompson, D. H. *Langmuir* **2007**, *23*, 6276.
(98) Jarrell, H. C.; Zukotynski, K. A.; Sprott, G. D. *Biochim. Biophys. Acta* **1998**, *1369*, 259.
(99) Benvegnu, T.; Brard, M.; Plusquellec, D. *Curr. Opin. Coll. Interface Sci.* **2004**, *8*, 469.
(100) Halter, M.; Nogata, Y.; Dannenberger, O.; Sasaki, T.; Vogel, V. *Langmuir* **2004**, *20*, 2416.
(101) Kai, T.; Sun, X. L.; Faucher, K. M.; Apkarian, R. P.; Chaikof, E. L. *J. Org. Chem.* **2005**, *70*, 2606.
(102) Patwardhan, A. P.; Thompson, D. H. *Langmuir* **2000**, *16*, 10340.
(103) Svenson, S.; Thompson, D. H. *J. Org. Chem.* **1998**, *63*, 7180.
(104) Wang, G. J.; Hollingsworth, R. I. *J. Org. Chem.* **1999**, *64*, 4140.
(105) DiMeglio, C.; Rananavare, S. B.; Svenson, S.; Thompson, D. H. *Langmuir* **2000**, *16*, 128.
(106) Holland, D. P.; Struts, A. V.; Brown, M. F.; Thompson, D. H. *J. Am. Chem. Soc.* **2008**, *130*, 4584.
(107) Cuccia, L. A.; Morin, F.; Beck, A.; Hebert, N.; Just, G.; Lennox, R. B. *Chem. Eur. J.* **2000**, *6*, 4379.
(108) Delfino, J. M.; Schreiber, S. L.; Richards, F. M. *J. Am. Chem. Soc.* **1993**, *115*, 3458.
(109) Longo, G. S.; Thompson, D. H.; Szleifer, I. *Biophys. J.* **2007**, *93*, 2609.
(110) Thompson, D. H.; Wong, K. F.; Humphry-Baker, R.; Wheeler, J. J.; Kim, J.-M.; Rananavare, S. B. *J. Am. Chem. Soc.* **1992**, *114*, 9035.
(111) Fan, Q.; Relini, A.; Cassinadri, D.; Gambacorta, A.; Gliozzi, A. *Biochim. Biophys. Acta* **1995**, *1240*, 83.
(112) Tanaka, M.; Sackmann, E. *Nature* **2005**, *437*, 656.

(113) Castellana, E. T.; Cremer, P. S. *Surf. Sci. Rep.* **2006**, *61*, 429.
(114) Renner, L.; Osaki, T.; Chiantia, S.; P.Schwille; Pompe, T.; Werner, C. *J. Phys. Chem. B* **2008**, *112*, 6373.
(115) Naumann, C. A.; Prucker, O.; Lehmann, T.; Ruhe, J.; Knoll, W.; Frank, C. W. *Biomacromolecules* **2002**, *3*, 27.
(116) Zhang, H.; Salinas, S.; Sundaresan, V. *Smart Mater Struct* **2011**, *20*, 094020.
(117) Zhang, L.; Longo, M. L.; Stroeve, P. *Langmuir* **2000**, *16*, 5093.
(118) Ma, C.; Srinivasan, M. P.; Waring, A. J.; Lehrer, R. I.; Longo, M. L.; Stroeve, P. *Colloid. Surface. B* **2003**, *28*, 319.
(119) Wong, J. Y.; Majewski, J.; Park, C. K.; Seitz, M.; Israelachvili, J. N.; Smith, G. S. *Biophys. J.* **1999**, *77*, 1445.
(120) Wong, J. Y.; Park, C. K.; Seitz, M.; Israelachvili, J. N. *Biophys. J.* **1999**, *77*, 1458.
(121) Majewski, J.; Wong, J. Y.; Park, C. K.; Seitz, M.; Israelachvili, J. N.; Smith, G. S. *Biophys. J.* **1998**, *75*, 2363.
(122) Ye, Q.; Konradi, R.; Textor, M.; Reimhult, E. *Langmuir* **2009**, *25*, 13534.
(123) Deng, Y.; Wang, Y.; Holtz, B.; Li, J.; Traaseth, N.; Veglia, G.; Stottrup, B.; Elde, R.; Pei, D.; Guo, A.; Zhu, X. *J. Am. Chem. Soc.* **2008**, *130*, 6267.
(124) Tutus, M.; Rosetti, F. F.; Schneck, E.; Fragneto, G.; Forster, F.; Richter, R.; Nawroth, T.; Tanaka, M. *Macromol. Biosci.* **2008**, *8*, 1034.
(125) Goennenwein, S.; Tanaka, M.; Hu, B.; Moroder, L.; Sackmann, E. *Biophys. J.* **2003**, *85*, 646.
(126) Baumgart, T.; Offenhausser, A. *Langmuir* **2003**, *19*, 1730.
(127) Delajon, C.; Gutberlet, T.; Steitz, R.; Mohwald, H.; Krastev, R. *Langmuir* **2005**, *21*, 8509.
(128) Fischlechner, M.; Zaulig, M.; Meyer, S.; Estrela-Lopis, I.; Cuellar, L.; Irigoyen, J.; Pescador, P.; Brumen, M.; Messner, P.; Moya, S.; Donath, E. *Soft Matter* **2008**, *4*, 2245.
(129) Bunge, A.; Fischlechner, M.; Loew, M.; Arbuzova, A.; Herrmann, A.; Huster, D. *Soft Matter* **2009**, *5*, 3331.
(130) Schiller, S. M.; Naumann, R.; Lovejoy, K.; Kunz, H.; Knoll, W. *Angew. Chem. Int. Ed. Engl.* **2003**, *42*, 208.
(131) Knoll, W.; Naumann, R.; Friedrich, M.; Robertson, J.; Losche, M.; Heinrich, F.; McGillivray, D.; Schuster, B.; Gufler, P.; Pum, D.; Sleytr, U. *Biointerphases* **2008**, *3*, FA125.
(132) Seitz, M.; Ter-Ovanesyan, E.; Hausch, M.; Park, C. K.; Zasadzinski, J. A.; Zentel, R.; Israelachvili, J. N. *Langmuir* **2000**, *16*, 6067.
(133) Seitz, M.; Wong, J. Y.; Park, C. K.; Alcantar, N. A.; Isaelachvili, J. *Thin Solid Films* **1998**, *327-329*, 767.
(134) Zhang, H.; Hill, R. *J. R. Soc. Interface* **2011**, *8*, 312.
(135) Munro, J. C.; Frank, C. W. *Langmuir* **2004**, *20*, 10567.
(136) Wagner, M. L.; Tamm, L. K. *Biophys. J.* **2000** *79*, 1400.
(137) Kiessling, V.; Crane, J. M.; Tamm, L. K. *Biophys. J.* **2006**, *91*, 3313.
(138) Kiessling, V.; Tamm, L. K. *Biophys. J.* **2003**, *84*, 408.

(139) Crane, J. M.; Kiessling, V.; Tamm, L. K. *Langmuir* **2005**, *21*, 1377.
(140) Albertorio, F.; Diaz, A. J.; Yang, T. L.; Chapa, V. A.; Kataoka, S.; Castellana, E. T.; Cremer, P. S. *Langmuir* **2005**, *21*, 7476.
(141) Purrucker, O.; Fortig, A.; Jordan, R.; Tanaka, M. *Chem. Phys. Chem.* **2004**, *5*, 327.
(142) Purrucker, O.; Fortig, A.; Jordan, R.; Sackmann, E.; Tanaka, M. *Phys. Rev. Lett.* **2007**, *98*.
(143) Lin, J.; Szymanski, J.; Searson, P. C.; Hristova, K. *Langmuir* **2010**, *26*, 3544.
(144) Merzlyakov, M.; Li, E.; Gitsov, I.; Hristova, K. *Langmuir* **2006**, *22*, 10145.
(145) Diaz, A.; Albertorio, F.; Daniel, S.; Cremer, P. *Langmuir* **2008**, *24*, 6820.
(146) Kaufmann, S.; Papastavrou, G.; Kumar, K.; Textor, M.; Reimhult, E. *Soft Matter* **2009**, *5*, 2804.
(147) Nikolov, V.; Lin, J.; Merzlyakov, M.; Hristova, K.; Searson, P. *Langmuir* **2007**, *23*, 13040.
(148) Renner, L.; Pompe, T.; Lemaitre, R.; Dreschel, D.; Werner, C. *Soft Matter* **2010**, *6*, 5382.
(149) Ide, T.; Takeuchi, Y.; Aoki, T.; Tabata, K.; Noji, H. *J. Surf. Sci. Nanotech.* **2005**, *3*, 70.
(150) Smith, E. A.; Coym, J. W.; Cowell, S. M.; Tokimoto, T.; Hruby, V. J.; Yamamura, H. I.; Wirth, M. J. *Langmuir* **2005**, *21*, 9644.
(151) Elender, G.; Kuhner, M.; Sackmann, E. *Biosens. Bioelectron.* **1996**, *11*, 565.
(152) Deverall, M.; Garg, S.; Ludtke, K.; Jordan, R.; Ruhe, J.; Naumann, C. A. *Soft Matter* **2008**, *4*, 1899.
(153) Deverall, M. A.; Gindl, E.; Sinner, E.-K.; Besir, H.; Ruehe, J.; Saxton, M. J.; Naumann, C. A. *Biophys. J.* **2005**, *88*, 1875.
(154) Siegel, A. P.; Murcia, M. J.; Johnson, M.; Reif, M.; Jordan, R.; Ruhe, J.; Naumann, C. A. *Soft Matter* **2010**, *6*, 2723.
(155) Berquand, A.; Mazeran, P.; Pantigny, J.; Proux-Delrouyre, V.; Laval, J.; Bourdillon, C. *Langmuir* **2003**, *19*, 1700.
(156) Kataoka-Hamai, C.; Higuchi, M.; Iwai, H.; Miyahara, Y. *Langmuir* **2010**, *26*, 14600.
(157) Reich, C.; Andruzzi, L. *Soft Matter* **2010**, *6*, 493.
(158) Wang, T.; Ingram, C.; Weisshaar, J. C. *Langmuir* **2010**, *26*, 11157.
(159) Shen, W. W.; Boxer, S. G.; Knoll, W.; Frank, C. W. *Biomacromolecules* **2001**, *2*, 70.
(160) Daniel, C.; Sohn, K.; Mates, T.; Kramer, E.; Radler, J.; Sackmann, E.; Nickel, B.; Andruzzi, L. *Biointerphases* **2007**, *2*, 109.
(161) Giess, F.; Friedrich, M. G.; Heberle, J.; Naumann, R. L.; Knoll, W. *Biophys. J.* **2004**, *87*, 3213.
(162) Raguse, B.; Braach-Maksvytis, V.; Cornell, B.; King, L.; Osman, P.; Pace, R.; Wieczorek, L. *Langmuir* **1998**, *14*, 648.
(163) Deme, B.; Marchal, D. *Eur. Biophys. J.* **2005**, *34*, 170.

(164) Kujawa, P.; Moraille, P.; Sanchez, J.; Badia, A.; Winnik, F. M. *J. Am. Chem. Soc.* **2005**, *127*, 9224.
(165) Richert, L.; Lavalle, P.; Payan, E.; Shu, X. Z.; Prestwich, G. D.; Stoltz, J.-F.; Schaaf, P.; Voegel, J.-C.; Picart, C. *Langmuir* **2004**, *20*, 448.
(166) Bunge, A.; Loew, M.; Pescador, P.; Arbuzova, A.; Brodersen, N.; Kang, J.; Dahne, L.; Liebscher, J.; Herrmann, A.; Stengel, G.; Huster, D. *J. Phys. Chem. B* **2009**, *113*, 16425.
(167) Croll, T. I.; O'Connor, A. J.; Stevens, G. W.; Cooper-White, J. J. *Biomacromolecules* **2006**, *7*, 1610.
(168) Gerelli, Y.; Di Bari, M. T.; Deriu, A.; Clemens, D.; Almasy, L. *Soft Matter* **2010**, *6*, 2533.
(169) Mansouri, S.; Fatisson, J.; Miao, Z.; Merhi, Y.; Winnik, F. M.; Tabrizian, M. *Langmuir* **2009**, *25*, 14071.
(170) Pavinatto, F. J.; Caseli, L.; Oliviera, O. N. *Biomacromolecules* **2010**, *11*, 1897.
(171) Koper, I. *Mol. Biosyst.* **2007**, *3*, 651.
(172) Prime, K. L.; Whitesides, G. M. *Science* **1991**, *252*, 1164.
(173) Lee, J. H.; Lee, H. B.; Andrade, J. D. *Prog. Polym. Sci.* **1995**, *20*, 1043.
(174) Du, H.; Chandaroy, P.; Hui, S. W. *Biochim. Biophys. Acta* **1997**, *1326*, 236.
(175) Chapman, R. G.; Ostuni, E.; Takayama, S.; Holmlin, R. E.; Yan, L.; Whitesides, G. M. *J. Am. Chem. Soc.* **2000**, *122*, 8303.
(176) Arnold, K.; Zschoernig, O.; Barthel, D.; Herold, W. *Biochim. Biophys. Acta* **1990**, *1022*, 303.
(177) Zhao, J.; Tamm, L. K. *Langmuir* **2003**, *19*, 1838.
(178) Wagner, M. L.; Tamm, L. K. *Biophys. J.* **2001**, *81*, 266.
(179) Munro, J. C.; Frank, C. W. *Langmuir* **2004**, *20*, 3339.
(180) Merzlyakov, M.; Li, E.; Gitsov, I.; Hristova, K. *Langmuir* **2006**, *22*, 10145.
(181) Szleifer, I. *Curr. Opin. Solid St. M.* **1997**, *2*, 337.
(182) McPherson, T.; Kidane, A.; Szleifer, I.; Park, K. *Langmuir* **1998**, *14*.
(183) Carignano, M. A.; Szleifer, I. *Interface Sci.* **2003**, *11*, 187.
(184) Bowie, J. U. *Nature* **2005**, *438*, 581.
(185) Lee, A. G. *Biochim. Biophys. Acta* **2003**, *1612*, 1.
(186) Nielsen, C. H. *Anal. Bioanal. Chem.* **2009**, *395*, 697.
(187) Woolley, A. G.; Wallace, B. *J. Membrane Biol.* **1992**, *129*, 109.
(188) Wong, D.; Jeon, T. J.; Schmidt, J. *Nanotechnology* **2006**, *17*, 3710.
(189) Becucci, L.; Carbone, M. V.; Biagiotti, T.; D'Amico, M.; Olivotto, M.; Guidelli, R. *J. Phys. Chem. B* **2008**, *112*, 1315.
(190) Woodbury, D. J.; Miller, C. *Biophys. J.* **1990**, *58*, 833.
(191) Bayburt, T. H.; Grinkova, Y. V.; Sligar, S. G. *Nano Lett.* **2002**, *2*, 853.
(192) Bayburt, T. H.; Sligar, S. G. *FEBS Lett.* **2010**, *584*, 1721.
(193) Baas, B. J.; Denisov, I. G.; Sligar, S. G. *Arch. Biochem. Biophys.* **2004**, *430*, 218.

(194) Denisov, I. G.; Grinkova, Y. V.; Baas, B. J.; Sligar, S. G. *J. Biol. Chem.* **2006**, *281*, 23313.

(195) Denisov, I. G.; Baas, B. J.; Grinkova, Y. V.; Sligar, S. G. *J. Biol. Chem.* **2007**, *282*, 7066.

(196) Shaw, A. W.; Pureza, V. S.; Sligar, S. G.; Morrissey, J. H. *J. Biol. Chem.* **2007**, *282*, 6556.

(197) Bayburt, T. H.; Sligar, S. G. *Protein Sci.* **2003**, *12*, 2476.

(198) Leitz, A. J.; Bayburt, T. H.; Bamakov, A. N.; Springer, B. A.; Sligar, S. G. *BioTechniques* **2006**, *40*, 601.

(199) Boldog, T.; Grimme, S.; Li, S.; Sligar, M.; Hazelbauer, G. L. *Proc. Natl. Acad. Sci.* **2006**, *103*, 11509.

(200) Dalal, K. *J. Biol. Chem.* **2009**, *284*, 7897.

(201) Mi, L. Z.; Grey, M. J.; Nishida, N.; Walz, T.; Lu, C.; Springer, T. A. *Biochemistry* **2008**, *47*, 10314.

(202) Anderson, J. L.; Frase, H.; Michaelis, S.; Hrycyna, C. A. *J. Biol. Chem.* **2005**, *280*, 7336.

(203) Friday, B. B.; Adjei, A. A. *Biochim. Biophys. Acta* **2005**, *1756*, 127.

(204) Kratz, C. P.; Niemeyer, C. M.; Zenker, M. *J. Mol. Med.* **2007**, *85*, 223.

(205) Patra, S. K. *Exp. Cell Res.* **2008**, *314*.

(206) Adjei, A. A.; Erlichman, C.; Davis, J. N.; Cutler, D. L.; Sloan, J. A.; Marks, R. S.; Hanson, L. J.; Svingen, P. A.; Atherton, P.; Bishop, W. R.; Kirschmeier, P.; Kaufmann, S. H. *Cancer Res.* **2000**, *60*.

(207) Whyte, D. B.; Kirschmeier, P.; Hockenberry, T. N.; Nunez-Oliva, I.; James, L.; Catino, J. J.; Bishop, W. R.; Pai, J. K. *J. Biol. Chem.* **1997**, *272*, 14459.

(208) Romano, J. D.; Michaelis, S. *Mol Biol Cell* **2001**, *12*, 1957.

(209) Mulligan, K.; Brownholland, D.; Carnini, A.; Thompson, D. H.; Johnston, L. J. *Langmuir* **2010**, *26*, 8525.

(210) Brownholland, D. P.; Longo, G. S.; Struts, A. V.; Justice, M. J.; Szleifer, I.; Petrache, H. I.; Brown, M. F.; Thompson, D. H. *Biophys. J.* **2009**, *97*, 2700.

(211) Patwardhan, A. P.; Thompson, D. H. *Langmuir* **2000**, *16*, 10340.

(212) Patwardhan, A. P.; Thompson, D. H. *Org. Lett.* **1999**, *1*, 241.

(213) Benvegnu, T.; Brard, M.; Plusquellec, D. *Curr. Opin. Coll. Interface Sci.* **2004**, *8*, 469.

(214) Kim, J.-M.; Thompson, D. H. *Langmuir* **1992**, *8*, 637.

(215) Montier, T.; Benvegnu, T.; Jaffres, P. A.; Yaouanc, J. J. *Curr. Gene Ther.* **2008**, *8*, 296.

(216) Svenson, S.; Thompson, D. H. *J. Org. Chem.* **1998**, *63*, 7180.

(217) Lehtonen, J. Y. A.; Holopainen, J. M.; Kinnunen, P. K. J. *Biophys. J.* **1996**, *70*, 1753.

(218) Longo, G. S.; Schick, M.; Szleifer, I. *Biophys. J.* **2009**, *96*, 3977.

(219) Connell, S. D.; Smith, A. *Mol. Memb. Biol.* **2006**, *23*, 17.

(220) Johnston, L. J. *Langmuir* **2007**, *23*, 5886.

(221) Goksu, E. I.; Vanegas, J. M.; Blanchette, C. D.; Lin, W.-C.; Longo, M. L. *Biochim. Biophys. Acta* **2009**, *1788*, 254.

(222) Veatch, S. L.; Keller, S. L. *Biochim. Biophys. Acta* **2005**, *1746*, 172.

(223) Buboltz, J. T.; Bwalya, C.; Williams, K.; Schutzer, M. *Langmuir* **2007**, *23*, 11968.
(224) Reviakine, I.; Brisson, A. *Langmuir* **2000**, *16*, 1806.
(225) Wacklin, H. P.; Thomas, R. K. *Langmuir* **2007**, *23*, 7644.
(226) Reinl, H. M.; Bayerl, T. M. *Biochem.* **1994**, *33*, 14091.
(227) Callow, P.; Fragneto, G.; Cubitt, R.; Barlow, D. J.; Lawrence, M. J.; Timmins, P. *Langmuir* **2005**, *21*, 7912.
(228) Baumgart, T.; Hess, S. T.; Webb, W. W. *Nature* **2003**, *425*, 821.
(229) Blanchette, C. D.; Lin, W.-C.; Orme, C. A.; Ratto, T. V.; Longo, M. L. *Biophys. J.* **2008**, *94*, 2691.
(230) Garcia-Saez, A. J.; Chiantia, S.; Schwille, P. *J. Biol. Chem.* **2007**, *282*, 33537.
(231) Frolov, V. A. J.; Chizmadzhev, Y. A.; Cohen, F. S.; Zimmerberg, J. *Biophys. J.* **2006**, *91*, 189.
(232) Kuzmin, P. I.; Akimov, S. A.; Chizmadzhev, Y. A.; Zimmerberg, J.; Cohen, F. S. *Biophys. J.* **2005**, *88*, 1120.
(233) Blanchette, C. D.; Lin, W.-C.; Orme, C. A.; Ratto, T. V.; Longo, M. J. *Langmuir* **2007**, *23*, 5875.
(234) Jensen, M. H.; Morris, E. J.; Simonsen, A. C. *Langmuir* **2007**, *23*, 8135.
(235) Seeger, H. M.; Marino, G.; Alessandrini, A.; Facci, P. *Biophys. J.* **2009**, *97*, 1067.
(236) Mulligan, K.; Jakubek, Z.; Johnston, L. J. *Langmuir* **2011**, *27*, 14352.
(237) Vockenroth, I. K.; Atansova, P. P.; Long, J. R.; Jenkins, A. T. A.; Knoll, W.; Koper, I. *Biochim. Biophys. Acta* **2007**, *1768*, 1114.
(238) Kycia, A. H.; Wang, J.; Merrill, A. R.; Lipkowski, J. *Langmuir* **2011**, *27*, 10867.
(239) Tanaka, M.; Tutus, M.; Kaufmann, S.; Rossetti, F. F.; Schneck, E.; Weiss, I. M. *J. Struct. Biol.* **2009**, *168*, 137.
(240) Garg, S.; Ruhe, J.; Ludtke, K.; Jordan, R.; Naumann, C. A. *Biophys. J.* **2007**, *92*, 1263.
(241) Lapcik, L., Jr.; Lapcik, L.; De Smedt, S.; Demeester, J.; Chabrecek, P. *Chem. Rev.* **1998**, *98*, 2663.
(242) Kumar, M. N. V. R.; Muzzarelli, R. A. A.; Muzzarelli, C.; Sashiwa, H.; Domb, A. J. *Chem. Rev.* **2004**, *104*, 6017.
(243) Kujawa, P.; Sanchez, J.; Badia, A.; Winnik, F. M. *J. Nanosci. Nanotechnol.* **2006**, *6*, 1565.
(244) Kujawa, P.; Schmauch, G.; Viitala, T.; Badia, A.; Winnik, F. M. *Biomacromolecules* **2007**, *8*, 3169.
(245) Salomaki, M.; Kankare, J. *Biomacromolecules* **2009**, *10*, 294.
(246) Machan, R.; Hof, M. *Biochim. Biophys. Acta* **2010**, *1798*, 1377.
(247) Bayerl, T. M.; Bloom, M. *Biophys. J.* **1990**, *58*, 357.
(248) Lin, W.-C.; Blanchette, C. D.; Ratto, T. V.; Longo, M. L. *Biophys. J.* **2006**, *90*, 228.
(249) Cha, T.; Guo, A.; Zhu, X.-Y. *Biophys. J.* **2006**, *80*, 1270.

(250) Ira; Zou, S.; Carter Ramirez, D. M.; Vanderlip, S.; Ogilvie, W.; Jakubek, Z.; Johnston, L. J. *J. Struct. Biol.* **2009**, *168*, 78.
(251) Merzlyakov, M.; Li, E.; Hristova, K. *Langmuir* **2006**, *22*, 1247.
(252) Sugihara, K.; Vanos, J.; Zambelli, T. *ACS Nano* **2010**, *4*, 5047.
(253) Bunge, A.; Loew, M.; Pescador, P.; Arbuzova, A.; Brodersen, N.; Kang, J.; Dahne, L.; Liebscher, J.; Herrmann, A.; Stengel, G.; Huster, D. *J. Phys. Chem. B* **2009**, *113*, 16425.
(254) Goksu, E. I.; Hoopes, M. I.; Nellis, B. A.; Xing, C.; Faller, R.; Frank, C. W.; Risbud, S. H.; Satcher, J. H.; Longo, M. L. *Biochim. Biophys. Acta* **2010**, *1798*, 719.
(255) Roiter, Y.; Ornatska, M.; Rammohan, A. R.; Balakrishnan, J.; Heine, D. R.; Minko, S. *Langmuir* **2009**, *25*, 6287.
(256) Lee, S.-W.; Na, Y.-J.; Lee, S.-D. *Langmuir* **2009**, *25*, 5421.
(257) Sanii, B.; Smith, A. M.; Butti, R.; Brozell, A. M.; Parikh, A. N. *Nano Lett.* **2008**, *8*, 866.
(258) Tristram-Nagle, S.; Petrache, H. I.; Suter, R. M.; Nagle, J. F. *Biophys. J.* **1998**, *74*, 1421.
(259) Yang, Z.; Galloway, J. A.; Yu, H. *Langmuir* **1999**, 8405.
(260) Hung, W. C.; Chen, F. Y.; Huang, H. W. *Biochim. Biophys. Acta* **2000**, *1467*, 198.
(261) Peyratout, C.; Donath, E.; Daehne, L. *J. Photochem. Photobiol. A* **2001**, *142*, 51.
(262) Maeda, H. *Langmuir* **1997**, *13*, 4150.
(263) Milhiet, P.-E.; Gubellini, F.; Berquand, A.; Dosset, P.; Rigaud, J.-L.; Le Grimellec, C.; Levy, D. *Biophys. J.* **2006**, *91*.
(264) Slade, A.; Luh, J.; Ho, S.; Yip, C. M. *J. Struct. Biol.* **2002**, *137*, 283.
(265) Schmid, E. L.; Tairi, A. P.; Hovius, R.; Vogel, H. *Anal. Chem.* **1998**, 1331.
(266) *Protein stability and storage*, Pierce Biotechnology Inc, 2005.
(267) Li, E.; You, M.; Hristova, K. *Biochemistry* **2005**, 352.
(268) Henderson, J. N.; Ai, J.; Campbell, R. E.; Remington, S. J. *Proc. Natl. Acad. Sci.* **2007**, *104*, 6672.
(269) Heller, W. T.; Waring, A. J.; Lehrer, R. I.; Harroun, T. A.; Weiss, T. M.; Yang, L.; Huang, H. W. *Biochemistry* **2000**, *39*, 139.
(270) Ludtke, S. J.; He, K.; Wu, Y.; Huang, H. W. *Biochim. Biophys. Acta* **1994**, *1190*, 181.
(271) Hrycyna, C. A.; Clarke, S. *Mol. Cell Biol.* **1990**, *10*, 5071.
(272) Duan, H. *Arch. Biochem. Biophys.* **2004**, *424*, 141.
(273) Davydov, D. R. *Biochemistry* **2005**, *44*, 13902.
(274) Bayburt, T. H. *J. Biol. Chem.* **2007**, *282*, 14875.
(275) Whorton, M. R. *Proc. Natl. Acad. Sci.* **2007**, *104*, 7682.
(276) Alvarez, F. J.; Orelle, C.; Davidson, A. L. *J. Am. Chem. Soc.* **2010**, *132*, 9513.
(277) Denisov, I. G. *J. Am. Chem. Soc.* **2004**, *126*, 3477.
(278) Shih, A. Y. *Biophys. J.* **2005**, *88*, 548.

(279) Griggs, A. M.; Hahne, K.; Hrycyna, C. A. *J. Biol. Chem.* **2010**, *285*, 13380.
(280) Carlson, J. W.; Jonas, A.; Sligar, S. G. *Biophys. J.* **1997**, *73*, 1184.
(281) Zweytick, D.; Deutsch, G.; Andra, J.; Blondelle, S. E.; Vollemer, E.; Jerala, R.; Lohner, K. *J. Biol. Chem.* **2011**, *286*, 21266.
(282) Blanchette, C. D.; Cappuccio, J. A.; Kuhn, E. A.; Segelke, B. W.; Benner, W. H.; Chromy, B. A.; Coleman, M. A.; Bench, G.; Hoeprich, P. D.; Sulcheck, T. A. *Biochim. Biophys. Acta* **2009**, *1788*, 724.
(283) Carlson, J. W.; Jonas, A.; Sligar, S. G. *Langmuir* **2000**, *16*, 3927.
(284) Boldog, T.; Li, M.; Hazelbauer, G. L. *Methods Enzymol.* **2007**, *423*, 317.
(285) Nath, A.; Atkins, W. M.; Sligar, S. G. *Biochemistry* **2007**, *46*, 2059.